



**The Development of Automatic On-Machine
Metrology**

By

Matthew Bibby


This thesis is submitted in partial fulfilment of the requirements for the
degree of Doctor of Philosophy

National Centre for Ultra Precision Surfaces
Department of Physics and Astronomy
University College London

February 2015

Declaration of Authorship

I, Matthew Bibby confirm that the work presented in this thesis is my own. Where information has been derived from other sources, I confirm that this has been indicated in the thesis.

A handwritten signature in black ink, appearing to read 'M Bibby', with a long horizontal stroke extending to the right.

Matthew Bibby

For Samantha Lambert

Acknowledgements

The author would like to thank two groups of people:

Those without whom this PhD would never have been started. Carole Bibby, Andrew Bibby, Joyce Stoddart and George Stoddart for having helped develop the required self-belief and determination. Janet Lambert and David Lambert for their acceptance and understanding. Richard Freeman and Zeeko for the opportunity and support to peruse this project.

Those without whom this thesis would not have been completed. The author's supervisor, David Walker for his guidance and support. Christopher King for his tutelage throughout the project. Pim Messelink for many hours of illuminating discussion. Finally, Samantha Lambert for the constant support, belief, and patience provided throughout this project.

Abstract

The manufacture of large off-axis aspheric optics for the next generation of extremely large telescopes presents a number of unique challenges. For example, the European Southern Observatory (ESO) Extremely Large Telescope (E-ELT) requires the manufacture of one 1.4 m class ultra-precision mirror segment per week in order to satisfy the first-light deadline. One of the factors limiting the pace of manufacture is metrology. Many of the tasks associated with measurement, such as optic positioning, alignment and acquisition are carried out manually. It is also common for the optic to be removed to a laboratory for measurement, which can be time consuming and risk damage.

This thesis presents research into the development of new on-machine metrology techniques, which allow measurement to be carried out in the manufacturing environment. This work is supported by a software application developed by the author to allow the design and control of on-machine metrology. This application uses the computer numerical control (CNC) polishing system as part of the positioning and alignment system. The inclusion of CNC has enabled the development of a close-loop control system which facilitates automatic alignment and acquisition of metrology data. The software presented uses a modular architecture, allowing many different types of metrology to be planned and control using a single application. This is demonstrated using two case studies, which allow automatic on-machine sub-aperture stitching metrology using a metrology tower placed over the machine, and automatic on-machine texture measurement. The use of a closed loop software application to control automatic on-machine texture

measurement is a novel step. It is also demonstrated that on-machine metrology in the manufacturing environment can produce measurement data of comparable quality to that of the laboratory. Automatic measurements systems such as those presented are likely to play an increasing role in the large and high-volume optical fabrication sectors.

Table of Contents

DECLARATION OF AUTHORSHIP	2
ACKNOWLEDGEMENTS	3
ABSTRACT	5
TABLE OF CONTENTS.....	7
LIST OF TABLES	14
LIST OF FIGURES	15
GLOSSARY	21
1 INTRODUCTION	23
1.1 CONTROL OF THE SURFACE.....	23
1.2 TECHNIQUES FOR THE MANUFACTURE OF OPTICAL SURFACES	27
1.2.1 <i>Classical Manufacturing Techniques</i>	27
1.2.2 <i>Application of Computer Numerical Control to Optical Surface Manufacturing</i>	30
1.2.3 <i>Sub-aperture Polishing Techniques</i>	34
1.2.3.1 Magneto-Rheological Fluid Polishing	35
1.2.3.2 Zeeko Inflatable Membrane Polishing.....	37
1.2.4 <i>Conclusion</i>	39
1.3 CHARACTERISATION OF SURFACES	40

1.3.1	<i>Form Characterisation</i>	43
1.3.2	<i>Texture Characterisation</i>	48
1.4	LIMITATIONS OF EXISTING MEASUREMENT TECHNIQUES.....	50
1.5	WORK PRESENTED	52
2	ON-MACHINE METROLOGY	54
2.1	ZEEKO IRP MACHINE	54
2.1.1	<i>Polishing Operation</i>	57
2.1.1.1	Supporting the Part.....	58
2.1.1.2	Part Alignment	59
2.1.1.3	Non-Linear Correction	60
2.1.1.4	Polishing.....	61
2.1.2	<i>Conclusion</i>	61
2.2	H-AXIS MOUNTED METROLOGY	62
2.2.1	<i>On-Machine Stitching Interferometer</i>	63
2.2.2	<i>Surface Texture Analyser</i>	65
2.2.3	<i>The [0,0,1] Condition</i>	66
2.2.3.1	The [0,0,1] Condition During Polishing.....	67
2.2.3.2	The [0,0,1] Condition During Metrology.....	67
2.2.4	<i>Conclusion</i>	70
2.3	5-AXIS STAGE AND TESTING TOWER	71
2.3.1	<i>OpTIC Glyndwr Testing Tower</i>	72
2.3.2	<i>Zeeko Metrology Station</i>	74

2.3.3	<i>Conclusion</i>	75
2.4	ON-MACHINE SURFACE TEXTURE MEASUREMENT	76
2.4.1	<i>IRP 1200 Machine Specification</i>	76
2.4.2	<i>Surface Texture Analyser Specification</i>	77
2.4.3	<i>Suitability for On-Machine Metrology</i>	78
2.4.3.1	Vibration Analysis	78
2.4.3.2	Manufacturing Environment Repeatability	81
2.4.4	<i>On-Machine Operation</i>	83
2.4.4.1	Fringe Location Using the STA	83
2.4.5	<i>Conclusion</i>	85
2.5	SUB-APERTURE MEASUREMENT	86
2.5.1	<i>Metrology Station Base Unit</i>	86
2.5.2	<i>Fizcam 3000</i>	91
2.5.3	<i>Suitability for Automated Metrology</i>	92
2.5.3.1	Metrology Station Tilt Table Assembly	92
2.5.3.2	Metrology Loop	94
2.5.4	<i>Manual System Operation</i>	96
2.5.4.1	Fringe Location Using the Fizcam 3000	97
2.5.5	<i>Conclusion</i>	98
2.6	SOFTWARE REQUIREMENTS FOR ON-MACHINE METROLOGY	99
2.7	CONCLUSION	101
3	METROLOGY DESIGNER.....	102

3.1	<i>METROLOGY DESIGNER DEVELOPMENT</i>	104
3.1.1	<i>Surface Design</i>	104
3.1.1.1	Device Configuration	106
3.1.2	<i>Optics database</i>	108
3.2	MEASUREMENT PLANNING	111
3.2.1	<i>Sub-aperture planning</i>	112
3.2.1.1	Spherical Sub-aperture Measurement Planning	113
3.2.1.2	Plano Sub-aperture Measurement Planning	127
3.2.1.3	Overlap optimisation	130
3.2.2	<i>Point measurement planning</i>	136
3.2.3	<i>Manual Editing of Sub-Aperture and Point Measurement Plans</i>	138
3.2.4	<i>Measurement Plan Description File Generation</i>	141
3.3	CONCLUSION	141
4	METROLOGY CONTROLLER DEVELOPMENT	143
4.1	COMMUNICATION.....	144
4.1.1	<i>Web Service Error Handling</i>	145
4.2	AUTOMATIC MEASUREMENT WORK FLOW	146
4.3	MEASUREMENT SETUP	147
4.3.1	<i>Sub-aperture Measurement</i>	148
4.3.1.1	Part Clacking	148
4.3.1.2	Pivot Distance	152

4.3.2	<i>Point Measurement</i>	155
4.3.2.1	Co-ordinate System Set Up.....	156
4.3.2.2	Non-linear Correction	157
4.3.3	<i>Conclusion</i>	160
4.4	SYSTEM INVERSE KINEMATICS	161
4.4.1	<i>Metrology Station</i>	161
4.4.2	<i>STA on the IRP Machine</i>	163
4.4.3	<i>Conclusion</i>	164
4.5	DEVICE ALIGNMENT	165
4.5.1	<i>Sub-aperture Measurement Alignment</i>	166
4.5.2	<i>Point Measurement Alignment</i>	178
4.5.2.1	Fringe Detection for the STA	192
4.5.2.2	Mitigation of the [0,0,1] Condition for H-axis Mounted Metrology 204	
4.5.3	<i>Conclusion</i>	209
4.6	MEASUREMENT ACQUISITION	210
4.7	APPLICATION OF METROLOGY CONTROL SYSTEM TO AUTOMATIC MANUFACTURING CELL 211	
4.8	CONCLUSION	213
5	RESULTS AND DISCUSSION	215
5.1	SURFACE TEXTURE ANALYSER.....	216
5.1.1	<i>Application of STA to ESO segment measurement</i>	216

5.1.2	<i>Automatic On-Machine Measurement</i>	219
5.1.3	<i>Comparison of STA with Existing Texture Analysis Techniques</i>	223
5.1.3.1	ADE Phaseshift White Light Interferometer	223
5.1.3.2	Surface Replication	227
5.1.4	<i>Conclusion</i>	232
5.2	METROLOGY STATION	233
5.2.1	<i>Application of Automatic Sub-Aperture Stitching Interferometry</i>	234
5.2.1.1	Spherical Pass-Off Measurement	235
5.2.1.2	Plano Pass-Off Measurement	243
5.2.2	<i>Comparison of sub-aperture and full-aperture metrology</i>	247
5.2.3	<i>Conclusion</i>	252
5.3	AUTOMATIC OPERATION	253
5.3.1	<i>Measurement Duration</i>	255
5.3.1.1	Measurement Acquisition	255
5.3.1.2	Device and SUT Positioning	256
5.3.1.3	Setup Procedures.....	257
5.3.2	<i>User Interface</i>	258
5.3.3	<i>Software Requirements Compliance</i>	259
5.3.4	<i>Conclusion</i>	261
5.4	OVERALL CONCLUSION	262
6	CONCLUSIONS AND FURTHER WORK.....	264
6.1	FUTURE WORK.....	267

6.1.1	<i>Metrology Control Suite</i>	267
6.1.2	<i>Automatic Measurement of Aspheric Surfaces</i>	270
6.1.2.1	Non-Null Testing	270
6.1.2.2	Wavefront Correction	271
7	LIST OF PUBLICATIONS	274
7.1	PAPERS.....	274
7.2	ESO CERTIFICATION DOCUMENTS.....	274
8	BIBLIOGRAPHY	275
9	APPENDICES	284
9.1	<i>METROLOGY CONTROL SUITE</i> USER MANUAL.....	284
9.2	METROLOGY CONTROL SUITE DEBUG MODE APPLICATION NOTE.....	328
9.3	<i>STA TILTED SPIGOT ASSEMBLY</i>	334

List of Tables

Table 1.1: Command codes used in example program and compatible with Fanuc control units	34
Table 2.1: IRP1200 axis specifications.....	77
Table 2.2: STA specification (10x objective).....	78
Table 2.3: Metrology Station base unit axis specification	90
Table 2.4: Fizcam 3000 specification	92
Table 2.5: Metrology Control Suite software requirements.....	100
Table 3.1: Device configuration file overview.....	107
Table 3.2: Device configuration file example.....	108
Table 3.3: Optics database parameters	110
Table 3.4: Optics database example	111
Table 3.5: Sub-aperture angles table	123
Table 3.6: Example sub-aperture angles table.....	123
Table 4.1: Zernike polynomials used in fine alignment correction - reproduced from [91]	178
Table 5.1: Summary of ESO E-ELT texture specification	217
Table 5.2: Summary of Metrology Station pass-off specification and achieved results	235
Table 5.3: Measurement statistics for the delta between the six repeat measurements and the computed mean	241
Table 5.4: Metrology Station plano pass-off measurement delta results.....	247
Table 5.5: Metrology Control Suite software compliance matrix.....	260

List of Figures

Figure 1.1: Overarm spindle machine lap mechanism taken from [19]	28
Figure 1.2: Birr telescope primary installed on UCL 2.4 m lap system	30
Figure 1.3: Simplified CNC system model schematic of 3-axis machine.....	31
Figure 1.4: Modern CNC system with dedicated controller	32
Figure 1.5: Example G-code program	33
Figure 1.6: Schematic of the MRF process taken from [31]	36
Figure 1.7: Variation of polishing spot size with Z-offset	38
Figure 1.8: Zeeko semi-rigid inflatable bonnet tool.....	38
Figure 1.9: Optical plate testing using a sodium lamp.....	42
Figure 1.10: Fizeau interferometer schematic.....	44
Figure 1.11: ADE Phaseshift MicroXAM white light interferometry.....	49
Figure 2.1: IRP1200 machine with interferometer test tower at OptIC, North Wales	56
Figure 2.2: A and B axis arrangement of the type-2 virtual pivot of the IRP1200.....	57
Figure 2.3: IRP1600 operator console PC.....	58
Figure 2.4: Zeeko OMSI CAD model fitted to a type-2 VP spindle (courtesy of Zeeko)	64
Figure 2.5: 4D Technology NanoCam with tripod tilt alignment assembly (courtesy of 4D Technology)	65
Figure 2.6: STA mounted on the IRP1600 machine and while testing a prototype ESO E-ELT segment at OptIC Glyndwr, North Wales.....	66
Figure 2.7: Measurement plan used during characterisation of the [0,0,1] condition	69

Figure 2.8: Resultant MSS testing plan designed to avoid region affected by the [0,0,1] condition	70
Figure 2.9: Lower path of the OpTIC Glyndwr optical testing tower used for ESO E-ELT segment full-aperture measurement (Top sphere assembly not shown)	72
Figure 2.10: Prototype ESO E-ELT segment mounted on 27-point support	73
Figure 2.11: Zeeko Metrology Station installed at customer site.....	74
Figure 2.12: SIOS SP2000 distance measuring interferometer mounted to IRP1200 machine during vibration analysis	79
Figure 2.13: Approximate vibration analysis locations on the 1.3 m diameter machine table.....	80
Figure 2.14: Sample IRP1200 vibration analysis FFT result.....	81
Figure 2.15: Comparison of STA repeatability in laboratory and on-machine regimes	82
Figure 2.16: STA course alignment and focus system (a) correctly aligned and focused, (b) correctly focused and misaligned, (c) poor focus and misaligned	84
Figure 2.17: Metrology Station tilt table assembly.....	87
Figure 2.18: Metrology Station 5-axis stage axes configuration (courtesy of Zeeko)	88
Figure 2.19: Fizcam 3000 access door on the Metrology Station.....	89
Figure 2.20: Metrology Station control console	91
Figure 2.21: Close-up view of the Metrology Station rotary tilt table.....	93
Figure 2.22: Example of the metrology loop of the Zeeko Metrology Station system	95
Figure 2.23: Metrology Station Fizcam 3000 alignment screen (l) and 4Sight measurement screen (r).....	98
Figure 3.1: <i>Metrology Designer</i> main GUI.....	104
Figure 3.2: Screen shot of Zeeko <i>Surface Designer</i> (courtesy of Zeeko)	106
Figure 3.3: Transmission optic parameters for spherical test	110
Figure 3.4: Initial planning function flow	112

Figure 3.5: Spherical sub-aperture angles calculation work flow.....	114
Figure 3.6: Sub-aperture rotation calculation schematic	116
Figure 3.7: SUT centre to edge distance calculation (Top) using all points on perimeter (Bottom) using points located along X-axis only	118
Figure 3.8: First sub-aperture at each ring of measurement plan.....	120
Figure 3.9: Ring azimuth angle calculation schematic	121
Figure 3.10: Single ring spherical measurement plan.....	122
Figure 3.11: Spherical sub-aperture planning work flow.....	125
Figure 3.12: Spherical sub-aperture measurement plan prior to coverage optimisation and using a small overlap value.....	126
Figure 3.13: Plano sub-aperture planning work flow	129
Figure 3.14: Measurement plan overlap optimisation work flow	131
Figure 3.15: SUT mask used for SUT coverage optimisation	132
Figure 3.16: (Top) Sub-aperture mask used for SUT coverage optimisation and (Bottom) the equivalent sub-aperture placed on the SUT	134
Figure 3.17: Resultant coverage mask following SUT mask multiplication with a single sub-aperture mask.....	135
Figure 3.18: Point measurement angles table planning	137
Figure 3.19: Point measurement plan - concentric rings.....	138
Figure 3.20: Manual sub-aperture measurement placement window	139
Figure 3.21: Manual point measurement placement window	140
Figure 3.22: Overall work flow of <i>Metrology Control Suite</i>	142
Figure 4.1: Direct Ethernet communication topology	144
Figure 4.2: Overall automatic measurement work flow	146
Figure 4.3: <i>Metrology Controller</i> main GUI screenshot.....	147
Figure 4.4: SUT optical axis alignment	149

Figure 4.5: Coarse alignment camera input displayed on <i>Metrology Controller</i> console PC using application developed by C.W. King	151
Figure 4.6: Schematic representation of required corrective translations following T-axis rotation to measure concentric sub-aperture ring of spherical SUT (image by C.W. King)	153
Figure 4.7: Metrology Station table assembly representation showing T-axis pivot offset distance	154
Figure 4.8: Non-linear correction map generated using <i>Zeeko TPG</i>	157
Figure 4.9: Residual test location focus error for the same part (Top) before and (Bottom) after test plan correction using non-linear probing data.....	159
Figure 4.10: Plano auto-alignment work flow	167
Figure 4.11: Plano auto-alignment work flow continued	168
Figure 4.12: Spherical auto-alignment work flow.....	169
Figure 4.13: Spherical auto-alignment work flow continued	170
Figure 4.14: Coarse spot sensitivity calculation.....	172
Figure 4.15: STA automatic alignment work flow.....	180
Figure 4.16: STA auto focus work flow	181
Figure 4.17: STA auto focus work flow continued	182
Figure 4.18: Interferometric fringes of the STA exhibiting large surface tilt error..	183
Figure 4.19: STA fitted to the IRP1200 machine testing a 200 mm cross-corners hexagonal part	187
Figure 4.20: Tilt correction of STA mounted on IRP machine.....	189
Figure 4.21: Relationship between STA camera and IRP machine co-ordinate frames when rotating IRP machine A-axis	190
Figure 4.22: Sobel filter output	195
Figure 4.23: Fringe detection using the Hough transform	198
Figure 4.24: Hough transform in the presence of noise	201

Figure 4.25: Edge detection result prior to cluster filtering	202
Figure 4.26: Edge detection result with cluster filtering	203
Figure 4.27: H-axis adjustment integrated into the STA automatic alignment script	207
Figure 4.28: H-axis correction function for [0,0,1] condition mitigation.....	208
Figure 4.29: Prototype optic production cell including a Zeeko IRP600 and Fanuc M20i-A robot arm	212
Figure 5.1: Example of ESO E-ELT segment measurement, witnessed by ESO	218
Figure 5.2: STA automatic metrology measurement plan.....	220
Figure 5.3: Modified test point locations table for STA automatic control testing.	221
Figure 5.4: STA on-machine automatic measurement example of a small-scale E-ELT process development component	222
Figure 5.5: Phaseshift ADE FFT analysis result	224
Figure 5.6: 4D Technology Surface Texture Analyser FFT result	225
Figure 5.7: Spatial frequency performance comparison between ADE Phaseshift and 4D Technology devices.....	226
Figure 5.8: Direct measurement of Zerodur sample using ADE Phaseshift.....	228
Figure 5.9: Polymer replication measurement using ADE Phaseshift	229
Figure 5.10: UV cure replication measurement using ADE Phaseshift	230
Figure 5.11: 465 mm ROC convex sphere used for Metrology Station pass-off testing	236
Figure 5.12: Measurement plan used for Metrology Station pass-off at customer site. SUT: 300 mm, 465 mm ROC Convex	237
Figure 5.13: Sub-aperture angles editor configuration for pass-off test of Metrology Station	238
Figure 5.14: Stitched result of Metrology Station pass-off test (image by C.W. King)	240

Figure 5.15: Example delta between stitched measurement and mean result for Metrology Station pass-off (image by C.W. King)	242
Figure 5.16: Metrology Station plano pass-off measurement plan.....	244
Figure 5.17: Plano pass-off measurement stitched result (image by C.W. King)	246
Figure 5.18: Schematic of test setup for comparison between stitched and full-aperture measurement (image by C.W. King)	248
Figure 5.19: 3-sphere test measurement plan	249
Figure 5.20: 3-sphere measurement result (image by C.W. King).....	250
Figure 5.21: Stitched measurement result (image by C.W. King)	250
Figure 5.22: Difference between 3-sphere and stitched results (image by C.W. King)	251
Figure 5.23: Metrology Station working volume temperature variation during stitching measurement for full-aperture and stitching comparison	252
Figure 5.24: Time constraints associated with current ESO segment processing steps	255
Figure 6.1: IRP600XL combined with metrology testing tower	270

Glossary

CAD – Computer Aided Design

CGH – Computer Generated Hologram

CMM – Co-ordinate Measuring Machine

CNC - Computer Numerical Control

COC – Centre of Curvature

E-ELT – European Extremely Large Telescope

ESO – European Southern Observatory

FOV – Field of View

GUI – Graphical User Interface

MRF – Magneto-Rheological Fluid

MSS – Master Spherical Segment

NaN – Not a Number.

NC – Numerical Control

OMM – On-Machine Metrology

PC – Personal Computer

ROC – Radius of Curvature

RSS – Root Sum Squared

STA – Surface Texture Analyser

SUT – Surface under Test

TPG – Tool Path Generator

1 Introduction

1.1 Control of the surface

Throughout our lives, we interact with the surrounding world by perceiving objects using our senses of sight, hearing and touch. Most of what we view is a series of surfaces, light interacting at an interface between an object and the air. A surface may be defined as;

'The outermost boundary (or one of the boundaries) of any material object, immediately adjacent to air, fluid or empty space, or to another object.' [1]

A surface is an infinitesimally fine layer, which forms the boundary between two media. However, this interface can often shape our perception of an object; its value, its quality, what it means to us and its function.

At the beginning of human civilisation, commodities were traded based upon their perceived value. The first recorded use of money was that of shell currency [2]. These were commonly cowry shells found washed up on beaches near to settlements, collected primarily for their aesthetics. Being different from artefacts man could readily make, they were difficult to counterfeit. Shells held value based upon their size and colour, possibly due to the rarity of such specimens. Over time, these shells began to be drilled and threaded onto string for ease of carrying and trading. Eventually, people began to manufacture shell-like beads instead of collecting shells. Materials such as wood, bone, and stone were selected and subsequently modified into currency. This marks one of the earliest examples at which humans sought to modify surfaces for requirements not directly associated

with survival (tools or weapons) or aesthetics (jewellery) but for a function: The surface in this case forms a robust, easily recognised symbol of value. When currency came to be manufactured in pressed metal, some eastern cultures retained the central hole in their coinage. This is still seen today in examples such as the Japanese 5¥ and 50¥ coins.

As technology developed, humanity began to make increasingly elaborate changes to surfaces for the purposes of functionality. In medicine, smooth, sharp needles allow the delivery of vaccination and curative preparations [3]. In aeronautics, the interaction of air with the refined surface of a wing provides lift and enables us to travel the world. These surfaces are modified and controlled purely for their functional quality rather than aesthetics, as with ancient currency.

However, the origin of optics may predate all but the earliest forms of currency. One of the earliest known lenses, The Nimrud Lens (plano-convex), dates back to around 750BC to 710BC and was created from quartz [4]. This example was found in what is now Northern Iraq, but similar examples have been located in Greece [5] and Egypt. There is some evidence of Egyptian optics dating back to 2600 BC, however no specimens have been recovered [6]. Most of these early optics are considered to have been used for carving, or as burning glasses.

Only much later did compound systems, of two or more lenses, become available. There remains debate over the origin of such systems. The compound microscope is often credited to either Zacharias Janssen, Hans Lippershey or Galileo Galilei between 1590 AD and 1605 AD [7], while the first refractive telescope is widely credited to Hans Lippershey in 1608, following a demonstration to Count Maurits of

Nassau [8]. Even after forming a commercial deal with the army, Lippershey was not granted a patent, as many others came forward to claim themselves as the inventors. The reason for the contention surrounding the origins of both the microscope and the telescope are two-fold; the potential for material gain and existing subconscious knowledge. It is thought that many were aware of the effects of compound optics, though there was little conscious awareness as to the applications. Regardless of this debate, it is certain that a revolution of astronomy followed the development of the telescope. By this time, society had developed such that basic survival was generally not a preoccupation. Many scholars were now able to turn their energy to exploration, not for material gain, but for the advancement of collective knowledge.

Observational astronomers could now observe more than points of light. New details and objects, previously invisible due to their faintness, were revealed. A multitude of discoveries followed, such as Jupiter's four largest moons, craters on Earth's moon and the phases of Venus by Galileo Galilei alone.

Following a further 400 years of development direct imaging of exoplanets, planets outside of our solar system, is a plausible pursuit [9]. One such example designed to allow characterisation of Earth sized exoplanets is the European Southern Observatory (ESO) European Extremely Large Telescope (E-ELT) [10]. This instrument is designed to deliver sufficient image quality and sensitivity to also study the era of first galaxy formation following the Big Bang, and the apparent acceleration of the expansion of the universe. Construction of the E-ELT will also challenge current practice in other fields, such as optical manufacturing and

metrology, as a result of system optical design. The E-ELT is scheduled for first light in 2024, with ESO adopting a 2-phase approach to construction in order to minimise risk of further delays and maximise instrument competitiveness [11]. One of the greatest challenges of the construction of the E-ELT is the fabrication of the primary mirror. As detector quantum efficiency nears 100%, obtaining greater optical performance becomes a matter of constructing a larger primary [12].

The E-ELT primary mirror design was originally a 42 m diameter F1 parabola consisting of 984 closely tessellated hexagonal mirrors (plus 133 spares). This specification was reduced to a 39 m diameter F0.88 primary in 2011 to save cost, not only of optical components, but also by reducing enclosure size. The individual segments are off-axis aspheres which must be polished edge to edge. This allows the segments to be placed closely together (4 mm gaps), minimising near-field infra-red emissions entering the optical chain from between components which degrades signal-to-noise ratio [13]. The University College London team at OpTIC Glyndwr is part of a consortium involving Zeeko Ltd and led by Glyndwr University which has been commissioned to produce seven prototype segments for the E-ELT primary, as per the original specification. Later in this chapter, techniques used to manufacture and measure these prototypes will be discussed as well as how they must be improved to satisfy the project goals.

Parallel to the development of optical technology is that of manufacturing. The E-ELT requires mass production of metre-scale optical components of high quality in order to meet the first light target and achieve the specified science goals. As will be demonstrated in the remainder of this chapter, capability in manufacturing is

interwoven with that in metrology. These developments are driven forward, not by the human need to survive but because we are driven to learn. Although the modification of a surface can change our perception of an object, that surface can also be used to change our perception of the world around us.

1.2 Techniques for the Manufacture of optical surfaces

This section will discuss how optical components are commonly made and how recent developments in this field have facilitated the new work presented in this thesis.

Optics such as the Nimrud lens were polished by hand or using simple equipment, such as that shown in [5]. This type of system was manually powered and labour intensive, especially with quartz being harder than other contemporary materials [14] [15]. Though crude by modern standards, such techniques are similar to those referred to as 'classical polishing'.

1.2.1 Classical Manufacturing Techniques

Production of an optical surface is usually a subtractive process, where material is removed from a ground blank until the surface shape matches that of the specification. The blank is a glass or ceramic slab which is ground into shape to ensure compatibility with the available tooling and minimise processing time. The grind is carried out on a rigid system so that an accurate shape is imparted to the surface, using a tooling similar to a cup wheel or a lap.

Lapping achieves removal by moving the work piece against an abrasive surface, or a non-abrasive surface in the presence of abrasive slurry. The lap is about the same size as the component to be polished and of equal and opposite radius of curvature

(ROC), ensuring it conforms to allow removal. With the two surfaces in contact, lateral movement is applied to achieve abrasion, typically by rotating the tool while moving the surface back and forth across the surface, as demonstrated in Figure 1.1 using the overarm spindle machine. The lap material is varied through the process, from a steel grinding lap to a pitch lap. The former imparts the correct form to the surface while the pitch tool is typically used to control roughness [16]. The pitch tool will slowly conform to the surface shape, removing small features while maintaining the ROC.

Originally manually operated, the lap has been increasingly automated and the speed at which the system worked can be accurately controlled. The rate of removal was found to be dependent upon the speed of motion across the surface (feedrate) and the amount of pressure exerted on the surface [17]. Slurry particle size and chemical composition also affect the removal and final finish of the process [18].

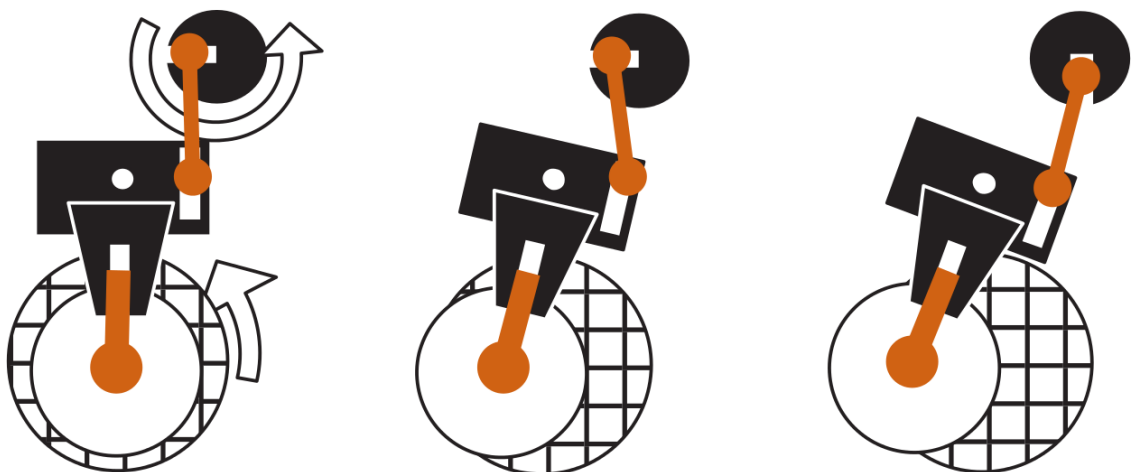


Figure 1.1: Overarm spindle machine lap mechanism taken from [19]

Although the lapping process is well-used, it has limitations. Each surface of a different ROC produced requires tooling of the correct radius, which can become a large source of expenditure for the optical manufacturer. Furthermore, aspheres and free-form optics cannot easily be produced through lapping and the process is generally limited to rotationally symmetric parts of plano or spherical prescription and some mild aspheres. As the requirement for large optics has increased, larger full-aperture polishing systems have been constructed. However, the tooling costs associated with such large systems mean they are typically purpose built or adapted for specialist projects. Figure 1.2 shows the aluminium primary mirror of the Birr telescope being restored at UCL on a 2.5 m grinding and polishing machine. In this case the mirror was a 1.8 m diameter parabola, however, adapting this system to polish other prescriptions would incur substantial cost and time [20]. In the case of the UCL polishing system described, some computerisation was added to the polishing system and the final aspherisation was performed using a sub-aperture regime [21].

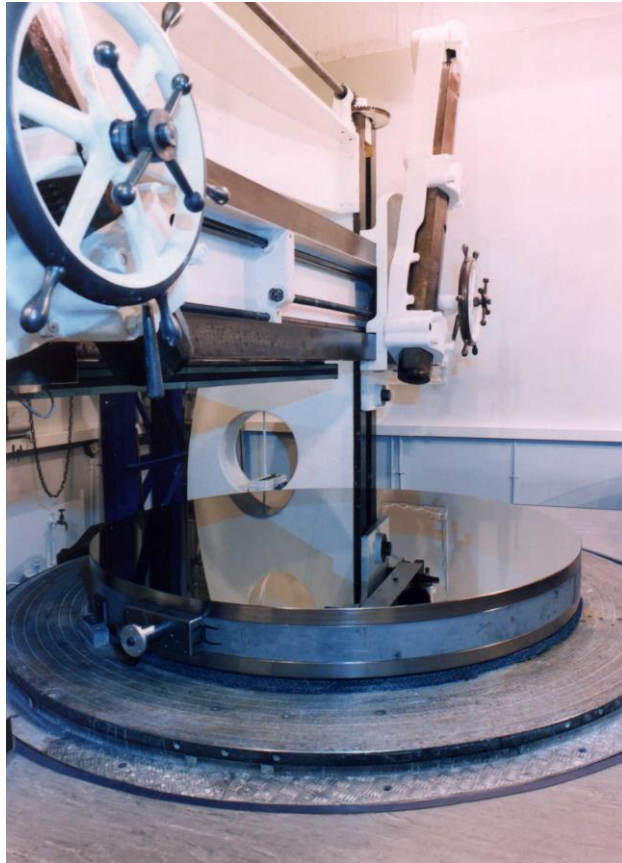


Figure 1.2: Birr telescope primary installed on UCL 2.4 m lap system

This application of Computer Numerical Control (CNC) and sub-aperture tooling allows the removal of some of the cost limitations of classical techniques. Although CNC systems have been available commercially since the 1940s [22], they were not used in optical manufacturing until much later. CNC techniques have been combined with lapping to develop the stressed or active lap which allow the production of aspheric surfaces [23] [24]. However, greater flexibility has been achieved through the development of finishing using generic tooling smaller than the work piece, called sub-aperture polishing [25].

1.2.2 Application of Computer Numerical Control to Optical Surface Manufacturing

The use of CNC and sub-aperture polishing techniques enable greater complexity optical surfaces to be produced, and so increased performance of the resultant

optical systems [26] [27]. CNC also forms a fundamental component in the work presented in this thesis. This section will therefore provide an overview of computer numerical control and discuss application to the field of optical manufacture.

A CNC system is one in which a computer controls the motorised axes of a machine to behave as prescribed by a program. A single machine may perform many different tasks by changing the program. Figure 1.3 shows a schematic of a simplified system, where three motorised axes are controlled via a program loaded onto a computer. CNC machines have no intelligence, and only execute the program. If the program places the machine into a configuration such that a crash occurs, (an unplanned interaction between axes and/or the work piece) the machine will comply. It is therefore common for Numerical Control (NC) programs to be generated using a computer application, allowing the toolpath to be previewed and checked.

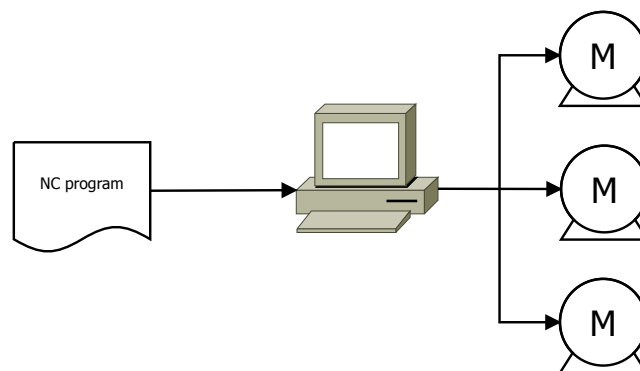


Figure 1.3: Simplified CNC system model schematic of 3-axis machine

While early CNC systems stored programs of punched paper tape, contemporary systems use the computer for program storage, allowing more complex programs between which the computer can rapidly switch. Modern systems also use a

dedicated controller to handle complicated axis arrangements while providing highly accurate control and the monitoring of safety systems. This dedicated computer allows, multiple systems to be controlled simultaneously from a single console computer. Figure 1.4 shows a schematic diagram of such a system with a single console controlling two three-axis systems. Such a system could be further scaled and the limiting factor tends to be the capability of the operator to monitor and control the system. This ability to control multiple dedicated CNC controllers will be shown to enable highly flexible operation by combining sub-systems as required.

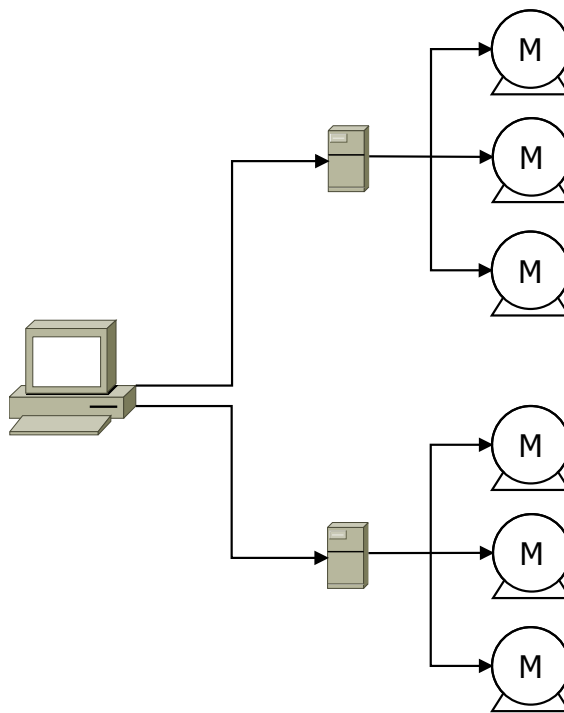


Figure 1.4: Modern CNC system with dedicated controller

NC files are often written in a language called G-code, which provides a sequence of simple instructions for the CNC controller to interpret and follow. Figure 1.5 shows an example G-code program automatically produced by the *Metrology Controller* application, written by the author and discussed in Chapter 4. The program begins

with a title (O1889 in this case), which enables the system to differentiate between many programs stored in memory. Modal instructions are then given, which may instruct the system to make absolute or relative moves, for example and remain in effect until changed. Axis moves are specified by an axis label (e.g. X) followed by a number, which, depending on mode, could specify the absolute or relative target. The machine controller reads and executes a single line before moving onto the next. Therefore, multiple axis commands placed on the same line are interpolated as per the modal commands. In this way, complex and co-ordinated movements can be built.

```
1      %  
2 -    O1889  
3 -    G90 G01 F250.000;  
4 -    W 71.902;  
5 -    V -11.327;  
6 -    U -420.000;  
7 -    B 0.000;  
8 -    A 0.000;  
9 -    Y 0.000;  
10 -   X 0.000;  
11 -   Z -7.131;  
12 -   M30  
13    %
```

Figure 1.5: Example G-code program

Although ISO6983 is a global definition of G-code functionality, this standard is not mandatory [28]. Typically, each manufacturer of CNC control systems implements the language differently to facilitate specific requirements. For the example given, the G and M codes used are provided in Table 1.1 and are correct for the Fanuc control systems used in all work presented. These differences in syntax result in a lack of code portability between systems.

Table 1.1: Command codes used in example program and compatible with Fanuc control units

Command	Definition
G90	Absolute move command
G01	Linear interpolation
F	Feed rate. Followed by desired value (mm/min)
M30	Program end

The application of CNC to the production of precision surfaces allowed a step change in production techniques. CNC of itself does not provide a great gain in surface quality achievable, as a skilled optical shop technician may produce similar surfaces by hand. However, CNC does offer versatility. The ability to control the process by changing the program allows the generation of any part within the capability of the machine. To realise the potential of CNC for optical manufacture, a machine is required which may support a wide range of part sizes and shapes, and uses similar tooling on many parts. The following sections presents two example systems, demonstrating how flexible state-of-the-art, high precision manufacturing systems have become. Fundamental to the developments presented in this thesis is that CNC based machines are able to operate automatically. Although CNC systems simply interpret instructions, it will be demonstrated that when combined with control software capable of automatically generating G-code programs, a more comprehensive control system may be developed.

1.2.3 Sub-aperture Polishing Techniques

Some of the limitations associated with the classical polishing of aspheres occur due to the aspheric misfit between the tooling and the part. Using a sub-aperture tool, to address an area smaller than the part, the polishing system can process a flat, sphere, asphere or free-form workpiece using generic tooling. This approach

presents the manufacturer with greater flexibility as well as the benefits of CNC. The example sub-aperture polishing systems presented here are QED's Magneto-Rheological Fluid (MRF) and the Zeeko Intelligent Robotic Polisher (IRP), although there are many more [29] [30].

1.2.3.1 Magneto-Rheological Fluid Polishing

MRF is distinct from most other optical processing in that the tool is rotated out of the plane of the work piece. Figure 1.6 shows a schematic depicting the MRF system tool assembly, taken from a patent filed by manufacturer QED [31]. The tool is made up of a vertically rotating wheel (12) on which a membrane is placed (14). A slurry made up of a colloidal suspension of magneto rheological particles (Carbonyl Iron) and abrasive (E.g. Cerium Oxide) is passed in between the workpiece and the wheel (22) [32] [33]. A magnetic field is applied to the gap, via an electro magnet (30), causing the slurry to stiffen. The interaction of the stiffened slurry between the workpiece and the membrane acts to produce a removal function on the workpiece. This removal function is adjusted through active control of the electromagnetic field, to achieve deterministic removal. Having been passed against the work piece, the slurry is collected (20) and re-circulated for continual use.

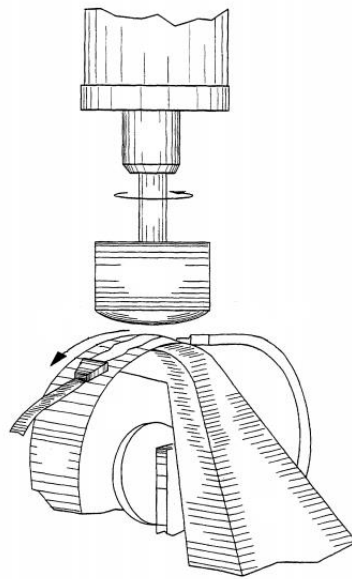


Figure 1.6: Schematic of the MRF process taken from [31]

The tool path is pre-computed from knowledge of the surface error with respect to the specification and the removal function is adjusted in real time to maximise process determinism.

The MRF process relies upon the accurate control of slurry flow during processing. In order to minimise the effect of gravity, the work piece is supported from above while the tool wheel is placed on the machine bed. While this has benefits for small parts, such as minimising slurry contamination of the part and support system, the work piece size is limited. Due to the aspect ratio of the E-ELT segments (1.4 m x 50 mm), part deformation is a concern and supporting the part from below allows the use of gravity as part of the system [34]. QED have developed larger machines such as the Q22-2000F which use a downward facing tool wheel to allow the processing of much larger parts. A system of this type would be capable of processing segments of the E-ELT. However polishing of short radius surfaces beyond 30°

slope, or materials which will interact with the magnetic field is not possible. As well as the usual factors to be considered when developing a polishing process, such as tool path, temperature, pH, slurry concentration, etc., the MRF operator must consider the concentration of Carbonyl Iron in the slurry [35]. This extra variable can serve to further complicate process development, however, there is evidence to suggest rapid processing of high quality surfaces is possible [36] [37] [38].

1.2.3.2 Zeeko Inflatable Membrane Polishing

The Zeeko process uses a spherical rubber membrane or bonnet, reinforced to ensure shape is retained when forced against the workpiece. A flat spot is produced against the surface, which is controlled in size by the displacement of the bonnet beyond the point of contact, the Z-offset. Offset adjusts the amount of force the bonnet exerts upon the work piece but this can also act to adjust the process footprint size shown in Figure 1.7 [39]. As the bonnet is rotated to produce removal, it must also be tilted, or precessed, to avoid the dead-spot at the centre of the axis of rotation, as shown in Figure 1.8.

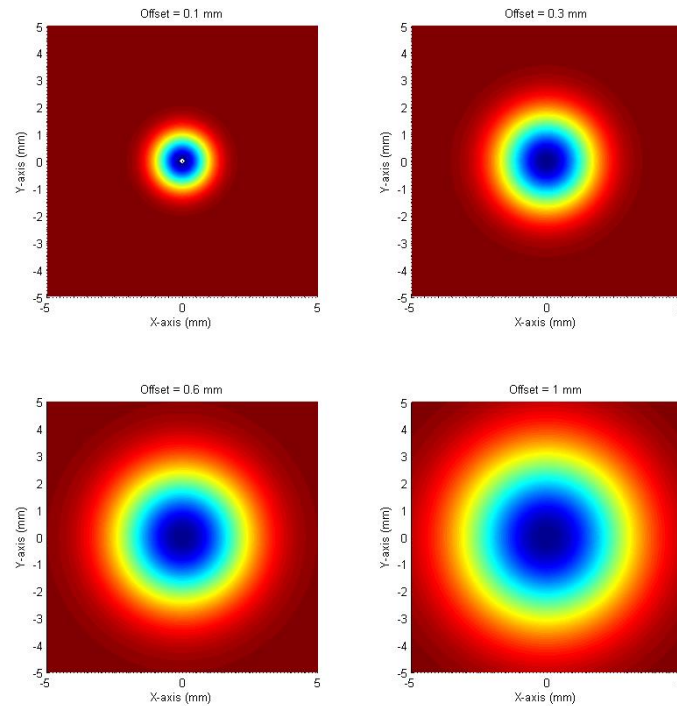


Figure 1.7: Variation of polishing spot size with Z-offset

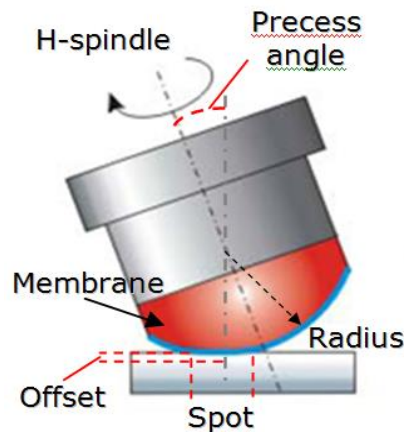


Figure 1.8: Zeeko semi-rigid inflatable bonnet tool

Slurry is fed into the interface between the bonnet and work piece, producing a Gaussian shaped removal function [40]. The bonnet is held at a constant precess angle relative to the surface normal, while being moved across the surface. With knowledge of the surface error, the feed rate may be modulated to cause the bonnet to move over high areas more slowly, reducing relative height. This process

is referred to as dwell time moderation, where the feed rate map is created from the error map and the tool influence function, characterised for the system operating conditions [41].

The process removal rate can be varied by adjusting slurry concentration, slurry material, pH, feed rate, tool rotation speed, bonnet material and pressure, and offset [42]. Many of these variables are interlinked, further complicating the process of full process characterisation. Even when a stable, convergent process has been developed, many parameters must be adjusted to apply it to another material.

Unlike the MRF polishing, the Zeeko machine can access any vector within a hemisphere and is able to process ferromagnetic materials. The Zeeko process can also make use of a wider range of tooling to achieve different removal rates and finishes [43]. However, in terms of the number of process variables, both are highly complicated and rely on accurate control of many parameters in order to produce reliable performance.

1.2.4 Conclusion

In this section, methods of pre-polishing and polishing surfaces have been reviewed as well as their limitations. The two sub-aperture systems discussed exemplify modern, complex polishing processes, which depend upon the control of multiple parameters to produce constant removal. In terms of the new work presented in this thesis, the integration of CNC into polishing machines is fundamental to the metrology systems developed, as will be discussed in Chapter 2. Although there has been a general progression towards deterministic processing, there remain many

variables which must be controlled in any polishing system. The polishing of glass is not fully deterministic and sub-aperture processing relies upon iterations, as controlling removal rate for material removal of comparable magnitude with the Z-offset remains difficult. Following each iteration the surface is measured to determine error relative to the desired shape.

There is a saying in the optical manufacturing industry;

'If you can't measure it, you can't make it!'

Measurement is used to provide feedback to the manufacturing process and ensure convergence. If this feedback is inaccurate, the subsequent tool path generated is unlikely to improve the surface condition beyond a certain point. In this situation, metrology will become the limiting factor of the final surface quality. The next section will provide background into the methods used to measure optical surfaces, and how these techniques led to the development of on-machine metrology.

1.3 Characterisation of Surfaces

Though there are many methods of characterising a surface at various spatial frequencies, such as profilometry, test plates and co-ordinate measuring machines (CMM), optical measurement performed using a phase-shifting interferometer will be concentrated on here. Measurement techniques which involve physical contact with the part are avoided as these pose greater risk of mechanical damage to the surface under test (SUT). Generally, two aspects of the surface property are of interest during metrology; form and texture. Although these are both essentially measurement of surface deviation from a reference, they provide information in

different spatial frequency ranges, require different measurement techniques and provide information about different aspects of optical performance [44]. Mid-spatial frequencies ($0.01 / \text{mm} - 1 / \text{mm}$) fall in the overlap region between form and texture.

One of the earliest optical methods of testing the shape of surfaces during process was the use of optical test plates. This involves placing the SUT in contact with a test plate known to be of better quality than the SUT target. A small air gap will remain between the two surfaces and if nominally monochromatic light, such as a Sodium or mercury lamp [45], is used to illuminate the two surfaces, Newton fringes become visible [46]. The presence of fringes depends upon the illumination source exhibiting sufficient coherence length to produce interference. Pressure exerted on the top surface will adjust the relative tilt of the surfaces and thus the fringe pattern. Each fringe represents half a wavelength of height variation and interpretation of the fringe pattern allows the skilled craftsperson to understand how the SUT deviates from the desired shape. Figure 1.9 shows a Sodium lamp test plate set up with a test flat placed on a wedged surface, with the slope running laterally across the image.

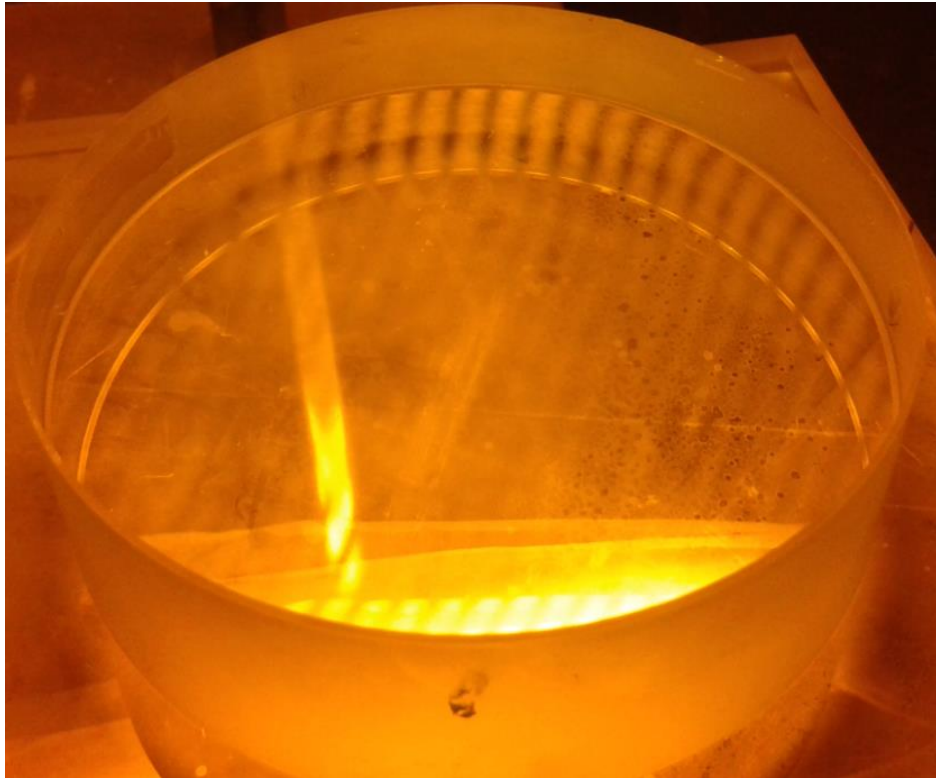


Figure 1.9: Optical plate testing using a sodium lamp

Though optical plate testing allows the metrologist to observe the surface error with reference to the test plate, the result can only be considered relative, as any error in the test plate cannot easily be separated from that of the reference without computerisation of the test. Test plate error must therefore be negligible compared with that of the SUT to enable convergence. Furthermore, this test is subjective, unless it is captured into a computer for analysis. This means there is little way of referencing the measurement back to the surface, nor of observing small features, too fine for the naked eye.

State-of-the-art digital data-acquisition interferometers, do not require contact between the reference surface and the SUT, and allow the capture of interferograms, typically using an area CCD, for computer analysis [47]. Although the recording of fringes provides great flexibility, such as allowing the quantification

of surface deviations and the opportunity of using CNC assisted polishing, these systems are sensitive to vibration [48] and air turbulence [49]. In the next section, current form measurement techniques are reviewed and their advantages and limitations discussed.

1.3.1 Form Characterisation

Form interferometry generally observes the variation of low slope, slow spatial frequency errors across a surface and provides information about the SUT departure from a reference radius of curvature. This is often applied as a full aperture technique, meaning that the whole surface is measured in a single field of view. Measured spatial frequency range is limited both by the instrument optical transfer function (OTF) and by the Nyquist limit of the CCD used to image the resulting interference pattern [50]. Both of these limitations vary depending upon the reference surface and SUT combination used. The Nyquist limit, and tolerable retrace error determine the maximum amount of asphericity which can be tested non-null with a spherical wavefront before a computer generated hologram (CGH) [51] or similar device must be employed. Retrace error results from mismatch between the test wavefront and SUT, preventing the retroreflection of light to the interferometer. This can cause poor image contrast and degrade measurement accuracy as the test and reference beams are no longer truly common path [52].

Figure 1.10 shows a schematic Fizeau interferometer configuration for testing a concave spherical optic. The Fizeau system is a widely used configuration because the reference and test beams are common path, meaning they encounter the same

surfaces and thus aberrations. This provides some cancelling of systematic errors, not possible with instruments such as the Twyman-Green [53].

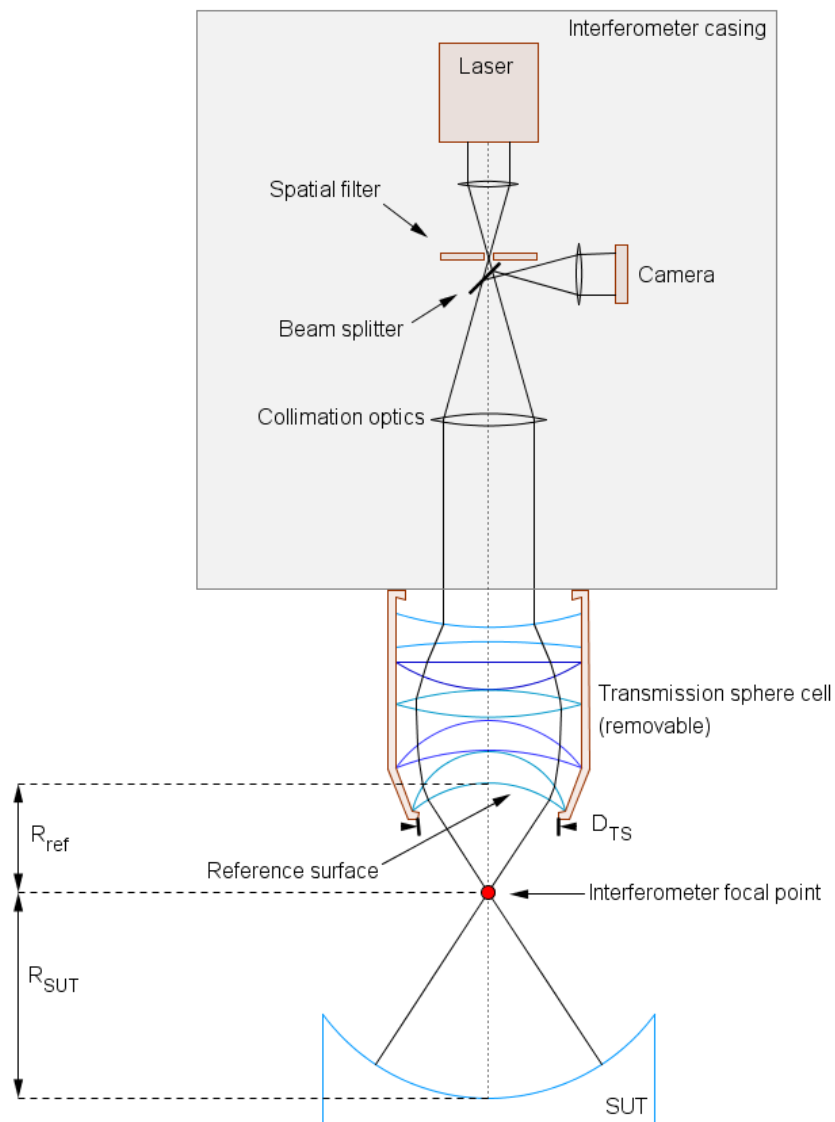


Figure 1.10: Fizeau interferometer schematic

The space between the transmission sphere and the SUT is referred to as the test cavity. The cavity length, D_c , is the sum of the radius of curvature of SUT and the reference optic and is given by (1.1) for spherical tests as shown in Figure 1.10.

$$D_c = R_{SUT} + R_{ref} \quad (1.1)$$

Where R_{SUT} is the SUT ROC and R_{ref} is the effective ROC of the transmission sphere. R_{ref} is given by (1.2).

$$R_{ref} = FD_{TS} \quad (1.2)$$

Where D_{TS} is the diameter of the transmission sphere and F is the F#. The transmission sphere is selected such that the test wavefront and SUT radii match at the surface, allowing the interferometer beam to strike the SUT normal and achieve retro-reflection with minimum retrace error when optimally aligned.

In practice plano measurement test cavity lengths are minimised to avoid, atmospheric turbulence in the test path and diffraction effects. Reduction of the spherical test cavity length to minimise environmental effects requires the addition of further optical elements. For the ESO E-ELT segment test system, further power has been introduced to the test path using a 1.5 m diameter concave spherical mirror, reducing the cavity size from 84 m to 10 m for both signal-to-noise and space reasons. However, additional components may introduce further sources of error into the test. Optimisation of the design allows much of the additional error to be calibrated out, however, some trade-off is made between environmental and system errors.

Recently, stitching interferometry has become commercially available. This technique parallels the move from full-aperture into sub-aperture processing, in that the SUT does not have to be examined as a single body. Instead of imaging the entire clear aperture of the SUT, the surface is split into a number of overlapping regions which are measured individually. Stitching interferometry allows the metrologist to select the optical testing configuration to minimise cavity length and

maximise spatial resolution. The resultant measurement data is then recombined, or stitched, using a computer algorithm, resulting in equivalent full-aperture data. The ability to increase spatial sampling frequency also allows increased system tolerance to tilt, increasing the scope to carry out non-null testing of aspheres [54]. In order to carry out stitching interferometry, good positional registration (ideally sub-pixel) of sub-apertures is required, so that the data may be accurately stitched [55]. Commercial units such as the QED SSI and AS, which can stitch highly aspheric surfaces using variable null optics, are available [56]. There are further examples of systems developed in academia [57] [58]. Zeeko have also applied a stitching algorithm developed in-house by C.W. King [59] to the development of the Metrology Station, presented in this thesis [60].

Currently, most metrology is carried out by first removing the SUT from the polishing machine and transporting it to a metrology laboratory. As the metrology environment is generally temperature controlled, a “soaking” period is required to allow the SUT to stabilise in this atmosphere. As the thermal conductivity of glass is relatively low, there can be a large thermal gradient across the material during soaking and internal stresses can cause the glass to deform [61]. Although most precision optical mirrors are manufactured using materials exhibiting a low coefficient of thermal expansion, measurement using averaged acquisitions can have a lower accuracy and repeatability during the acclimatisation period, than when fully acclimatised.

The SUT is supported such that no stresses are induced and aligned with the interferometer for measurement. Alignment is generally carried out manually,

either by physically adjusting screws or commanding an actuated system to tilt either the SUT or interferometer itself. In order to minimise error resulting from effects such as air turbulence, electrical noise and vibration during measurement, a number of acquisitions are typically averaged. The level of averaging is chosen such that repeatability error is negligible compared with the measured SUT error. It is also possible to remove some systematic error associated with the interferometer by subtracting a calibration from the measurement dataset. Though residual tilt may be removed from the measurement using fitting algorithms, best results are obtained through optimal alignment, as system retrace error is minimised. Discretion must be used when removing terms from measurement data as the metrologist must ensure any component removed is the result test error and not present on the SUT. Removal of such aberrations from data can limit the convergence of subsequent corrective polishing and so limit convergence. Although applications may be written to obtain data, it is considerations such as those mentioned which currently prevent the automatic analysis of measurement data beyond well-defined situations.

Form interferometry data is used as feedback for the corrective polishing process, when using CNC sub-aperture polishing. Measurement data is used to vary dwell time such that areas on the surface which are high relative to the desired ROC are preferentially polished to remove more material. Over a series of corrections, assuming proper polishing parameter selection, the surface is observed to converge to the desired form. However, even an optic of correct form may exhibit poor optical performance due to excessive scattering of light. Scattering is caused by

poor surface texture, which must also be controlled. The latter stages of polishing typically use a low removal tool to optimise surface texture. Measurement of texture is not used for corrective polishing, but to judge when sufficient smoothing has been applied. The following section outlines the techniques used for texture measurement and their limitations.

1.3.2 Texture Characterisation

Texture or micro-roughness characterisation allows analysis of SUT errors at spatial frequencies beyond the range of the form interferometer ($> 1/\text{mm}$) which influence surface scattering properties [62]. Systems such as grazing incidence x-ray optics are particularly sensitive to texture [63] [64], and various measurement techniques are employed to enable proper quantification, such as atomic force microscopy (AFM), profilometry, and interferometry [65].

It is generally the case that surface texture requirements form part of the optic specification and so the manufacturer must be able to adequately characterise the SUT. For example the prototype E-ELT specification [10] stipulates average texture must be $< 2 \text{ nm}$ arithmetic average (Ra). As with form interferometry, the SUT is commonly removed from the processing area and placed in the metrology lab. Most laboratory based instruments have the configuration of a bench top microscope, requiring that the SUT be placed underneath the objective for measurement [66], such as the ADE Phaseshift white light interferometer used at OpTIC Glyndwr, shown in Figure 1.11. This bench top configuration becomes impractical for surfaces greater than $\sim 400 \text{ mm}$ in diameter as the part can no longer be accommodated on the sample stage. In contrast with form interferometry,

texture measurement is generally carried out by taking a small, discrete measurements of the surface. Sufficient samples must be taken to ensure results are statistically representative but sample numbers are in practice limited. Though full-aperture techniques such as the Lyot test have been proven, they are generally not employed due to the amount of light required for sufficient image contrast, and can exhibit orientation dependent detection of errors [67].



Figure 1.11: ADE Phaseshift MicroXAM white light interferometry

In-situ texture measurement allows the SUT to remain in the manufacturing environment, avoiding the logistical problems associated with large optics. These systems are deployed onto the SUT, where they sit in contact with the surface [68] [69]. Depending upon the length of acquisition, some level of temperature control

may be required to prevent thermal drift during measurement acquisition. Though the application of such instruments negates the requirement to move the optic, accessing the central portion of large components is difficult as the operator has to lean over the surface to place the instrument.

There are some reports of manufacturers employing surface replication for texture measurement [70]. This uses a material which is pressed into the SUT, and assumes the inverse surface texture. The material is then set or cures into a rigid state, retaining the negative surface impression. This replication is removed and tested as normal. Although this technique is labour intensive, it does alleviate many of the logistic issues of performing texture measurement on large surfaces. However, the available literature relates to the use of surface replication for SUTs with a texture of around 100 nm to $> 1 \mu\text{m Ra}$. There is little material which discusses the accuracy of such techniques for reproduction of texture at the nanometre level. Some experimental data of a replicated smooth sample is presented in Chapter 5 for comparison with the systems discussed in this thesis.

1.4 Limitations of Existing Measurement Techniques

The existing measurement techniques discussed are acceptable in small volume production of prototypes and where the SUT is easily handled. However, most commonly involve the removal of the SUT from the manufacturing system and transport to the measurement environment. Together with temperature soaking, this can account for a large portion of the overall manufacturing time, depending on part mass and dimensions, and introduce risk of damage due to handling. It has been estimated by Walker and Bingham that around 6% of large optics produced

between 1960 and 1995 were damaged [71] [72]. For example, during manufacture of the Birr Telescope primary at UCL, 91% of manufacturing time was spent either measuring or in set up activities associated with switching between polishing and measurement [73].

Furthermore, both state-of-the-art form and texture measurement lack the flexibility to accommodate the range of optics required by diverse projects such as the ESO E-ELT, laser fusion, for x-ray mandrels, steep aspherical components of next generation photography optics as well as medical implants and moulds for consumer electronics casings. Although these examples require an array of different polishing techniques, all can be accommodated by a member the IRP machine family. There is no such case for measurement.

Lab based metrology requires transport of large optics which is potentially risky. Modern on-machine interferometry generally relies on the use of a testing tower, which limits the range of SUTs which can be accommodated with a given range of Z-axis motion and transmission spheres available. It is often the case that the testing tower specification is produced around a single large project. This approach can lead to the test system requiring a refit before another project may be accommodated and so a lack of flexibility. Other available form measurement techniques such as profilometry and CMMs pose many of the same limitations and provide a sparser dataset, unsuitable for certification against a specification for high precision optics.

The greatest limitation of current texture measurement solutions is the inability to accommodate large and/or heavy components. Again the SUT must be relocated

from the manufacturing environment. The limited Field of View (FOV) of white light interferometers also causes practical difficulty measuring of the same region following subsequent treatments, for example edge effects or scratches. Existing on-machine texture measurement requires that a stand be placed in contact with the SUT, which does little to mitigate the damage risks associated with transport to lab based devices. Surface replication techniques offer reduced accuracy on smooth surfaces, when compared with interferometric techniques and require manual work in close proximity to the SUT.

In order to address the identified limitations associated with state-of-the-art metrology, particularly of large surfaces, this thesis presents the development of on-machine metrology systems combining modern, vibration insensitive interferometers with a new control system. It will be demonstrated that these systems can support a range of measurement devices and machine hardware configurations to enable automatic on-machine metrology, which offers enhanced versatility compared with state-of-the-art systems.

1.5 Work Presented

The contribution of the author presented in this thesis is a software application, referred to as the *Metrology Control Suite*. This application is made up of two sub-modules; *Metrology Designer* and *Metrology Controller*. The development of this application is presented using two case studies, concerned with on-machine form and texture measurement.

Chapter 2 presents discussion of the elements which make up the on-machine metrology systems presented and their suitability for this application. Suitable

devices are outlined and a feasibility study conducted to establish the viability of on-machine metrology. Following this discussion, the requirements for the *Metrology Control Suite* are outlined.

The functionality of the *Metrology Designer* application is described in Chapter 3, with examples of how the developed software is used with both case study instruments. The measurement plans developed with *Metrology Designer* are then executed with *Metrology Controller*, which is discussed in Chapter 4.

Metrology Controller allows the metrology instrument to be automatically positioned at each measurement location and aligned by interfacing with the CNC controller. This is a novel step in terms of on-machine texture metrology. Chapter 4 discusses the two modes of on-machine metrology operation: open-loop and closed-loop. Open-loop being the initial positioning of the measurement device at a location specified in the measurement plan. Closed-loop operation allows the correction of residual misalignment between the device and surface under test by using feedback from the interferometer compute correction moves.

Chapter 5 presents discussion of measurement results obtained using the systems developed, and makes assessment of the planning and control functionality of *Metrology Controller*. The work presented is then summarised in Chapter 6 and conclusions drawn about the impact of automatic on-machine metrology. Finally, an overview is presented of the work required in order to fully realise the potential of automatic on-machine metrology.

2 On-Machine Metrology

Having observed the practical limitations of state-of-the-art metrology, it is clear that significant benefit would result from applying metrology in the manufacturing environment. Given that most corrective polishing at the OpTIC facility is carried out using the three Zeeko IRP machines, the greatest gain would result from integrating metrology with one of these platforms. The machine itself is then used as a positioning system, minimising additional hardware requirements and allowing automation of the measurement process.

This chapter will outline the features of the IRP machine as well as the limitations and advantages of using a system specifically designed for polishing as part of a metrology system. The various options of integrating metrology onto the machine will be discussed, along with those selected for development. Finally, the requirements of the software application used to facilitate automatic system operation will be outlined.

2.1 Zeeko IRP machine

The IRP machine has been developed to allow deterministic polishing of ultra-precision surfaces using an iterative process of metrology and corrective polishing. Incorporating metrology more directly into this manufacturing process therefore seems a logical step, given the time lost and risk imposed during part transport, soaking and clocking prior to measurement, particularly for large parts. The existing IRP machines range in size from those capable of processing 50 mm parts up to the 1.6 m system installed at the OpTIC facility. Owing to the size constraints of smaller

machines, the work presented here has been applied only to machines with capacities larger than 1 m. This allows early development work to proceed without considering the physical limitations of the polishing enclosure, which could pose a crash risk to the metrology device. Though the name, 'Intelligent Robotic Polisher' implies the machine has intelligence, it is a standard CNC machine and follows instructions provided by the operator, either manually or via a program.

Figure 2.1 shows the UCL IRP1200 machine at OpTIC Glyndwr. This machine accommodates up to a 1.2 m component. In this case, the machine includes an opening roof system, allowing an interferometer positioned on the test tower above to view the part secured to the machine table. This is the first example of on-machine interferometry developed by Zeeko, and requires the operator to climb the test tower and manually align the interferometer using screws on the 5-axis stage, visible at the top of the image. This system is currently configured to allow full-aperture measurement of 3 m ROC concave parts of approximately 300 mm diameter, which are used for E-ELT process development work.



Figure 2.1: IRP1200 machine with interferometer test tower at OptIC, North Wales

The IRP machine is typically made up of linear X, Y and Z-axes as well as a rotary C-axis table. The C-axis is used to mount the optical component during polishing and is capable of continual rotation. The machine also has A and B-axes which effectively simulate an azimuth and elevation system respectively, as shown in Figure 2.2. However, the B-axis operates in a 45° plane to the Z-axis. This arrangement is designed to rotate the tool spindle (H-axis) about a point 10 mm from the front face of the spindle, known as the Virtual Pivot (VP). This allows a change in pointing vector of the polishing tool, while ensuring contact is maintained with the surface being processed. The A and B-axis arrangement allows the machine to access any surface-normal within a hemisphere and, combined with X, Y, and Z translation, is able to process at these vectors anywhere within the

machine limits. When carrying out on-machine metrology using the IRP machine, the system configuration falls broadly into two categories, outlined in Section 2.2 and Section 2.3. The following sections outline the operation of the machine for polishing, as many of the set up tasks are analogous to those required for automatic on-machine metrology.

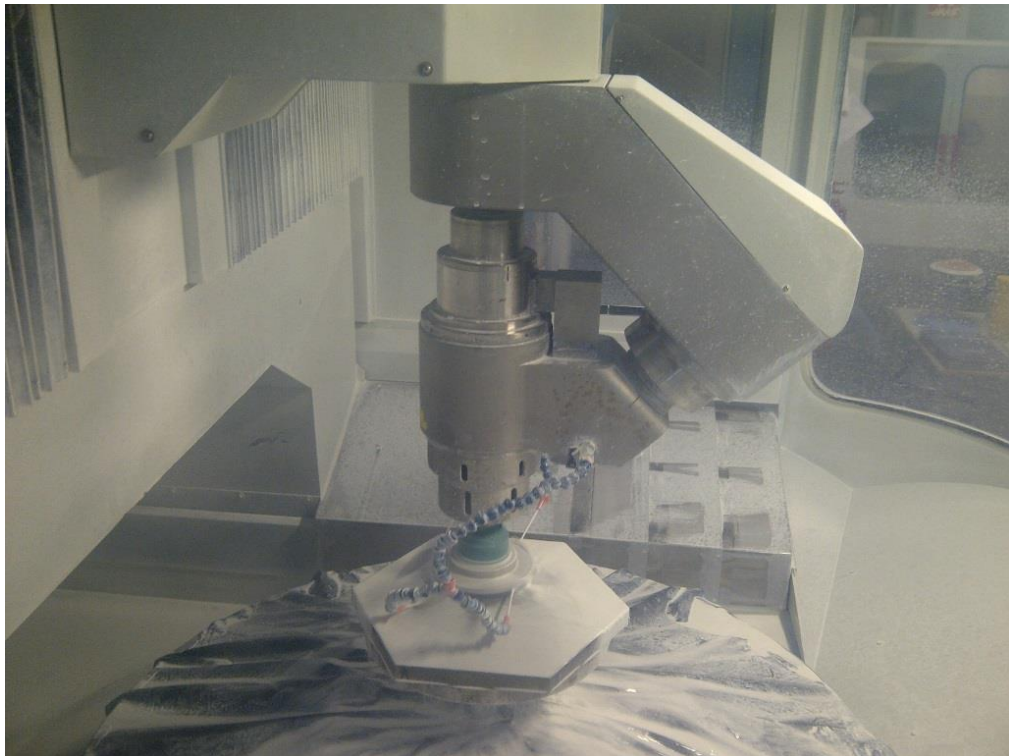


Figure 2.2: A and B axis arrangement of the type-2 virtual pivot of the IRP1200

2.1.1 Polishing Operation

During automatic polishing operation, the IRP machine follows a set of instructions provided via a G-code program loaded into the control system. Programs are loaded via the operator console, shown in Figure 2.3, which also allows manual control and monitoring of machine position and status. The console machine communicates with the CNC controller via a High-Speed Serial Bus (HSSB) which

consists of an optical fibre connection. This CNC configuration is similar to that shown in Figure 1.4, but using a single dedicated controller.



Figure 2.3: IRP1600 operator console PC

Prior to execution of the polishing NC program, the operator must perform a series of set up tasks to ensure the process is accurately applied to the surface. These activities are summarised in the following sections.

2.1.1.1 Supporting the Part

When preparing for a polishing run, the part is mounted to the machine table via a suitable support system. The support system is designed to prevent the movement or deformation of the part under gravity or the loads of polishing. A significant deformation with respect to the Z-offset, would result in variation of polishing spot

size which would affect process convergence. For on-machine metrology, the part must be supported, while allowing it to be aligned with the measurement device. The support must remain dimensionally stable in the presence of expected environmental thermal drift, so as not to introduce distortion of the part through induced stress. Such distortions may invalidate the resulting data. The part support requirements for metrology are therefore more stringent, as the part must remain stable at the interferometric level for the duration of measurement.

The complexity of a component support varies with the diameter and weight of the optic. A small part (<200 mm diameter), for example, may be waxed onto a metal plate, whereas the E-ELT prototype segments sit on a 3-point hard stand for polishing, minimising deformation under load, and are raised up on a 27-point hydrostatic support for metrology. Both of these supports are arranged into one structure, with the 27-point support emulating those of the E-ELT primary mirror. The configuration of the E-ELT segment support for metrology minimises the risk of error between test and operational optical performance when the telescope is pointing at zenith. Despite the variation in requirements between polishing and metrology, the E-ELT segment support is an example that both activities may be accommodated by a single support system, even for large components.

2.1.1.2 Part Alignment

Alignment should set the part co-ordinate frame to a known relationship with that of the machine. Part alignment is particularly important for corrective processes using a small polishing spot size, as the process footprint can miss the targeted

error, if not properly oriented and centred [74]. This is critical when polishing edges of components such as E-ELT segments.

To ensure the specified spot size is used, the origin of the machine and part co-ordinate frames must coincide. To simplify the setup of this arrangement, the IRP machine H-axis has a load cell incorporated, which allows the system to detect force as the bonnet contacts the surface. A G-code program instructs the machine to move the H-axis towards the surface, until just in contact. This program is executed when the bonnet is close but not in contact with the part and, with the surface found, the machine co-ordinate frame is offset to define the origin. Setting the co-ordinate frame origin is common to all CNC machines, as the system has no prior knowledge of where the workpiece is located in space. It will be shown in Chapter 4 that the same process is required for the correct operation of on-machine metrology.

2.1.1.3 Non-Linear Correction

No matter how well designed the support system, and how well mounted the part, some residual slope due to mounting error of the part with respect to the machine coordinate frame, or wedge in the glass, will remain. Correction is possible by building tilt adjustment into the part support structure or by shimming the part. However, both methods can reduce the stability of the supporting system and, in the case of tilt adjustment, add significant weight and complexity.

The approach typically employed by Zeeko is to measure the tilt (and other non-linear terms) using a process called non-linear probing. In this process, the bonnet is used to probe the surface in a specified grid, while a record is made of co-ordinates

at which the surface is found. This file is then used to fit a tilt plane (or other terms) and correct the Z-coordinates of the polishing tool path for the measured error. This process can be repeated in between each run to ensure any shift of the part or support system during processing is accounted for. It will also be shown in Section 4.3.2.2 that non-linear correction may be applied to improve on-machine metrology positional accuracy in a similar manner.

2.1.1.4 Polishing

With the pre-polish set up activities completed, a G-code program containing the corrected toolpath is loaded into the CNC controller and executed. Once polishing is underway and the process is stable, supervision is not required until the polishing cycle is complete.

Polishing is the application for which IRP machine was designed, and there is a strong economic argument that the optical manufacturer should organise workflow to maximise the percentage of time spent polishing. All other activity such as aligning, metrology, mounting and un-mounting is an overhead and should be minimised. This work presented in this thesis takes a step in the direction of minimising these overheads, while maximising the accuracy of the polishing process though improved quality of metrology.

2.1.2 Conclusion

This section has outlined the configuration and operation of the Zeeko IRP machine, which will go on to form a core part of the on-machine metrology system presented in this thesis. Some of the routine activities required in order to prepare for polishing have also been briefly described. Even when using a small part on a simple

support system, the processes of mounting, aligning and carrying out non-linear correction can occupy 1-2 hours and is a potential source of error in the surface quality finally produced. These processes must be carried out each time a part is removed from the machine, such as for off-machine measurement. Though effort has been made to automate as many of these tasks as possible, they are still relatively labour intensive and become increasingly difficult as the part-size scales up and handling becomes difficult and risky.

The logical approach is to move the part as little as possible. Instead of taking the part to the metrology laboratory, metrology should be carried out at the machine. However, in order to operate efficiently, the IRP machine should spend as much time as possible processing the surface rather than measuring. Therefore, any metrology carried out at the machine should be completed in less than the time otherwise lost in the usual cycle of part movement and repeating pre-polish procedures, and result in no greater surface measurement error. In order to minimise duration of metrology, and yet maintain quality, it is likely that some degree of automation will be required.

As discussed, the IRP machine may be used to perform automatic on-machine metrology. However, one must first consider how to mount the metrology instrument. The next sections will review the options of supporting the metrology device and provide examples of instruments which may be used.

2.2 H-axis Mounted Metrology

As mentioned, polishing is carried out by fitting a tool to the precision Schunk chuck situated at the front of the H-axis spindle. In order to use the machine to position a

metrology device fitted to this chuck, the polishing tool must be removed. The device is then mounted so that, ideally, the optical axis is parallel to the machine H-axis. Any misalignment between the H-axis and device optical axis would need to be removed by adding angular offset to the machine co-ordinate frame. It will also be seen in Section 2.2.3 that misalignment perpendicular to the B-axis arm can cause problems when attempting to align the measurement device.

With the measurement device mounted to the spindle, the A and B-axes may be used for tilt alignment correction. However, as these axes are non-orthogonal, a compound move is required to effect correction. Furthermore, as the centre of rotation is about the machine VP, not necessarily the device focal point, a translation may also be required in order to maintain FOV at a constant position on the SUT, depending upon the measurement device optical configuration.

2.2.1 On-Machine Stitching Interferometer

Following the development of a commercial sub-aperture stitching software package, which allows multiple small-area measurements of a single surface to be joined in data to create a full-aperture map, Zeeko sought to develop a measurement device which could be installed on the IRP machine. The On-Machine Stitching Interferometer (OMSI) is designed to mount to the side of the machine VP, shown in Figure 2.4. The bonnet tool and slurry guard at the front of the H-axis remain in place for clarity. It is expected that, during measurement, these would be removed to minimise the risk of contamination of the interferometer by polishing slurry.

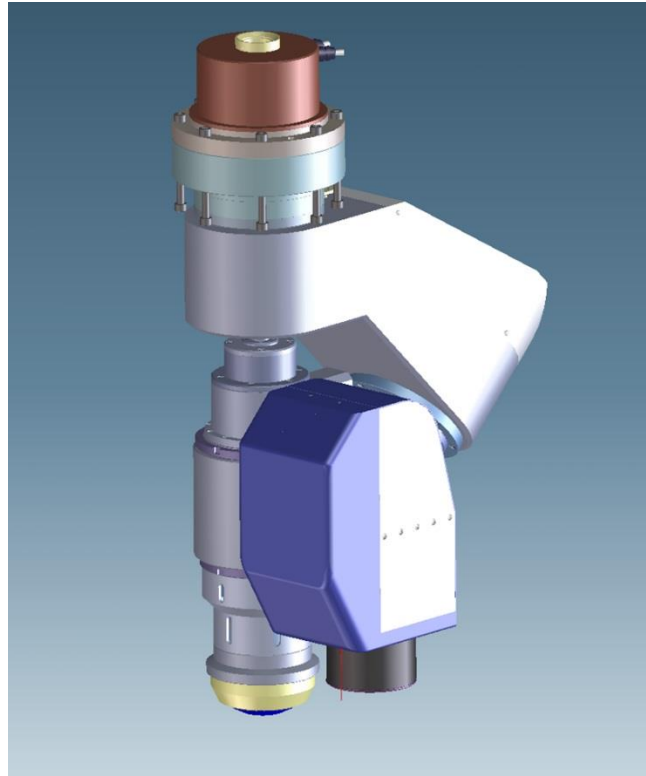


Figure 2.4: Zeeko OMSI CAD model fitted to a type-2 VP spindle (courtesy of Zeeko)

The OMSI design incorporates a compact PC6000 interferometer, supplied by 4D Technology, along with an in-house reflex beam expander to allow a compact form-factor. The system chassis is designed to maintain internal optical alignment under a frequently changing gravity vector during tilt alignment. A SIOS SP2000 distance measuring interferometer was included in the design to allow accurate measurement of variations in distance between the OMSI and the SUT. Due to the semi-rigid mechanics of the IRP machine, it is possible that A and B-axis sag could alter the cavity length sufficiently to affect the stitching result. Knowledge of these variations would be used to adjust the stitching parameters and ensure erroneous form did not propagate into the resultant synthetic dataset.

However, during testing of an early prototype, the chassis of the OMSI proved insufficiently rigid to maintain internal alignment under a sufficient range of B-axis

motion for practical operation. Therefore, internal realignment was frequently required. Following a project review in April 2012, Zeeko decided that the concept of mounting the measurement module onto the machine VP was too ambitious and should be reconsidered.

2.2.2 Surface Texture Analyser

Another example of an H-axis mounted metrology device is the Surface Texture Analyser (STA), which was developed by Zeeko in partnership with 4D Technology. 4D Technology supplies the device as the NanoCam, which sits on a tripod placed on the SUT, as shown in Figure 2.5 [75]. The STA features a Schunk chuck compatible spigot, replacing the original carry handle. The STA, therefore, does not require placement upon the SUT during testing, as with the NanoCam.



Figure 2.5: 4D Technology NanoCam with tripod tilt alignment assembly (courtesy of 4D Technology)

Figure 2.6 shows the STA in use on the IRP1600 machine during testing of the SPNO4 ESO E-ELT segment [76]. H-axis mounting of the STA is preferred to the tripod of the NanoCam as, the metrologist does not have to reach over the segment

to place the device, removing a potential risk of damage. Adjustments to the device are made prior to using the IRP machine axes to position the device over the SUT.

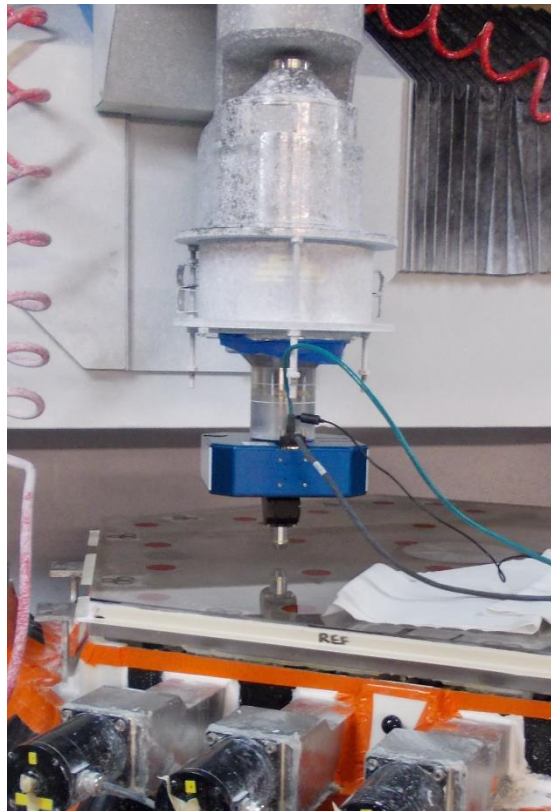


Figure 2.6: STA mounted on the IRP1600 machine and while testing a prototype ESO E-ELT segment at OpTIC Glyndwr, North Wales

Although mounting the metrology instrument as a replacement for the bonnet is convenient, devices in this configuration suffer a systematic limitation of the A and B-axis configuration. This is known as the [0,0,1] condition, referring to direction cosines, and is described in the following section.

2.2.3 The [0,0,1] Condition

The [0,0,1] condition is observed when the IRP machine VP attempts to align with a surface where the local surface normal vector is parallel, or near-parallel to, the Z-axis. Polishing, and H-axis mounted on-machine metrology, are affected differently.

Although both conditions are referred to as the [0,0,1] condition, they are two distinct phenomena.

2.2.3.1 The [0,0,1] Condition During Polishing

As discussed, the IRP machine affects the media to be polished by rotating a tilted, or precessed, bonnet against the surface in the presence of slurry. The machine is instructed to move the bonnet along a prescribed toolpath, while varying the A and B-axis angles to maintain the precess angle relative to the local surface normal vector. However, in the example where the tool is passed over the centre of a spherical surface and must pass through the [0,0,1] surface normal vector, the A-axis must rapidly rotate by 180° in order to maintain the relationship between the tool and part, while maintaining feedrate. In practice this cannot be achieved, and so a variation in removal rate is observed. This is analogous to the zenith blind spot for an alt-azimuth telescope.

This issue may be overcome through adjustment of the code which produces the machine toolpath to avoid situations where very high angular velocity rotations are required. In this case the [0,0,1] condition is due to machine dynamic performance limitations, which can be allowed for. However, during metrology, a static condition occurs which has a greater impact upon metrology.

2.2.3.2 The [0,0,1] Condition During Metrology

The [0,0,1] condition also arises when testing a position with a local surface normal vector parallel to the machine Z-axis with an H-axis mounted device. To address such an orientation, the B-axis value is zero and variation of the A-axis serves only to rotate the instrument about the Z-axis. In this case a residual tilt error is

observed via interferometric fringes perpendicular to the B-axis, which remain constant for any A-axis orientation. Therefore, proper alignment of instrument and SUT cannot be achieved. This error is caused by a systematic error in the alignment of the B-axis relative to the A-axis, resulting in the B-axis not sitting exactly in the 45° plane, as designed. This manifestation of the [0,0,1] condition has made measurement of plano surfaces on the IRP machine difficult. Therefore, other methods of mitigating the effects of the situation have been used such as tilting the SUT such that the B-axis is not equal to zero at any testing location.

In order to analyse the effect of the [0,0,1] condition, an observation was made of the area of an E-ELT segment which would be affected. The STA was used to measure the ESO E-ELT master spherical segment (MSS), which is a hexagonally shaped 84 m ROC spherical part, with a 1.4 m cross-corner diameter. A series of points were measured in a line arranged from centre to corner, as shown in Figure 2.7. The blue lines indicate the part boundary and the red points the STA testing locations.

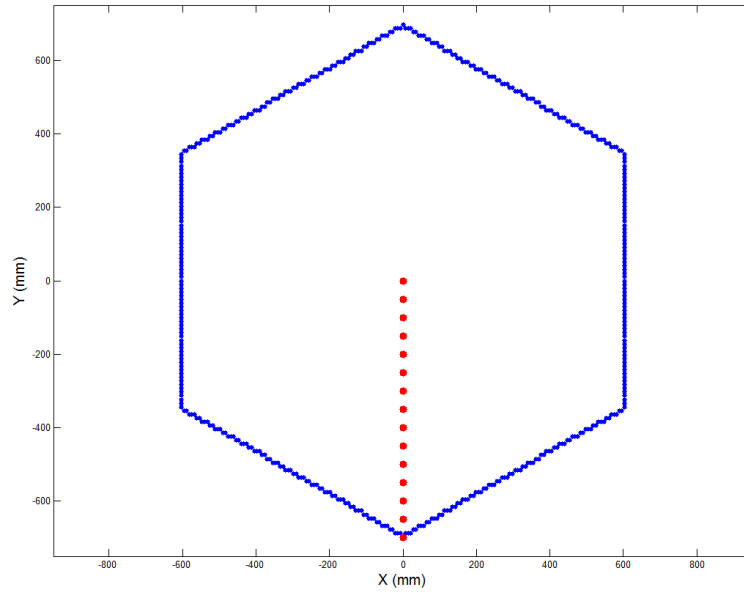


Figure 2.7: Measurement plan used during characterisation of the [0,0,1] condition

During testing it was found that locations greater than 600 mm from the centre could be measured without encountering the [0,0,1] condition. The SUT local normal vector at this test location corresponds to a limit of $> \sim 0.5^\circ$ from the axis about which the A-axis rotates, before becoming amenable to measurement. In the example of testing the E-ELT MSS, this would leave around 85% area of the SUT inaccessible, without modifying the system. Figure 2.8 shows an example testing plan which demonstrates the limitations of avoiding the region in which the [0,0,1] condition impacts performance. These plans were created with an early version of the *Metrology Control Suite*, presented in Chapter 3 and Chapter 4.

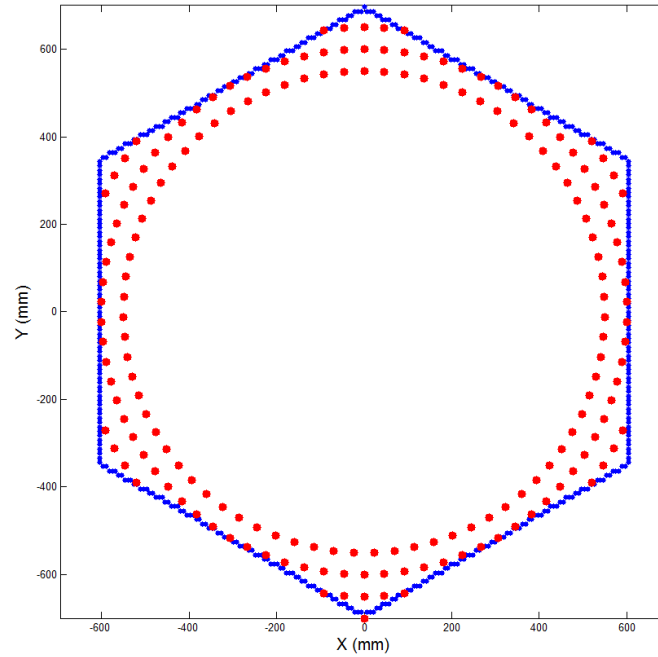


Figure 2.8: Resultant MSS testing plan designed to avoid region affected by the [0,0,1] condition

An inability to characterise such a large area of the SUT is unacceptable. In order to measure in the presence of the [0,0,1] condition, the metrologist must tolerate increased retrace error associated with having multiple fringes of tilt in the FOV. This systematic limitation exemplifies the restrictions which must be overcome in order to perform precision metrology on a machine primarily designed for manufacturing. A solution to the stated problem, allowing the STA device to test in the presence of the [0,0,1] condition, is discussed in Chapter 4.

2.2.4 Conclusion

This section has reviewed the potential solution of mounting the metrology device onto the IRP machine H-axis, either as a bonnet replacement or via a side-clamp arrangement. The potential problems caused by the machine [0,0,1] condition have been discussed, which affect instruments in either configuration.

During measurement, the device will also be repeatedly rotated and repositioned potentially to any vector within a hemisphere. The gravity vector of the device will therefore be repeatedly changed, which could cause internal optical alignment to become compromised, as with the OMSI. Devices operating in this arrangement may be subject to reduced service intervals or suffer internal failure.

2.3 5-axis Stage and Testing Tower

Many interferometric testing configurations designed to measure the SUT in a full-aperture regime on long ROC parts require the interferometer to be positioned at a large distance from the part. This may prohibit mounting the device on the H-axis and so the instrument is commonly located on a testing tower, placed over the IRP machine.

As the instrument is no longer mounted to the IRP machine, the A and B axis combination cannot be used to effect alignment correction, and so a supplementary tilt and translation system is used. The 5-axis stage usually includes orthogonal X, Y and Z-axes for translation and A and B-axes for tilt correction [77]. The key kinematic difference between 5-axis stage measurement and IRP machine spindle mounting is that the A and B-axes of the 5-axis stage are orthogonal tilt axes. Therefore, when making an alignment correction, a single tilt move may be made, as the resultant translation is typically sub-pixel and so negligible. Figure 2.1 shows an example of the arrangement described. Further examples of such measurement systems are discussed in the following sections.

2.3.1 OpTIC Glyndwr Testing Tower

The ESO E-ELT project consortium has constructed a 10 m tall testing tower to allow full-aperture testing of E-ELT segments. As mentioned in Section 1.3.1, a Fizeau test requires that the cavity length be greater than the SUT ROC. In this case the interferometer would be at least 84 m from the SUT, resulting in an impractically long cavity. Therefore, the consortium opted to reduce the path length by placing a concave element at the top of the testing tower. The test tower is shown in Figure 2.9, with the top sphere located out of the top of the image.

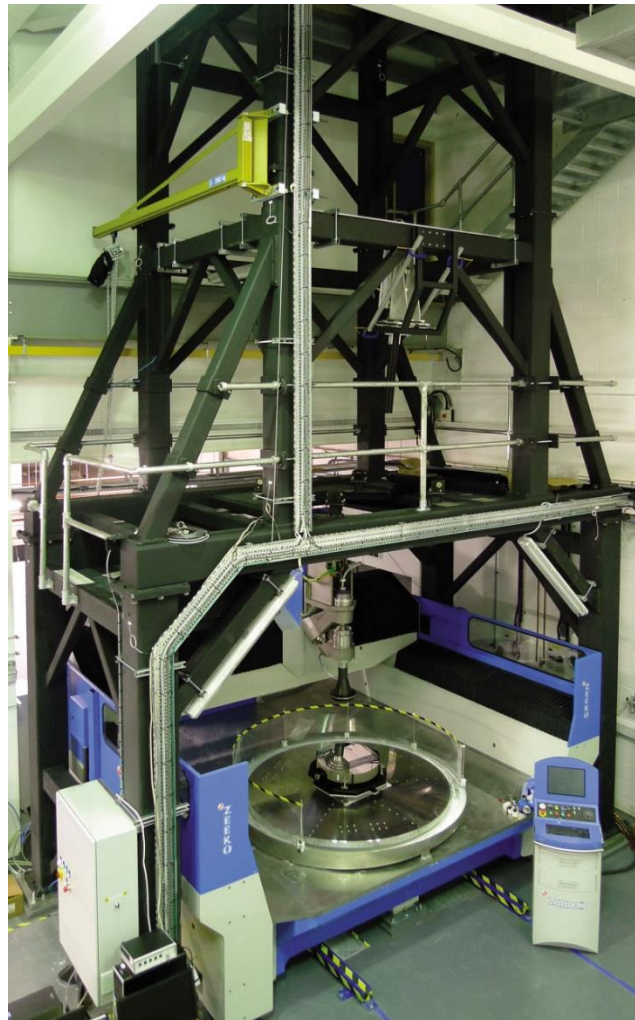


Figure 2.9: Lower path of the OpTIC Glyndwr optical testing tower used for ESO E-ELT segment full-aperture measurement (Top sphere assembly not shown)

An IRP1600 machine located beneath the testing tower is used for polishing and positioning the SUT for measurement. Figure 2.10 shows the segment mounted on the 27-point support, with the support covered by black polythene to prevent slurry ingress during processing. The support contact points with the rear of the segment are visible as red circular patches. The support system and SUT weigh ~250 kg therefore moving these components repeatedly is undesirable. The part support system has three vertical tilt actuators, spaced at 120° intervals around the support periphery to allow adjustment of tilt alignment and piston.

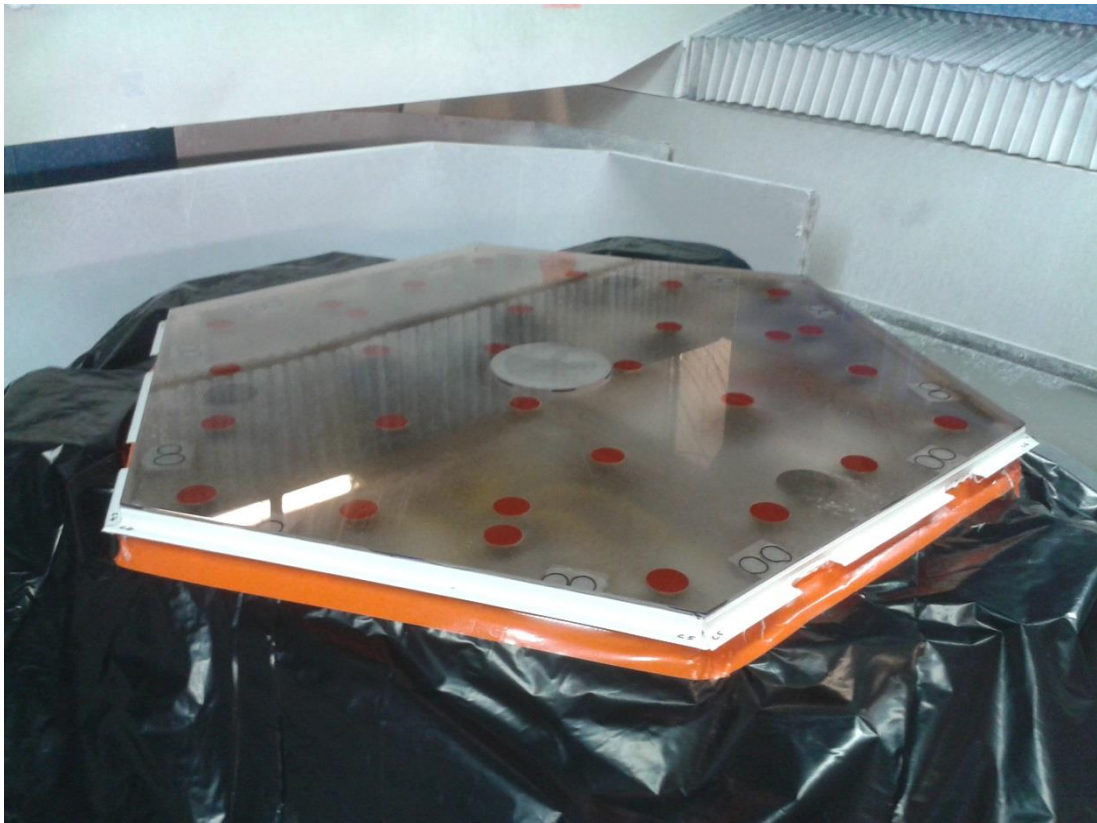


Figure 2.10: Prototype ESO E-ELT segment mounted on 27-point support

Due to the complex optical chain of the testing system, as well as air currents in the large testing volume, achieving adequate signal-to-noise performance is difficult and measurement dominates the operational time. Automation of such a system

would reduce the duration of the measurements by being able to perform measurement continually, with automatic alignment.

2.3.2 Zeeko Metrology Station

The Metrology Station system was manufactured by Zeeko in 2012 as a platform for stitching interferometry and is also capable of some full-aperture measurement. Figure 2.11 shows the Metrology Station system installed at a customer laboratory. This system has the same base as an IRP600 machine, with an axis configuration which includes a tilting table system. The system uses a 4D Fizeau 3000 interferometer, which is housed in the cabinet fitted to the test tower. The interferometer is installed in a 5-axis stage (X,Y,Z,A,B) to allow tilt correction.

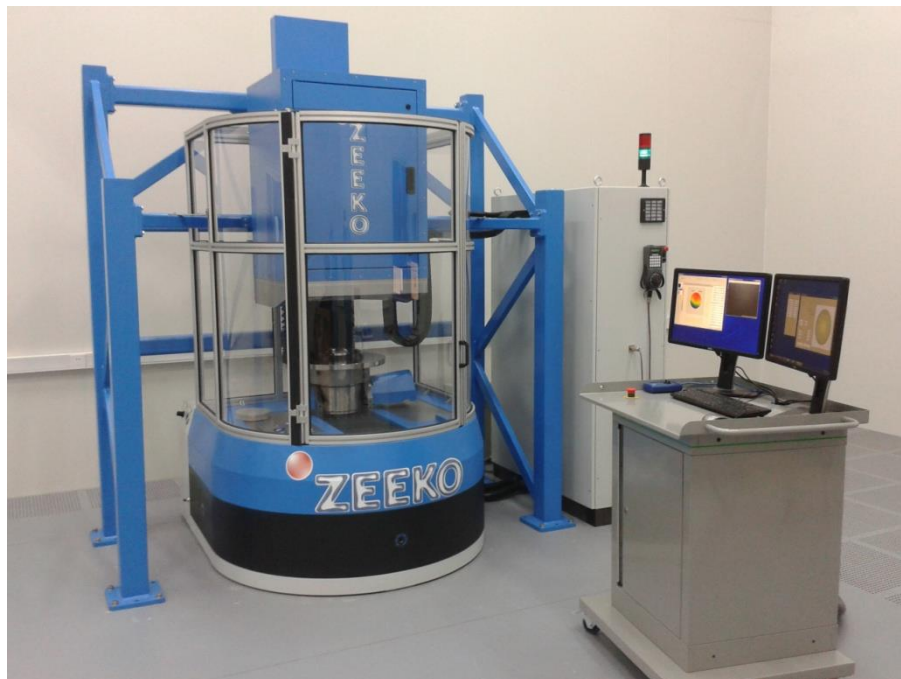


Figure 2.11: Zeeko Metrology Station installed at customer site

To the right of the test tower, the electrical cabinet is visible behind the operator console and is separated from the system in order to minimise induced vibration.

The operator console allows the user to view measurement progress and control the system, in a similar manner to that of the IRP machine.

Although the system hardware configuration is somewhat different, the Metrology Station provides the same data as the OMSI, and demonstrates the ability of the software presented in this thesis to automatically carry out sub-aperture measurement.

2.3.3 Conclusion

This section has reviewed the option of carrying out on-machine metrology by placing a tower structure over the polishing machine. Though the Metrology Station presented here is a specialised system and does not perform polishing, it does have many common characteristics with an IRP machine. In practice, such an arrangement could be executed using a testing tower over an IRP machine, as shown in Figure 2.1, which would represent little operational difference and provide an on-machine solution.

The use of the testing tower presents the opportunity to rapidly switch between polishing and measurement. When compared with having to move the SUT to the metrology lab, up to a 1.5 days per cycle (estimated for the E-ELT) could be saved in pre-polish set up time. The test tower would also be quicker than mounting the metrology device to the H-axis as removal of the bonnet and slurry guard is not required. When used for sub-aperture interferometry, the test tower provides more flexibility in terms of range of ROC which can be measured compared with full-aperture metrology.

2.4 On-Machine Surface Texture Measurement

In this section, the systems selected for development for automatic on-machine texture measurement will be outlined. The CNC machine and metrology instrument form a system and so neither can be considered in isolation. Deficiencies in performance of any part of the system are likely to impact data quality. Therefore the specifications of both the IRP machine and the STA interferometer are presented, and their suitability for on-machine metrology are assessed. The STA device was selected to provide an example of H-axis mounted metrology, and to support texture measurement for the ESO E-ELT project.

2.4.1 IRP 1200 Machine Specification

Table 2.1 reproduces the pertinent IRP1200 axis specifications [78]. The H-axes of the IRP machine available during development were configured in the CNC system as “spindles” rather than “axes”, and so may rotate freely when not powered. Therefore, in order to fix the relationship between the STA camera and the machine A-axis during measurement, adhesive tape was applied across the H-axis mounting during testing as a short term solution. This is visible in blue, above the STA in Figure 2.6. IRP machines currently in production offer an axis configuration for the H-axis, negating this requirement.

The IRP machine base is formed from polymer granite, which sits upon rubber isolation legs, which provide a degree of passive damping to ambient vibration. However, the machine is internally semi-rigid and relies upon the compliance of the inflated bonnet tool to damp any residual axis vibration and prevent ripple in the process footprint. When the A and B-axis combination is not balanced, the machine

must apply holding torque to the drives in order to maintain axis position. The application of holding torque is dependent on feedback from the axis encoders. It is observed during testing that torque may be applied intermittently and acts to induce some vibration. The effects of such self-induced vibration are characterised in Section 2.4.3.

Table 2.1: IRP1200 axis specifications

Axis	X	Y	Z	A	B	C	H
Travel	1300 mm	1300 mm	500 mm	±360 deg	±90 deg	N/A	N/A
Step resolution	1 µm	1 µm	1 µm	0.001 deg	0.001 deg	0.001 deg	N/A
Accuracy	< 20 µm	< 20 µm	< 15 µm	±1 arcmin	±1 arcmin	±2 arcmin	N/A
Alignment	X-Y	X-Z	Y-Z				
Circular interpolation	< 0.05 mm	< 0.05 mm	< 0.05 mm				
Squareness	< 10 arcsec	< 10 arcsec	< 10 arcsec				

2.4.2 Surface Texture Analyser Specification

The relevant aspects of the STA specification are presented in Table 2.2. During testing and development of this system, only a 10x objective was available and so the specification related to this configuration is shown. The STA uses a 460 nm Light Emitting Diode (LED) light source. While this is practical for on-machine metrology, (sources such as Helium-Neon lasers tend to be larger) depth of focus is reduced due to the limited coherence length of LEDs. In practice, it is observed that moving ± 1 µm from best focus causes a loss of fringe contrast such that fringe acquisition is not possible. This results in fringes generally not being visible when arriving at a testing location. Some vertical scanning is therefore required to locate the surface.

Table 2.2: STA specification (10x objective)

Item	Specification
Light source	Pulsed LED, $\lambda = 460$ nm
Camera	1.4 MPixels 12-bit
Weight	4.6 kg
RMS repeatability	< 0.005 nm
RMS Precision	< 0.1 nm
Spatial sampling (10x objective)	0.7 μ m
FOV (10x objective)	0.9 mm X 0.9 mm

2.4.3 Suitability for On-Machine Metrology

This section discusses the limitations of the separate system elements outlined in Section 2.4.1 and 2.4.2 and how they are likely to impact overall system performance. Understanding the performance of the STA and IRP machine together as a system is fundamental to establishing viability.

2.4.3.1 Vibration Analysis

As mentioned in the previous section, the IRP machine servo motors can act to induce vibration while attempting to maintain position. Although the acceleration parameters of the IRP control system may be tuned to minimise vibration during metrology, the machine is optimised for the primary task of polishing. The STA uses simultaneous phase shifting to minimise vibration sensitivity [79]. However, large oscillations at frequencies of around 1 kHz can reduce image contrast and increase fringe print through, where fringes are visible in analysed data [80]. To evaluate if such vibration is present, measurements were carried out using a SIOS SP2000 distance measuring interferometer. This was secured to the IRP1200 machine H-axis via a spigot and L-shaped bracket. The SIOS was aligned normal to a glass sample mounted on a tilt stage clamped to the IRP1200 machine C-axis table, as shown in Figure 2.12. The SIOS SP2000 can measure relative changes in distance

along the beam length with a resolution of 0.1 nm and a sampling frequency up to 1 MHz.

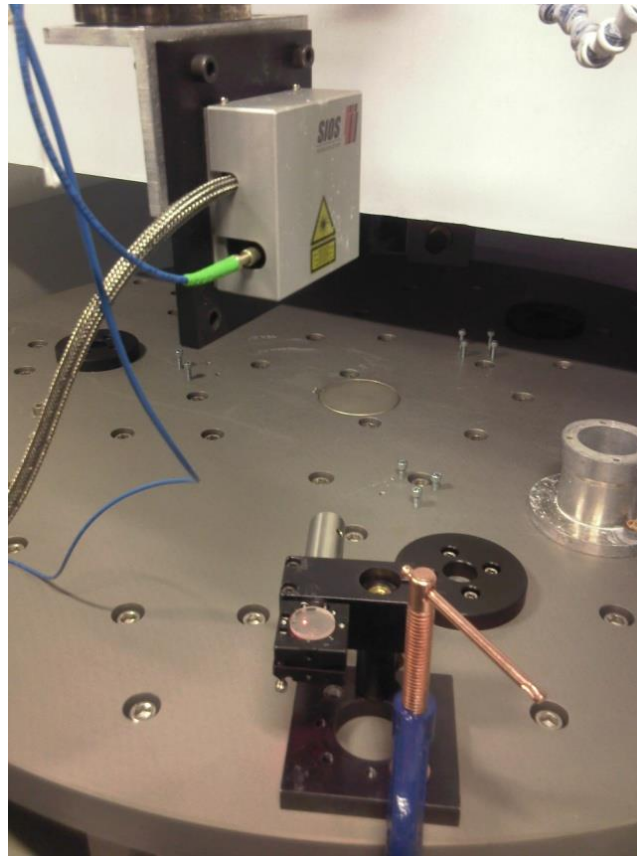


Figure 2.12: SIOS SP2000 distance measuring interferometer mounted to IRP1200 machine during vibration analysis

Measurements were taken at four locations on the machine table, involving different combinations of axis positions, with some variation of A and B-axes in order to align the SP2000 with the reflector. Figure 2.13 shows the approximate test locations.

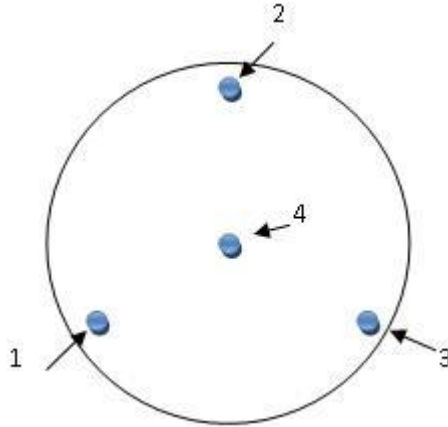


Figure 2.13: Approximate vibration analysis locations on the 1.3 m diameter machine table

During initial testing, little lateral vibration was observed, therefore only oscillation normal to the machine C-axis was measured in detail. Observation of the vibration spectra at the locations indicated in Figure 2.13 revealed no component exceeded 23 nm displacement or 300 Hz in frequency. A result representative of the test is shown in Figure 2.14. Although the measured vibration amplitude is significant in comparison to that of expected measured texture, the frequency of these vibrations are well below that reported to affect the STA. Provided exposure time is minimised, the resultant surface displacement occurring during exposure is negligible. This was confirmed by operating STA on the IRP1200 machine and measuring an ultra-smooth reference flat of <0.1 nm RMS texture. A measurement repeatability of < 1 Å was obtained when averaging 256 frames.

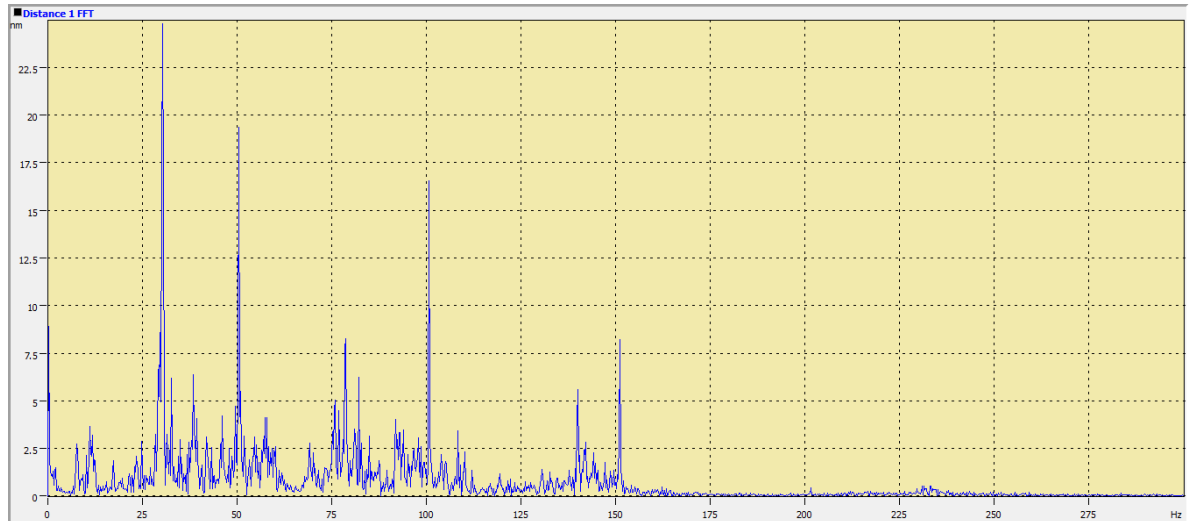


Figure 2.14: Sample IRP1200 vibration analysis FFT result

2.4.3.2 Manufacturing Environment Repeatability

In order to minimise the effects of residual mechanical or environmental instability on measurement data, it is normal practice to average several measurement acquisitions. Table 2.2, which reproduces data from the STA specification, indicates that the STA has repeatability of <0.005 nm (one standard deviation of RMS of 10 datasets of 64 averaged frames) when tested in optimal conditions. However, application to the manufacturing environment is likely to degrade this performance through reduced environmental control and the presence of residual vibration, as established in Section 2.4.3.1.

In order to observe how the on-machine application of STA affected measurement repeatability, static testing was carried out both in the metrology laboratory and on the IRP 1200 machine at OptIC Glyndwr. Two measurements were carried out at each averaging level and subtracted to provide an indication of how measurement repeatability varies with number of frames averaged. The test result is shown in Figure 2.15.

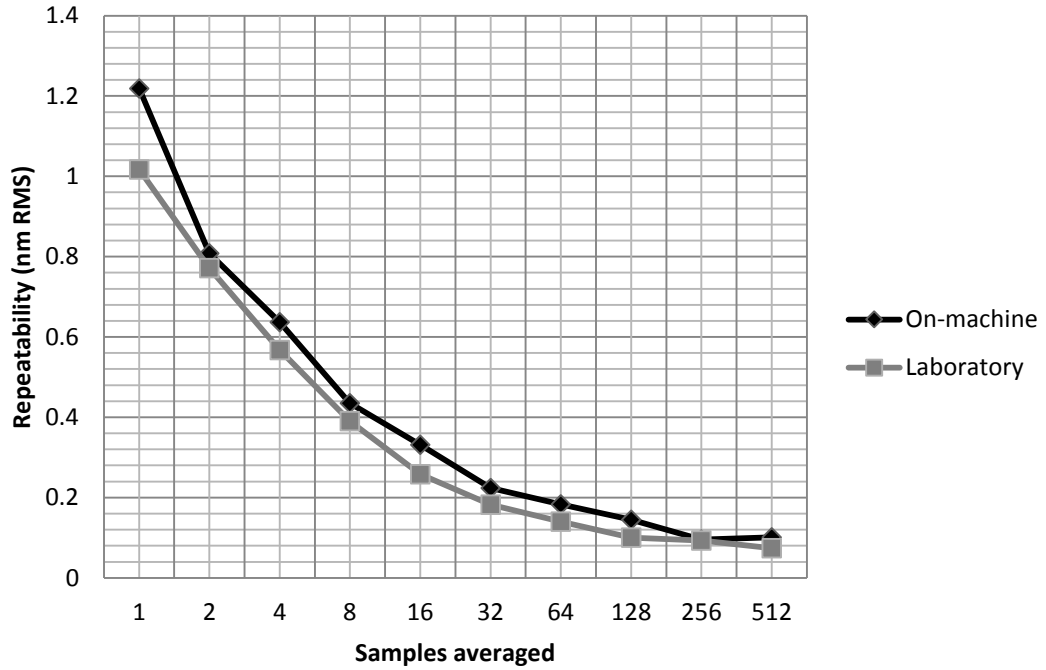


Figure 2.15: Comparison of STA repeatability in laboratory and on-machine regimes

It was observed that system repeatability was reduced by an average of 16.6% when operating the STA on machine. At low averaging levels (<4 frames), fringe print through dominates the resultant dataset, indicating that some residual vibration is present which is not found in the laboratory. For averaging levels up to 256 frames, comparable repeatability to the laboratory is obtained by increasing the measurement averaging. However, at high averaging levels, e.g. 512 frames and greater, repeatability is reduced and obtaining measurement data without significant numbers of invalid pixels becomes difficult. This is due to thermal drift during the acquisition period. As the STA acquires around 1 – 1.2 frames per second, measurements using averaging of 512 frames take more than 10 minutes to complete and so thermal drift can act to reduce image contrast. However, when averaging 512 frames, the difference in repeatability between lab and machine is ~ 0.03 nm RMS which is at the atomic scale and generally negligible. Differences in

repeatability could be reduced further through improved thermal control of the manufacturing environment, should measurement of super-smooth surfaces be required. This demonstrates that on-machine operation of the device imposes no constraints on measurement performance for the majority of surfaces.

2.4.4 On-Machine Operation

During these tests, the IRP machine was operated in manual mode (using the machine console to move individual axes) to position the STA. Achieving optimal instrument alignment with the SUT requires compound moves, using at least 3-axes for a basic alignment correction (A, B and Z) and 5-axes in order to maintain the point of interest in the FOV (also X and Y). This difficulty stems from the mentioned limited coherence length of the STA light source, and the IRP machine kinematics.

When carrying out on-machine metrology, it is more convenient for the operator if the H-axis could rotate about the centre of the FOV of the measurement device, especially with the STA. However, this cannot be achieved manually without modification of either the IRP machine or the STA. It will be demonstrated in Chapter 4 that the device can maintain a position of interest in the FOV with the use of the control system developed by the author.

2.4.4.1 Fringe Location Using the STA

The short coherence length source of the STA limits the range within which fringes can be observed. This can make obtaining fringes difficult when arriving at a measurement location. The STA has an alignment mode in which the image returned from both the reference mirror and the SUT are displayed to the user. A

set of example images taken from the 4Sight software application, showing the alignment mode return images, are given in Figure 2.16.

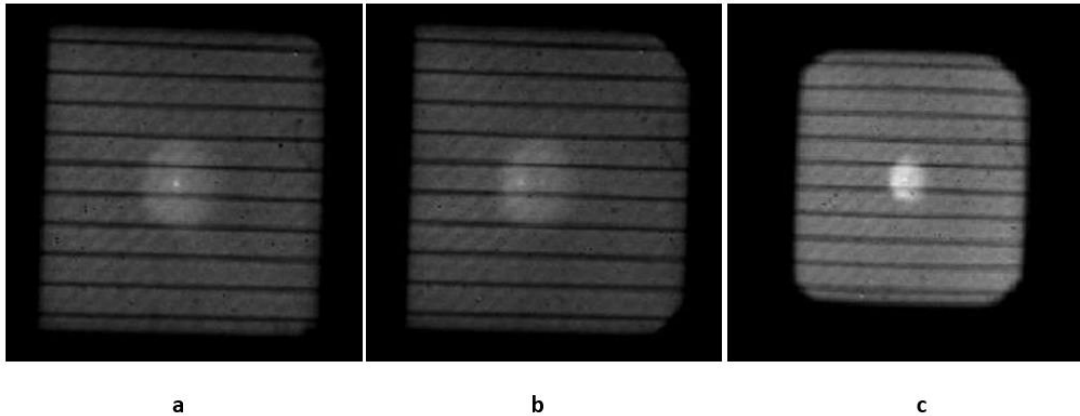


Figure 2.16: STA course alignment and focus system (a) correctly aligned and focused, (b) correctly focused and misaligned, (c) poor focus and misaligned

Figure 2.16(a) shows the return image properly aligned and focused. The SUT return image is near symmetrical and square in shape. Figure 2.16(b) has the right hand corners have rounded as the image is truncated by an internal optical stop of the device, owing to the STA being tilted relative to the SUT. Figure 2.16(c) shows the SUT return image when the STA is not positioned the optimum distance from the SUT. The return is diminished in size and all corners are truncated.

It is expected that some combination of both tilt and focus error will be encountered when arriving at a test location. Alignment mode is designed such that when the two images are correctly aligned and focused, fringes should be visible. However, in practice it is found with the return image optimised, as in Figure 2.16(a), fringes are not visible in measurement mode. The device generally requires up to 50 μm of focus correction before fringes are located. Therefore, alignment mode is found to be of use only in providing a rough guide for device alignment and

focus under manual control. Coarse alignment mode is deemed unsuitable for automatic operation.

2.4.5 Conclusion

The results obtained from the vibration analysis of the IRP1200 indicate no significant vibration exists which is likely to cause displacement greater than one pixel in size laterally, nor significantly impact focusing performance. However, the repeatability test showed that, compared with the metrology laboratory measurements, on-machine repeatability performance was reduced. In order to minimise such a difference for a given acquisition averaging level, it is desirable to reduce camera exposure times. In order to allow any reduction in exposure time, fringe contrast should be maximised through optimal alignment. Although this will be influenced by SUT finish quality, reducing exposure time is the easiest way of minimising the deficit between on-machine and lab repeatability performance.

The accuracy of the machine linear axes is specified as $< \pm 20 \mu\text{m}$ error over the length of the axes. This corresponds to around 2.2 % of the STA FOV when measuring with the 10x objective. Therefore, should the operator wish to measure the same surface feature repeatedly following successive processing, the system should be able to return to the same position reliably and retain the point of interest in the FOV. This has been trialled using an early version of the control software presented in this thesis. It was found that the system could return to the same feature with a combined X and Y repeatability of $7.6 \mu\text{m}$. This initial work was published by the author [81].

Following the assessments made of combined STA and IRP1200 machine performance, both from specification and test, it was found that on-machine metrology with the system is practical. The potential performance limiting factors have been identified and solutions will be demonstrated in Chapter 4.

2.5 Sub-Aperture Measurement

Following the problem experienced with the OMSI when installed the H-axis assembly, the alternative concept of the test tower configuration remains as the preferred on-machine solution for measurement of form. Development of a sub-aperture stitching system will focus upon the Metrology Station system presented in Section 2.3.2. Although this system has no manufacturing capability, it will be demonstrated in Chapter 6 that the techniques developed for this system may be utilised for an exemplar on-machine metrology system. This section will outline the specification of the hardware forming the Metrology Station and discusses any limiting factors.

2.5.1 Metrology Station Base Unit

As mentioned, the Metrology Station base is derived from that of an IRP 600 machine, with the exception that the C-axis has been replaced with a tilting table arrangement. Figure 2.17 shows the tilt table assembly, which is able to translate along the W-axis. The U-axis is the equivalent of the IRP C-axis. The V-axis axis serves to rotate the table assembly about the X-axis, providing the tilt required to perform sub-aperture measurement of spherical parts. The table assembly sits below a cabinet which houses the interferometer and 5-axis stage.

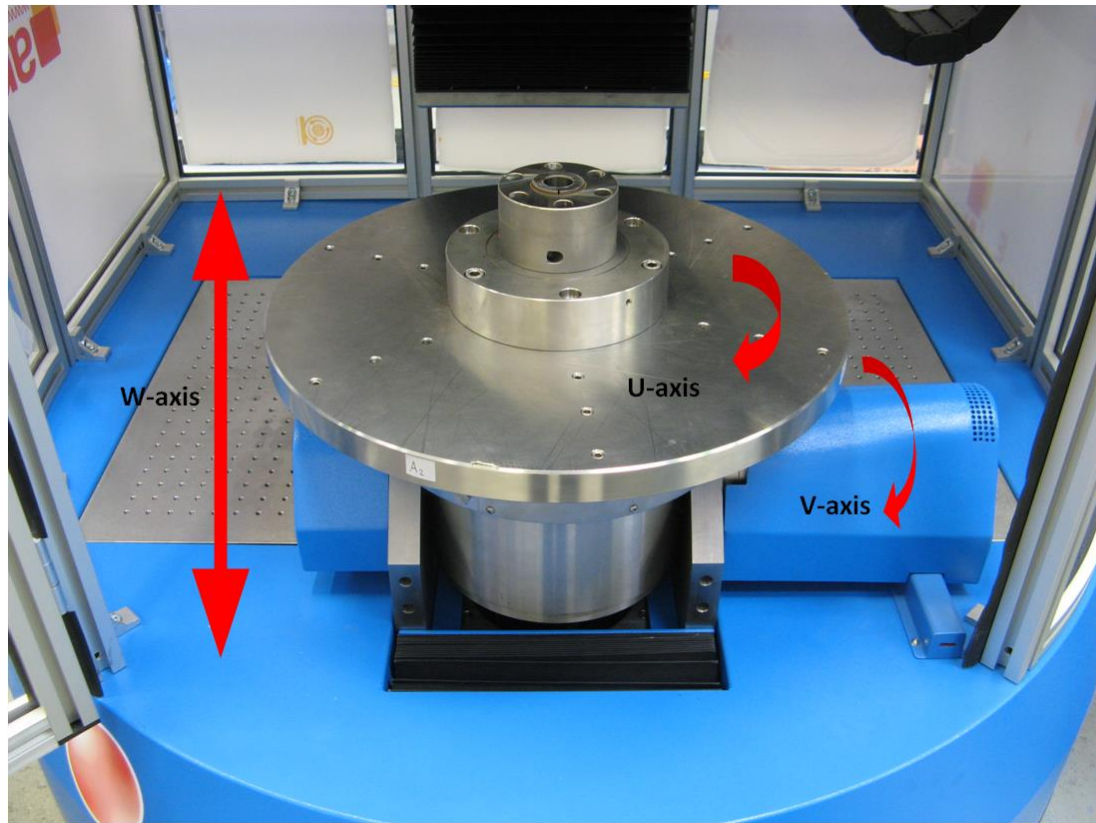


Figure 2.17: Metrology Station tilt table assembly

In order to affect tilt correction for both spherical and plano SUT types, the system must be able to tilt and translate the interferometer relative to the SUT. The required tilt axes are assembled into a 5-axis stage (X,Y,Z,A, B-axes), mounted inside the interferometer housing shown in Figure 2.11. The housing is mounted to the Z-axis which allows the whole assembly to move vertically to control the interferometer cavity length. Figure 2.18 shows a CAD rendering of the Metrology Station 5-axis stage assembly. In this image, the Y-axis is labelled and the X-axes can be seen running perpendicular. The A-axis is seen above the Y-axis label and the B-axis is hidden behind the interferometer mounting. The A and B-axes are configured as linear axes which drive a wedge under a radial bearing. The tilt stage is hinged at the opposing edge, and pivots as the corresponding wedge is driven.



Figure 2.18: Metrology Station 5-axis stage axes configuration (courtesy of Zeeko)

A protective cabinet is fitted around the interferometer mounting assembly with an access door to a small screen secured to the front of the interferometer mounting. This arrangement is shown in Figure 2.19.



Figure 2.19: Fizcam 3000 access door on the Metrology Station

The alignment screen to the bottom-right of Figure 2.19 allows the operator to observe the reference return spot while aligning the reference surface. The white case in the centre is the Fizcam 3000 interferometer [82], which is directed downward through the bottom of the cabinet. The interferometer is fitted with a 4"-to-6" beam expander, visible through the 5-axis stage. The Fizcam 3000 Fizeau interferometer was selected, in contrast with the Twyman-Green PC6000 used in the OMSI, because the common path reference provides some cancellation of systematic errors. This reduces device sensitivity to small internal misalignments resulting from tilt movements made for plano SUT alignment.

Table 2.3 shows the specifications of the Metrology Station axes. The Metrology Station is fitted with the same hardware used on IRP machines and so is of comparable performance.

Table 2.3: Metrology Station base unit axis specification

Axis	X	Y	Z	A	B	U	V	W
Travel	185 mm	85 mm	1180 mm	±2 deg	±2 deg	N/A	±45 deg	475 mm
Step resolution	1 µm	1 µm	1 µm	0.001 deg	0.001 deg	0.001 deg	0.001 deg	1 µm
Accuracy	< 20 µm	< 20 µm	< 15 µm	±1 arcmin	±1 arcmin	±2 arcmin	N/A	
Alignment	X-Y	X-Z	Y-Z					
Circular interpolation	< 0.05 mm	< 0.05 mm	< 0.05 mm					
Squareness	< 10 arcsec	< 10 arcsec	< 10 arcsec					

During measurement, the system hardware is operated automatically by the *Metrology Control Suite* application, developed by the author and described in Chapter 3 and Chapter 4. During operation, the user interacts with the system through the console PC (Figure 2.20), primarily to monitor system activity.

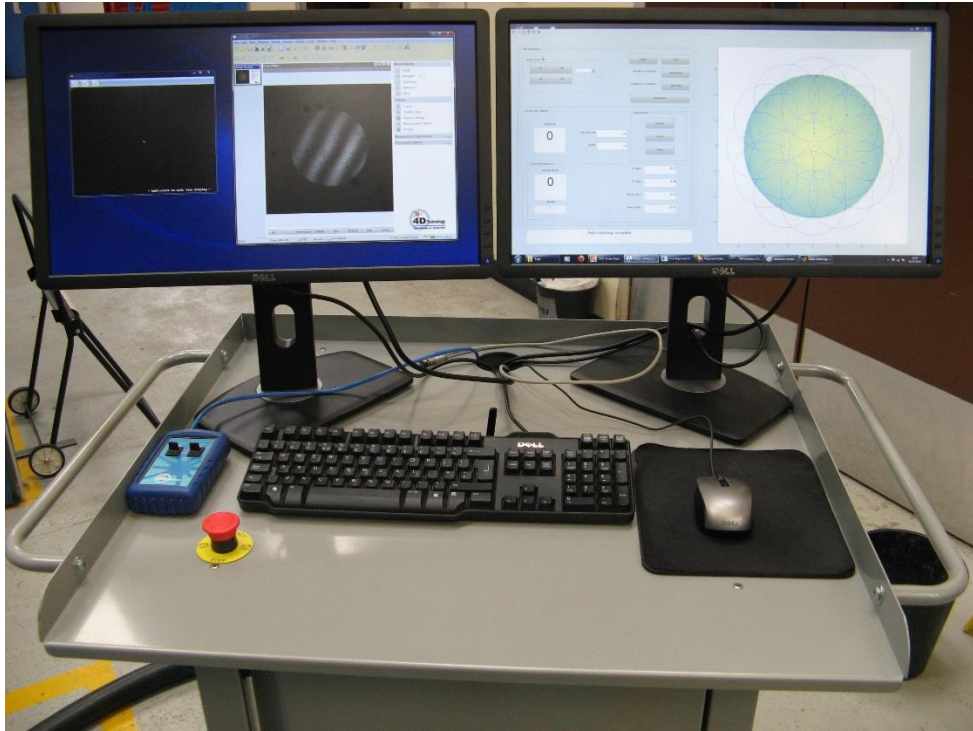


Figure 2.20: Metrology Station control console

Figure 2.20 shows the console PC with the left monitor containing the 4Sight window, displaying the interferometer image with a visible sub-aperture. The smaller window to the left shows the alignment screen output allowing the user to view the alignment camera return during measurement setup. The right-hand monitor shows *Metrology Control Suite*, presented in this thesis.

2.5.2 Fizcam 3000

The Metrology Station is fitted with a Fizcam 3000 interferometer manufactured by 4D Technology, Arizona. As with the STA, the Fizcam uses a CCD phase mask to allow simultaneous phase imaging to reduce sensitivity to vibration [83]. The Fizcam uses standard Fizeau transmission optics which are common to many other instruments such as Zygo and Wyco. The Fizcam also makes use of an integrated HeNe light source which provides a coherence length greater than that of the STA, making locating fringes easier as interference occurs over a greater displacement

range. Table 2.4 presents the specification of the Fizcam 3000 system. Items such as spatial sampling and FOV are omitted as they are influenced by the combination of transmission optic and SUT.

Table 2.4: Fizcam 3000 specification

Item	Specification
Light source	Helium-Neon, $\lambda = 663 \text{ nm}$
Camera	1.4 MPixels 12-bit
Weight	~25kg
RMS repeatability	< 0.7 nm
RMS Precision	< $\lambda/20$

2.5.3 Suitability for Automated Metrology

Following an overview of the Metrology Station system specification, this section presents discussion of the pertinent aspects of the system for automated metrology. The Metrology Station has been developed to acquire form data for a wide range of surfaces, some of which (such as 0.5 m class optics) cannot be accommodated on state-of-the-art systems, such as the QED's SSI [84].

2.5.3.1 Metrology Station Tilt Table Assembly

The rotary table installed on the Metrology Station presents a number of challenges during development. This system is designed to accommodate a half-metre scale part weighing up to 40 kg with slopes of up to 45° in both concave and convex forms.

Figure 2.21 shows a side view of the rotary tilt table from the side. Due to the requirements to tilt to 45° and accommodate large parts, the pivot point of the table has been sited low on the assembly. In many practical situations when a part is affixed, the rotary table can become top-heavy, and so inherently unstable [85].

In order to retain the SUT in the correct position during testing, the harmonic drive of the T-axis (table tilt) must therefore apply holding torque which, depending upon system tuning parameters selected, can induce oscillation of the table. Proper tuning of this assembly is difficult owing to the large range of part weights and sizes which the system may accommodate. During development, Zeeko engineers opted to tune the systems parameters such that the rotary table motion was over-damped to ensure oscillation could not occur.

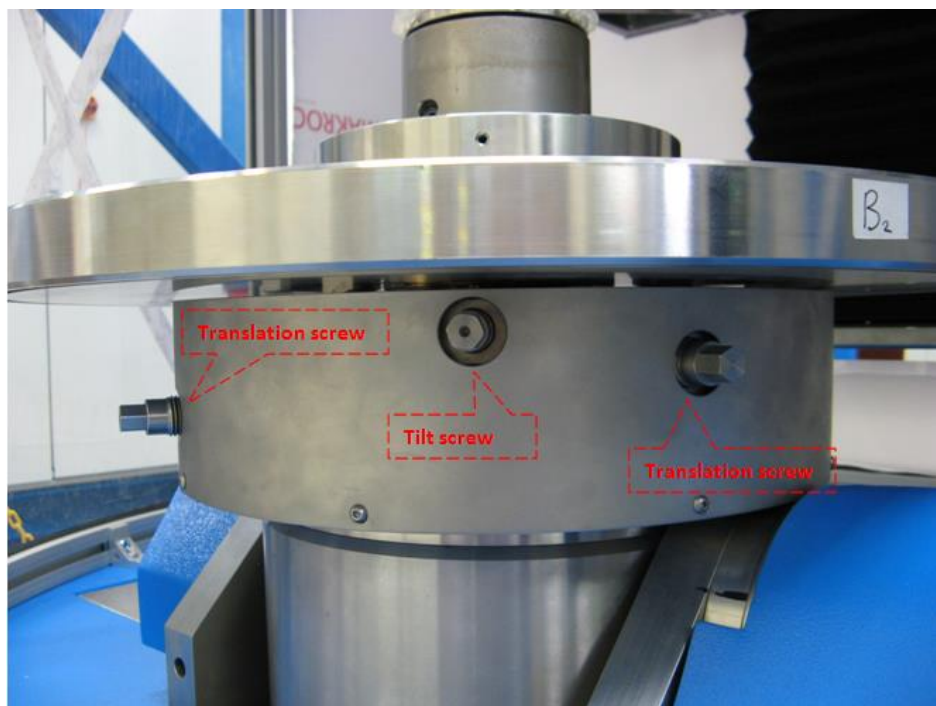


Figure 2.21: Close-up view of the Metrology Station rotary tilt table

While over-damped tuning offers stable and benign motion, it causes the system to respond more slowly to commands, and accelerations are reduced. In contrast, one of the great opportunities which system automation provides is that of increasing productivity. In the high-volume manufacturing facility, such sluggish motion of a single assembly can reduce efficiency, as the entire system is limited in speed by

the slowest component. This is an example of a trade-off between versatility and operational efficiency.

2.5.3.2 Metrology Loop

Optical metrology using an interferometer relies upon the comparison between the cavity length of the SUT against that of the reference. In order for this comparison to be valid, both the reference and the SUT should be secured so no significant movement occurs during measurement acquisition. When multiple frames are averaged to improve SNR, the measurement setup must be stable for the duration of acquisition. As demonstrated with the STA in section 2.4.3.2, even if the system exhibits stability for short measurements, external factors such as thermal drift can become significant over longer periods, on the order of 10 minutes. One of the factors which influences system sensitivity to such environmental factors is the metrology loop, as defined below.

If one were to trace the shortest mechanical path from the SUT around the metrology system to the interferometer, this would be the “metrology loop” of the machine. A change in physical length of any of the components forming the metrology loop will result in a reduction in the system measurement performance. Figure 2.22 provides a visualisation of the metrology loop of the Metrology Station system.

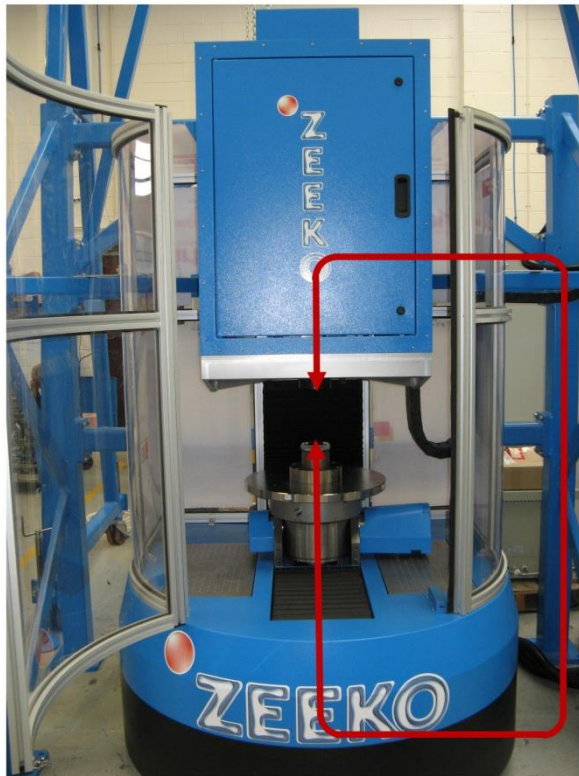


Figure 2.22: Example of the metrology loop of the Zeeko Metrology Station system

In the case of the STA and IRP machine combination, the metrology loop is simple, as the bridge of the machine is supported from the same rigid base as the C-axis. Any thermal drift experienced by the base is passed to the bridge and the C-axis, and so the two are well coupled. By contrast, the loop of the Metrology Station passes through the floor of the laboratory, increasing the length and complexity with comparison to the IRP machine and STA.

Existing systems use techniques to mitigate the impact of the metrology loop, such as hanging the SUT support and metrology device from the tower as a single element, similar to the principle of the NANOMEFOS system [86]. Careful selection of construction materials may be employed to ensure any thermal expansion is

passively compensated, minimising disruption to alignment and cavity length during acquisition. However, the Zeeko machine range has been designed principally for manufacturing and, for this, dynamic performance is of main concern. The Metrology Station is derived from such systems, and so exhibits many of the same characteristics.

It will be shown in this thesis that many of the issues associated with the complex metrology loop are reduced through proper environmental control. However the ultimate performance of any metrology system is determined at the design phase. In order to move metrology into the manufacturing environment, some compromise of performance may be inevitable.

2.5.4 Manual System Operation

The manual operation of the Metrology Station is similar to the IRP machine in the respect that a tilt correction requires multiple axes to be manipulated in order to hold position over the SUT test location. However, because the effective spatial sampling area is typically much larger than the STA, the lateral movement induced by a single axis to effect tilt correction is typically sub-pixel, and thus negligible. Therefore, tilt correction for plano testing requires only the use of the A and/or B-axes, and the use of X and/or Y axes for spherical configurations, as translation is equivalent to tilt at a small scale. Furthermore, because of the longer coherence length light source, the Fizeau 3000 fringe contrast is negligibly affected by, single-axis tilt correction moves and so subsequent Z-axis focus correction is not required.

Single axis correction moves allow simple manual operation and setup of the system. However, if the V-axis must be adjusted when moving between sub-

aperture locations, interferometric fringes are lost. There are also many configurations which can cause the table to crash into the Z-axis stage or bottom of the interferometer cabinet. The operator must therefore exercise caution when carrying out manual V-axis moves. Automation of the system can avoid such risks, because the kinematics equations used ensure that the table maintains clearance from other hardware.

2.5.4.1 Fringe Location Using the Fizcam 3000

The Fizcam 3000 includes an alignment camera, similar to that on the STA. However, owing to the larger coherence length of the Helium-Neon source, the system exhibits a larger range in both tilt and piston. This range is dependent upon the SUT ROC and reference optic F# combination for spherical tests. For the plano, tilt sensitivity is fixed and insensitive to Z-axis displacement.

The Fizcam alignment mode displays the return spots from the Fizcam reference optic and SUT. When the operator aligns the SUT return with that of the reference, fringes are visible on the measurement screen. Unlike the STA system, fringes are easily found when the two spots are properly aligned and focused and the alignment camera and measurement camera outputs may be viewed simultaneously, as shown in Figure 2.23.

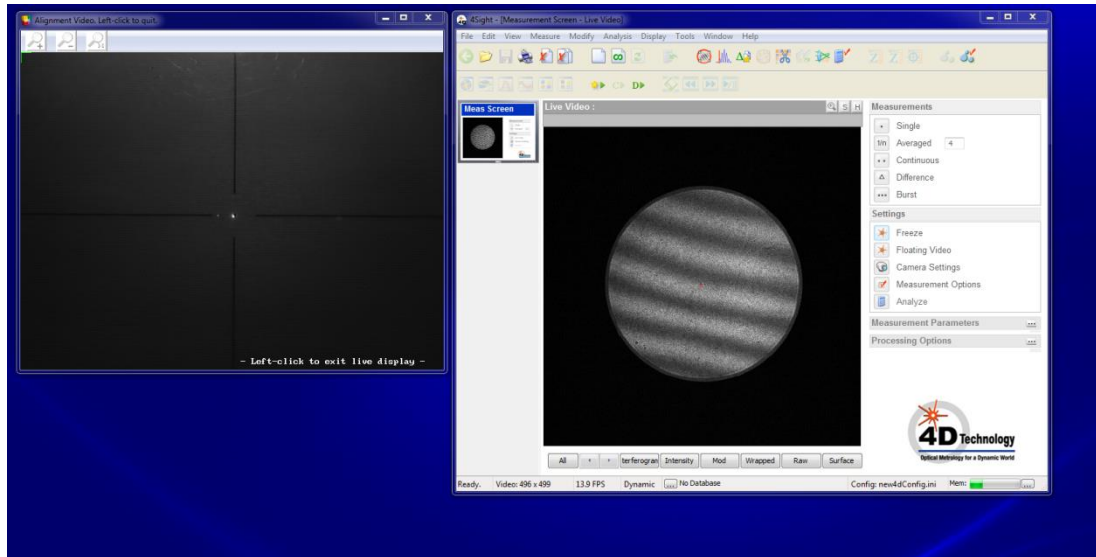


Figure 2.23: Metrology Station Fizecam 3000 alignment screen (l) and 4Sight measurement screen (r)

The alignment camera feed is displayed on the console PC using an application developed by Dr Christopher King (Zeeko). This application also captures still images for use in automatic alignment, as discussed in Chapter 4.

2.5.5 Conclusion

This section has outlined the Metrology Station specification and some of the factors limiting system performance. Manual control operation of the Metrology Station is easier compared with that of the STA due to the relative insensitivity to translation when performing alignment. While this may suggest manual operation the system to obtain sub-aperture data is viable, it does not take into account that some sub-aperture configurations, demonstrated later, contain large numbers of measurement locations and so take many hours to measure. The benefits of system automation both in terms of ease of use and operational efficiency must therefore be considered. Also, when measuring short ROC convex components, separation of the rotary table from the Z-axis and interferometer cabinet may be difficult to judge, posing risk of a hardware crash. The Metrology Station is well suited to

development into a fully automated measurement system, as will be discussed in the following chapters.

This chapter has discussed and compared two devices which are viable for application to automated on-machine metrology, as well as the OMSI. The remainder of this thesis will detail how these systems have been automated through the development of a flexible software application which allows the planning and execution of automated metrology. This application is sufficiently generalised to support other metrology systems, as will be discussed in Chapter 6. In order to develop such software, an understanding of what tasks are required to perform automated metrology must be developed. The following section provides a software specification for the application discussed in Chapter 3 and Chapter 4.

2.6 Software Requirements for On-Machine Metrology

As mentioned, although the use of on-machine metrology has parallels with processes of CNC polishing, the design and execution of a measurement plan has a set of unique requirements, not addressed by any existing application. These requirements are stated in Table 2.5.

In order to provide a clear description of software development, the application presented in the following chapters is divided into two parts, each addressing one of the key tasks required; planning and execution of metrology.

Table 2.5: Metrology Control Suite software requirements

Metrology Designer	
1.	Allow specification of the surface to be tested
2.	Allow specification of device and optical setup to be used for testing
3.	Allow simple design of metrology plan which will provide useful data
4.	Provide customisation of plan for more demanding measurements
5.	Prevent generation of a metrology plan which will cause damage to the machine, SUT, or present danger to personnel
6.	Allow the plan to be saved for future use or modification
Metrology Controller	
1.	Allow the measurement plan to be loaded and reviewed
2.	Interface with machine controller(s)
3.	Query system axis positions
4.	Dynamically generate g-code and upload to the controller
5.	Execute and delete g-code files from control system
6.	Display measurement progress and system status clearly to the user
7.	Prevent the system making movements which could damage the machine, SUT or pose a danger to the operator
8.	Control the measurement device to make automatic measurement acquisitions and save the data to file
9.	Ensure acquired data is useful for either correction or SUT measurement
10.	Analyse device alignment and compute correction moves
11.	Summarise measurement information to allow operator to interpret progress
12.	Allow user to pause or cancel the measurement process
13.	Record any system errors to allow remote debugging

2.7 Conclusion

This chapter has reviewed the available hardware which will form the building blocks of the on-machine measurement system. Methods of integrating such metrology with the IRP machine have been discussed, along with example devices which have been previously considered for development. The two systems selected for development, the Surface Texture Analyser and the Metrology Station have been presented in detail and compared and contrasted with their predecessor, the OMSI. For each of system, a feasibility study has been conducted, with potential performance limiting factors demonstrated. Both of the systems selected are deemed suitable for automation development.

In order to achieve full automation, a software application must be developed which allows both metrology planning and automatic execution of this plan. A set of requirements for such an application has therefore been stated, including the requirement to obtain feedback from the interferometer in order to compute subsequent correction moves, and properly align the device with the SUT. This software will therefore have two modes of operation; open-loop, where the machine moves the interferometer to the predicted measurement location, and closed-loop, where measurements are made in order to compute subsequent correction moves. The following chapters discuss the development of the planning and control applications respectively.

3 Metrology Designer

Integration of metrology with CNC systems allows the metrologist to benefit from the ability to perform a series of measurements with minimal operator interaction. However, as with the Zeeko polishing process, the user must first define the tasks to be performed in order for the system to operate unattended. Although CNC enabled metrology parallels polishing in that the system must address a given location along a specified vector, the activities carried out at these surface locations differ greatly. The Zeeko polishing process moves a rotating bonnet against the part surface, modulating dwell time in order to remove a target quantity of material. For measurement, the system must reach a target location and align the device with the SUT. Full automation also requires that the device then be commanded to measure prior to moving to the next location.

When planning a polishing run for the IRP machine, the operator computes a tool path using the *Zeeko TPG* software application. The tool path describes how the bonnet is moved across the surface of the part and typically consists of a chain of co-ordinates and vectors located closely together. At the end of the planning process a G-code file is generated, by converting the tool path from real to machine co-ordinates, using inverse kinematics equations. These equations describe the orientation of each axis to place the machine at a given position and attitude. On-machine metrology requires a similar plan to be created, however, instead of generating a tool path, a set of discrete testing locations must be specified. The initial location the measurement device will arrive is calculated from the surface design, and so does not include error in the SUT or machine and test configuration.

If the operator knew exactly what the SUT surface looked like, measurement would not be required at all. As the requirements of this metrology planning process are different to those of tool path generation, programs such as TPG are unsuitable. *Metrology Designer* was therefore developed in order to provide a simple measurement planning process, analogous to *Zeeko TPG*.

Following polishing tool path planning, the operator uploads the output G-code file to the machine control system at the start of polishing. The G-code file is executed sequentially and the CNC controller interpolates between the machine axis positions specified to produce a smooth movement over the surface. In the case of measurement, due to the subsequent alignment corrections required at each location, a single file cannot be used to address all measurement locations. A new file must be generated and uploaded for each individual move. This requires a more complex interface with the machine controller and is beyond the functionality available in the current Zeeko control system. For the purposes of this work, *Metrology Controller* was developed. *Metrology Controller* uses measurement device feedback to dynamically generate new G-code instructions and enable the measurement system to automatically correct misalignment in the initial measurement position calculation made by *Metrology Designer*. While it will be demonstrated that this closed-loop alignment system is capable of correcting for errors in the test setup, making an accurate initial guess is important in minimising the time spent making corrections and thus maximising the efficiency of automation.

3.1 Metrology Designer Development

The *Metrology Designer* application allows the user to generate a measurement plan to be executed by the *Metrology Controller* application. As the application is intended for customer use, all software functionality is compiled with a GUI (Figure 3.1) developed using Matlab. Full explanations of GUI button functionality can be found in the *Metrology Control Suite* Manual in Appendix 9.1.

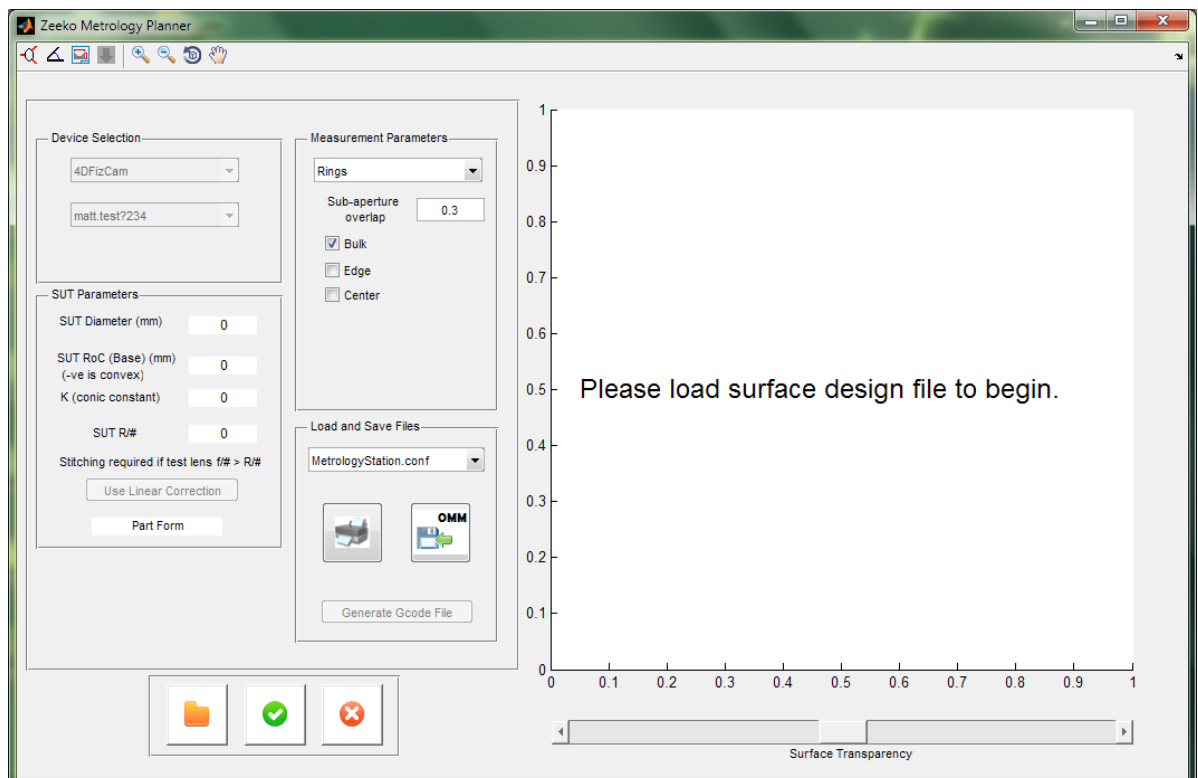


Figure 3.1: *Metrology Designer* main GUI

3.1.1 Surface Design

In order to begin planning metrology, the user must specify the surface to be measured. Knowledge of the surface shape, size, and form is required for the system to calculate how many measurement locations are required to address the surface completely, and in which direction to orient the metrology device to access these locations.

When carrying out polishing activities on the Zeeko IRP machines, the operator requires similar knowledge of the surface in order to generate tool paths. Surface design information is provided in the form of a Zeeko Design file. This contains meshes which describe the part form along with parameter information such as the part rotational base (plano, spherical, aspherical, etc.) and ROC. These parameters may be used as modal flags to switch the planning algorithms between modes without requiring extra computation, such as fitting.

The Zeeko Design file is created using the *Surface Designer* application (Figure 3.2) (written by Zeeko), which is incorporated into all existing Zeeko applications. In order to keep functionality of *Metrology Designer* consistent with other applications and ensure operation of on-machine metrology parallels polishing where possible, *Surface Designer* has been integrated to the *Metrology Designer* application. The *Surface Designer* application is launched by selecting the icon, located on the main toolbar. Instead of generating a new surface design each time a measurement plan is required, a surface design may also be loaded. This design file is therefore transferable between different software applications, allowing better control of designs and minimising the risk of incorrect file use.

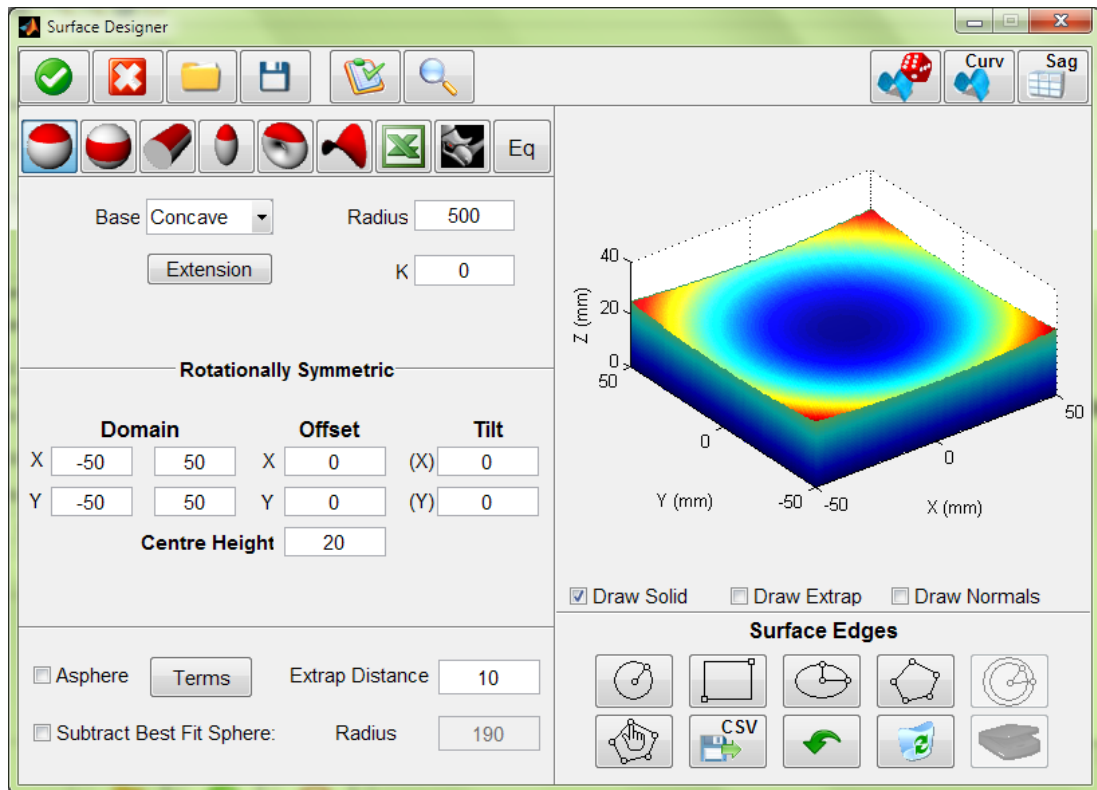


Figure 3.2: Screen shot of Zeeko *Surface Designer* (courtesy of Zeeko)

When a surface design is loaded, the design parameters are checked to ensure the surface is either plano or spherical. If the user loads a surface file of an aspherical or free-form surface, a warning is displayed as these are not currently supported by *Metrology Designer*. Alignment with aspheric or free-form surfaces would require further development of the automatic alignment algorithms. With a compatible surface design loaded, the characteristics such as diameter, ROC, and SUT R# are displayed to the user to allow confirmation of the intended surface design.

3.1.1.1 Device Configuration

When planning measurement, *Metrology Designer* must also have knowledge of the measurement device and optical configuration to ensure a valid design is produced. *Metrology Designer* currently supports the design of measurements for sub-aperture interferometry and texture interferometry. Sub-aperture metrology

design requires the placement of sub-apertures such that the entire region of interest on the SUT is covered, with sufficient sub-aperture overlap to ensure a good stitching result. Texture interferometry requires a set of measurement locations of sufficient number to allow the operator to understand how texture varies across the surface of the SUT. Texture measurement locations are discrete and are not required to overlap. In order to support both modes of measurement and allow the user to switch between them, *Metrology Designer* uses a configuration file for each metrology device. An outline of the parameters contained in the device configuration file are given in Table 3.1.

Table 3.1: Device configuration file overview

Parameter	Description
Mode	String used to describe planning mode of device.
XAxis	Double indicating the index of the X-axis. Provides the system with device orientation information relative to the CNC axes. This provides knowledge of which machine axis to use to effect alignment correction in a given camera axis.
YAxis	Double indicating the index of the Y-axis.
ZAxis	Double indicating the index of the Z-axis.
axisDirection	Array of doubles in indicating the directions of the above device axes. As it is possible for interferometers to introduce optical axis flips, this effect must be considered.
Brand	String describing the device manufacturer. This is used as a flag for device interfacing code as different manufacturers can require different communication methods.
Model	String indicating the model of the device. Different models from the same manufacturer have different features.
Name	String containing descriptive device name. This is used in the <i>Metrology Designer</i> GUI.

Two example device configurations are given in Table 3.2, for the *STA* on-machine texture interferometer and the *Fizcam 3000* discussed in Section 2.4 and Section 2.5.

Table 3.2: Device configuration file example

Parameter	STA1	Fizcam 3000
Mode	Point	Subaperture
XAxis	1	2
YAxis	2	1
ZAxis	3	3
axisDirection	[1,1,1]	[-1,-1,1]
Brand	4D	4D
Model	STA	Fizcam
Name	STA1	4DFizCam

As can be seen by comparing the two configuration files, the *STA1* operates in point mode, using small test areas which are modelled as points on the SUT. The *Fizcam* requires sub-aperture mode. The *Fizcam* is also mounted orthogonally with respect to the CNC system axes and has a negative sign convention in the X and Y-axes.

As *Metrology Designer* starts up, the device configuration file folder is searched for files and the drop down menu on the GUI is populated with those available for planning. When generating a measurement plan, the device configuration is included with the plan, binding the measurement plan to a single device, thus preventing the operator using the plan with another device, risking device and SUT damage.

3.1.2 Optics database

With the correct device selected for measurement, *Metrology Controller* populates a second drop down box with compatible optical configurations. These are required as the optical parameters of an objective determine the size of the device FOV on the SUT as well as the required working distance. The available optical configurations are further filtered by the form of the SUT; plano or spherical, for

sub-aperture measurement. Point measurement does not require specific objectives for a given form and so the entire selection is displayed.

In the case of sub-aperture interferometry, the optical parameters of the selected objective are used to calculate the number of sub-apertures to be placed and how they are arranged to provide the required overlap. The sub-aperture radii for a given transmission sphere or flat are given by (3.1) and (3.2) respectively.

$$R_{spherical} = \frac{|R_{SUT}|}{2F_{\#}} \quad (3.1)$$

$$R_{plano} = \frac{D_{TS}}{2} \quad (3.2)$$

Where R_{SUT} is the ROC of the surface under test and D_{TS} is the aperture diameter of the transmission sphere, as shown in Figure 3.3. R_1 is the reference surface ROC and R_2 is the effective ROC when considering the physical extent of transmission sphere cell. R_2 is compared with the SUT ROC to ensure the measurement is physically possible with the selected optical configuration. For example, should the user design a measurement of a convex sphere with a larger ROC than the selected transmission sphere R_2 value, the SUT would come into contact with the transmission optic cell during positioning. This condition must be avoided at the design stage, as the Metrology Station does not include proximity or crash detection systems. Test optic and SUT incompatibility is therefore avoided by checking R_2 and ROC_{SUT} during planning and warning the user accordingly.

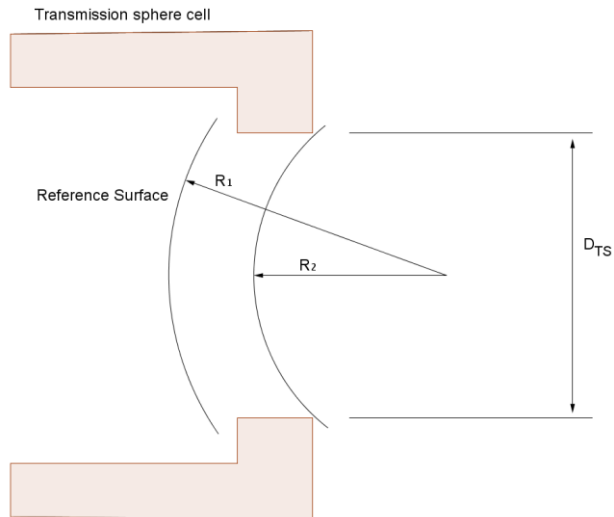


Figure 3.3: Transmission optic parameters for spherical test

The optical parameters outlined are stored as a cell array which is used as an optics database [87]. The user may add and edit the optics database through an editor built into the software. Each time a new SUT design is loaded into *Metrology Designer*, the optics database is filtered and the only optics of compatible form with the SUT form are presented for selection. Table 3.3 provides explanation of the parameters stored in the optics database and Table 3.4 an example for the two development devices.

Table 3.3: Optics database parameters

Parameter	Description
Name	String containing tem name displayed on <i>Metrology Designer</i> GUI
Working distance / F#	Double containing either (if applicable); Point measurement: Working distance of objective in mm Sub-aperture: F# of transmission optics
Mode	Double acting as flag to specify; 0: Sphere = transmission sphere 1: Plano = transmission flat 2 : Point measurement = microscope objective
R_1	Double, See Figure 3.3, if applicable
R_2	Double, See Figure 3.3, if applicable
D_0	Double, See Figure 3.3, if applicable

Table 3.4: Optics database example

Parameter	STA1 10X objective	Zygo F1.5 transmission sphere
Name	10x	F1.5
Working distance/ F#	25	1.5
Mode	2	0
R ₁	-	121.2
R ₂	-	115
D ₀	-	93.7

Should the optics database be empty, or not contain an optic suitable for the currently loaded SUT, measurement planning is not possible and a warning is displayed to the user.

3.2 Measurement planning

When the user has a valid surface design file, device configuration file and a suitable measurement optic, a measurement may be planned. When the user presses the plan measurement button, *Metrology Designer* uses the information provided to classify the measurement and decide which planning algorithm to apply. At present, there are two main plan types; point measurement and sub-aperture, which will be discussed in detail. This initial classification process is illustrated in Figure 3.4.

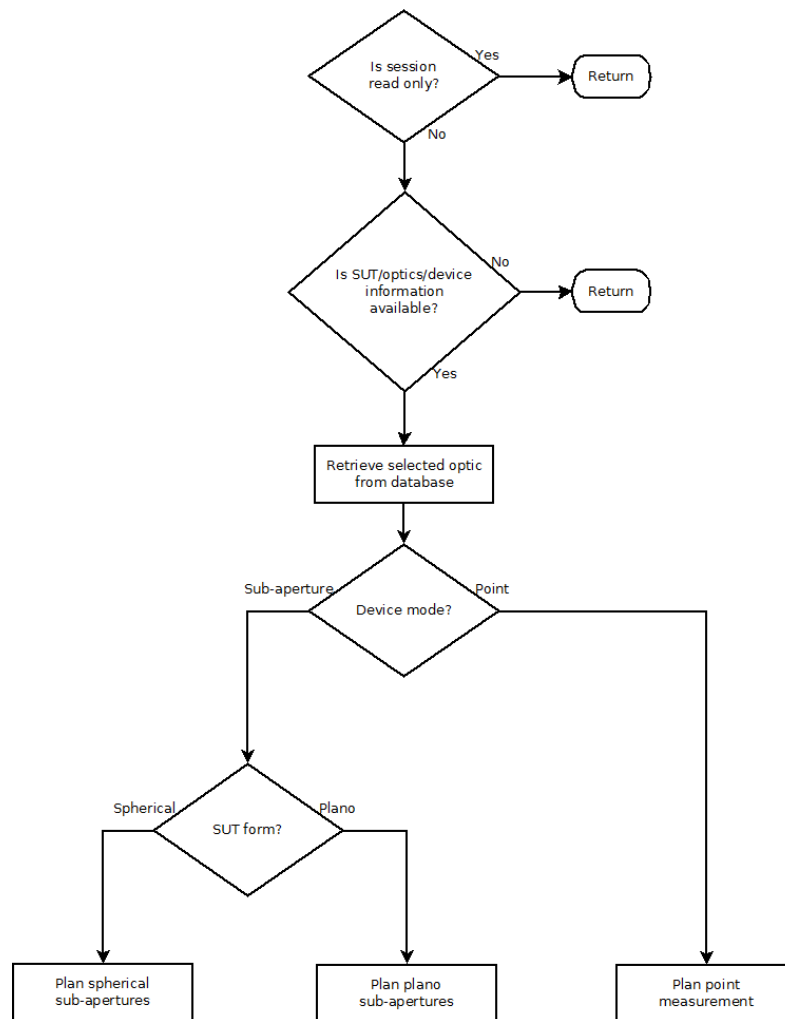


Figure 3.4: Initial planning function flow

Following classification of the plan to be designed, the appropriate planning algorithm is executed. Section 3.2.1 and Section 3.2.2 detail sub-aperture and point measurement planning respectively.

3.2.1 Sub-aperture planning

Sub-aperture planning mode contains two sub-modes (plano and spherical), as shown in Figure 3.4. Both modes contain functionality to allow the operator to create a plan based upon the entry of a minimum sub-aperture overlap value as well as a more comprehensive sub-aperture placement editor. Although the sub-

aperture stitching application used to stitch data can support aspheric surfaces, the required hardware is not included in the prototypes described in this thesis.

3.2.1.1 Spherical Sub-aperture Measurement Planning

Figure 3.5 shows the planning routine for a spherical sub-aperture test when using overlap optimisation mode. Vectors OC , OE , and OS are shown in Figure 3.6. As mentioned, in order to obtain a complete error map following data stitching, the measurement must contain data with sufficient overlap between adjacent sub-apertures. *Metrology Designer* therefore tests the measurement design for complete overlap and enters an optimisation routine when non-covered areas are found. For spherical measurements, *Metrology Designer* places sub-apertures on a series of concentric rings and only the sub-aperture centre co-ordinates are required for kinematics calculation. *Metrology Designer* outputs testing locations in real co-ordinates as conversion to machine co-ordinates requires machine configuration information which is obtained during measurement set up. As such, this inverse kinematics calculation is carried out in *Metrology Controller* and discussed in Chapter 4.

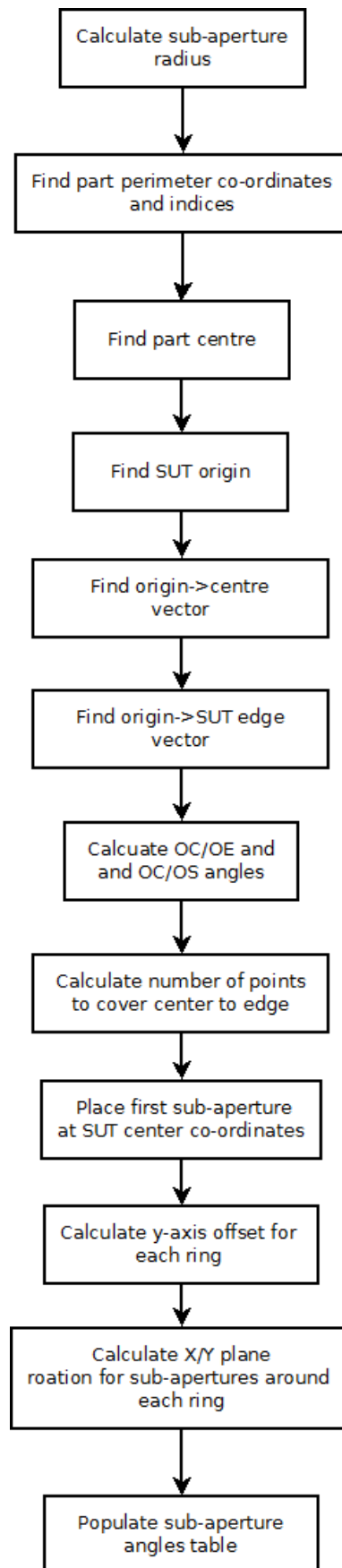


Figure 3.5: Spherical sub-aperture angles calculation work flow

At the start of the planning routine, the sub-aperture radius is calculated using (3.1) or (3.2) and the reference optic information. This provides information on how large the testing footprint is expected to be on the SUT when the interferometer is nulled. The part edge is then found to establish the measurement plan boundary. This is necessary in order to calculate the number of test locations required for full SUT coverage. Knowledge of the part centre from the design file is used to define the first test location and also to provide the (x,y) location of the SUT spherical origin. This has been defined in (3.3) and (3.4) for clarity.

The co-ordinate origin is defined as the SUT centre at the part surface as this will also define the machine co-ordinate origin, and minimises the number of subsequent offsets which must be applied. Figure 3.6 shows an example convex surface viewed in the X-Z plane. The red arc indicates the outline of the central sub-aperture.

$$C = [0,0,0] \quad (3.3)$$

Where C is defined as the SUT centre at the part surface.

$$O = [0,0,R_{SUT}] \quad (3.4)$$

Where O is defined as the part centre of curvature and R_{SUT} is the SUT ROC, which is negative for convex parts.

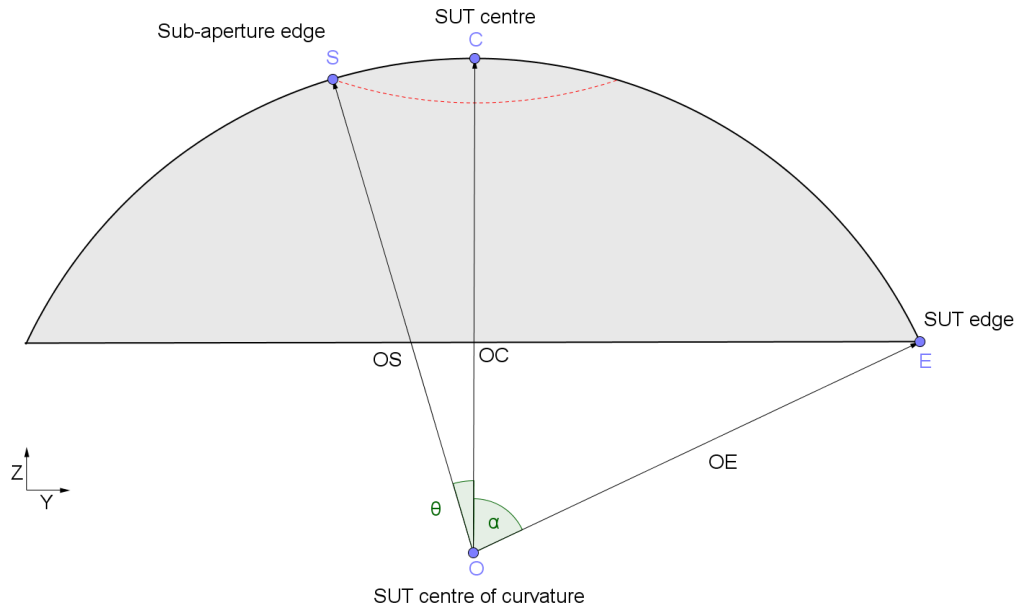


Figure 3.6: Sub-aperture rotation calculation schematic

Due to the spherical shape of the SUT, the first sub-aperture on subsequent rings may be placed by making an incremental rotation from the first sub-aperture position about the X-axis by an angle ϑ , which is effectively an elevation change.

This elevation angle is found by first calculating the elevation change to move from the part centre to the edge of the first sub-aperture, S given by (3.5).

$$S = [0, R_{spherical}, Z'] \quad (3.5)$$

Where Z' is found by subtracting the x and y components from the design file X and Y-meshes respectively and finding the indices of the resultant minimum. These indices are looked up in the design file Z-mesh to provide the nearest Z-axis value on the surface.

The SUT edge location is located in (x,y) at the SUT perimeter location found to be the furthest from the part centre. Although this may not lie along the Y-axis due to SUT orientation in the design file, this location is used only to calculate the

maximum number of expected sub-apertures to allow memory pre-allocation. The (x,y) position of the SUT edge, E , furthest from the part centre, C , is found by computing the distance between each perimeter point and the centre and finding the maximum.

$$E = [0, \frac{D_{SUT}}{2}, Z''] \quad (3.6)$$

Where D_{SUT} is the part diameter and Z'' is the height of the SUT edge, found in the part mesh. The use of all perimeter co-ordinates increases calculation time but removes sensitivity to SUT orientation in the design file. Figure 3.7 shows an example in which the top image is the result of a search using all perimeter co-ordinates, and the bottom a search using only points lying along the X and Y-axes. The SUT perimeter is shown in blue with the red and green points representing E . The area inside the dashed circles indicate the resultant measurement coverage. Measurement planning using the bottom search technique would result in the SUT corners being missed from measurement.

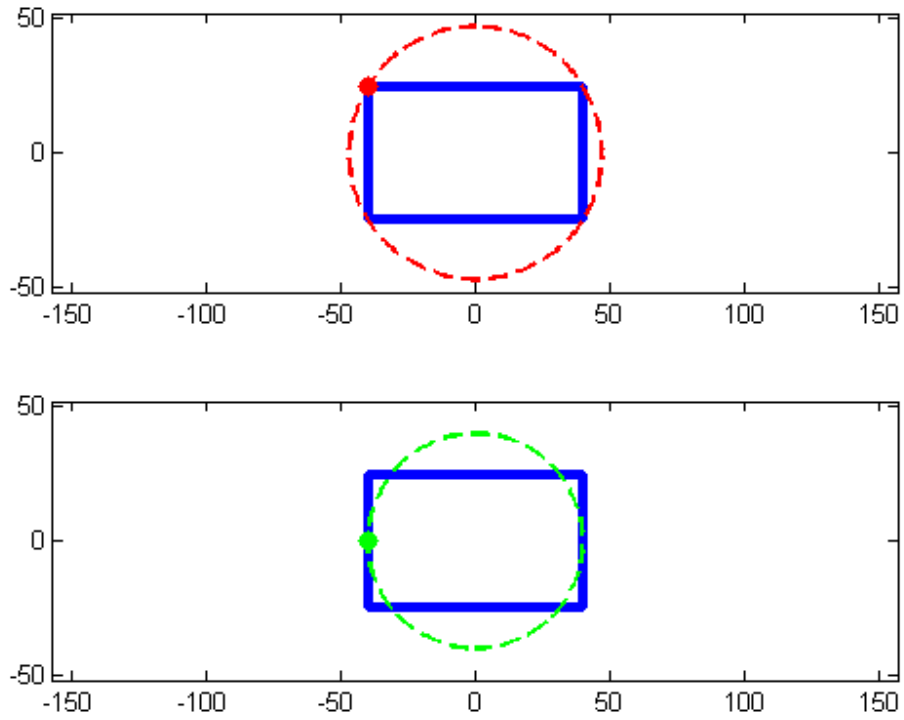


Figure 3.7: SUT centre to edge distance calculation (Top) using all points on perimeter (Bottom) using points located along X-axis only

With the fundamental locations in the measurement geometry defined, it is possible to compute vectors OC , OE , and OS indicated in Figure 3.6. Where OC is the SUT centre-of-curvature to part centre vector, OE is the SUT centre-of-curvature to part edge vector and OS is the SUT centre-of-curvature to sub-aperture edge vector. Therefore, the elevation increment angle, ϑ , is given by (3.7).

$$\theta = \cos^{-1} \left(\frac{\vec{OC} \cdot \vec{OS}}{|\vec{OC}| |\vec{OS}|} \right) \quad (3.7)$$

Similarly, the angle between OC and OE vectors, α , is given (3.8).

$$\alpha = \cos^{-1} \left(\frac{\vec{OC} \cdot \vec{OE}}{|\vec{OC}| |\vec{OE}|} \right) \quad (3.8)$$

The number of concentric sub-aperture rings, N_{rings} , is then given by (3.9).

$$N_{rings} = \left\lceil \frac{\alpha}{\theta(1 - \tau)} \right\rceil \quad (3.9)$$

Where τ is the overlap parameter input by the user, expressed as a decimal (0.5 for 50% overlap). This reduces the incremental elevation angle to allow overlap between sub-aperture rings. This overlap level can only be assured for the first row of sub-apertures, which are placed along a single axis. As rotations about the Z-axis are applied to create testing locations around each ring, the overlap level varies. However, provided the SUT is covered completely, no variation in measurement stitching quality has been observed, as many sub-apertures usually overlap the same inter-ring location, producing an averaging effect during data recombination. The number of rings, N_{rings} , is rounded up, to ensure adequate SUT coverage at the part edge.

Assuming the first sub-aperture is located at the part centre, it is possible to define a row of sub-apertures along a single axis between the SUT centre and edge, as shown in Figure 3.8. Each sub-aperture indicates the first test location at a new concentric ring and has the user specified overlap with those adjacent.

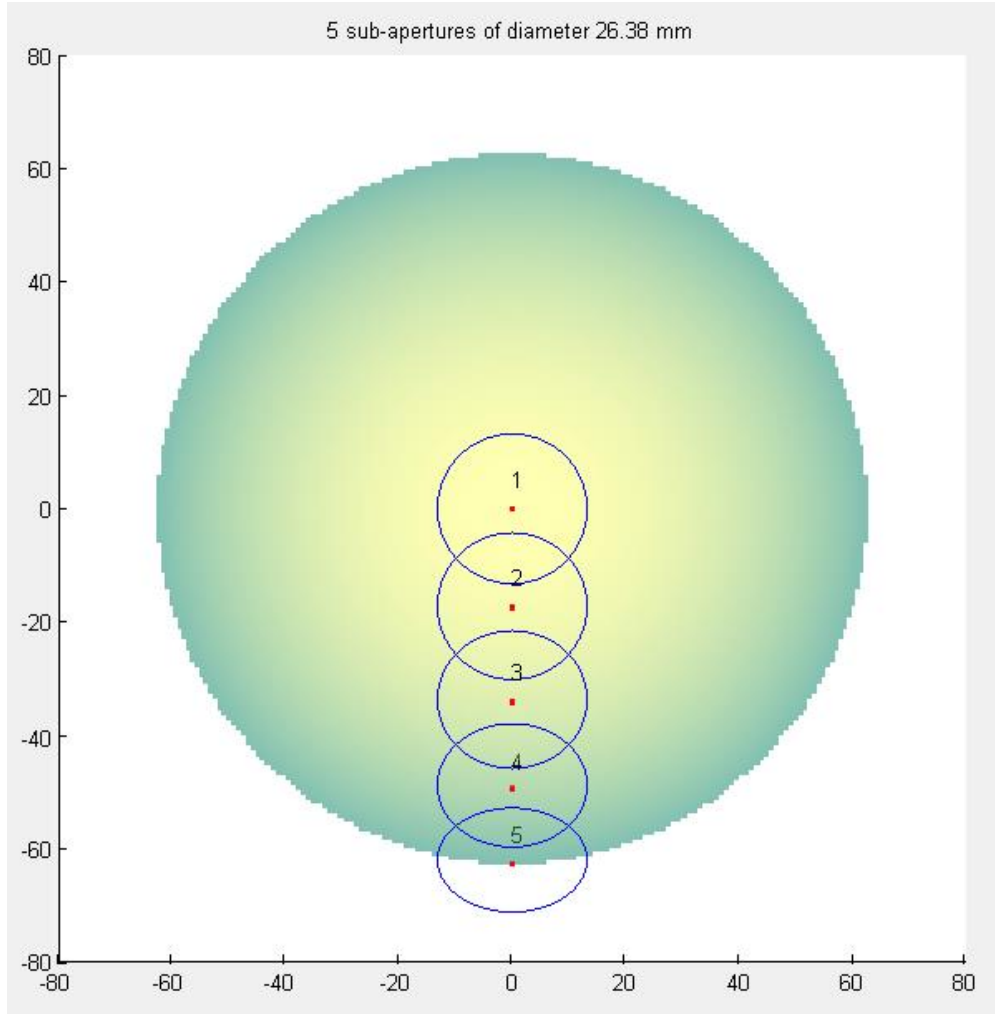


Figure 3.8: First sub-aperture at each ring of measurement plan

The radius of each concentric sub-aperture ring is computed by performing a rotation of the first sub-aperture location, about the X-axis by the incremental elevation, ϑ , for each ring in turn, given by (3.10). This is required for calculation of the incremental azimuth rotation angle, ϕ , used to place sub-apertures around each ring.

$$\begin{bmatrix} x_i' \\ y_i' \\ z_i' \end{bmatrix}_{i=1 \rightarrow N_{rings}} = \begin{bmatrix} 1 & 0 & 0 \\ 0 & \cos((i-1)\theta_i) & -\sin((i-1)\theta_i) \\ 0 & \sin((i-1)\theta_i) & \cos((i-1)\theta_i) \end{bmatrix} \begin{bmatrix} x_i \\ y_i \\ z_i \end{bmatrix} \quad (3.10)$$

Where i is concentric ring index number and N_{rings} is the number of rings. The ring radius is provided by y_i' , which may be used to calculate ϕ . Figure 3.9 shows an

example arrangement of a sub-aperture ring, indicated by the dashed line. Two sub-apertures are shown in red with centres placed upon the sub-aperture ring. The angle ρ is the azimuth rotation angle which is required to move from the centre to the edge of one sub-aperture, given by (3.11). Assuming two sub-apertures are placed with their centres lying on the concentric ring and arranged with perimeters just touching, the angle required to rotate from one centre to the next about the Z-axis is 2ρ . Figure 3.10 shows an example sub-aperture layout with a single ring on which the sub-apertures are just touching. The sub-apertures appear elliptical due to viewing an (x,y) projection of a 3-dimensional arrangement.

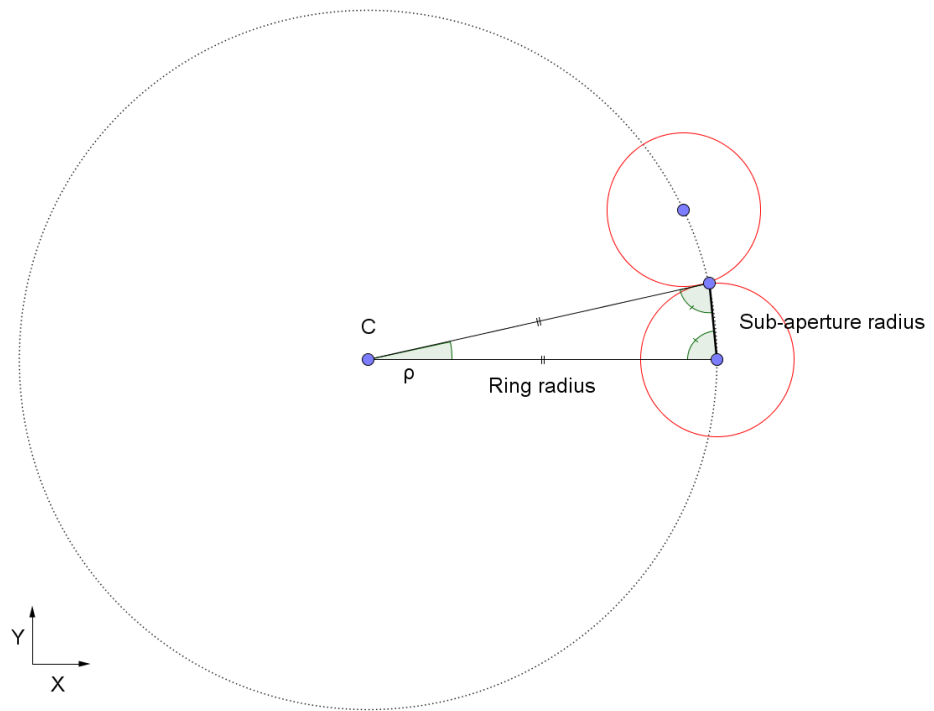


Figure 3.9: Ring azimuth angle calculation schematic

$$\rho_{spherical} = 2\sin^{-1}\left(\frac{R_{spherical}}{2y_i'}\right) \quad (3.11)$$

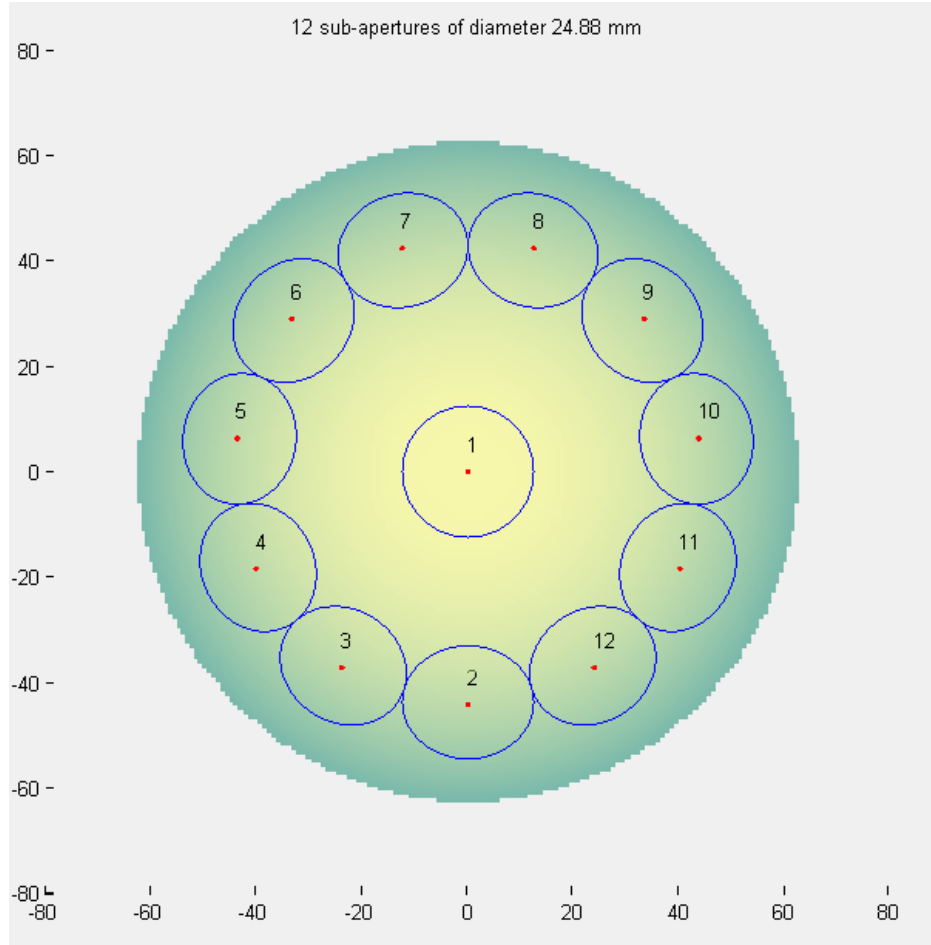


Figure 3.10: Single ring spherical measurement plan

The incremental azimuth angle to move between adjacent sub-apertures with overlap is given by (3.12).

$$\varphi = 2\rho(1 - \tau) \quad (3.12)$$

Where τ is the overlap input by the user to the GUI, represented as a decimal (e.g. 0.5 for 50%). The number of sub-apertures to be placed around a given ring, $N_{azimuth}$, is calculated using (3.13).

$$N_{azimuth} = \left\lceil \frac{2\pi}{\varphi} \right\rceil \quad (3.13)$$

The values resulting from (3.10), (3.12), and (3.13) are used to populate a sub-aperture angles table. The angle calculation step has been separated in code from

the sub-aperture layout procedure because the user has the ability to manually manipulate the sub-aperture placement angles. The sub-aperture angles table is a 4 column by N_{rings} -row table formatted as shown in Table 3.5. An example sub-aperture angles table is also given in Table 3.6 for a measurement plan with four concentric rings of sub-apertures.

Table 3.5: Sub-aperture angles table

Column number	Contents	Description
1	Index	Double. Incremental number providing the ring index.
2	Elevation angle	Double. Absolute elevation angle, specified in degrees with the Z-axis defined as zero.
3	Number of sub-apertures	Double. Used to calculate the incremental azimuth angle for each ring
4	Y-axis offset	Resultant y_i' from calculation of elevation. Provides the ring radius.

Table 3.6: Example sub-aperture angles table

Ring number	Elevation (°)	Sub-apertures	Y-axis offset (mm)
1	0	1	0
2	11.4928	6	-17.3482
3	22.9855	12	-34.0007
4	34.4783	17	-49.2898

Following calculation of the sub-aperture angles information, sub-aperture placement is carried out. This process follows procedure indicated in Figure 3.11 using the information contained in the sub-aperture angles table. A centre sub-aperture is first defined and recorded. This point is then rotated about the x-axis by the elevation angle for the first ring and recorded as the first sub-aperture in the second ring. Azimuth rotations are then performed and recorded as more sub-apertures. This process is repeated for each ring until a complete plan has been

formed. Once a set of sub-aperture centre co-ordinates for the plan has been calculated, the local surface normal vector for each location is also found. This is required to allow inverse kinematics calculation to transform the measurement plan co-ordinates into machine axis values. An example plan without overlap optimisation is shown in Figure 3.12, created by inputting Table 3.6 into the spherical sub-aperture planning procedure.

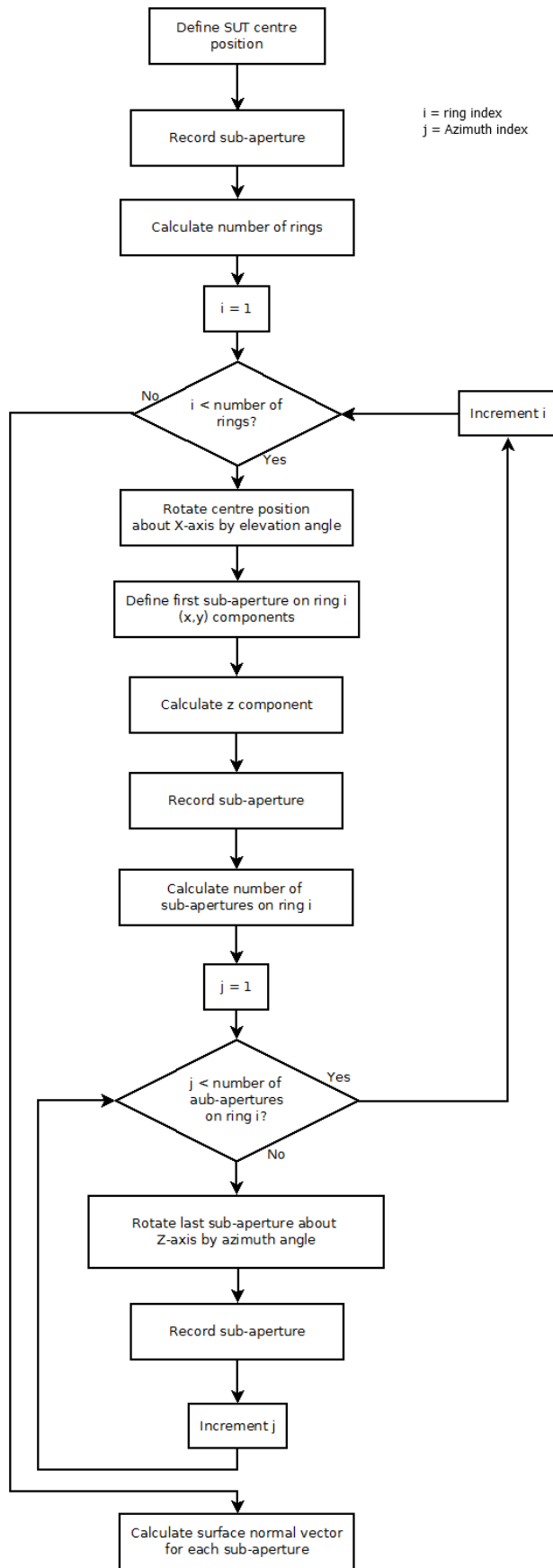


Figure 3.11: Spherical sub-aperture planning work flow

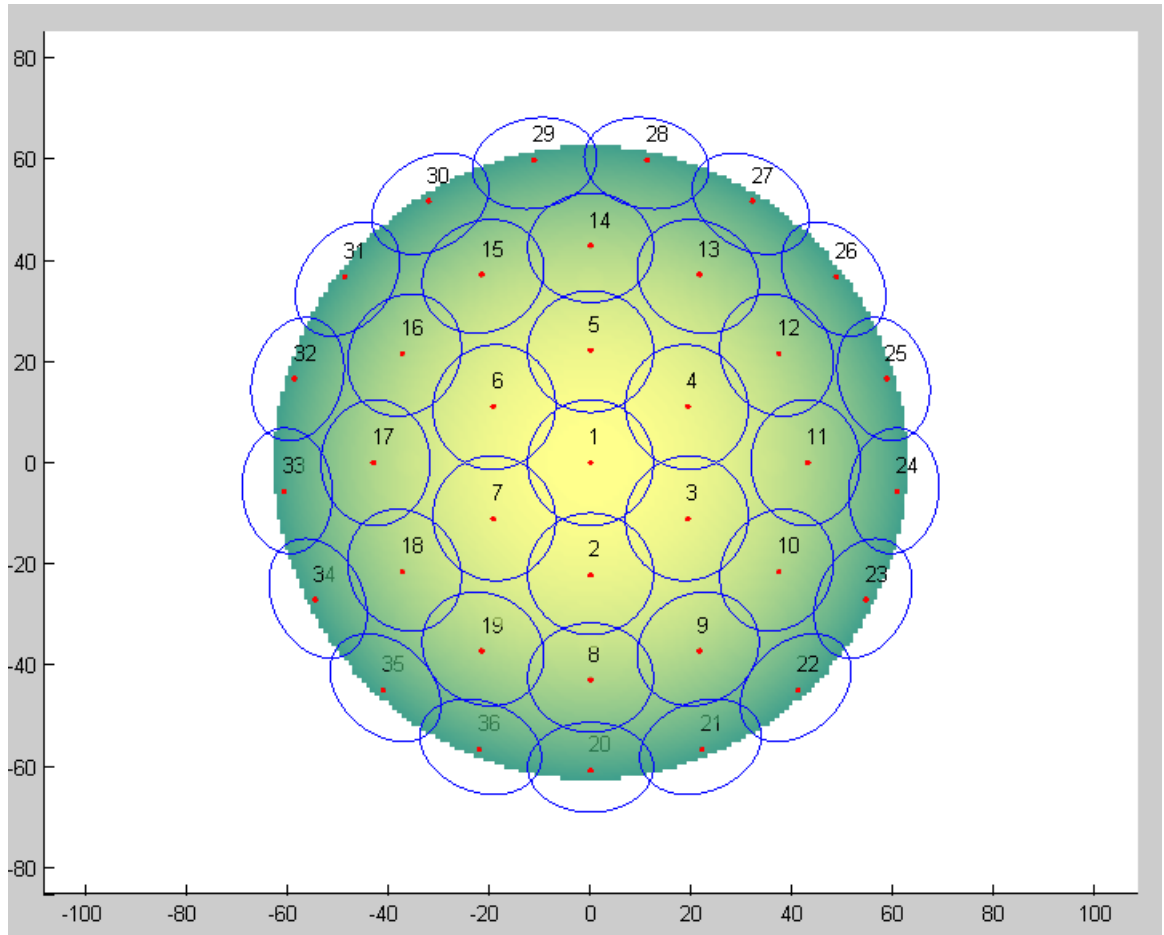


Figure 3.12: Spherical sub-aperture measurement plan prior to coverage optimisation and using a small overlap value

Although sub-aperture placement angles have been calculated to provide the specified level of overlap, complete coverage of the SUT is not assured. Following planning, the measurement plan must be tested to establish if the current level of overlap is sufficient to produce full coverage. The measurement plan shown in Figure 3.12 has been created without the use of overlap optimisation. In this case, an overlap of 10% was specified, which is insufficient to provide complete SUT coverage. If this plan were measured, the synthetic dataset obtained from stitching would contain gaps and be unsuitable for use to compute further corrective polishing. It is possible that the user can incrementally increase the overlap parameter manually, until complete coverage of the SUT is achieved, however, the

ethos behind the simple planning mode is that *Metrology Designer* will produce a basic plan which can be used immediately. The process of optimising surface coverage is discussed in Section 3.2.1.3.

3.2.1.2 Plano Sub-aperture Measurement Planning

The plano measurement planning regime is similar to that of spherical measurement planning, with the exception that no elevation changes are required. In this case the number of rings required is given by (3.14).

$$N_{plano\ rings} = \left\lceil \frac{R_{SUT}}{2R_{plano}(1 - \tau)} \right\rceil \quad (3.14)$$

Where R_{SUT} is the distance from the SUT radius. R_{plano} is given by (3.2) and τ is the user specified overlap. $N_{plano\ rings}$ is rounded up to ensure at sufficient rings are used to cover the SUT. The ring radii are calculated using (3.15).

$$R_{plano\ ring_{i=1:N_{rings}}} = 2(i - 1)R_{plano}(1 - \tau) \quad (3.15)$$

Where i is the ring index. To complete the plano sub-aperture angles table, the number of sub-apertures on a given ring is calculated in the same way as for spherical SUT testing, using (3.12) and (3.13), following the calculation of ρ , given by (3.16).

$$\rho_{plano} = 2 \sin^{-1} \left(\frac{R_{plano}}{2R_{plano\ ring_i}} \right) \quad (3.16)$$

Where ρ_{plano} is the azimuth rotation required to move between a sub-aperture centre and edge on a concentric ring, shown in Figure 3.9. The plano sub-aperture planning routine is shown in Figure 3.13. The plano planning algorithm differs in that the ring and elevation step of the spherical plan has been replaced by a

translation, owing to the difference in SUT form. The sub-aperture overlap optimisation and manual adjustment procedures in the following sections are generalised to allow the same code to serve both planning routines. This generalisation of code to support multiple planning applications enables a modular approach to be taken to implementing new metrology devices in the existing architecture.

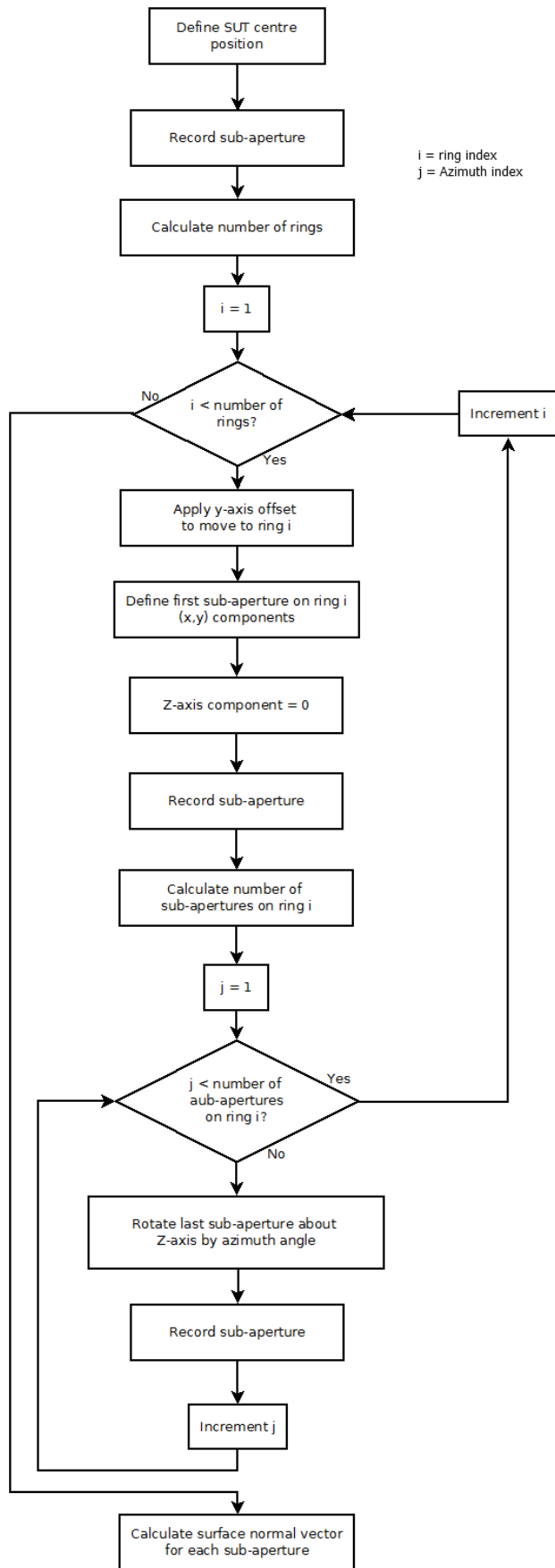


Figure 3.13: Plano sub-aperture planning work flow

3.2.1.3 *Overlap optimisation*

Overlap optimisation is the process of ensuring that any sub-aperture measurement developed using the simple design mode of *Metrology Designer* provides complete SUT coverage, and therefore yields useful sub-aperture measurement data. Useful data is defined as that which may be stitched to provide a representative full aperture map of the surface and can be used to generate tool paths for corrective polishing. The overall planning process for sub-aperture measurement is shown in Figure 3.14. This process includes the calculation of sub-aperture rotation angles and the layout processes discussed earlier, as well as checking to ensure complete surface coverage. If the operator were to enter a value of overlap which was too small to provide a measurement plan with complete coverage of the SUT, the planning routine would enter an iterative loop, increasing the overlap parameter by 1% on each pass until a viable measurement plan is computed. The final overlap parameter is used to replace the user input value on the GUI, to provide feedback. Finally, the testing locations are populated into a table to be saved in an OMM file.

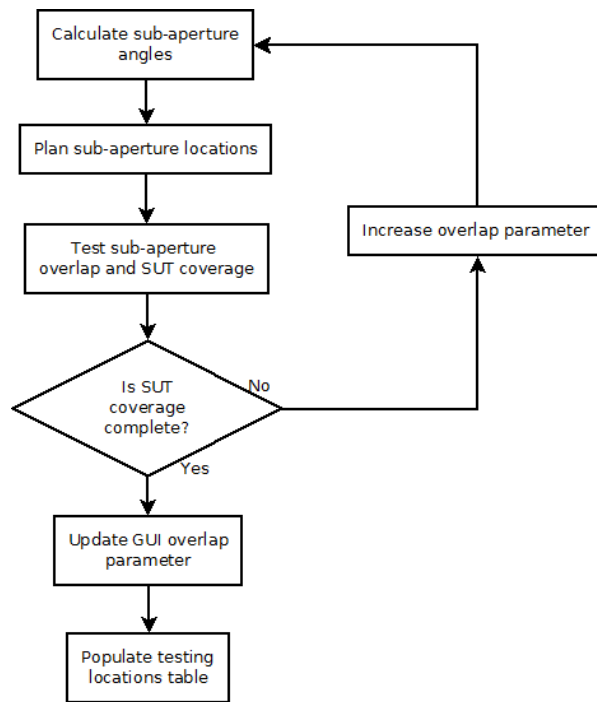


Figure 3.14: Measurement plan overlap optimisation work flow

SUT coverage checking is carried out by first creating a mask of zeros and ones using the part surface mesh dimensions. Figure 3.15 shows an example mask, red representing ones and blue for zeros. This process provides only a projection in the X-Y plane and so any information beyond the hemisphere is lost. *Metrology Designer* therefore can only support measurement requiring an elevation less than 90°.

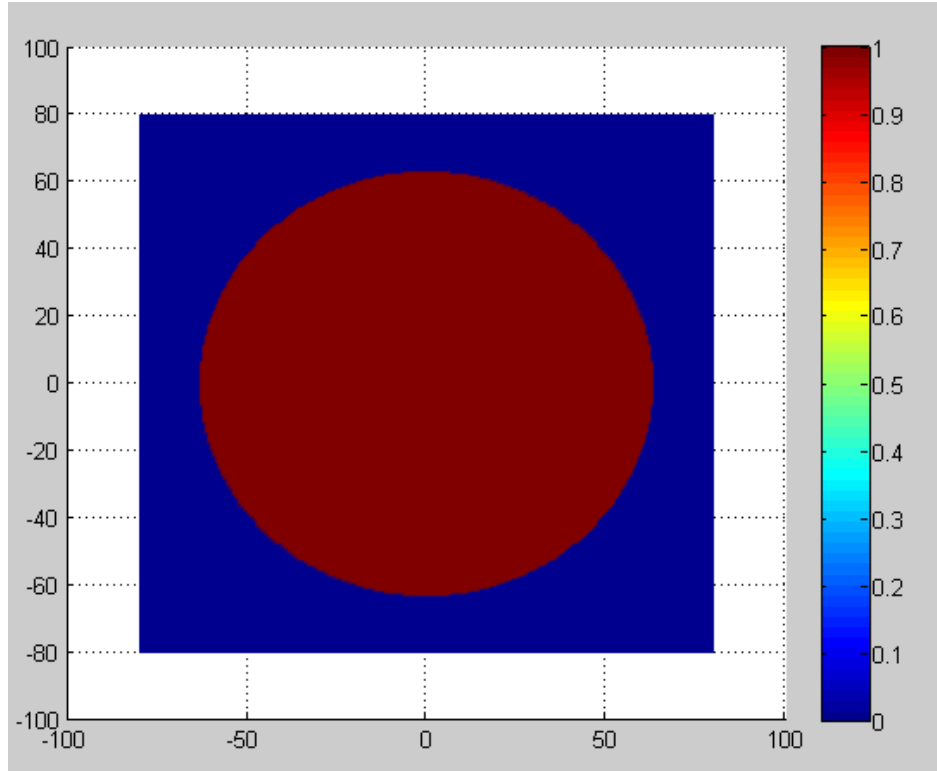


Figure 3.15: SUT mask used for SUT coverage optimisation

A mask is then created for each sub-aperture in turn. In the case of spherical surfaces, the sub-apertures may be rotated out of the X-Y plane when not at the part centre. Therefore, a simple circular mask cannot represent a sub-aperture for a spherical SUT. As the circle is a special case of an ellipse, it is possible to generally describe the sub-aperture shape in the X-Y plane with an ellipse for all SUT form types, as given by (3.17).

$$\begin{aligned}
 ax^2 + bxy + cy^2 - (2ax_0 + by_0)x - (2cy_0 + bx_0)y + ax_0^2 \\
 + bx_0y_0 + cy_0^2 = 1
 \end{aligned}
 \tag{3.17}$$

Where (x_0, y_0) is the ellipse centre co-ordinates and a, b, and c are given by (3.18), (3.19), and (3.20) respectively.

$$a = \frac{\cos^2(\gamma)}{r_A^2} + \frac{\sin^2(\gamma)}{r_B^2}
 \tag{3.18}$$

$$b = \frac{2 \cos(\gamma) \sin(\gamma)}{r_A^2 - r_B^2} \quad (3.19)$$

$$c = \frac{\sin^2(\gamma)}{r_A^2} + \frac{\cos^2(\gamma)}{r_B^2} \quad (3.20)$$

Parameters r_A and r_B are the major and minor radii of the sub-aperture, projected onto the X-Y plane. In the sub-aperture mask, all points within the sub-aperture are defined as ones and those outside zeros. Figure 3.16 shows an example sub-aperture mask in the upper plot and the sub-aperture from which it was generated in the lower plot. The sub-aperture mask consists of a mesh the same size as that of the design file. The SUT mesh in the bottom image appears circular due to the areas around surface being padded with NaNs, which are not plotted by Matlab.

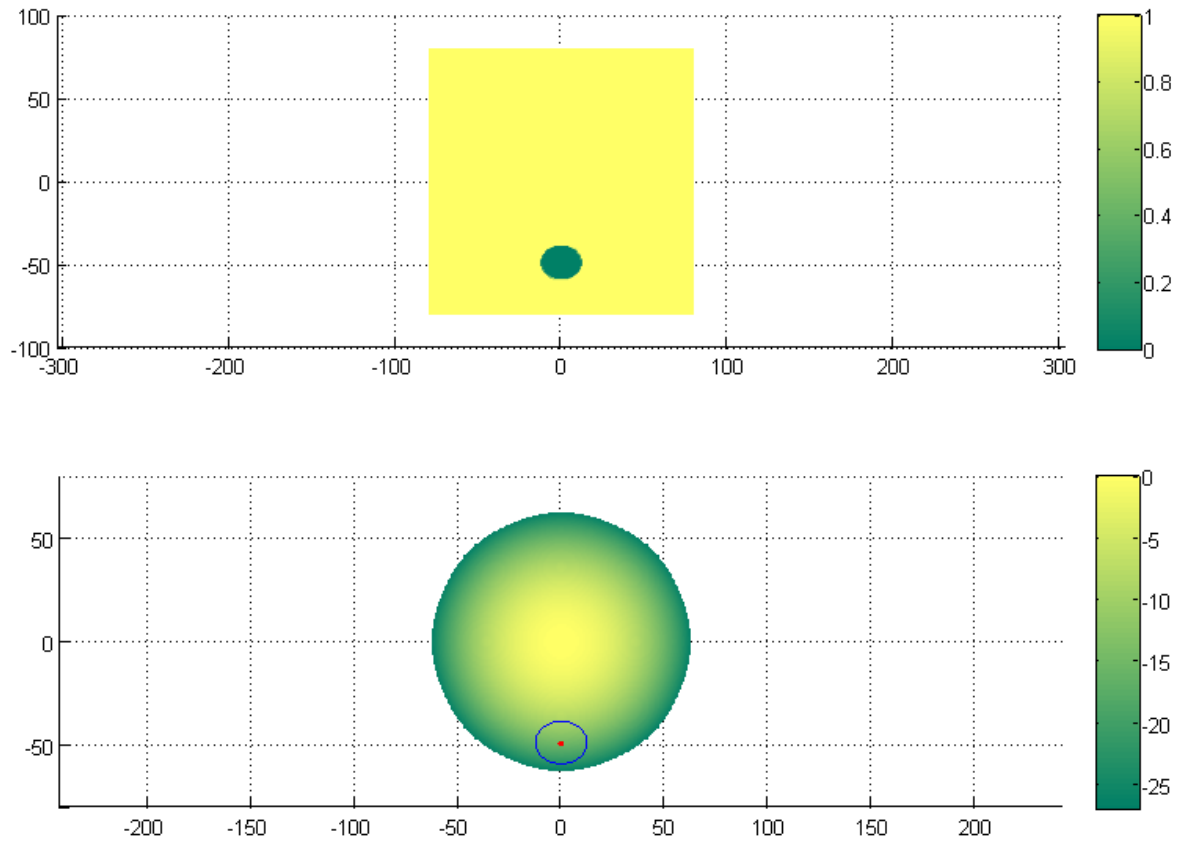


Figure 3.16: (Top) Sub-aperture mask used for SUT coverage optimisation and (Bottom) the equivalent sub-aperture placed on the SUT

The sub-aperture mask is then multiplied with the SUT mask, resulting in the area covered by the sub-aperture being removed from the resultant mesh, as shown in Figure 3.17. This process is carried out for each sub-aperture in the measurement plan. The resulting mesh is then summed. If the SUT mask is completely covered by sub-apertures, the sum of the resultant mesh is zero. If the sum of the SUT mask is greater than zero, the overlap parameter is increased and planning is carried out again. This process is iterated until the SUT is completely covered. Figure 3.17 shows the result of multiplying the SUT mask of Figure 3.15 with the sub-aperture mask of Figure 3.16, producing a cut out region. The overlap checking routine is also used to remove sub-apertures which lie outside the SUT. Such testing locations may occur due to rounding up the number of rings (N_{rings}) during the planning process. If

the sum of the resultant mesh does not change following multiplication with a sub-aperture mask, the sub-aperture is discarded.

Allowing measurement locations which do not lie on the SUT to remain in the testing plan is both inefficient and risky during automated measurement as the interferometer may return bad data. This may result in large, erroneous correction moves during alignment, which risks SUT and device damage.

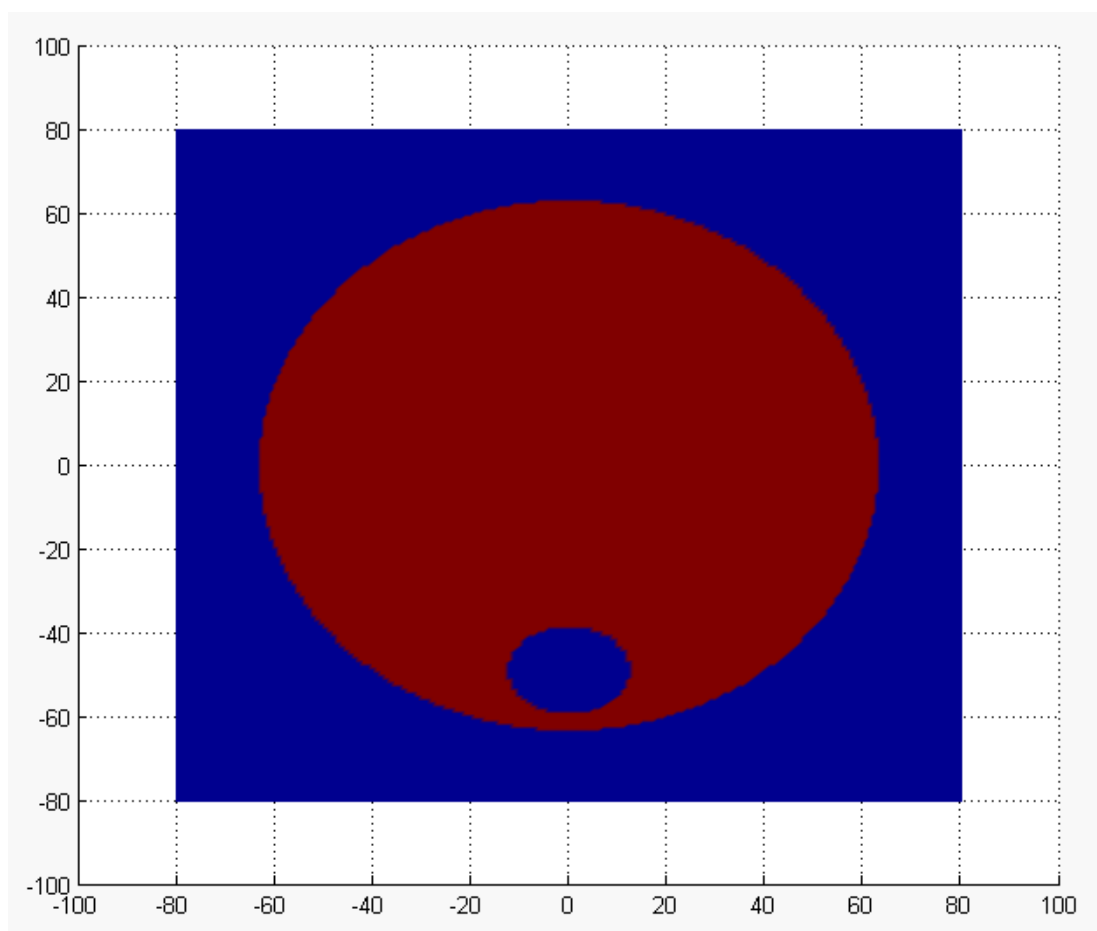


Figure 3.17: Resultant coverage mask following SUT mask multiplication with a single sub-aperture mask

This method of optimisation is inefficient as the measurement planning process may be carried out multiple times for overlap values far below that required for SUT coverage. The overlap value is currently incremented by 1% for each pass of the planning algorithm. When creating a design using a high F# transmission optic

and large diameter SUT, measurement planning can take a long time (2-3 minutes) due to the large number of small sub-apertures. It is possible to reduce planning time (<1 minute for large plans) by using a method such as gradient decent optimisation [88], and this is an area of expected future development. However, the incremental method has been found to be stable and, provided the correct R_{SUT} value is obtained, performs reliably. Calculation of an undersized R_{SUT} , due to problems in the search algorithm can cause optimisation to become stuck as the plan can never cover the SUT.

3.2.2 Point measurement planning

Metrology Designer is also used for the development of point measurement plans, for devices such as the STA. As this device is used to look at texture only, stitching of measurements is not required and therefore measurement overlap is not necessary. These measurements are performed over a small areas (typically < 1 mm²) and are therefore modelled as discrete points.

The planning process for point measurement is broadly similar to that of sub-aperture measurement. This allows a modular approach to measurement planning routines and simplifies the development process by allowing a standard format of function arguments and returns.

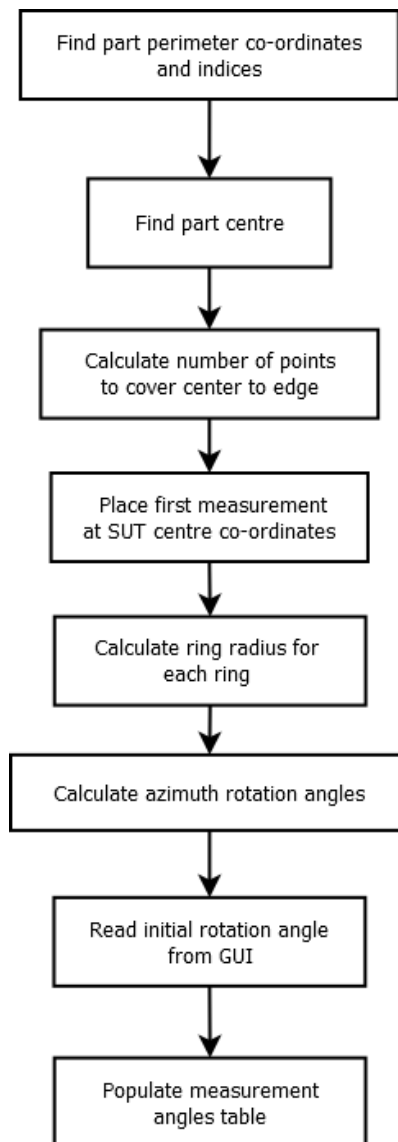


Figure 3.18: Point measurement angles table planning

Point measurement utilises a test location angles table, in a similar way to sub-aperture measurement design, however a bulk plan rotation is incorporated. This allows the operator to carry out measurement along straight edges, such as those of the hexagonal E-ELT segments, when using a square grid planning mode. Such measurement can aid in the characterisation of texture near the part edge, where different processing steps interact. Both concentric ring and square grid mode calculate measurement points so that a uniform point density is maintained across the SUT, when using simple planning mode. As IRP polishing tool paths often follow

a raster pattern across the surface, it should be ensured that the point spacing is not an integer multiple of raster track spacing as texture measurement may encounter a periodic variation, which has not been completely randomised by subsequent process runs. Figure 3.19 shows an example point measurement plan created by *Metrology Designer*.

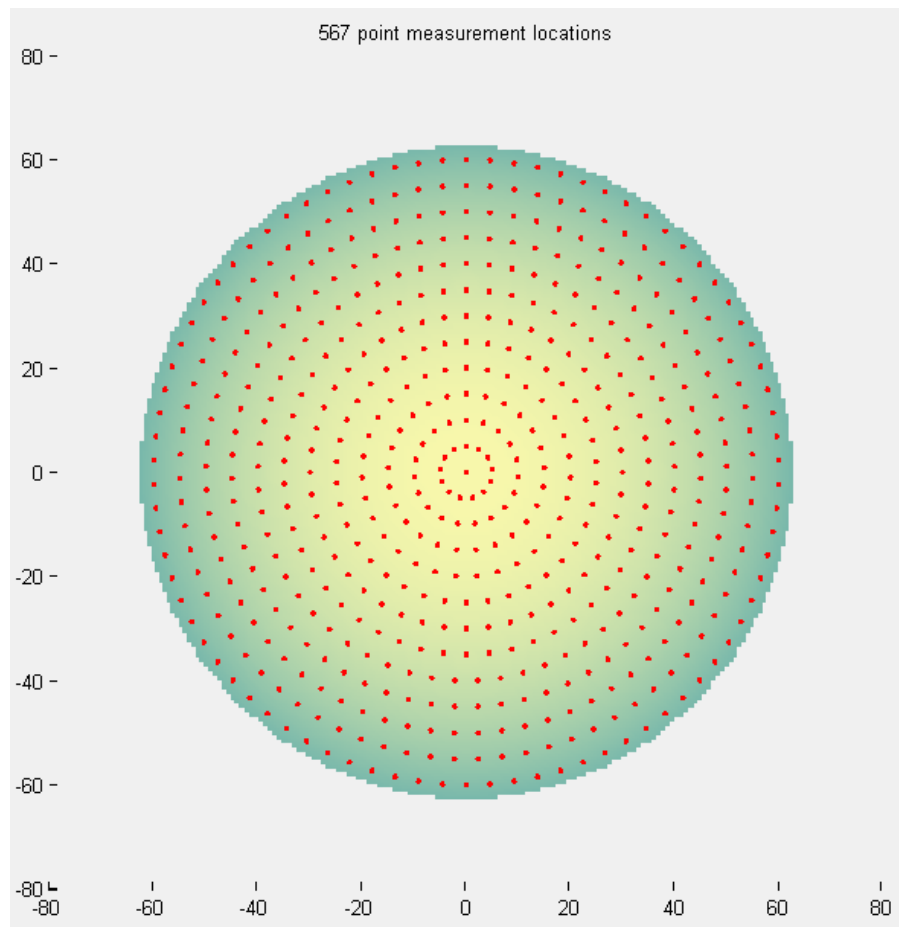


Figure 3.19: Point measurement plan - concentric rings

3.2.3 Manual Editing of Sub-Aperture and Point Measurement Plans

As well as the simple planning mode discussed, it is possible for the user to manually adjust azimuth and elevation angles between testing locations and create plans with incomplete coverage, in the case of sub-aperture measurement. This is often desirable in practical manufacturing due to aberrations such as edge roll-off,

where the slope at the part edge becomes so steep fringes become aliased or where the surface may be damaged. In this situation, interferometric measurement may become unreliable due to data dropout and so other measurement techniques are employed, such as a scanning probe. These regions should then be avoided during measurement due to unpredictable behaviour during automatic alignment.

In order to facilitate the manual adjustment of the measurement plan, the test location angles editor is used (Figure 3.20). This allows the user to directly edit the test point angles table to adjust placement and remove rings, as required. This menu is used for both sub-aperture and texture measurement planning.

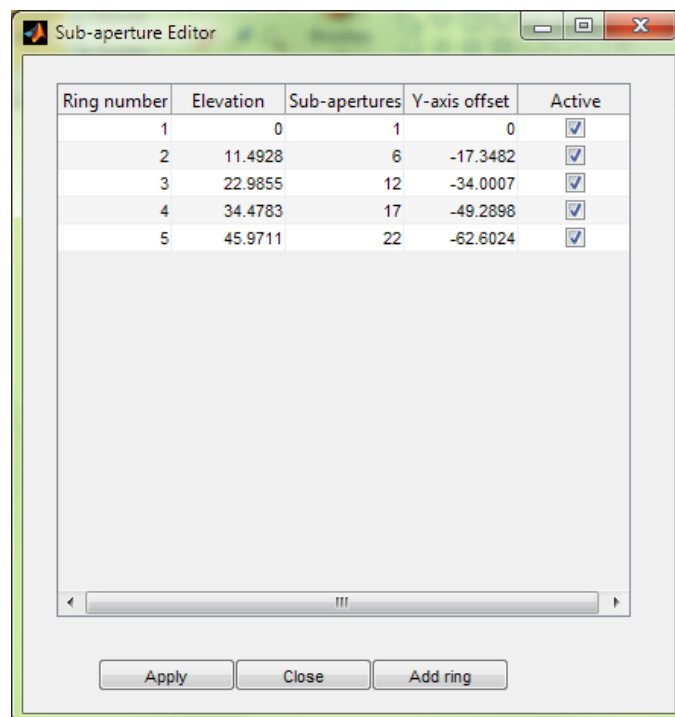


Figure 3.20: Manual sub-aperture measurement placement window

In order to adjust the plan, the user may edit some of the entries in the table shown in Figure 3.20, depending upon the SUT form. The sub-apertures column can be adjusted to vary the number of testing locations on a given ring. To adjust the inter-ring spacing for spherical tests, the elevation angle is adjusted. In the case of plano,

testing, the Y-axis offset is adjusted as the elevation value is always equal to zero. When the test location angles editor has been used to manually configure a plan, overlap optimisation is disabled (for sub-aperture measurement) and the calculation of the sub-aperture angle table is skipped and a table is generated from the user inputs to the angles editor window.

When used for adjusting point measurement plans, the editor menu is configured as shown in Figure 3.21. The user may also adjust the plan rotation to allow measurement along straight part edges. Should the user adjust any value in the plan rotation column, all rows are updated with the same value, ensuring measurement point density remains uniform over the surface.

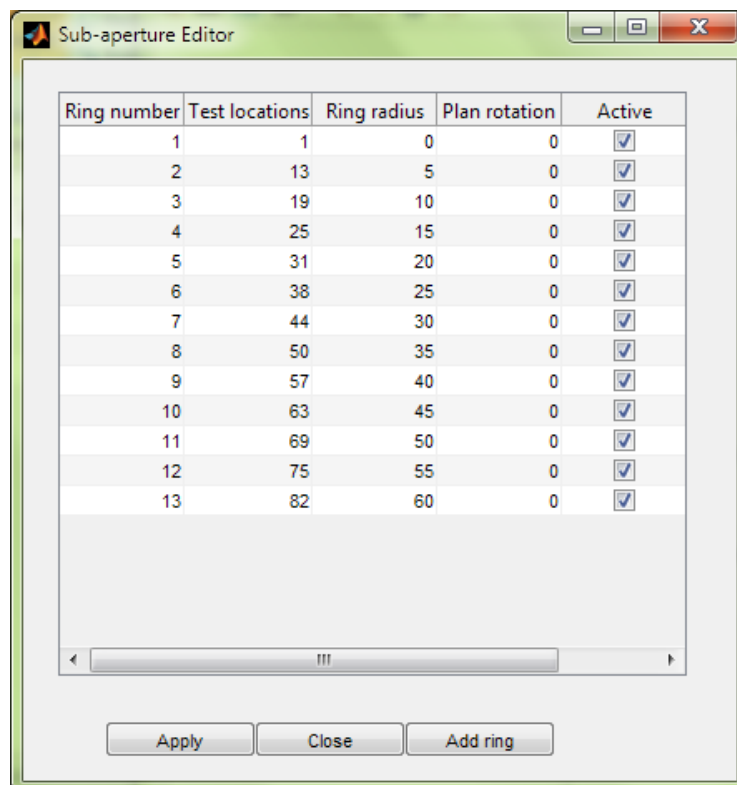


Figure 3.21: Manual point measurement placement window

3.2.4 Measurement Plan Description File Generation

The final step in the metrology planning process is to package the measurement plan along with the device file and optic information into an On-Machine Metrology (OMM) file. At this point the user should also select the correct system configuration from the drop down box on the *Metrology Control Suite* GUI. The system configuration file contains parameters which tell the control software how to use the hardware intended to carry out measurement. Modification of the system configuration file can greatly alter system behaviour and potentially cause a safety hazard and so the file is encrypted using the 128-bit AES standard [89]. The decryption key is hard coded into the *Metrology Control Suite* so the user cannot access the system configuration.

The device and system configuration are packaged with the measurement plan as a safety measure, to prevent the operator using an OMM file with hardware which may not support the measurement.

3.3 Conclusion

This chapter has outlined the procedures used for planning measurements for both the STA fitted to the IRP machine and the Metrology Station. The example devices have different requirements of the measurement planning process, as follows. The STA requires only a number of discrete points, evenly distributed across the surface to allow the metrologist to make an assessment of the behaviour of the process applied to the SUT. The Metrology Station system requires a series of sub-apertures, laid out with sufficient overlap to allow the stitching algorithm to reassemble a complete map of the surface. While the requirements of the two

systems differ, they have both been accommodated in the same application with the use of configuration files. This approach allows a common interface which may support many different metrology types while minimising operator training for new metrology systems. The OMM file is analogous to the polishing toolpath generated by *Zeeko TPG*, however, instead of directly instructing the system hardware to move, the metrology plan is interpreted by *Metrology Controller*. *Metrology Designer* fits into the overall work flow of *Metrology Control Suite* as shown in Figure 3.22. The development of *Metrology Controller* is discussed in Chapter 4.

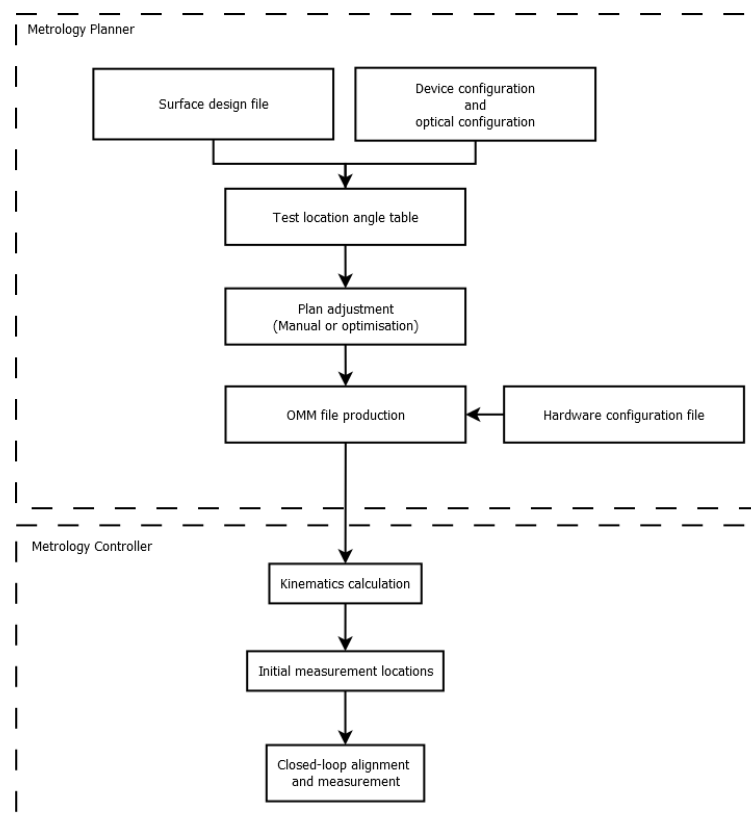


Figure 3.22: Overall work flow of *Metrology Control Suite*

4 Metrology Controller Development

Metrology Controller is an application, developed by the author as part of the *Metrology Control Suite*, which instructs the hardware forming the metrology system what to do throughout the measurement process in order to achieve the measurement plan outlined in Chapter 3. In order for the application to know what hardware is available, how to communicate with it, and where to go to carry out measurement, an OMM file generated using *Metrology Designer* is loaded. The metrology control system follows the instructions contained within the OMM file in a similar manner to the IRP machine following those contained within the NC file. The key difference between the two systems is the metrology control system uses feedback to dynamically generate G-code to correct residual alignment error found following arrival at a test location.

With the OMM file loaded, the measurement configuration is displayed to the user, allowing confirmation of the correct plan being used with the system. From the *Metrology Controller* GUI, the user can then alter various operating parameters such as measurement averaging level and the residual alignment error at which to begin measurement. If the OMM file is valid, the operator can connect the machine to the metrology system and commence measurement, following some set up procedures. This chapter will discuss the steps required to set up the measurement system of automatic metrology as well as how the system uses interferometer data as feedback to ensure proper alignment with the SUT.

4.1 Communication

Metrology Controller communicates with the CNC hardware available via a standard Ethernet connection [90]. The use of Ethernet allows direct communication with the CNC controller, as shown in Figure 4.1, allowing the metrology station to acquire status information and command CNC moves with minimal communication delay. The CNC console remains capable of overriding automatic metrology at any time and also displays the normal status information. However, the same information is accessed by the metrology console, allowing a single user interface for control and status monitoring of the entire system.

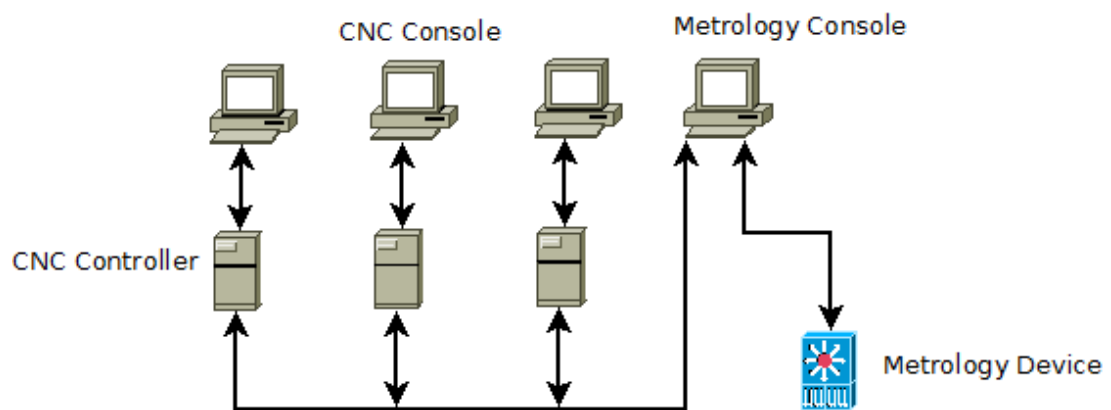


Figure 4.1: Direct Ethernet communication topology

The metrology devices used in systems discussed in this thesis have been manufactured by 4D technology and communication is carried out via a python web service running on the metrology console PC. Control commands are then sent to the device via HTTP over TCP/IP using a Soap protocol. As illustrated in Figure 4.1, this connection is kept separate from the CNC controller system on a separate interface provided by 4D. During system operation it is observed that measurement acquisition typically dominates the cycle time. The 4D Technology interferometers require up to 1 second to acquire a single frame, and depending upon

environmental stability and user accuracy requirements, an averaging level of 256 frames, for example, may be selected.

4.1.1 Web Service Error Handling

During operation it is common for the python web service to experience intermittent errors such as time outs, when a task duration exceeds that allowed by the control system. Such errors prevent the interferometer performing the requested tasks and so can terminate measurement. Therefore *Metrology Controller* includes error handling routines which detect that an error has occurred. The observed errors are typically transient, for example caused by large vibrations due to other activity in the manufacturing environment or electromagnetic interference. Though it is desirable to eliminate these phenomena, such disturbances are characteristic of performing metrology on-machine. *Metrology Controller* therefore reissues a failed command to the interferometer to allow measurement to continue.

It has been found in testing that the reissuing of commands is sufficient to allow the system to proceed with measurement. Occurrences of errors are logged for future debugging. The system configuration limits the number of times the same command may be reissued to prevent the system becoming stuck in a loop. Should this limit be exceeded, the *Metrology Controller* will abandon measurement. Errors resulting in automatic measurement being terminated by the control system typically result from incorrect measurement set up by the operator. Errors may be analysed by placing *Metrology Controller* into debugging mode, where all system information is output to the console (See Appendix 0).

4.2 Automatic Measurement Work Flow

When executing automatic measurement using *Metrology Control Suite*, measurement typically follows a standard work flow, as shown in Figure 4.2. Following an initial set up tasks, the system is placed into plan execution mode. From this point onward, the system requires no user intervention. Status information is presented via the *Metrology Controller* GUI to allow the operator to view progress. The measurement process may be paused or cancelled during execution at the user's request. The system can also take the decision to halt measurement if any errors occur from which the system cannot recover by itself. Such issues are reported to the user via the error logging system and *Metrology Controller* GUI status display, shown in Figure 4.3.

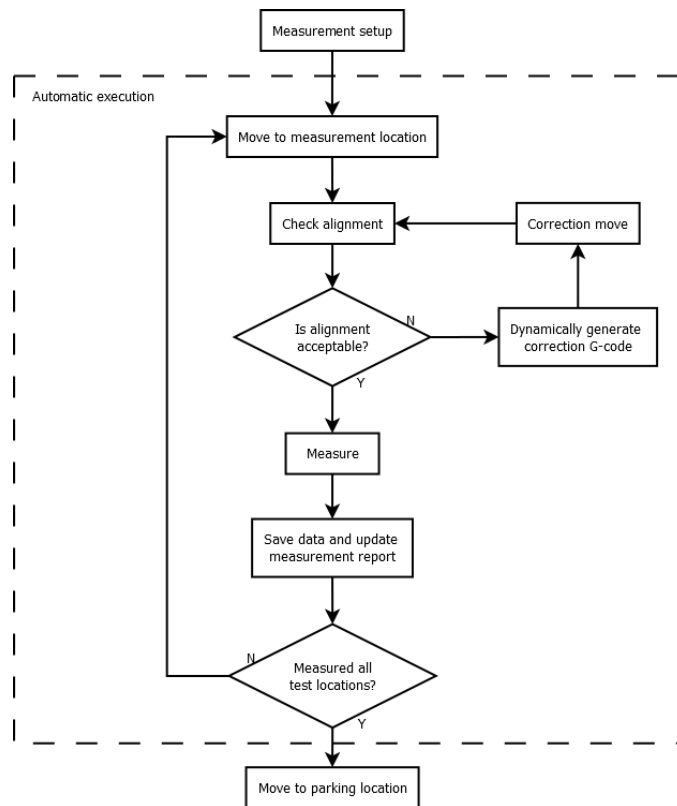


Figure 4.2: Overall automatic measurement work flow

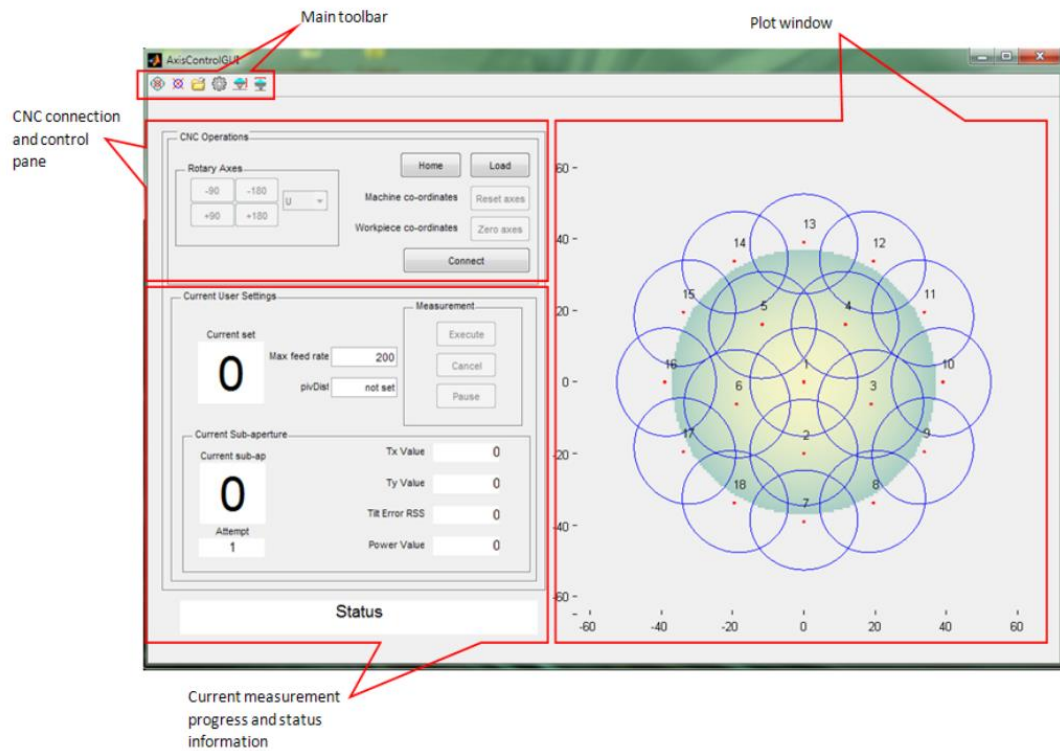


Figure 4.3: Metrology Controller main GUI screenshot

The remainder of this chapter discusses each of the main tasks contained in set up and automatic execution. The overall workflow is the same for both sub-aperture and texture metrology, however some of the specific tasks are dependent upon system hardware.

4.3 Measurement Setup

Measurement setup consists of the tasks carried out between applying power to the system and measurement execution. This can include optical setup of the measurement device, clocking of the SUT and defining the measurement coordinate system. Set up tasks are typically carried out with at least some user intervention and acceptable and reliable automatic operation depends upon their being performed correctly.

The set up tasks to be carried out are dependent upon the metrology system being used and the two example systems are discussed separately.

4.3.1 Sub-aperture Measurement

This section details the set up activities required prior to the automatic execution of sub-aperture measurement using the Metrology Station.

4.3.1.1 Part Clocking

When carrying out sub-aperture measurement, *Metrology Designer* places sub-apertures in a series of concentric rings as described in Chapter 3. This allows the system to rotate only the R-axis (Metrology Station table) when moving between sub-apertures on the same ring. In order to minimise subsequent correction moves at each measurement location, the SUT axis of symmetry should be coaxial with the rotary table axis. Should the SUT optical axis and the rotation axis have an angle between them, rotation of the R-axis will induce tilt and power error into the alignment at a new measurement location. Figure 4.4 shows an example test with an exaggerated error, θ .

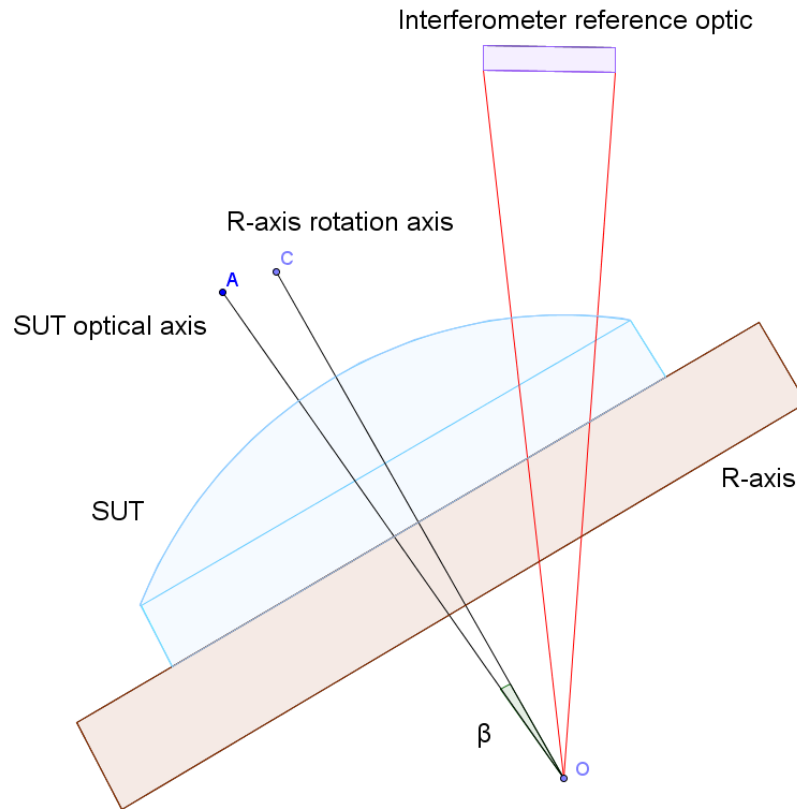


Figure 4.4: SUT optical axis alignment

The interferometer beam is shown in red and is confocal with the SUT centre of curvature (COC). Error between the optical axis and the R-axis can result from part wedge or the SUT not being centred on the table. Such a misalignment error does not typically prevent successful measurement but increases the number of alignment corrections required at each measurement location.

In order to minimise such setup error and aid the operator, *Metrology Control Suite* includes a semi-automatic procedure to enable the user to clock the part accurately to the R-axis. The operator first sets up the part and ensures there are non-aliased fringes in the interferometer FOV. Once the process is started, the system automatically nulls the interferometer to optimise alignment. The R-axis is then rotated by 180°, maximising the error in the return from the SUT. Figure 4.5 shows

a frame captured from the interferometer alignment camera using software written by C. W. King, displaying the reference surface return spot near the black cross-hair centre. The SUT return spot may be seen in the lower left quadrant. Unless the reference and SUT return spots are coincident and on the optical axis, no interference occurs and so measurement is not possible. The aim of the auto-clocking process is for the two return spots to remain coincident for any rotation of the R-axis.

Following the 180° R-axis rotation, if reference and return spot positions differ by more than a tolerance value (typically 5 pixels), the software instructs the operator to position the return spot on the green cross using the table translation (for spherical) or tilt (for plano) screws (shown in Figure 2.17). The green cross represents the centre of the SUT return spot orbit as the R-axis rotates. The angle, β , between the interferometer and R-axis is proportional to the radius of this orbit. As the operator adjusts the table screws, the R-axis tilt relative to the interferometer optical axis is adjusted. Placing the SUT return spot at the green cross will place the R-axis rotation axis parallel with the interferometer optical axis. Following placement, the system automatically realigns the reference and return spots. Another rotation is carried out and the process repeats until the returns spots are within tolerance.

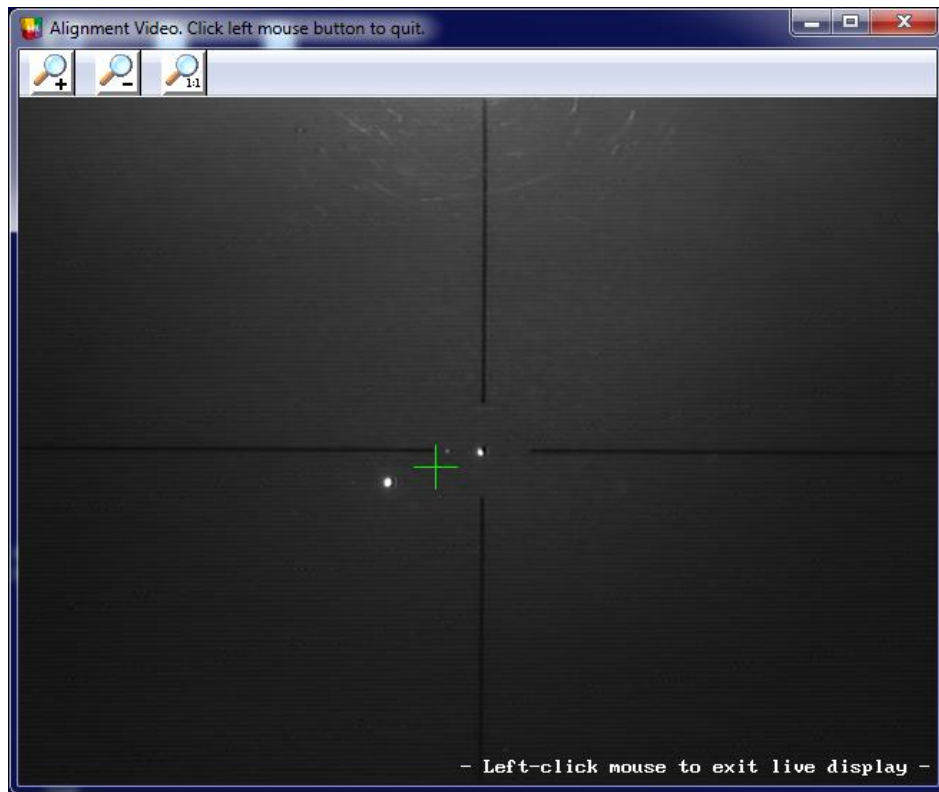


Figure 4.5: Coarse alignment camera input displayed on *Metrology Controller* console PC using application developed by C.W. King

During initial testing of the auto-clocking procedure, clocking to within the specified tolerance was found to be difficult. This was due to slight movement of the SUT return spot resulting from flexing of the rotary table chassis, caused by opening and closing the front access door of the Metrology Station. The CNC interlocking system required that this door be closed for automatic operation, but user access is required to the rotary table screws in order to make corrections following each rotation. This issue was resolved by including an interlock override facility to allow automatic operation during the auto-clocking procedure. The system feed rate is subsequently limited to minimise risk to the operator during the procedure, and the override is cleared upon completion.

With the R-axis and optical axis of the SUT properly aligned, the number of corrections required when arriving at sub-apertures on the same ring are minimised. This is particularly important for measurement plans featuring large numbers of measurement locations, as overall measurement time is also minimised.

4.3.1.2 Pivot Distance

In order to move between concentric rings within a spherical measurement plan, the Metrology Station must tilt the rotary table using the T-axis. Following this rotation, translations of both the Y and Z-axes are required owing to the T-axis not pivoting about the SUT COC, as shown in Figure 4.6. The size of this translation is dependent upon the elevation of the concentric sub-aperture ring, and proportional to the offset between the SUT COC and axis of rotation of the T-axis.

The surface design file used to create the measurement plan does not include information such as part thickness and fixture dimensions required to compute these translation. In order to allow a simplified calculation, an assistant has been incorporated into *Metrology Control Suite*, which guides the user through the process.

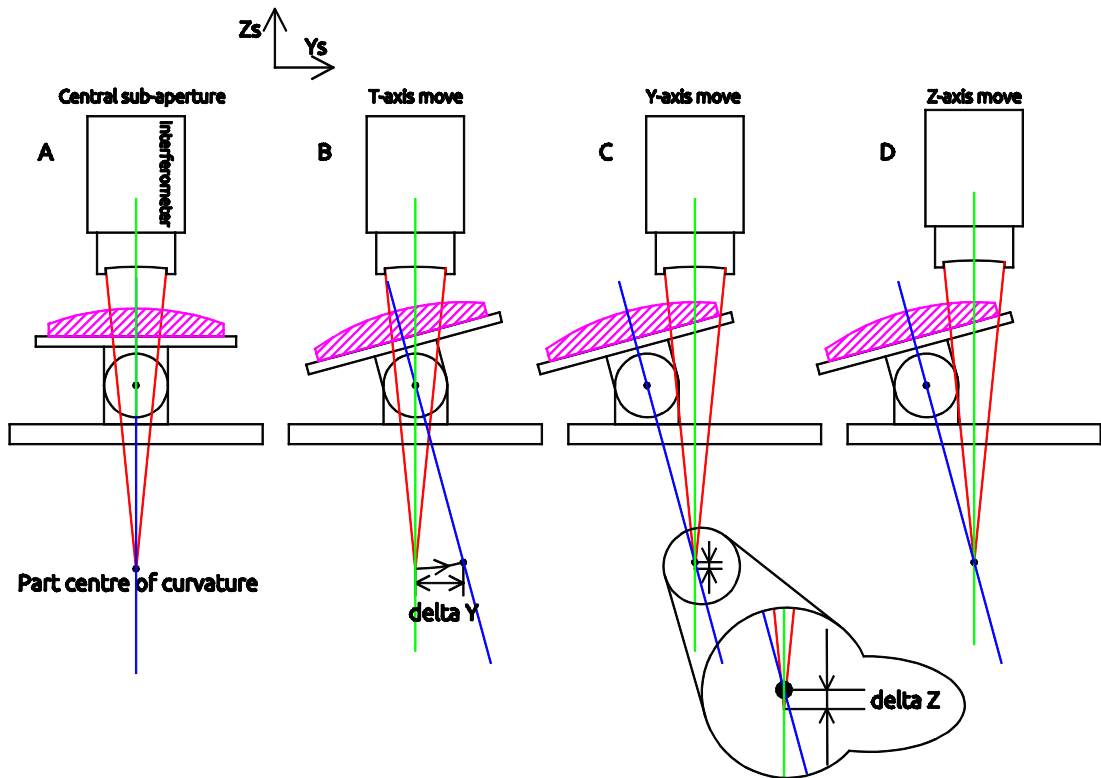


Figure 4.6: Schematic representation of required corrective translations following T-axis rotation to measure concentric sub-aperture ring of spherical SUT (image by C.W. King)

When the pivot distance calculation assistant is used, the user is instructed to place the interferometer focus at positions D_1 , D_2 , and D_3 indicated in Figure 4.7 in turn. At each location the system Z-axis value is recorded. As both the table surface and the SUT are reflective, positioning the interferometer focus at D_1 and D_2 produces interferometric fringes. By adjusting the Z-axis to remove power, positions D_1 and D_2 may be accurately established. D_3 is found by nulling the interferometer at the SUT, thereby matching the interferometer wavefront and SUT radii from the SUT centre of curvature.

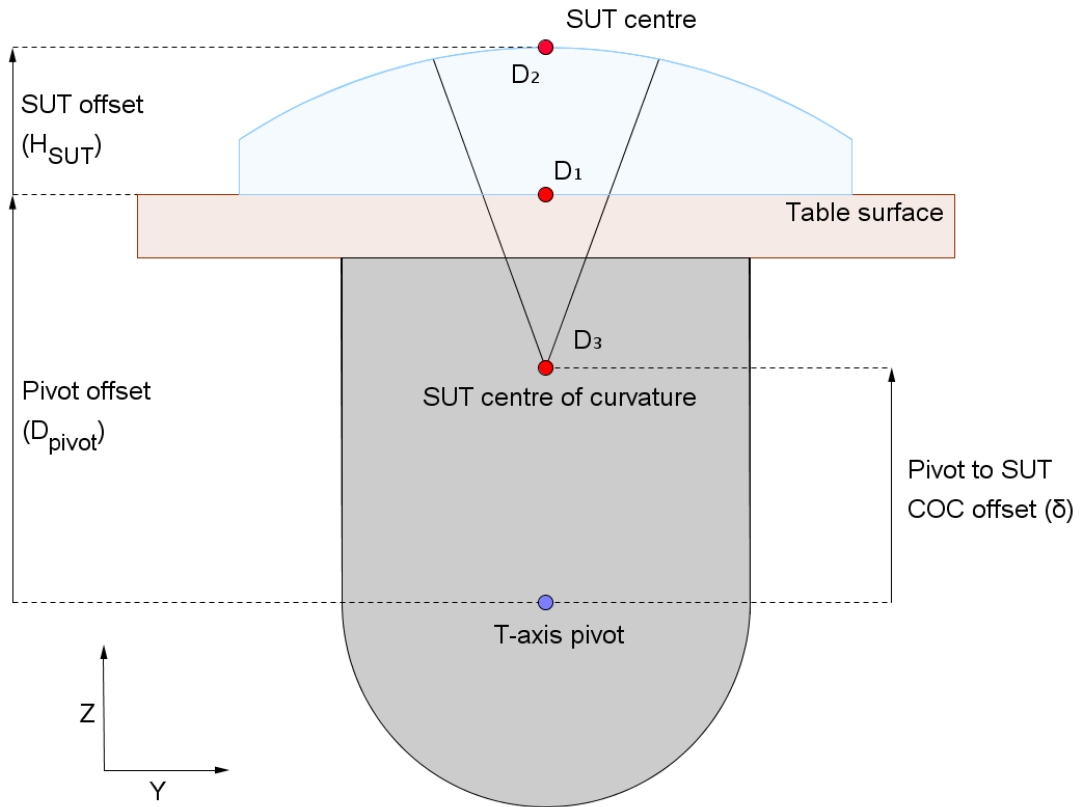


Figure 4.7: Metrology Station table assembly representation showing T-axis pivot offset distance

With the system Z-axis location recorded at each of the interferometer focus locations, the pivot offset distance, δ , is calculated using (4.1).

$$\delta = D_{pivot} + R_{SUT} + H_{SUT} \quad (4.1)$$

Where SUT radius of curvature, R_{SUT} , and the SUT offset, H_{SUT} are given by (4.2) and (4.3) respectively.

$$R_{SUT} = D_3 - D_2 \quad (4.2)$$

$$H_{SUT} = D_2 - D_1 \quad (4.3)$$

The pivot offset distance, D_{pivot} , cannot be characterised by the interferometer but does not change, and so is stored as part of the machine configuration. The SUT ROC has a negative sign convention for convex parts. With the pivot distance

characterised, the value is stored in the system configuration for use during kinematics calculation prior to measurement execution. The pivot distance value, along with the calculated ROC are displayed to the user to allow an opportunity to detect plan and SUT mismatch prior to measurement execution.

With knowledge of the pivot offset distance, each measurement location may be corrected during kinematics calculation using (4.4) and (4.5), as indicated in Figure 4.6.

$$\Delta y = \partial \sin(T) \quad (4.4)$$

$$\Delta z = \partial(1 - \cos(T)) \quad (4.5)$$

These corrections are only required for spherical surface measurement. During plano measurement, the T-axis is not required to rotate, therefore no correction is required. Following set up, interferometer is nulled at the first measurement location and the system axes are offset to zero to define the co-ordinate system origin at the SUT centre for measurement.

4.3.2 Point Measurement

As the STA is fitted to the IRP machine H-axis for on-machine measurement, it requires a different set of set up tasks to sub-aperture measurement using the Metrology Station. The set up tasks for the STA on the IRP machine are discussed in this section.

4.3.2.1 Co-ordinate System Set Up

Prior to commencing measurement, the IRP machine coordinate system must be set to ensure it is coaxial and concentric with that of the metrology plan. This ensures locations specified in the measurement plan have the same relationship with the surface design as the SUT. As the machine cannot correct for any SUT orientation error between the surface design file and the set up on the machine, the operator must manually align the part rotationally and define the machine co-ordinate frame origin.

Part rotational alignment is achieved by securing a dial gauge to the IRP machine H-axis. A flat datum is commonly machined onto the work piece edge, allowing alignment with one of the machine linear axes, such that change in the dial gauge reading when the axis is moves is negligible. In order to set the machine co-ordinate origin, the operator must locate the interferometer at the first measurement location in the plan and null the interferometer fringes. The IRP machine axes are then offset to define the first measurement location as the machine co-ordinate frame origin

With the machine co-ordinate frame configured accurately, co-ordinates specified the measurement plan are the same for the machine configuration, ensuring measurement is applied at the correct surface locations. This also minimises measurement duration as fewer correction moves are required as there is less error between where the surface is expected to be and where it is measured.

4.3.2.2 Non-linear Correction

In order to minimise measurement duration when operating the STA on the IRP machine, accuracy of the planned measurement location must be maximised. Focal error greater than $\pm 1 \mu\text{m}$ (10x objective) results in no visible fringes within the device FOV. Although the system has an algorithm to enable fringes to be located prior to performing alignment correction, this is slower than fine alignment correction alone, as discussed in Section 4.5.2.

In order to minimise the effects of part wedge and mounting error when polishing, *Zeeko TPG* can correct the polishing tool path using non-linear probing, as discussed in Section 2.1.1.3. In order to minimise the effects of part wedge and mounting error on STA measurement plan location accuracy, *Metrology Controller* is also able to accept the non-linear correction file. Currently, only a fitted plane is used for measurement plan correction, however more terms may be added in future. Figure 4.8 shows example resultant probing data with a fitted plane in green overlaid.

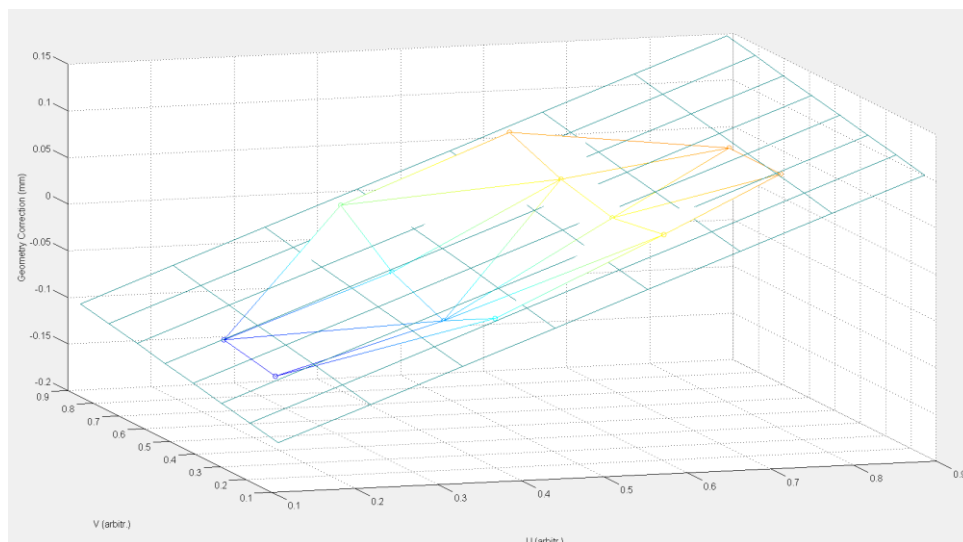


Figure 4.8: Non-linear correction map generated using *Zeeko TPG*

In order to assess any improvement when applying non-linear correction to automatic on-machine metrology a test was conducted. A 220 mm cross-corner hexagonal Zerodur test piece was secured to the IRP1200 machine. This piece was probed with a bonnet tool to produce probing data and plane fit shown in Figure 4.8. The SUT was tested using the STA both before and after the application of the non-linear correction file to the measurement plan. The residual focus error at each location in the measurement plan was recorded and used to create the residual error maps shown in Figure 4.9. Comparison of the error before and after the application of non-linear correction shows that the focus error when first arriving at a testing location has been reduced by ~67%. The residual error shown in the bottom plot exhibits some higher order terms such as power as well as some remaining tilt. The use of more fitting terms would yield further improvement and minimise the measurement duration for STA measurement on the IRP machine.

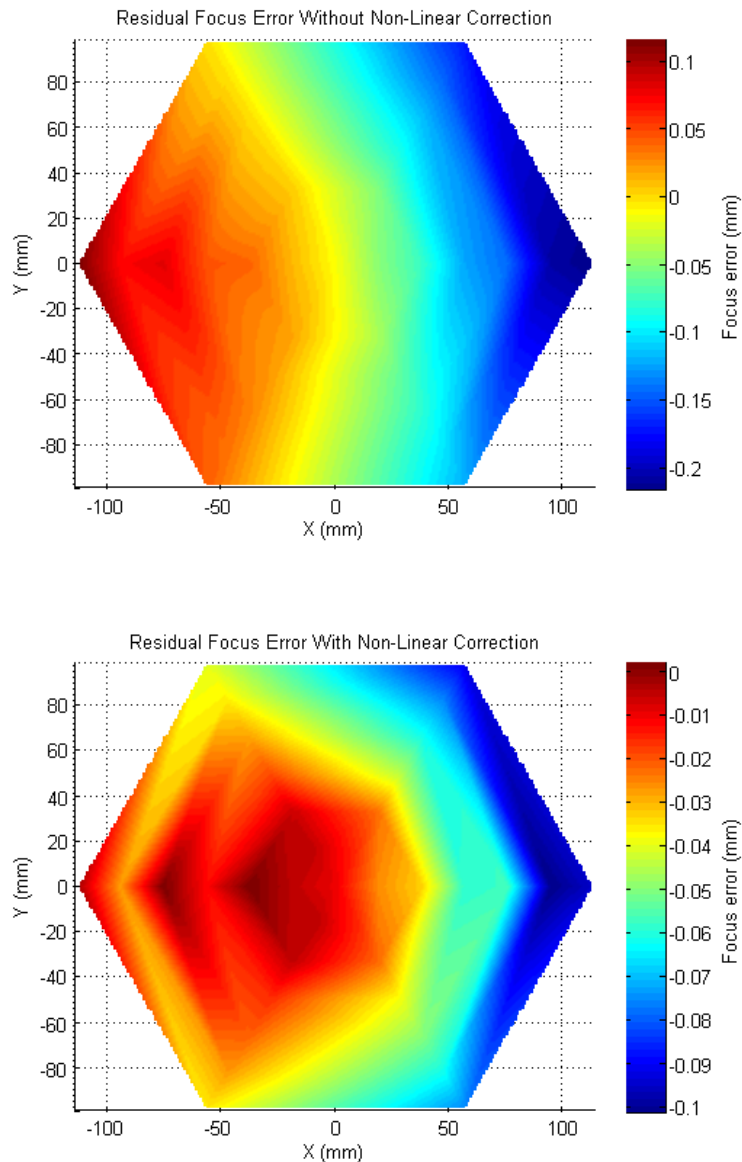


Figure 4.9: Residual test location focus error for the same part (Top) before and (Bottom) after test plan correction using non-linear probing data

In order for the non-linear probing data to be accurate, the part and fixturing must be properly acclimatised to the manufacturing environment as any thermal drift or mechanical settling may cause the set up error to change over time. However, as the objective behind on-machine testing is for the part to remain on the machine, thermal drift is unlikely to affect measurement processes applied in between successive processing runs as the part will have already acclimatised, assuming the manufacturing environment is stable.

4.3.3 Conclusion

The procedures outlined in this section are applied in order to ensure the correct relationship between the measurement plan and the system hardware. Activities such as clocking and non-linear probing are identical to those applied when preparing for polishing and, assuming the SUT support is stable, the same correction used in polishing may be applied. Interferometer specific tasks such as optical clocking have parallels with polishing as the part must also be clocked to the machine axes prior to processing to ensure accurate process application. Such parallel in set up procedures between polishing and metrology allow on-machine to become another routine task of the optical manufacturer. The aid of the CNC machine when carrying out alignment and clocking reduce the difficulty of these activities in comparison with manually adjusting the SUT in the metrology laboratory.

Where set-up tasks vary from the operations used on the IRP machine, such as pivot to SUT COC offset measurement or auto-clocking on the Metrology Station, software assistants have been used to guide the operator. The aim is to minimise the likelihood of any mistake resulting in the automatic measurement process either becoming stuck, or posing a risk of damage to part or machine. With the set up procedures completed, the measurement plan is automatically updated to maximise the accuracy of the predicted measurement locations, reducing measurement duration.

4.4 System Inverse Kinematics

The testing location co-ordinates contained within the measurement plan cannot be used directly with the measurement system axes. This is because measurement locations are specified in (X,Y,Z) which require conversion to machine co-ordinates. In order to produce machine co-ordinates, a set of inverse kinematics equations, describing the geometric relationship between the machine axes are applied. These equations take as arguments the measurement location co-ordinates (X,Y,Z) and local surface normal vectors (n_x, n_y, n_z) which are contained in the measurement plan.

Inverse kinematics calculation is also performed at the generation of an IRP machine tool path, prior to polishing. The main difference between the two processes is that polishing specifies a fine pitch of points, in order to create a smooth, pseudo-continuous tool path. On-machine metrology only requires that the end point of any move be correct in orientation and location, while avoiding crashes. This section will discuss the inverse kinematics for the example systems presented.

4.4.1 Metrology Station

Following auto-clocking of the part and the setting of the Metrology Station co-ordinate system, the measurement plan and machine are coaxial, therefore the measurement plan (X,Y,Z) locations can be used directly as machine axes. However, any measurement of a spherical surface requires T-axis rotations, and therefore the correction of the Y and Z components for the SUT COC to T-axis offset distance, as

discussed in Section 4.3.1.2. The corrected axis positions Y_c and Z_c are therefore given by (4.6) and (4.7) respectively.

$$Y_c = Y + \Delta y \quad (4.6)$$

$$Z_c = Z + \Delta z \quad (4.7)$$

Where Y and Z are the measurement location co-ordinates provided by the measurement plan. The correction offsets, Δy and Δz are given by (4.4) and (4.5) respectively. The table tilt axis value, T , is given by (4.8).

$$T = \frac{R_{SUT}}{|R_{SUT}|} \frac{\delta}{|\delta|} (\cos^{-1}(n_z) + \pi) \quad (4.8)$$

Where n_z is the Z-component of the local surface normal vector, R_{SUT} is the SUT ROC, and δ is the pivot to SUT COC offset, given by (4.1).

R is given by the negative of the azimuth angle of the sub-aperture, ϕ , shown in (4.9). This ensures the machine angle is given in part co-ordinates, allowing the sub-apertures to be addressed in the same order as those specified in the measurement plan.

$$R = -\phi \quad (4.9)$$

The A and B-axes contained within the interferometer housing cabinet are set to zero by default. These are only used to correct misalignment for plano measurements and, since alignment error is not predicted, zero error is assumed for initial positioning. Although it would be possible to make an improved

prediction of local tilt error based upon the tilt found at adjacent measurement locations, this has not been implemented in the current software version.

4.4.2 STA on the IRP Machine

When performing inverse kinematics calculations for the IRP machine, the same calculations are applied as when generating a tool path for polishing. As with Metrology Station, these calculations rely upon knowledge of the measurement point location (X,Y,Z) and the vector along which the device must be oriented in order to address the location (n_x, n_y, n_z) . The type-2 VP IRP machine inverse kinematic equations presented in this section are provided by W. Messelink of Zeeko. The machine A and B-axis values are calculated using (4.10) and (4.12) respectively for each test location in the measurement plan.

$$A = \tan^{-1}\left(\frac{n_y}{n_x}\right) + \Psi - \pi \quad (4.10)$$

Where Ψ is given by (4.11).

$$\Psi = \pi - \tan^{-1}\sqrt{2}\left[\frac{1 - n_z}{\sin(B)}\right] \quad (4.11)$$

$$B = \cos^{-1}(2n_z - 1) \quad (4.12)$$

As with the Metrology Station, the measurement plan (X,Y,Z) components are used as machine axis values. However, owing to the IRP machine VP being located 10 mm in front of the H-axis, some translation correction is required in order to accommodate the length of the STA. The corrected machine co-ordinates (X_c, Y_c, Z_c) are obtained by applying (4.13).

$$\begin{bmatrix} X_c \\ Y_c \\ Z_c \end{bmatrix} = \begin{bmatrix} 1 & 0 & 0 & Ln_x \\ 0 & 1 & 0 & Ln_y \\ 0 & 0 & 1 & Ln_z \\ 0 & 0 & 0 & 1 \end{bmatrix} \begin{bmatrix} X \\ Y \\ Z \\ 1 \end{bmatrix} \quad (4.13)$$

Where L is the length of the measurement device, specified in mm. As this parameter does not change, it is stored in the device file saved with the measurement plan. The current device length for the STA is measured with the 10x objective fitted. As 4D Technology supply alternative objectives, offering other magnifications, this parameter will need to be calculated from the device base unit length added to the objective length selected in *Metrology Designer*. Objective size would then be stored in as a parameter in the optics database.

The output from inverse kinematics calculation is a table of machine axis values, which will allow positioning of the measurement device at each measurement location in turn. Following calculation, the axis values are checked against the axis limits contained within the system configuration to ensure that the measurement locations are within the machine envelope. The axis values are used by *Metrology Controller* to generate G-code files to issue instructions to the system CNC controller. The correct kinematics set to use is selected using entries in the measurement configuration file, included with the OMM file.

4.4.3 Conclusion

This section has provided an overview the system inverse kinematics for both the Metrology Station and the STA measurement systems. These functions are used to transform the co-ordinates produced by Metrology Designer into machine axis values, directly compatible with G-code generation. As the system kinematics are selected using system configuration options, neither device is tied to any particular

hardware. However, practical limitations of mounting the STA onto the Metrology Station hardware result in incompatibility. However, such flexibility would allow a future OMSI device to be mounted on to the IRP machine, requiring only a modification to the system configuration file. Following inverse kinematics calculation, the systems moves to the first measurement location and automatic metrology commences.

4.5 Device Alignment

During automatic measurement plan execution, the measurement device is positioned, in turn, at each location specified in the measurement plan. To allow measurement acquisition, interferometric fringes must be located and nulled sufficiently to satisfy the user specified alignment error threshold. This threshold value is entered into the user configuration menu (See Appendix 9.1). The approach taken with both the Metrology Station and STA is to use feedback from the interferometer to form a closed-loop control system to iteratively correct residual alignment and power error (if applicable). In the case of on-machine texture measurement, this is a novel step. Both point and sub-aperture measurement routines have two main alignment modes; coarse and fine. Coarse alignment is defined as when fringes are not present in the device FOV, as determined by 4Sight, or are aliased and cannot be unwrapped. The point and sub-aperture systems presented have different routines for coping with coarse alignment due to the features and limitations of the two instruments, as outlined in Chapter 2. Fine alignment correction is carried out using a Zernike polynomial fit [91] to provide values of residual tilt along the device camera X and Y-axes. This section will discuss

the operation of both systems in coarse and fine alignment modes. Alignment correction is complete and measurement begins when residual fine alignment error falls below the user set threshold.

4.5.1 Sub-aperture Measurement Alignment

Sub-aperture measurement operations split tasks such as auto-alignment and measurement into one of two classes; plano or spherical. Automatic alignment therefore has separate work flows for each due to their differing requirements. Flow diagrams showing the plano and spherical auto-alignment function work flows are shown in Figure 4.10, Figure 4.11 and Figure 4.12, Figure 4.13 respectively. The star node symbol in both diagrams indicates the interrupt checking function. To allow the user to abort or pause execution of measurement at any time, a flag is raised when the user presses the pause or cancel buttons. The status of these flags are polled periodically during operation and the appropriate task is performed. This implementation has the drawback of having to wait until the preceding task has been executed before the user request may be serviced. All safety critical features, such as emergency stop, are hardware implemented. As the pause and cancel features are not used for safety critical inputs, this approach is acceptable.

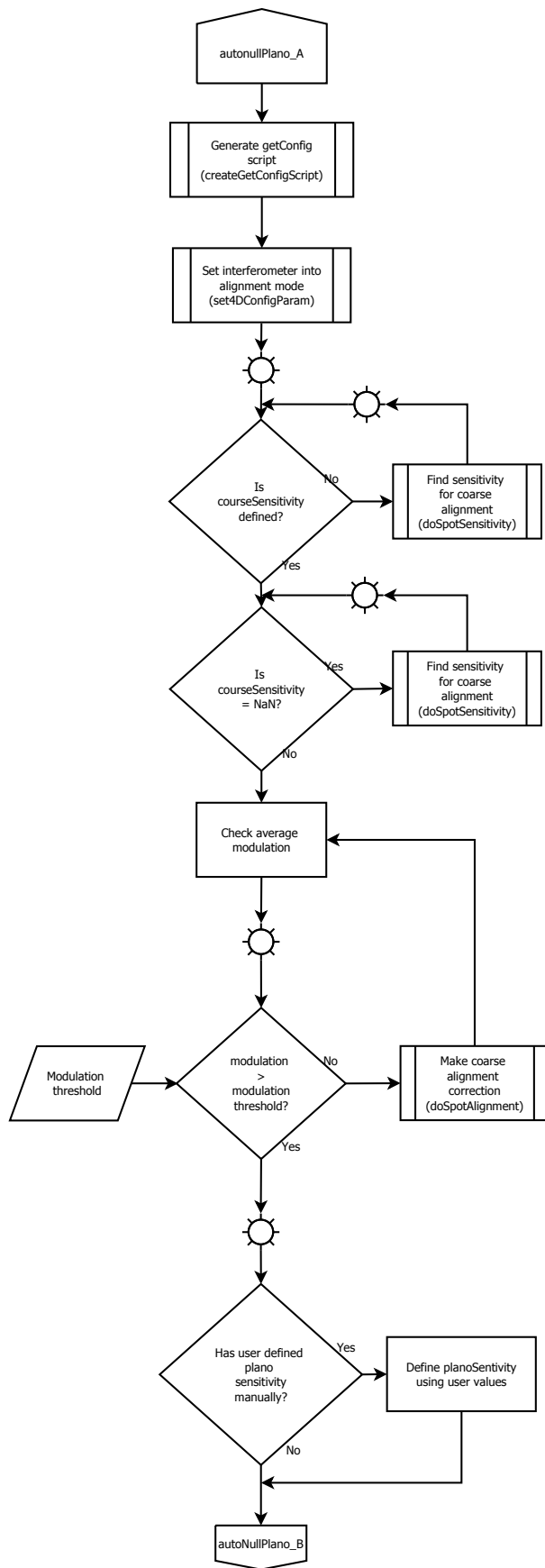


Figure 4.10: Plano auto-alignment work flow

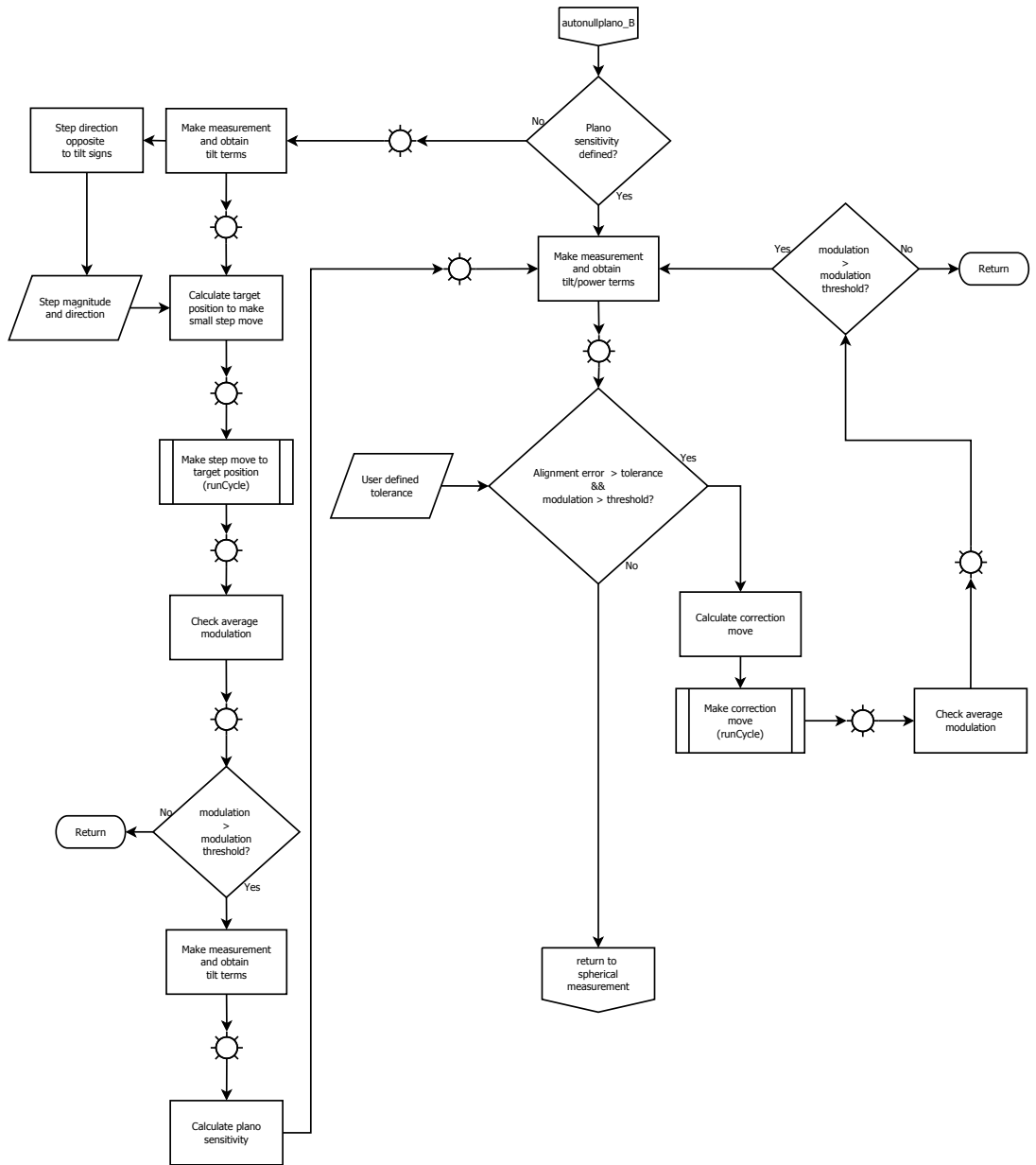


Figure 4.11: Plano auto-alignment work flow continued

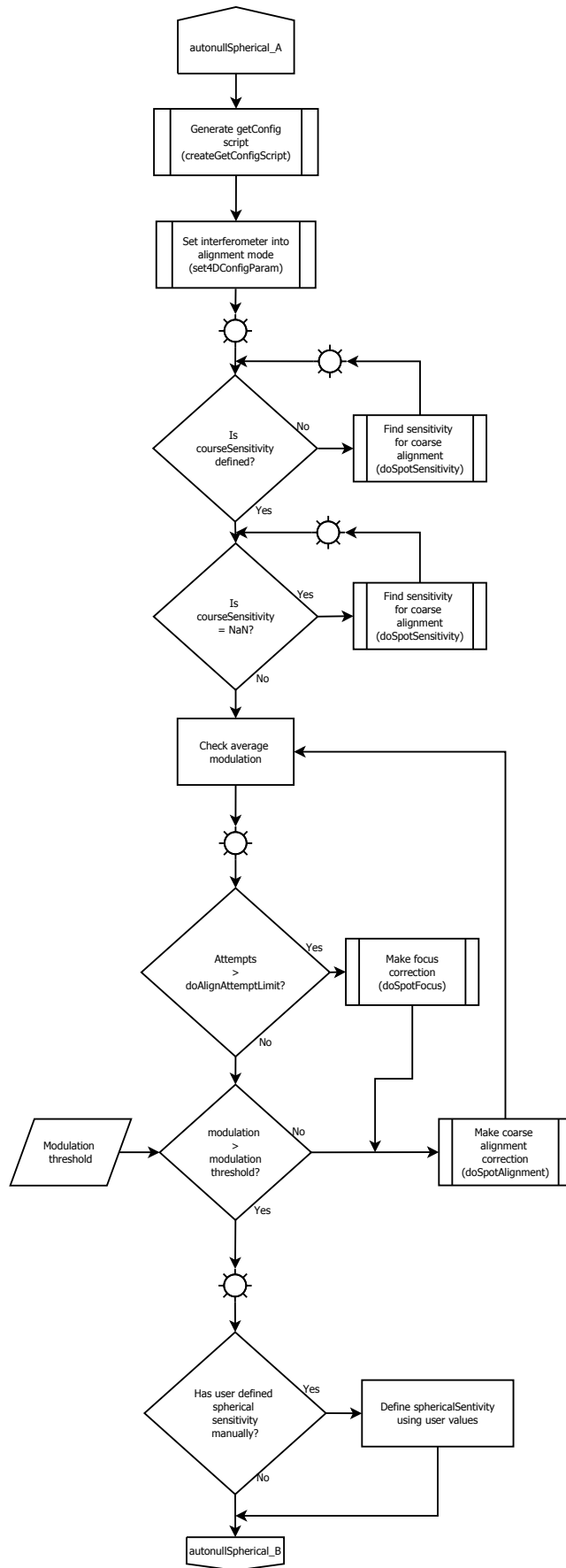


Figure 4.12: Spherical auto-alignment work flow

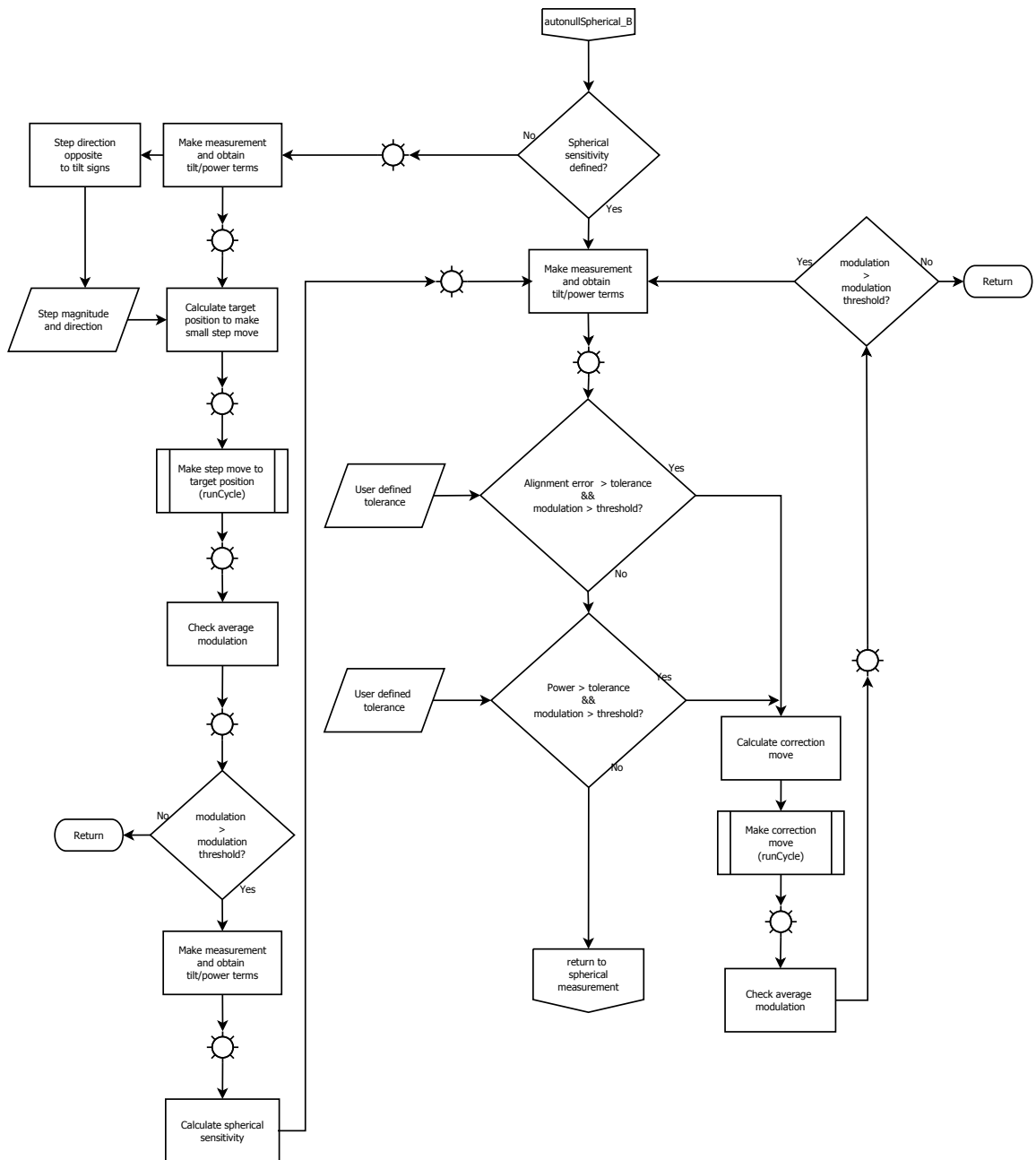


Figure 4.13: Spherical auto-alignment work flow continued

As both scripts start they set the interferometer into alignment move, which uses a low averaging level (typically around 4 frames) to reduce the measurement time required in between each correction iteration. The device configuration is changed via a python script which is executed by the web service. This python script is dynamically generated based upon the alignment averaging level selected by the user. Selection of the averaging value is a trade-off between the stability of the

environment in which the device is operating and the requirement to reduce iteration time. An increased averaging level will reduce the measurement uncertainty through noise and vibration print through reduction but will increase measurement time. If the overall measurement time is very large data stitching may be affected due to thermal drift during the measurement cycle.

In order for coarse alignment corrections to be made, both alignment error data and sensitivity values are required. The procedure for calculating the system coarse alignment sensitivity is shown in Figure 4.14.

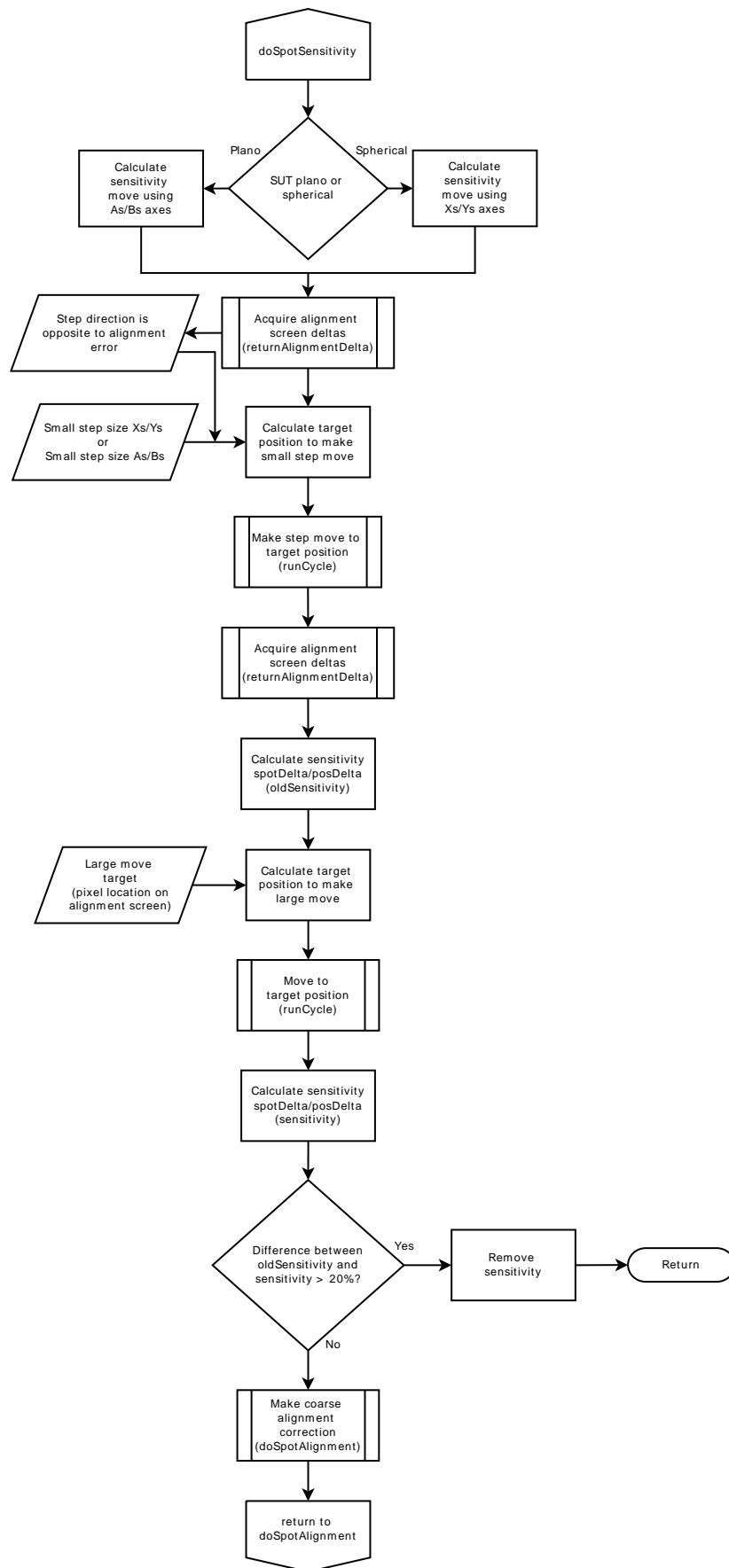


Figure 4.14: Coarse spot sensitivity calculation

Coarse alignment values are first calculated by recording the position of the test return spot on the interferometer alignment screen. The alignment spot is then moved by either translating (spherical) or tilting (plano) the interferometer relative to the SUT. The size of this move is calculated as a function of the transmission optic F# for spherical measurements and is constant for plano measurements. This initial step is designed to move the spot a small distance from the screen centre to minimise the risk of driving the spot off the screen during sensitivity calculation. The size of this translation step is given by (4.14).

$$\Delta X_{coarse} = \frac{S}{\left(\left(\frac{210.23}{F}\right) - 9.2707\right)} \quad (4.14)$$

Where S is the step parameter in μm , given by the machine configuration, and ΔX_{coarse} is the resultant X-axis translation requires for the small spot move. F is the transmission optic F#. (4.14) was determined by finding the SUT return spot tilt sensitivity for a set of transmission spheres. For each objective, the system X-axis was incremented by a small amount and the resultant shift in interferometer alignment spot recorded. This data was then used to calculate a sensitivity of each transmission optic, allowing an equation for sensitivity versus F# to be fitted. As sensitivity is equal in both X and Y, (4.14) may be used for both axes.

Although this sensitivity value could be used for automatic alignment of the system, in practice, it is found that the value can vary due to transmission sphere parameter accuracy and environmental conditions. Therefore, this value is used as an approximation to calculate a larger step move to position the alignment return at a target pixel, typically near the edge of the alignment screen. This move is much

larger than the previous and so a greater SNR ratio is achieved. A second sensitivity calculation is made at the target pixel and the two values obtained are compared. Should the sensitivity value of the large and small SUT spot moves vary by more than 20%, they are discarded and the process retried. The error handling system allows the sensitivity calculation to be retried a specified number of times before halting measurement to prevent the process becoming stuck in a loop.

For example, if the user attempts to test a lens assembly (with multiple return spots due to there being several elements stacked together), the spot detection algorithm may switch between spots following axis moves, as the algorithm centroids the region of maximum intensity. This can cause erroneous values, preventing correct operation. In this case the error handling function would prevent the system becoming stuck in a loop. Phantom return spots have also been observed from some transmission optics, which can cause the same problem. A possible solution is to improve the alignment spot algorithms to track the SUT return spot during movement to retain the same feature for each calculation.

Following the successful calculation of a coarse sensitivity value, the function performs coarse alignment to place the SUT return spot at the same position as the reference return spot. This allows interferometric measurement, permitting the computation of Zernike terms and their use in fine alignment correction. During coarse alignment, an image of the alignment screen is captured (using acquisition functions written by C.W. King) and the screen centre pixels, containing the reference return spot, are masked out. A threshold is applied and the SUT return spot centre is found. A correction may be computed from the spot centre position

obtained. This correction is dynamically written into a G-code file and uploaded to the control system for execution. However, in practice it has been found that the system behaviour may be unstable during coarse alignment. When making large correction moves, the system tends to oscillate around the target. This overshoot results from spatial distortion associated with the alignment screen imaging optics. Such distortion can manifest as a pin cushion effect, a non-linear stretching of the distance between the frame centre and edge. This would cause a surface return spot near the frame edge to produce an erroneously large correction move, producing an overshoot. The use of error bisection, moving half the correction distance between acquiring feedback, decreases the tendency to oscillate through over correcting.

Following coarse correction, fringes are visible within the interferometer FOV and the system returns to the main alignment routine (Figure 4.10 or Figure 4.12) to perform fine alignment correction. In this mode, the interferometer is commanded to acquire data and a Zernike fit is calculated using 4Sight. The Zernike coefficients are returned to the control application for correction calculation. As with the coarse alignment algorithm, fine correction requires the calculation of a sensitivity value as tilt sensitivity varies with F# for spherical measurement. The sensitivity value is obtained by making a measurement from the initial location, followed by making a step move in both translation and power for spherical testing. The magnitude of these moves are given by (4.15) and (4.16) respectively. Plano measurement uses a fixed initial step value, specified in the system configuration and found empirically.

$$\Delta X_{fine} = \frac{715.1}{F} \quad (4.15)$$

Where ΔX_{fine} is the translation move, which is equal to that used for the system Y-axis. F is the transmission sphere F#.

$$\Delta Z_{fine} = \frac{125}{F^2} - \frac{17}{F} \quad (4.16)$$

Where ΔZ_{fine} is the Z-axis translation required for fine sensitivity calculation. F is the transmission sphere F#. (4.15) and (4.16) were derived by characterising the sensitivity of different F# transmission spheres for tilt and power and fitting the resultant trends.

Should fringes be lost during sensitivity calculation, the function will return to the main measurement function. The system will then return to the predicted sub-aperture measurement location and start the process again.

$$S_{spherical} = \frac{P'_{(x,y,z)} - P_{(x,y,z)}}{Z'_{(2,3,4)} - Z_{(2,3,4)}} = \frac{\Delta P_{(x,y,z)}}{\Delta Z_{(2,3,4)}} \quad (4.17)$$

Where $S_{spherical}$ is the fine sensitivity for spherical testing configurations, $P_{(x,y,z)}$ is the starting position and $P'_{(x,y,z)}$ the resultant position following a move by ΔX_{fine} in translation and by ΔZ_{fine} in power, given by (4.15) and (4.16) respectively. $Z'_{(2,3,4)}$ are the resultant residual tilt and power Zernike terms following the move and $Z_{(2,3,4)}$ the initial Zernike terms. The definition of $Z_{(2,3,4)}$ are given in Table 4.1. Terms contained within the shaded area are not currently required during sensitivity or alignment calculation. However, terms Z_5 to Z_9 can be used develop a procedure for the automatic alignment of a CGH for aspheric testing. A similar process to (4.17) may be used to calculate fine tilt sensitivity for a plano test, S_{plano} .

$$S_{plano} = \frac{P'_{(a,b)} - P_{(a,b)}}{Z'_{(2,3)} - Z_{(2,3)}} = \frac{\Delta P_{(a,b)}}{\Delta Z_{(2,3)}} \quad (4.18)$$

Where $P'_{(a,b)}$ are the system A and B-axis positions following a step move of size given by the system configuration from position $P_{(a,b)}$.

Having calculated the fine alignment sensitivity values, the system enters a cycle of iterative measurements followed by corrections until the residual error falls below the user set threshold. The new target (X,Y,Z) position at each iteration of a spherical test, $T_{spherical}$, is given by (4.19).

$$T_{spherical} = P_{(x,y,z)} - \frac{Z_{(2,3,4)}}{S_{spherical}} \quad (4.19)$$

Where $P_{(x,y,z)}$ is the current position of the X,Y, and Z axes, read from the CNC control unit. $Z_{(2,3,4)}$ are the residual tilt and power terms in the interferometer FOV, obtained by remotely commanding the device to make a measurement and perform a Zernike fit on the resultant data. $S_{spherical}$ is the spherical sensitivity, given by (4.17). Similarly, the target position for a correction move of a plano test, T_{plano} , is given by (4.20).

$$T_{plano} = P_{(a,b)} - \frac{Z_{(2,3)}}{S_{plano}} \quad (4.20)$$

Where $P_{(a,b)}$ is the current A and B-axis position and S_{plano} is the fine plano sensitivity, given by (4.18).

Table 4.1: Zernike polynomials used in fine alignment correction - reproduced from [91]

j	n	m	$Z_j(\rho, \theta)$	Aberration name
1	0	0	1	Piston
2	1	1	$2\rho \cos \theta$	x tilt
3	1	1	$2\rho \sin \theta$	y tilt
4	2	0	$\sqrt{3}(2\rho^2 - 1)$	Defocus
5	2	2	$\sqrt{6}\rho^2 \sin 2\theta$	Primary astigmatism at 45°
6	2	2	$\sqrt{6}\rho^2 \cos 2\theta$	Primary astigmatism at 0°
7	3	1	$\sqrt{8}(3\rho^3 - 2\rho) \sin \theta$	Primary y coma
8	3	1	$\sqrt{8}(3\rho^3 - 2\rho) \cos \theta$	Primary x coma
9	3	3	$\sqrt{8}\rho^3 \sin 3\theta$	
10	3	3	$\sqrt{8}\rho^3 \cos 3\theta$	
11	4	0	$\sqrt{5}(6\rho^4 - 6\rho^2 + 1)$	Primary spherical
12	4	2	$\sqrt{10}(4\rho^4 - 3\rho^2) \cos 2\theta$	Secondary astigmatism at 0°
13	4	2	$\sqrt{10}(4\rho^4 - 3\rho^2) \sin 2\theta$	Secondary astigmatism at 45°
14	4	4	$\sqrt{10}\rho^4 \cos 4\theta$	
15	4	4	$\sqrt{10}\rho^4 \sin 4\theta$	
16	5	1	$\sqrt{12}(10\rho^5 - 12\rho^3 + 3\rho) \cos \theta$	Secondary x coma
17	5	1	$\sqrt{12}(10\rho^5 - 12\rho^3 + 3\rho) \sin \theta$	Secondary y coma
18	5	3	$\sqrt{12}(5\rho^5 - 4\rho^3) \cos 3\theta$	
19	5	3	$\sqrt{12}(5\rho^5 - 4\rho^3) \sin 3\theta$	
20	5	5	$\sqrt{12}\rho^5 \cos 5\theta$	
21	5	5	$\sqrt{12}\rho^5 \sin 5\theta$	
22	6	0	$\sqrt{7}(20\rho^6 - 30\rho^4 + 12\rho^2 - 1)$	Secondary spherical
23	6	2	$\sqrt{14}(15\rho^6 - 20\rho^4 + 6\rho^2) \sin 2\theta$	Tertiary astigmatism at 45°
24	6	2	$\sqrt{14}(15\rho^6 - 20\rho^4 + 6\rho^2) \cos 2\theta$	Tertiary astigmatism at 0°
25	6	4	$\sqrt{14}(6\rho^6 - 5\rho^4) \sin 4\theta$	
26	6	4	$\sqrt{14}(6\rho^6 - 5\rho^4) \cos 4\theta$	
27	6	6	$\sqrt{14}\rho^6 \sin 6\theta$	
28	6	6	$\sqrt{14}\rho^6 \cos 6\theta$	
29	7	1	$4(35\rho^7 - 60\rho^5 + 30\rho^3 - 4\rho) \sin \theta$	Tertiary y coma
30	7	1	$4(35\rho^7 - 60\rho^5 + 30\rho^3 - 4\rho) \cos \theta$	Tertiary x coma
31	7	3	$4(21\rho^7 - 30\rho^5 + 10\rho^3) \sin 3\theta$	
32	7	3	$4(21\rho^7 - 30\rho^5 + 10\rho^3) \cos 3\theta$	
33	7	5	$4(7\rho^7 - 6\rho^5) \sin 5\theta$	
34	7	5	$4(7\rho^7 - 6\rho^5) \cos 5\theta$	
35	7	7	$4\rho^7 \sin 7\theta$	
36	7	7	$4\rho^7 \cos 7\theta$	
37	8	0	$3(70\rho^8 - 140\rho^6 + 90\rho^4 - 20\rho^2 + 1)$	Tertiary spherical

4.5.2 Point Measurement Alignment

When comparing point and sub-aperture measurement alignment routines, the greatest difference results from the limited depth of field, and lack of alignment screen of the STA. The limited focal depth is caused by the use of an LED light source, exhibiting a limited coherence length. It is observed that interference does not occur beyond $\pm 5 \mu\text{m}$ from best focus (poor contrast beyond $\pm 1 \mu\text{m}$) and, without an alignment screen and SUT return spot, the system has limited information to aid in fringe location. This forces a different approach to automatic system alignment, which unlike sub-aperture measurement is negligibly affected by

SUT form. Furthermore, due to the non-orthogonal configuration of the IRP machine axes, alignment correction in one direction cannot be achieved through a single axis move. Every alignment correction requires a compound move of the A and B-axes, with a translation of the X, Y and Z-axes in order to hold station over the measurement location. Figure 4.15 shows the system work flow when performing alignment and Figure 4.16 and Figure 4.17 the fringe location routine.

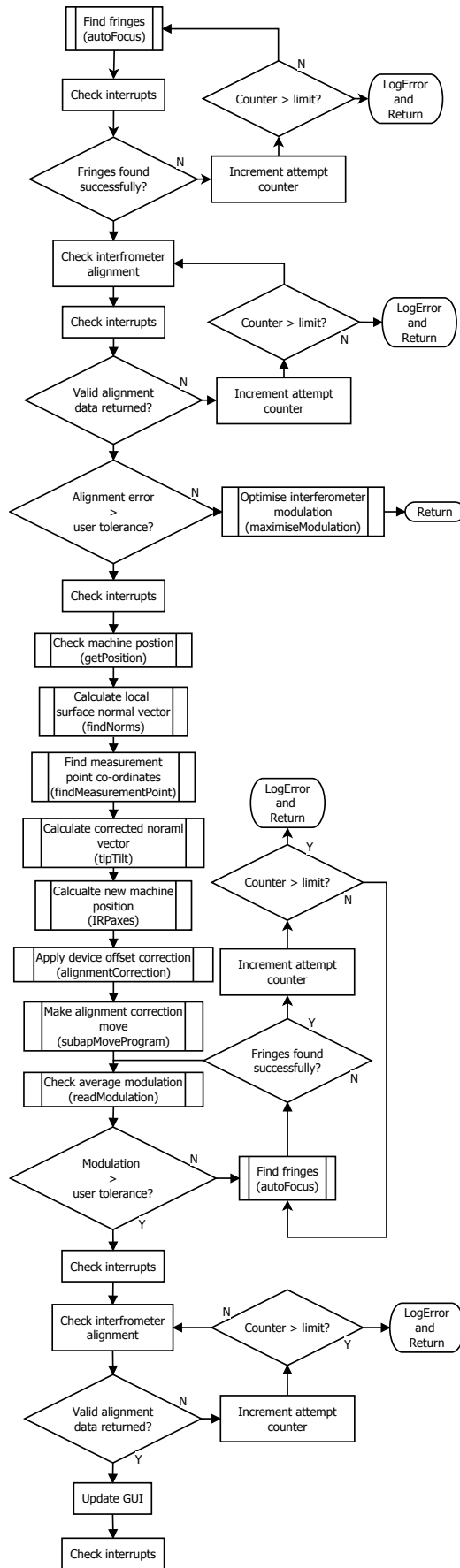


Figure 4.15: STA automatic alignment work flow

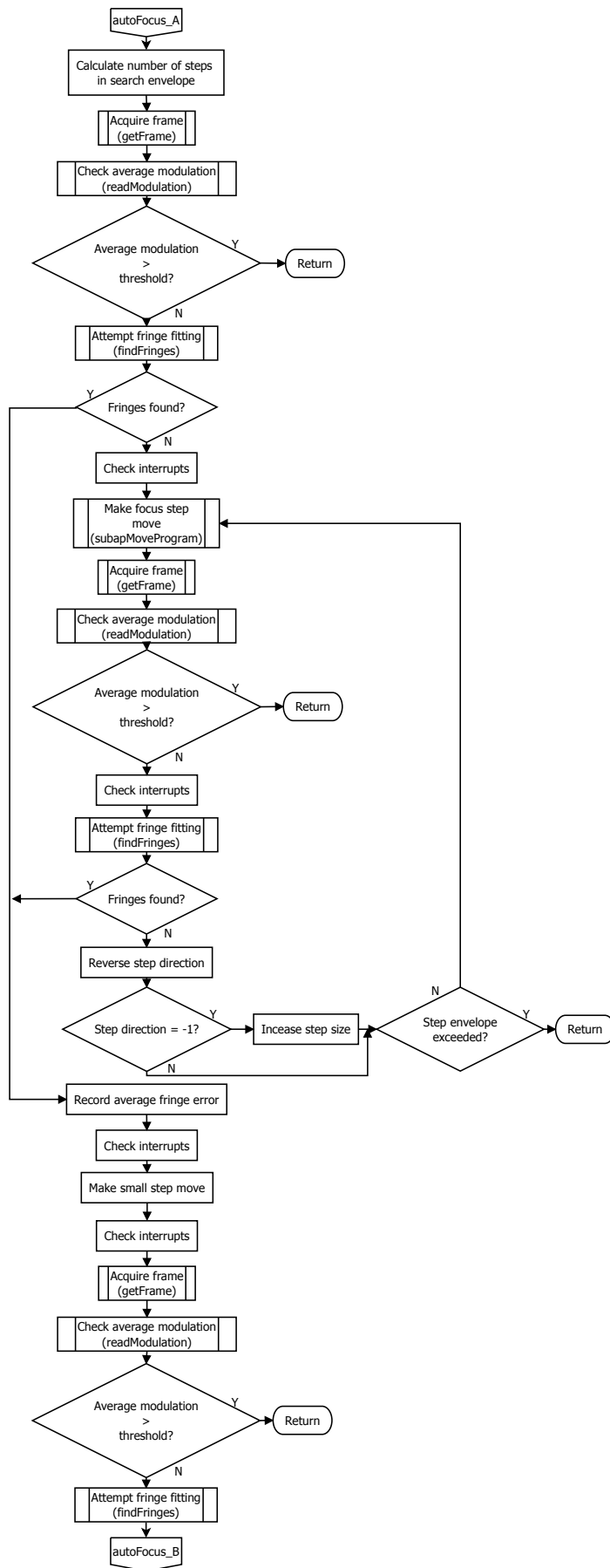


Figure 4.16: STA auto focus work flow

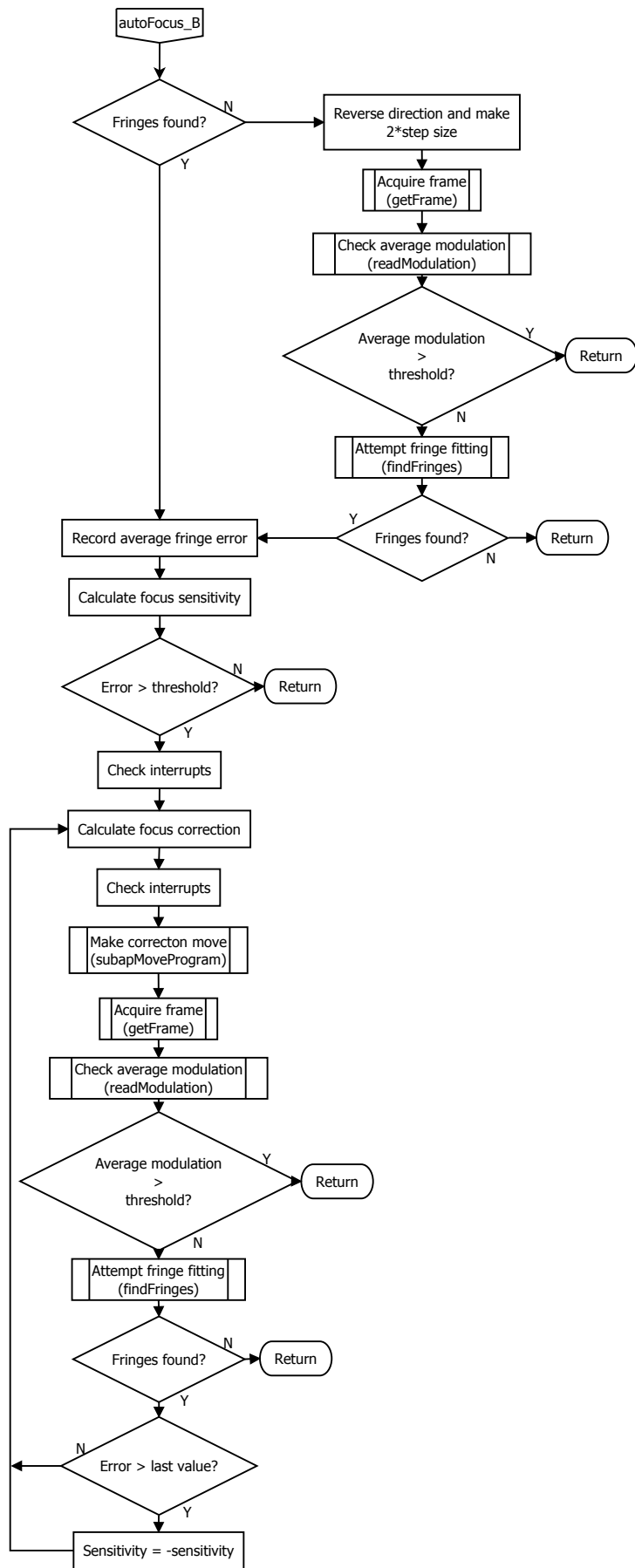


Figure 4.17: STA auto focus work flow continued

It is likely that no fringes will be visible when first arriving at the measurement location. The alignment routine therefore begins by locating fringes. The long range focus and tilt sensors of the device were deemed unsuitable for automation (as discussed in Section 2.2.2) and so fringe location is carried out by scanning the device along the IRP machine H-axis direction vector and acquiring raw interferometric frames. The average modulation of these images is obtained from 4Sight and compared with a threshold level defined in the system configuration. If sufficient tilt error is present, the fringes form a narrow band across the FOV and the average modulation falls to around the background noise level. An example of this situation is shown in Figure 4.18.

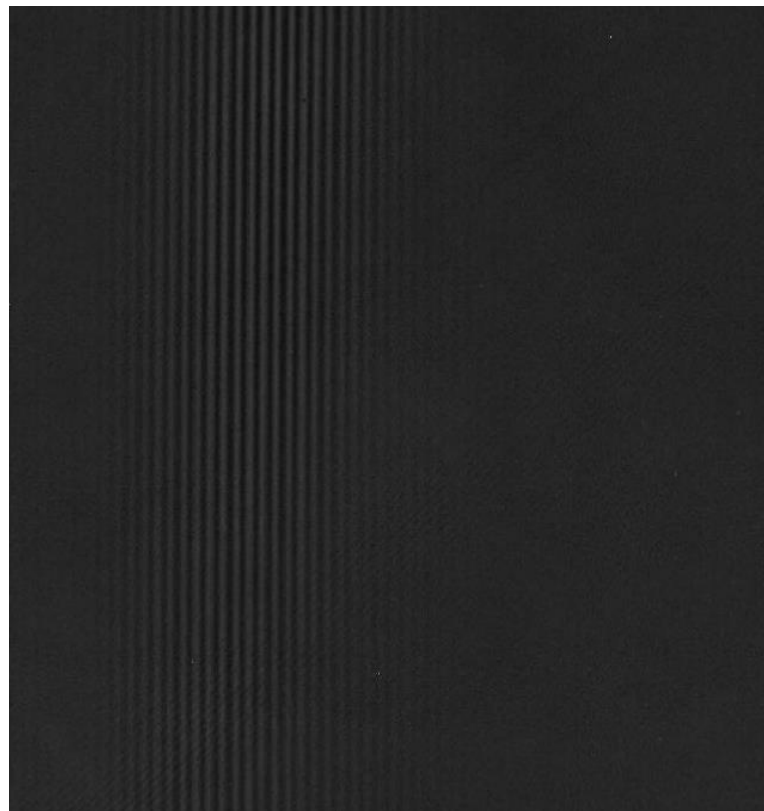


Figure 4.18: Interferometric fringes of the STA exhibiting large surface tilt error

As it is possible for this situation to occur during measurement, due to a poor non-linear correction or inaccurate surface design, reading the average modulation level

during scanning can cause fringes to be erroneously ignored. In order to create a general solution for such cases, the captured frames are processed by a pattern recognition algorithm to detect lines in the image. The operation of this fringe detection algorithm is discussed in Section 4.5.2.1. However, each time a frame is acquired, modulation is checked and if the value is found to be sufficient, focus scanning is abandoned and alignment correction is carried out.

During fringe detection, the system scans along the IRP machine H-axis direction vector. A working envelope is defined by the scan size specified in the system configuration and the step size. In testing, only a 10x objective was available and so an envelope of $\pm 150 \mu\text{m}$ and a step size of $2 \mu\text{m}$ were found to give reliable results, giving 75 steps. When other objectives become available, this function will be adapted to use a calculation to provide these values. Instead of starting at one extreme of the search envelope and scanning to the other end, the system starts at the centre (the measurement location specified in the plan) and reverses direction every other move. As the best prediction is that at which the system first arrived, those scan positions closest to this location are most likely to yield viable fringes. Should the search envelope be exceeded without locating fringes, the system will skip this measurement location and continue to the next. It is critical that the search step size is set sufficiently small that the device does not pass through focus without detecting fringes.

Following each step move modulation is checked and, if insufficient compared with the threshold given in the system configuration, fringe detection is attempted. If fringes are not found within the image, the system steps in the opposite direction

along the normal vector. If the last step direction was negative (towards the SUT) the size of size of the step is incremented by the step size. If fringes are found, the system attempts to place these fringes at the centre of the device FOV. This is done by first calculating the sensitivity of fringe lateral movement in the FOV to device translation along the H-axis vector. As well as indicating the presence of fringes, the fringe detection algorithm provides the co-ordinates of the centre of the detected fringe pattern. Device focus sensitivity, S_{focus} , is given by (4.21)

$$S_{focus} = \frac{\sqrt{(C'_x - C_x)^2 + (C'_y - C_y)^2}}{(P'_F - P_F)} \quad (4.21)$$

To calculate focus sensitivity, a device frame is acquired at position P_F , providing fringe pattern centre co-ordinates (C_x, C_y) . A 1 μm move along the H-axis vector is made, placing the device at P'_F . A second frame is acquired, providing fringe pattern centre co-ordinates (C'_x, C'_y) .

Following sensitivity calculation, the system makes correction moves using the calculated value and subsequent error values obtained from fringe fitting. After each move, a new interferometric frame is captured and the fringe pattern position is re-evaluated. This process continues until the distance between the pattern centre and the FOV centre falls below a threshold specified in the system configuration. Should the error increase, the sign of the sensitivity value is inverted. If fringes are lost, the focus routine is abandoned. When the auto focus function is aborted due to fringes being lost, the system uses the standard error handling procedure.

When interferometric fringes have been located and centred, the system switches to fine alignment mode. When correcting fine alignment, data is acquired from the interferometer and 4Sight performs a Zernike analysis to obtain tilt terms. Tilt information can then be used to calculate a correction move. However, unlike the Metrology Station example, alignment correction with the IRP machine cannot be carried out with X or Y-axis translation alone as fringes are easily lost through introduction of focal error. As the instrument FOV is also small, a residual translation could also cause features of interest to move out of the frame. It is therefore important that the interferometer hold station over measurement location during all correction moves. Figure 4.19 shows the STA device fitted to the tool chuck of the IRP1200 machine, with the interferometer beam visible on the SUT. In order to maintain focus and translation of the FOV, alignment corrections must be performed relative to the position at which the beam meets the SUT. When computing an alignment correction for the STA, the system first queries the machine position. From the machine position information, the H-axis direction vector, (n_x, n_y, n_z) , is calculated by applying the IRP machine forward kinematic equations, provided by A. Beaucamp of Zeeko and given in (4.22), (4.23), and (4.24).

$$n_x = \frac{\cos(A) (1 - \cos(B))}{2} - \frac{\sin(B) \sin(A)}{\sqrt{2}} \quad (4.22)$$

$$n_y = \frac{\sin(A) (1 - \cos(B))}{2} - \frac{\sin(B) \cos(A)}{\sqrt{2}} \quad (4.23)$$

$$n_z = \frac{\cos(B) + 1}{2} \quad (4.24)$$

Where A and B are the IRP machine A and B-axis positions respectively.

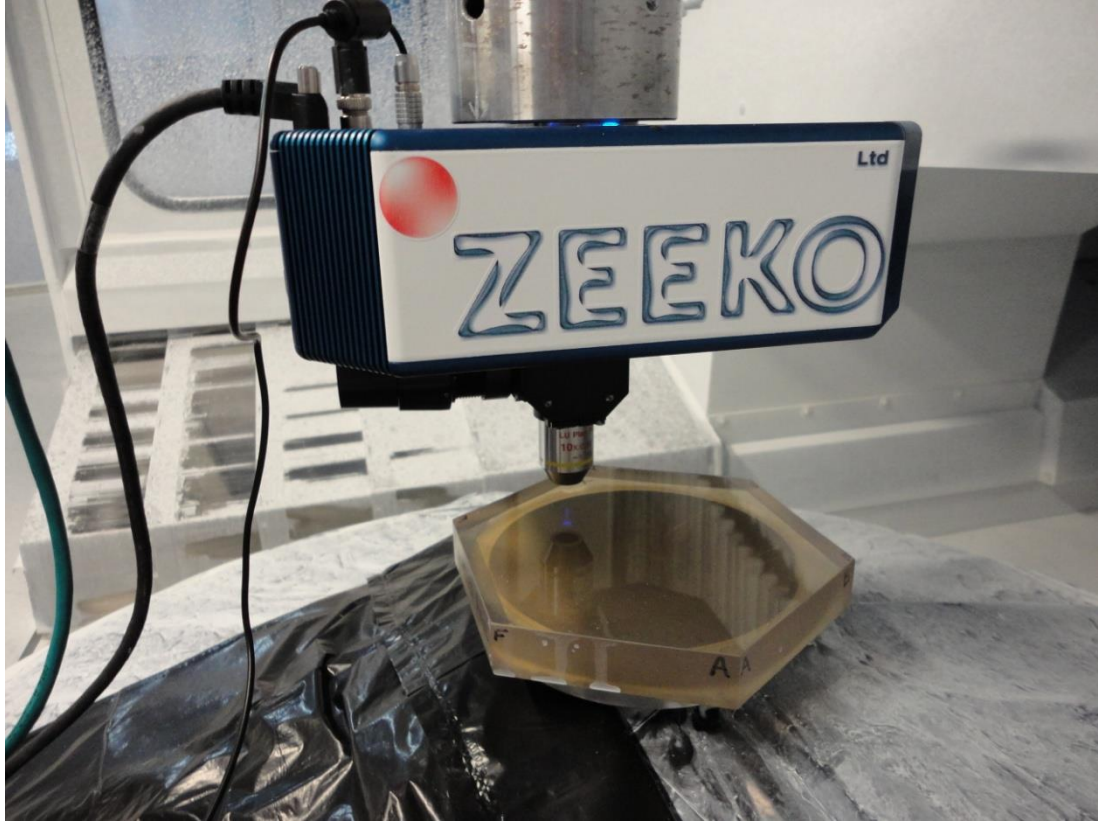


Figure 4.19: STA fitted to the IRP1200 machine testing a 200 mm cross-corners hexagonal part

To compute an alignment correction and retain the point of interest within the device FOV, the co-ordinates of the test location on the SUT must be found. Using the device and optical configuration information, an offset distance between the H-axis front face, D_{VT} , may be calculated as given by (4.25).

$$D_{VT} = D_{STA} + D_{OB} + D_W \quad (4.25)$$

Where D_{STA} is the STA body height, D_{OB} is the objective height and D_W is the objective working distance from the SUT, as shown in Figure 4.20. The test location co-ordinates, (X, Y, Z) , are computed by projecting along the H-axis vector, (n_x, n_y, n_z) , by D_{VT} , given by (4.26).

$$\begin{bmatrix} X \\ Y \\ Z \end{bmatrix} = \begin{bmatrix} 1 & 0 & 0 & D_{VT}n_x \\ 0 & 1 & 0 & D_{VT}n_y \\ 0 & 0 & 1 & D_{VT}n_z \\ 0 & 0 & 0 & 1 \end{bmatrix} \begin{bmatrix} X_m \\ Y_m \\ Z_m \\ 1 \end{bmatrix} \quad (4.26)$$

Where (X_m, Y_m, Z_m) are the machine X, Y, and Z-axis positions which are read from the CNC controller. The error angle, α , between the local surface normal vector and the STA is then computed by acquiring measurement data and performing a Zernike fit to obtain residual tilt align the camera X and Y-axes to which (4.27) is applied.

$$\alpha_{(x,y)} = \frac{\tan^{-1}(\lambda Z_{(1,2)})}{D_{(x,y)}} \quad (4.27)$$

Where λ for the STA is 460 nm, which is stored in the device configuration file. $Z_{(1,2)}$ are the Zernike terms for tilt in X and Y respectively. $D_{(x,y)}$ is the dimensions of the STA FOV in millimetres given in the device optical configuration. The H-axis vector is rotated about the test location (X, Y, Z) by α to obtain a corrected H-axis vector by calculating the angle between the H-axis X and Y components and the X and Y-axis respectively using (4.28).

$$\beta_{(x,y)} = \cos^{-1}(n_{(x,y)}) \quad (4.28)$$

Where β is the angle between the IRP machine X and Y-axes and the H-axis vector. $n_{(x,y)}$ are the current H-axis vector X and Y components. $B_{(x,y)}$ is subsequently modified error angle, α , given by (4.27). This results in the corrected angles, $\omega_{(x,y)}$, given by (4.29). The corrected angles are used to compute a new H-axis vector.

$$\omega_{(x,y)} = \alpha_{(x,y)} + \beta_{(x,y)} \quad (4.29)$$

Finally, a projection is made along the resultant vector by D_{VT} to find the corrected virtual pivot position. This new co-ordinate and vector are used to compute a new set of machine axis positions using the inverse kinematics equations ((4.10) and

(4.12)) and the machine is moved. In practice, it is observed that surface features move slightly (typically < 10 pixels) in the FOV. This can be reduced through improved calibration of the instrument length at setup.

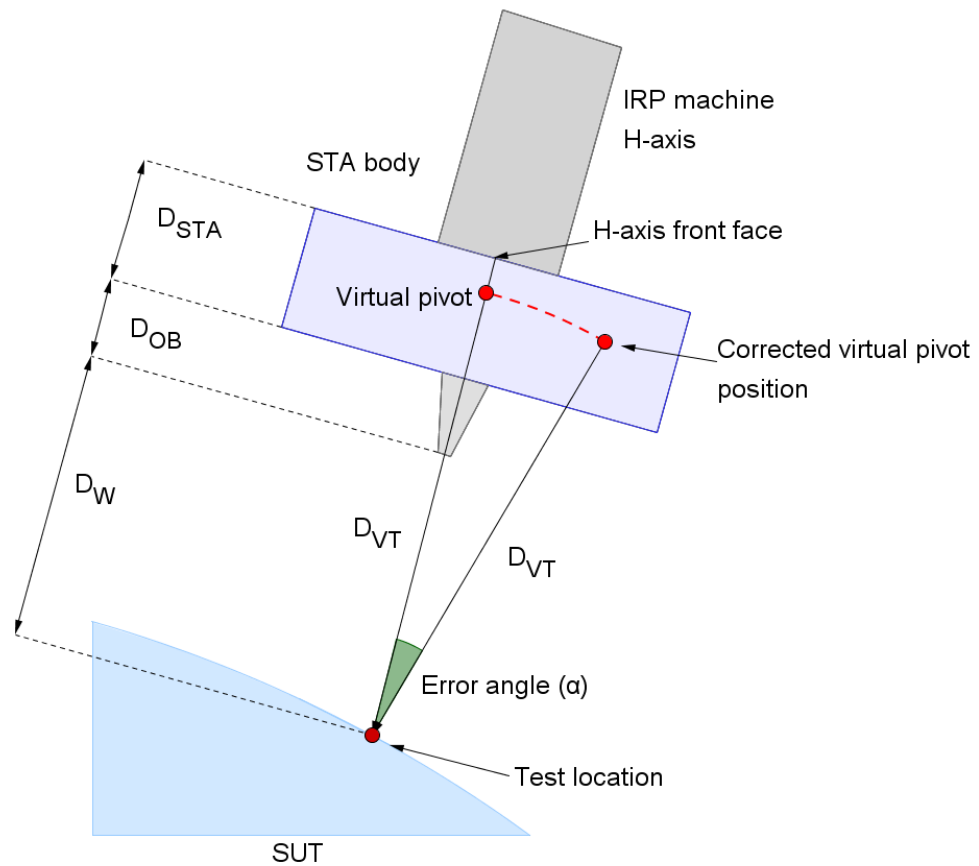


Figure 4.20: Tilt correction of STA mounted on IRP machine

In order to make an alignment correction as described, the orientation of the device camera relative to the IRP machine co-ordinate frame must be accounted for. All co-ordinates read from, and passed to the machine control system in the form of G-code are specified with respect to the IRP machine co-ordinate frame. When 4Sight returns Zernike alignment terms, they are given in the camera co-ordinate frame. As the A-axis of the IRP machine rotates the STA camera plane out of alignment with the machine axes, alignment correction using the provided Zernike terms cannot be applied directly to the H-axis vector. Figure 4.21 shows the A-axis

assembly of the IRP machine when viewed from above, with the STA secured to the H-axis and the B-axis set to zero. It can be seen that, as the STA maintains a fixed relationship with the H-axis, rotations of the A-axis result in the misalignment of the STA camera co-ordinate frame with respect to that of the machine. During initial STA testing, it was found that co-ordinate frame error owing to camera and machine co-ordinate frame misalignment prevents alignment convergence.

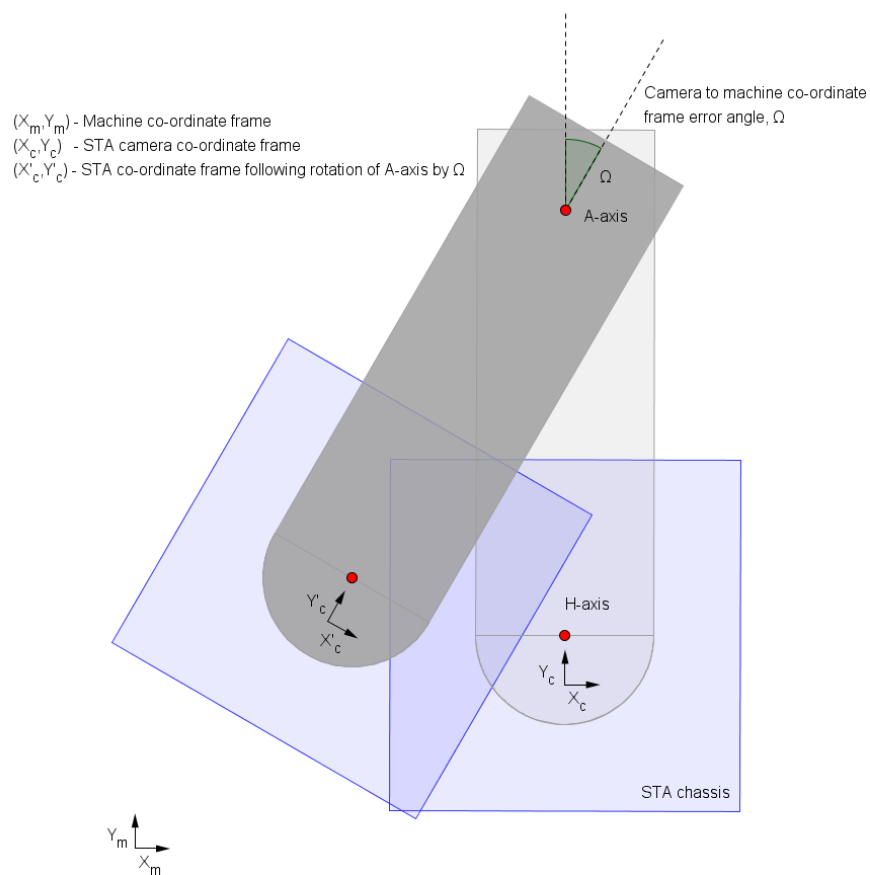


Figure 4.21: Relationship between STA camera and IRP machine co-ordinate frames when rotating IRP machine A-axis

To account for the machine to STA camera co-ordinate frame error, the H-axis vector is computationally rotated about the Z-axis by the A-axis value using (4.30), to effectively place the STA camera axes consistent with those of the IRP machine. Following this correction, the Zernike terms may be applied to correct the H-axis

vector for misalignment using (4.27). The resultant vector is rotated by the A-axis value back to the original rotation. This allows the system to make camera relative alignment corrections, despite the machine and camera axes not residing in the same co-ordinate frame.

$$\begin{bmatrix} n'_x \\ n'_y \\ n'_z \end{bmatrix} = \begin{bmatrix} \cos(-A) & -\sin(-A) & 0 \\ \sin(-A) & \cos(-A) & 0 \\ 0 & 0 & 1 \end{bmatrix} \begin{bmatrix} n_x \\ n_y \\ n_z \end{bmatrix} \quad (4.30)$$

Where (n_x, n_y, n_z) is the H-axis vector obtained by applying (4.22), (4.23), and (4.24) to the machine position, obtained from the CNC controller. A is the A-axis value and (n'_x, n'_y, n'_z) is the resultant corrected vector. Large B-axis rotations will also produce error between the camera and machine co-ordinate frames owing to the B-axis acting at a 45° in the Y-Z plane, with the A-axis at zero. For the relatively shallow (typically $< 10^\circ$) slopes measured during development, this affect proved negligible. However, this will be addressed in future work as control system performance on steep surfaces will be degraded.

While tilt correction is ongoing, the system remains in an iterative loop of measuring and correction moves until the residual tilt error falls below a user defined threshold. At the start of each iteration of the fine alignment routine, the system checks the average modulation of the interferometer and, if fringes are lost, the auto focusing procedure will be executed.

This section has discussed how, after arriving at a test location defined in the measurement plan, the STA locates fringes and is automatically aligned with the SUT prior to measurement. This process involves acquiring measurement data and using a Zernike fit to obtain tilt information relative to the SUT. This tilt information

is used to calculate an improved position and move the IRP machine. The application of this technique to on-machine texture interferometry is a novel step. When there is large tilt or focus error between the STA and the SUT, a pattern recognition algorithm is employed to allow fringe detection. This technique is discussed in Section 4.5.2.1.

4.5.2.1 Fringe Detection for the STA

As mentioned in Section 4.5.2, the average fringe modulation value calculated by 4Sight cannot be reliably used for fringe detection in the presence of high tilt error (>~5 fringes) because the fringe pattern under fills the device FOV. The 4Sight application does produce modulation maps, frames where modulation with adjacent pixels is mapped to intensity. However, requesting these frames via the Python Web service causes the application to crash, and a solution to this could not be found. It is possible to check modulation by computing pixel-to-pixel variation in intensity from a raw frame. However, using this method, it would be difficult to implement a computationally efficient algorithm which would operate robustly in the presence of noise. Therefore this section presents the novel approach of applying a Hough transform to aid the detection of fringes for on-machine metrology. The Hough transform is a pattern recognition algorithm which allows feature extraction of imperfect objects based upon a voting system in parameter space.

In the presence of large tilt error the interferometer remains capable of unwrapping fringes provided they are non-aliased, however it is difficult to determine if fringes are present. Measuring at each point in the scanning envelope

during coarse focusing would be time consuming and could potentially lead to false plane fitting and pose a collision risk to the instrument. It was therefore decided that pattern recognition would be used to identify fringes within the image.

In order to carry out a Hough transform, a raw interferometric frame is captured from the interferometer. Background subtraction is used to remove any systematic error associated with the device optics, such as internal reflections or dust. The resultant image is passed through a Sobel filter to perform edge detection. The Sobel filter is a discrete differentiation operator which emphasises edges within the image. Though there are many common edge detection operators such as Canny and Gaussian, the Sobel operator was selected for ease of implementation.

The Sobel filter convolves two 3x3 kernels with the image data, given in (4.31) and (4.32), producing two matrices containing the X-axis, G_x , and Y-axis, G_y , gradient magnitudes respectively. A root sum squared (RSS) matrix is then calculated from the X and Y matrices, providing an image containing slope information within the original image given by (4.33).

$$G_x = \begin{bmatrix} -1 & 0 & 1 \\ -2 & 0 & 2 \\ -1 & 0 & 1 \end{bmatrix} * I \quad (4.31)$$

$$G_y = \begin{bmatrix} -1 & -2 & -1 \\ 0 & 0 & 0 \\ 1 & 2 & 1 \end{bmatrix} * I \quad (4.32)$$

Where I is the raw frame acquired from the STA.

$$I_E = \sqrt{G_x^2 + G_y^2} \quad (4.33)$$

Where I_E is the resultant RSS edge image of G_x and G_y . As the Hough transform used for pattern recognition accepts as an input a matrix containing logic values, a threshold is applied. All pixels with a value greater than the threshold are set to one, and all below are set to zero. The return from the SUT is observed to vary in intensity depending upon factors such as sample reflectivity, alignment error, and device camera settings and so a fixed threshold value is unsuitable. Therefore the applied threshold is calculated from the mean value of I_E , as shown in (4.34).

$$T_E = 1.5\overline{I_E} \quad (4.34)$$

Where T_E is the threshold value applied to edge image, I_E , to provide a logical matrix for application of the Hough transform. The factor of 1.5 was established empirically as the most suitable. However, (4.34) will be reviewed when other objectives are used with the STA. An example resultant image following application of the threshold is shown in Figure 4.22. This image was generated by applying the Sobel filter discussed to Figure 4.18. It is observed that the fringe pattern becomes clearly visible in the resultant image along with some regions of noise.

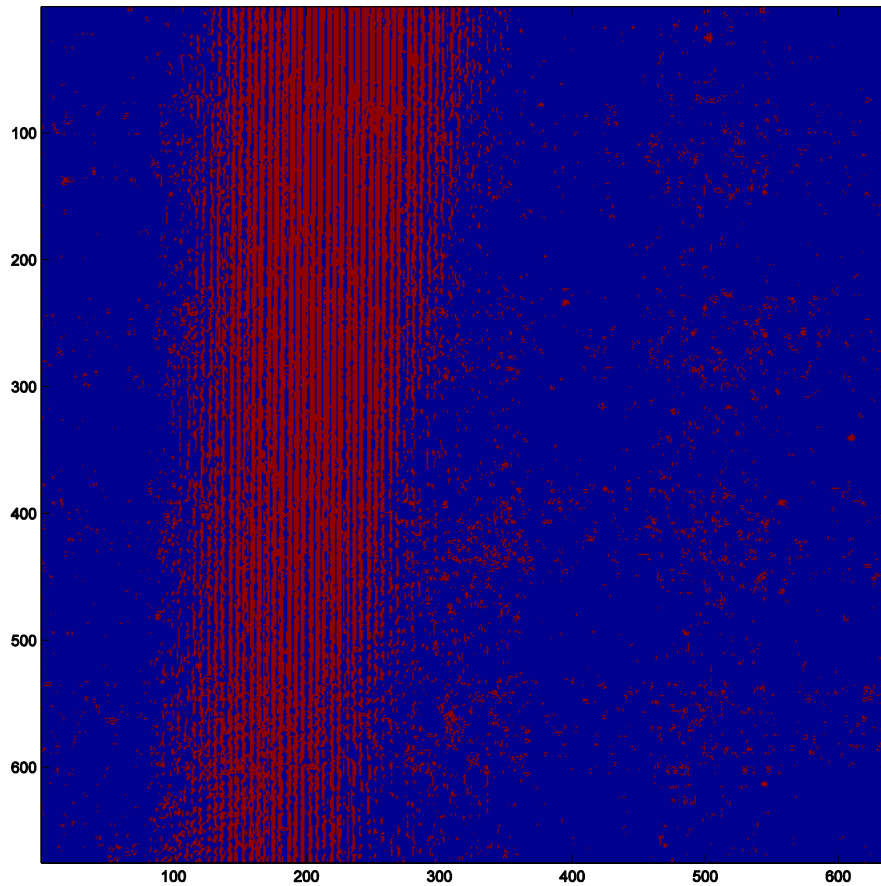


Figure 4.22: Sobel filter output

The Hough Transform was selected pattern recognition at it is particularly well suited to determining the presence of non-perfect patterns yet sufficiently flexible to allow the function to be reused for other applications [92]. When using the Hough transform, the problem is parameterised in terms of the distance of a line from the origin (r), defined as the bottom left of the image, and the orientation of that line within the image (ϑ_l). In parameter space, the equation of a line may be represented by (4.35).

$$r(\theta_l) = x\cos(\theta_l) + y\sin(\theta_l) \quad (4.35)$$

Where r is limited in size by the image dimensions in pixels, and ϑ_i specified from 0 to π . The number of increments ϑ_i is divided into controls the sampling resolution of the Hough transform and the processing time required. Each pixel detected as part of an edge in I_E has (4.36) applied to it, mapping it to a sinusoid for every value of ϑ_i and is stored in a table called the accumulator. The algorithm then iterates through the accumulator placing votes for each combination of r and ϑ_i , thereby identifying all possible lines which pass through the pixels contained in I_E . The r and ϑ_i combinations with the highest number of votes indicate the best fit line for the pixel contained in the image. Due to this voting process, the Hough transform is able to detect imperfect patterns and so can function with incomplete lines or those which may be slightly curved. This is useful in the case of fringe detection, as on small ROC surfaces with a low magnification objective, the fringe pattern may appear curved.

Figure 4.23 shows an example Hough transform, produced during on-machine testing of the STA. The top-left image shows a raw frame acquired from the interferometer with fringes visible across the full frame. The top-right image shows the image following Sobel filtering. The remaining fringes are shown in white and are greatly diminished in number due to the thresholding process preserving only those of greatest contrast. The green lines are the inverse transforms of the lines detected by the Hough transform, which have been overlaid on the edge detection image to assess the fit. The inverse transform is performed using (4.36). It can be seen that some of the green lines run almost horizontal across the bottom of the image. This occurs because the Hough transform has placed votes in regions which

contain large areas of pixels and so may form a part of many different combinations of r and ϑ_l . Possible solutions to this are discussed later.

The bottom-left image is a visualisation of the Hough space following the voting process. The black regions indicate no votes. The light yellow regions are those with the highest votes. The green crosses show the regions which have been selected for use in fitting and are those which have been inverse transformed and displayed in the top-right image.

$$y = -\left(\frac{\cos(\theta_l)}{\sin(\theta_l)}\right)x + \frac{r}{\sin(\theta_l)} \quad (4.36)$$

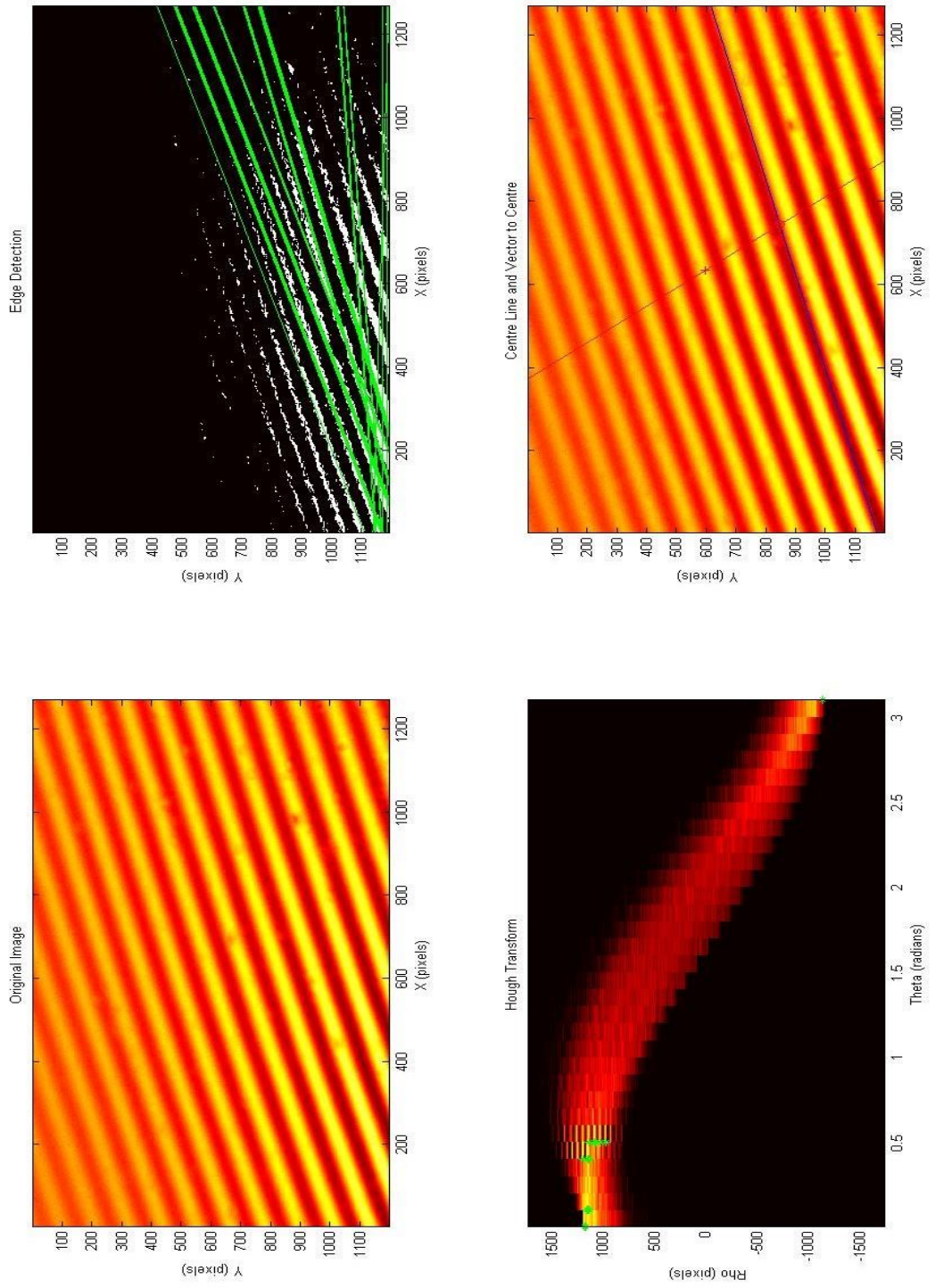


Figure 4.23: Fringe detection using the Hough transform

In this example the 50 Hough regions with the highest number of votes have been used for fitting. This value was arrived at empirically based upon the observed performance of Hough transform during on-machine testing. The selected r and ϑ_i values are averaged to reduce the effects of any combinations which produce a poorly fitted lines. Finally, the bottom-right image in Figure 4.23 shows the raw frame with a blue line, indicating the average line obtained from the 50 averaged Hough space values. The red line shows the vector between the frame centre, which is the target position for the fringe pattern centre, and the average fit line. The distance in pixels between the fringe pattern centre and the camera centre pixel is finally calculated. The error value is then used to obtain a focus sensitivity and monitor the progress of subsequent error correction moves, as described earlier in this section.

The Hough transform is capable of fitting patterns to incomplete features or noise. While this is of benefit in situations where contrast can vary across an image, noise and surface defects can result in poorly fitted lines. During testing with a typical SUT used for process development of the E-ELT work, it was found that some light was returned from the back of the SUT. The source of these returns occur where the part was blocked to an aluminium runner using wax. When the STA first arrived at the predicted measurement location and began scanning for fringes, some of these features became visible. Figure 4.24 shows the resultant Hough transform of this image, with many of the discrete regions allowing line fitting. When these features detected, the systems stops scanning for fringes and attempts to calculate a focus sensitivity value with the erroneous data. This causes invalid values and the system

becomes stuck. In order for the STA to become a viable automatic on-machine metrology tool, the system must be able to cope with such features as surface dig or scratches. In order to reduce the effects of such practical problems, a cluster size filter was implemented.

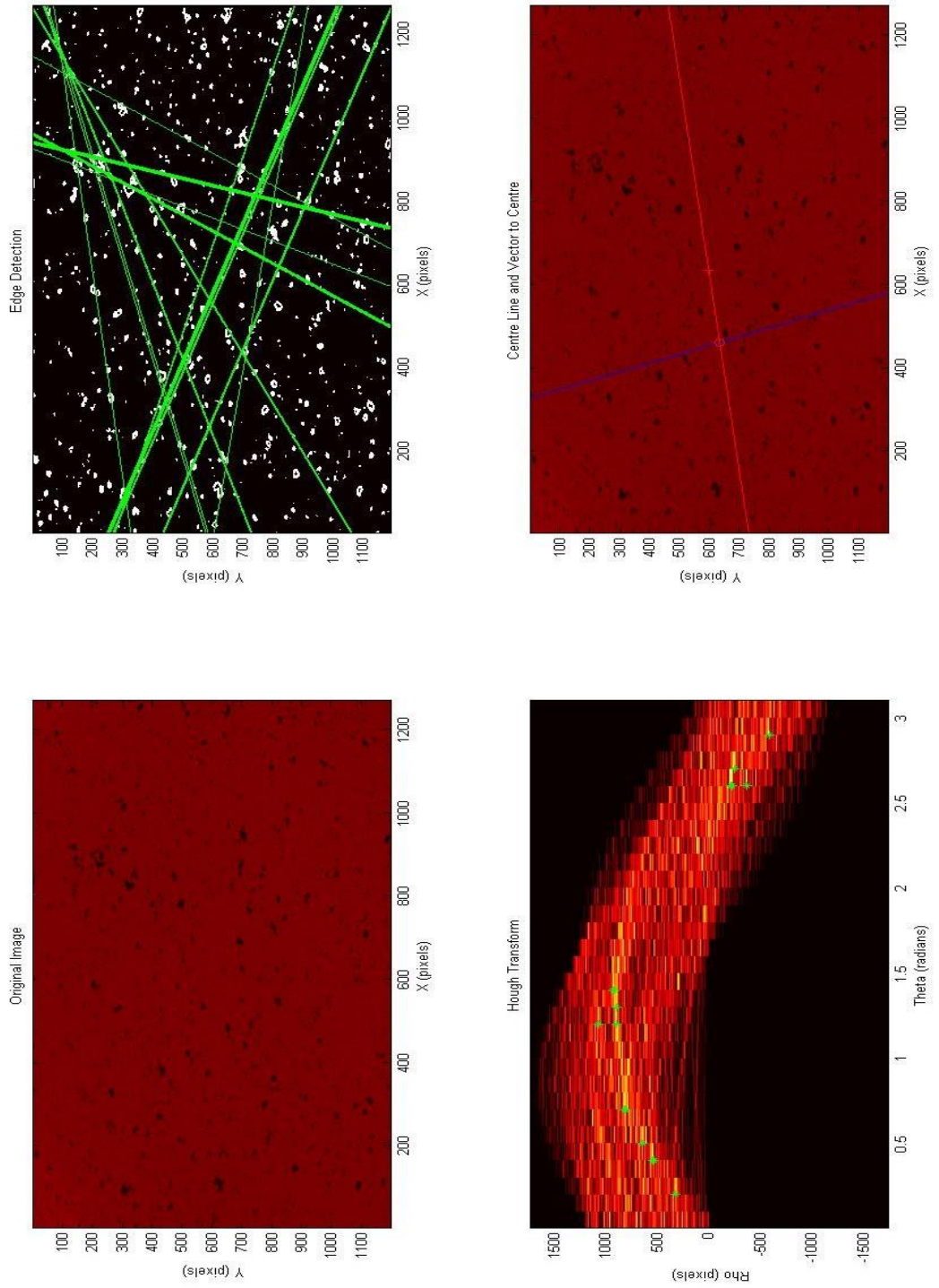


Figure 4.24: Hough transform in the presence of noise

The problem illustrated in Figure 4.24 occurs because many small, discrete regions of pixels tend to remain following edge filtering, which can be fitted to many lines. Typically, fringes are larger regions of contiguous pixels. A filter was therefore created which scans a window across the edge image output by the Sobel filter. All pixels within this window are summed and the pixel at the centre of the window is set to the total value. A threshold is then applied to the resultant image to specify a minimum feature size which may remain in the image. Figure 4.25 shows an example frame following Sobel edge detection but without cluster filtering. Figure 4.26 shows the same dataset following the application of the cluster filter discussed.

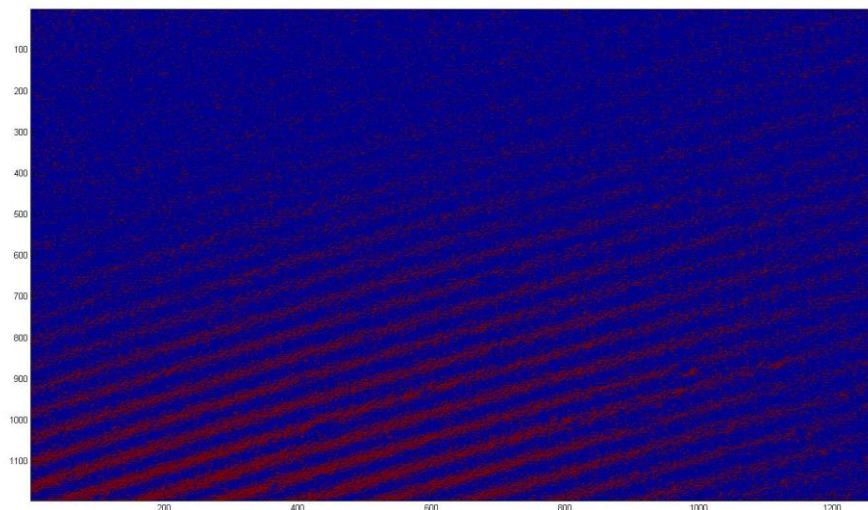


Figure 4.25: Edge detection result prior to cluster filtering

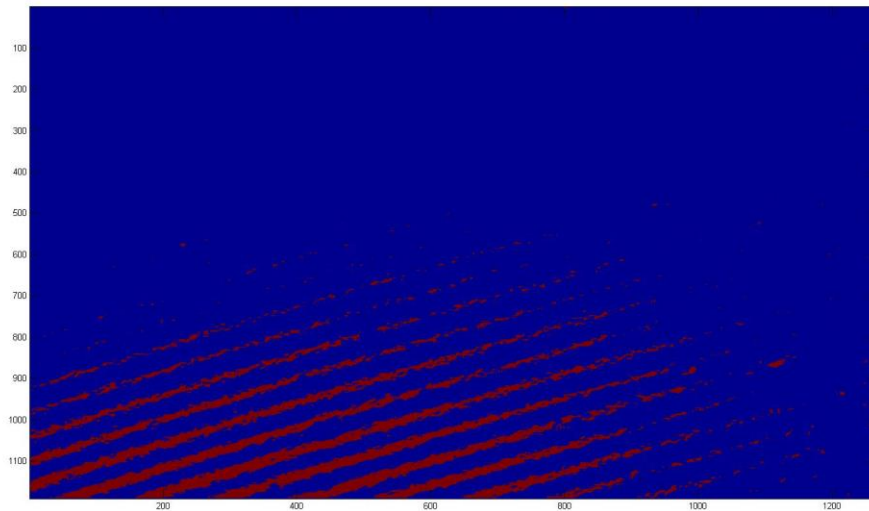


Figure 4.26: Edge detection result with cluster filtering

It can be seen that the occurrence of noise in the image is greatly reduced, leaving high contrast fringe edges. Given input data such as that shown in Figure 4.24, it is found that the small regions do not survive the cluster filter. The filter was tested with the same part which previously exhibited the problem of erroneous fringe detection and the issue could not be replicated.

This section has discussed the application of a Hough transform to the detection of fringes for situations when the modulation value provided by 4Sight becomes unreliable. This unreliability occurs in the presence of large tilt errors, causing fringes to arrange in a band across the device FOV. It has been demonstrated that the Hough transform in combination with a Sobel filter and a cluster filter provides a robust method to detect the presence of interferometric fringes, while avoiding erroneous detection of noise and spurious features associated with part blocking and glass inhomogeneities.

Though the implementation discussed provides reliable operation, further improvements may be made to increase speed of operation. At present the Hough transform step alone takes approximately 1.5 seconds to complete. Execution time is directly proportional to the number of points contained within the accumulator. At present the Sobel filter provides an image containing bands of contiguous pixels, representing fringes. However, only lines a single pixel thick are required for fringe detection. Therefore a line thinning filter can be applied to reduce the thickness of the bands returned by the Sobel filter, and thus the number of points contained in the Hough accumulator. The application of a further filtering step must be evaluated to ensure a net decrease to processing time is achieved. This is to be addressed in future development.

4.5.2.2 Mitigation of the [0,0,1] Condition for H-axis Mounted Metrology

As mentioned in Section 2.2.3.2, the [0,0,1] condition can make proper alignment of any device mounted to the tool chuck of the IRP machine difficult. Avoiding areas prone to the [0,0,1] condition is not a viable for components such as the ESO E-ELT, due to the long base ROC of the part. This section discusses a method of minimising the effects of the condition, allowing proper alignment of the device without modification of the IRP machine.

When aligning a device fitted to the machine H-axis to a part which is near plano or plano, interferometric fringes cannot be completely nulled. Instead a small number of fringes typically remain. In the case of the STA, these fringes are arranged vertically, indicating they occur perpendicular to the B-axis when projected onto an X-Y-plane. Under such conditions, the B-axis is usually near zero and so a rotation of

the A-axis does not provide adjustment. One option explored is to fit an extra axis in the form of a piezoelectric tilt system to the device, however, such a solution would require the addition of further control modules and system interfaces. The decision was taken to add as little additional hardware as possible, while not modifying the IRP machine in a manner which could impact the ability to manufacture optical surfaces or perform other metrology. The spigot by which the STA is mounted to the IRP machine was therefore modified to include a tilt of 1.9° , as shown in Appendix O. This angle was found by testing a series of locations on the ESO MSS part, and calculating the angle at which proper alignment becomes possible from knowledge of the local surface normal vector at the first unaffected location.

When the STA is fitted to the IRP machine, the spigot tilt is arranged such that the STA optical axis is tilted along the X-axis of the machine with respect to the H-axis. During setup the A and B-axes of the machine must offset to compensate for the spigot tilt and null the device to the first measurement location. Thereafter, the system behaves as normal. When encountering the $[0,0,1]$ condition, the control software can command the H-axis of the machine to rotate, thereby adjusting the orientation of the spigot tilt to compensate for the error in the B-axis which causes the condition to occur. The vertical fringes, which previously could not be nulled, are observed to be rotated to a horizontal orientation by the H-axis rotation. These horizontally arranged fringes may be nulled by adjusting the B-axis. Using a tilted spigot has allowed the use of the IRP machine H-axis, negating the requirement to add further axes or hardware.

However, in order to implement this solution to mitigate the [0,0,1] condition, the IRP machine H-axis must be integrated into the Fanuc control system as an axis, rather than as a spindle, where the motor is configured only to rotate at a known speed. The IRP1200 and IRP1600 machines installed at the OptIC Glyndwr facility use H-axes which are configured as spindles only. Therefore, this solution has been verified experimentally with alignment and H-axis rotations performed manually. This solution was found to successfully remove the effects of the [0,0,1] condition, allowing the STA to be properly aligned for measurement of plano surfaces, which was previously not possible.

To fully integrate this solution into the automatic operation of *Metrology Controller*, modifications of the control application are required. Knowledge of the instrument camera orientation with respect to the IRP machine must be maintained. To date, the STA has been mounted such that the device camera X and Y-axes are parallel with those of the machine, with the A-axis at zero. When rotating the H-axis, the camera co-ordinate frame becomes rotated compared with that of the machine. This requires the modification of the work presented in Section 4.5.2 to perform correction for the H-axis axis as well as the A-axis. Figure 4.27 shows the IRP automatic nulling function, which has been updated to determine whether the measurement point falls within the region affected by the [0,0,1] condition. This decision is made by observing the angle between the local surface normal vector and the machine Z-axis. If this angle is less than the minimum beyond which normal auto-alignment is possible, H-axis correction is required. Figure 4.28, shows the prototype function to perform the H-axis correction.

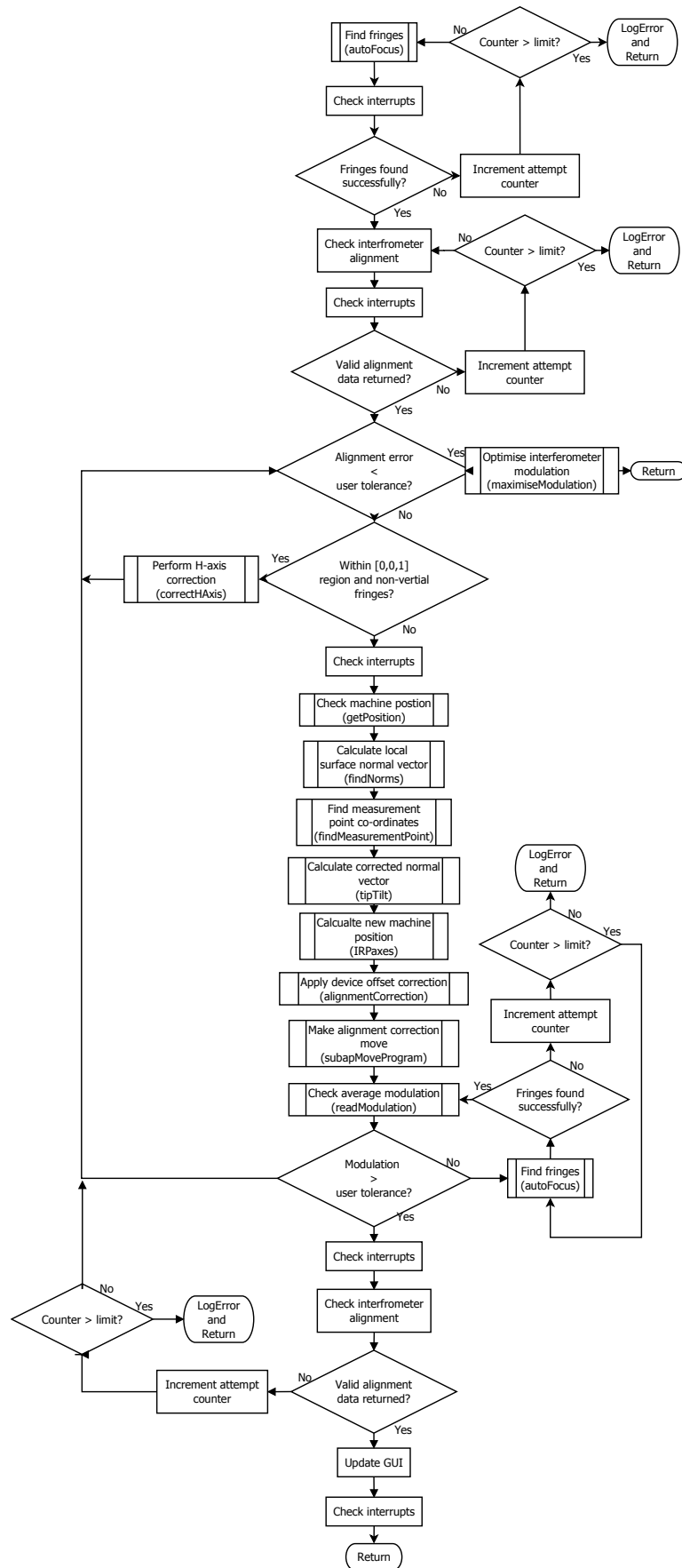


Figure 4.27: H-axis adjustment integrated into the STA automatic alignment script

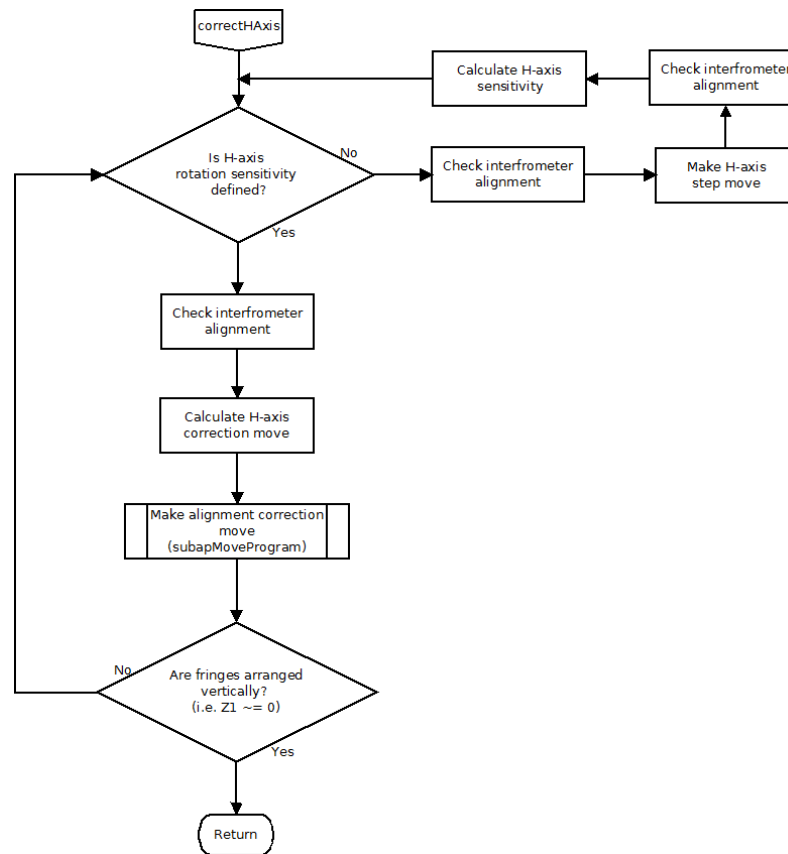


Figure 4.28: H-axis correction function for [0,0,1] condition mitigation

Having corrected the fringes to be horizontal in the device FOV, the function returns. Normal alignment is then performed and measurement proceeds as normal. It is likely that some further correction will be required to take into account that interferometer objective will be tilted out of the X-Y plane of the machine by the tilted spigot, however no noticeable problems were found during initial testing.

This section has presented a solution to allow the STA to be operated on the type-2 virtual pivot machine without modification to the machine, nor significant modification to the instrument itself. The tilted spigot used here can be easily removed and refitted with a normal mounting for other testing work. The solution given has been initially tested on the IRP1200 to confirm performance, however, full integration into the automatic control routines has not been possible owing to the spindle configuration of the H-axis on the systems at OpTIC. All modern type-2

virtual pivot IRP machines have H-axes configured as axes and therefore properly encoded to support this solution.

4.5.3 Conclusion

This section has discussed the automatic alignment of both point and sub-aperture measurement systems using closed-loop operation with feedback provided via 4Sight and the alignment camera acquisition software for the Metrology Station. The alignment routines of both measurement systems have two modes of close-loop operation: coarse and fine alignment. Owing to the differing hardware configurations of the STA and the Fizcam 3000, different coarse alignment routines are required.

The Fizcam 3000 uses an internal alignment camera for coarse alignment, producing return spots from both the reference optic and the SUT. Placing both of these returns coincident at the centre of the alignment screen produces interference and allows the system to switch to fine alignment. However, the sensitivity of both coarse and fine alignment modes to translation (for spherical surfaces) is dependent upon the F# of the transmission optic used. Therefore, the alignment routine includes functionality to characterise this sensitivity for both coarse and fine alignment modes.

Although the STA does include a coarse alignment mode, wherein the return from the objective is overlaid with that from the source, optimising this alignment does not generally produce interference in measurement mode. Therefore, a procedure of scanning the device along the H-axis vector has been adopted. In order for this procedure to prove effective in the presence of high tilt error, when

4sight cannot detect the presence of fringes, a pattern recognition algorithm has been successfully employed. With the fringe pattern located and centred in the device FOV, the alignment routine switches into fine mode.

For both measurement systems, fine alignment mode uses Zernike terms computed by 4Sight from measurement data, to calculate subsequent correction moves. The residual error achievable in this mode is limited by the step resolution of the hardware. The step resolution for linear axes supplied by Zeeko is currently 1 μm , however this can be reduced to 100 nm by modifying the Fanuc control system. Even with the 1 μm step resolution, the Metrology Station is capable of 0.03 waves residual tilt error for a F1.5 test configuration when averaging 4 frames for Zernike fitting. Similar performance has been obtained with the STA using a 10x objective.

4.6 Measurement Acquisition

When sufficiently aligned, the system changes the interferometer configuration into measurement mode, which increased acquisition averaging to minimise vibration print through. Measurement acquisition is carried out and the data checked to ensure sufficient valid pixels are present, compared with a user specified threshold percentage. Should there be insufficient pixels, the system will check alignment and attempt measurement again, using the standard error handling procedure. Following a successful measurement, the interferometer data file is saved and the measurement report is updated. The measurement report is a text file which contains surface statistics for each measurement along with the valid pixel percentage and any notes of any problems. This allows the user to quickly

understand where any problems with the measurement process lie. The system can then be instructed to repeat single sub-apertures to fill in missing data, if required.

When all measurement locations have been addressed, the system will return the axes to the home location and indicate to the operator that measurement is complete. If the user has requested more than one data set, the system will immediately start the next set.

4.7 Application of Metrology Control System to Automatic Manufacturing Cell

At the point of completing the initial development of *Metrology Control Suite*, there was in place automated polishing and automated metrology. Both of these processes do not require human intervention during execution. However, setup and initialisation do require manual work. The next logical step must be to attempt to automate these intermediate tasks also. Therefore, Zeeko in partnership with Glyndwr University have engaged in a TSB project [93] to integrate a robotic arm with an IRP machine. This project aims to enable the automation of loading and unloading of optical components and tooling to the IRP machine, as well as wash-down between process and metrology. Such work provides the ambitious prospect of developing a *completely automated cell*, containing an IRP machine, metrology and a robotic arm, to carry out part and tool handling activities. A prototype cell system is currently under construction at OpTIC Glyndwr, as shown in Figure 4.29.



Figure 4.29: Prototype optic production cell including a Zeeko IRP600 and Fanuc M20i-A robot arm

As part of the *Metrology Control Suite*, a series of control and communications functions has been developed. These functions are currently being augmented to include interfacing for the robotic arm and will, in the future, include an interface to *Zeeko TPG* to allow the system to plan polishing activities. The amalgamation of tool path generation, metrology planning and control functionality will be governed by a decision making system which will include task scheduling algorithms to maximise cell productivity. This application of the work discussed in this thesis illustrates the flexibility of the architecture, in that new functionality can be added while maintaining the same performance used in other projects. The operator would control, not just an IRP machine or a metrology station but a whole production cell. In terms of process development for projects like the ESO E-ELT, which has taken around 7-years to date, small scale prototypes could be processed continually,

automatically exploring the parameter space and producing large quantities of process data. The process engineer is then freed from moving parts around manually to focus on analysing data to find the best possible route to a convergent process and the development of new finishing techniques.

4.8 Conclusion

This chapter has presented the development of a control application which allows a system comprised of both interferometer and CNC hardware to conduct automatic on-machine metrology, based upon a measurement plan created using the *Metrology Designer* module discussed in Chapter 3. The decision making behaviour of the system when operating in both open-loop and closed-loop modes has been discussed. Solutions to some of the problems identified in Chapter 2, such as the STA [0,0,1] condition and operation in the presence of an unstable environment.

Although the STA and Fizecam 3000 have been applied to the IRP machine and Metrology Station respectively, there is no limit in software to prevent using each instrument with either machine. This is possible because the *Metrology Control Suite* is of a modular design and the choice of which kinematics to use during measurement is specified in the system configuration file. Therefore, new hardware may easily be supported in the future with little variation to either the existing code, or the behaviour of the user interface. This approach has been adopted both to enable simplified integration of further systems into the application and to minimise time spent developing the GUI. It was observed at various points during development that debugging the user interface takes a disproportionately large amount of time compared with the functionality it provides. However, the GUI

provides an essential window into the operation of an automated system, and so from the perspective of safety alone, a clear and effective interface serves an important role in a fully automatic system. As automatic metrology is expanded in both capability and complexity, it is critical that the human factors of such automation are understood [94].

Chapter 5 will provide an assessment of the features of the *Metrology Control Suite* and the data produced by both the STA and the Metrology Station. It will be demonstrated that automatic on-machine metrology is capable of producing data of comparable quality with that of state-of-the-art techniques, even in an unstable testing environment.

5 Results and Discussion

As discussed in Chapter 1, many state-of-the-art measurement techniques are unsuitable for the manufacture of next generation extremely large telescope optics. The combination of large, heavy optics, and their support systems, results in logistical problems transporting such components to the metrology laboratory. Many early on-machine solutions suffer from having to control the manufacturing environment and, in the case of texture measurement, require contact with the optical surface. The development of vibration insensitive interferometers and sub-aperture stitching metrology has provided an opportunity to remove some of the problems currently associated with on-machine metrology. The author has combined these new techniques with existing CNC systems to enable automatic on-machine metrology, as well as produce more reliable metrology in the manufacturing environment.

Following the development of the *Metrology Control Suite*, the software has been used to carry out a series of measurements with both the Metrology Station and STA automatically. This chapter will discuss measurement results as well as the performance of the control system, and demonstrate that the techniques developed can support future production of ultra-precision large optics. Where possible, comparison will also be drawn between state-of-the-art techniques and those presented in this thesis.

5.1 Surface Texture Analyser

As discussed in Chapter 1, surface texture measurement of large surfaces such as E-ELT segments currently presents practical challenges due to the physical configuration of state-of-the-art instruments and the requirement to transport the SUT. On-machine instruments generally require placement onto the surface and manual alignment, posing a risk of surface damage. Also, in order to achieve the production rate required for the E-ELT to meet the first light deadline, duration of metrology must be minimised. Therefore, systems such as the STA used with *Metrology Control Suite*, provide an advantage over existing devices.

As discussed in the preceding chapters, the STA device is fitted to the IRP1200 machine and is classed by the control system as a point measurement device. This means the measurement design process produces a set of discrete points which are not required to overlap. This section will present example data taken with the STA mounted to the IRP machine and make comparison with existing texture measurement techniques. The measurements presented here were taken without the use of the tilted spigot arrangement, used to overcome the [0,0,1] condition.

5.1.1 Application of STA to ESO segment measurement

As part of the ESO E-ELT prototype project, the consortium are required to provide texture measurement data. A summary of the segment texture specification is given in Table 5.1. No requirements for sampling area or resolution are made, which demonstrates that there is no established best practice of how to measure texture for optics of this scale. This is in contrast to form measurement, for which the specification is more comprehensive [34].

As the E-ELT is difficult to move and cannot be accommodated on existing texture measurement systems, the STA is fitted to the IRP1600 machine to perform these measurements. As discussed earlier, most of the ESO segment falls within the region affected by the IRP machine [0,0,1] condition due to the long radius of curvature of the surface. Therefore, tilt actuators fitted to the segment support (discussed in Section 2.3.1) are driven to their extreme in order to introduce sufficient tilt to allow measurement over most of the surface.

Table 5.1: Summary of ESO E-ELT texture specification

Specification	Requirement
Maximum microroughness in useful area	3 nm
Average microroughness in useful area	2 nm
Number of samples to be taken	3

It was found during testing that control system still struggles with this setup due to some regions remaining affected by the [0,0,1] condition. Use of automatic testing would also require the use of non-linear probing to correct the measurement plan for the extra tilt introduced by the segment support. As the operators of the IRP1600 use a non-standard method to perform non-linear probing, development would be required to enable compatibility with *Metrology Designer*. It was therefore decided that *Metrology Controller* would be used in semi-automatic mode for the ESO E-ELT segment pass-off measurements. Semi-automatic mode allows the user to interpret the live fringes in 4Sight and select which way the system should tilt. This reduces the effects of the [0,0,1] condition by allowing assessment of when alignment can no longer be improved. Semi-automatic mode uses the same control functions as fully automated measurement but accepts instructions from the operator. This mode is an improvement over manual

operation as orthogonal moves are produced by the control system, allowing simpler alignment control but without automatic alignment.

Figure 5.1 shows an example ESO E-ELT prototype segment measurement (SPN04). The measurement was taken with the STA using the 10x objective over an area of approximately 0.9 mm x 0.9 mm. The STA has been used in the pass-off of 3 segments and the master spherical segment (MSS) to date.

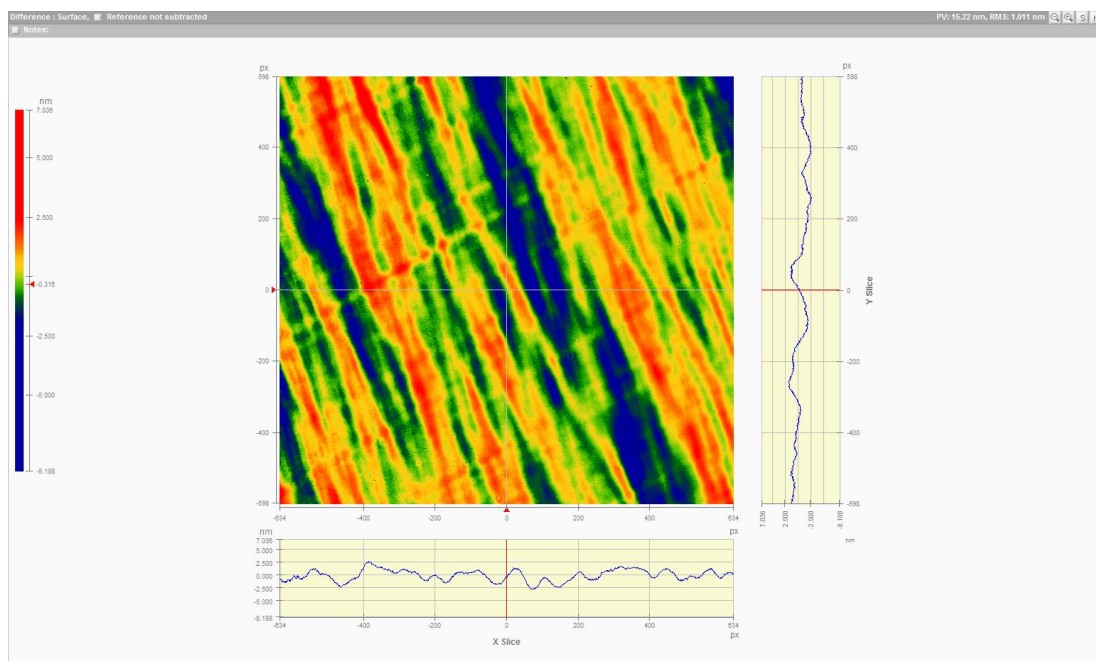


Figure 5.1: Example of ESO E-ELT segment measurement, witnessed by ESO

This measurement produced a result of 15.22 nm PV and 1.01 nm Sa and was calibrated by subtracting a reference dataset created by averaging 16 randomly arranged measurements of a super-smooth reference flat. During the course of the ESO E-ELT segment prototype production, STA measurements have been collected by the author to allow certification of segment texture for customer pass-off.

5.1.2 Automatic On-Machine Measurement

During development, measurements were also carried out on the IRP1200 machine using the STA in automatic mode. This section reviews the data obtained during these measurements, as well as the performance of the control system during operation. Figure 5.2 shows the measurement used for this test, which was performed on a hexagonal 3000 mm ROC concave spherical surface with a corner-to-corner diameter of 200 mm. This test was performed prior to the implementation of the tilted spigot (Section 4.5.2.2) and so the central measurement location was skipped in order to avoid the [0,0,1] condition during the test. It was found that the SUT slope was sufficient at all subsequent locations for measurement to proceed without problem. Measurement points were laid out in three lines from centre to corner. As the target of measurement was to assess control system performance, uniform surface coverage was not required.

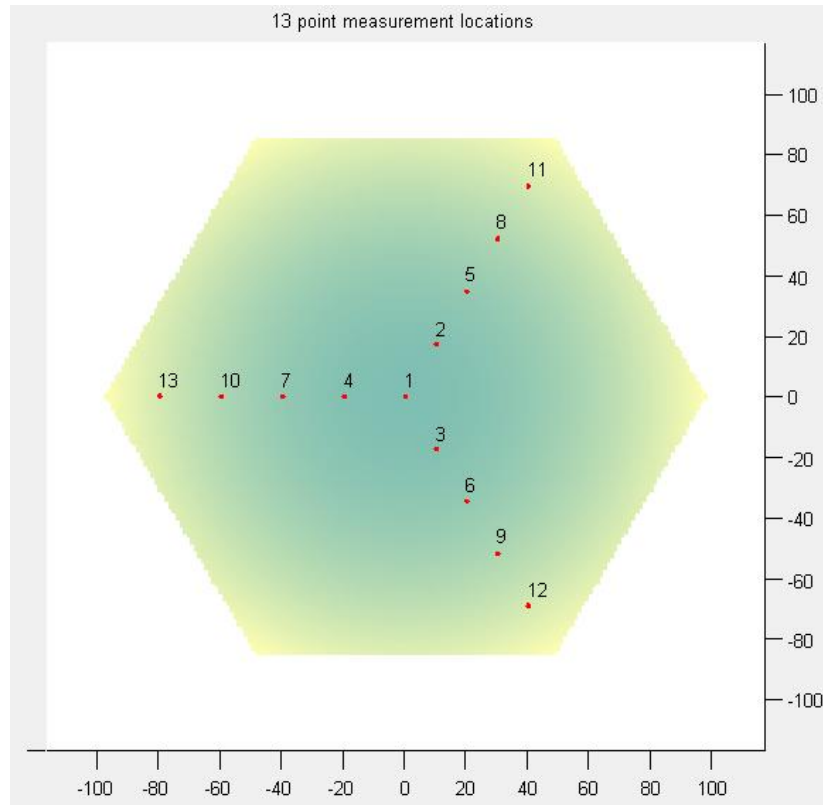


Figure 5.2: STA automatic metrology measurement plan

The modified test location position table is shown in Figure 5.3. This shows that a bulk rotation of 30° has been applied to allow the measurements to run into the part corners.

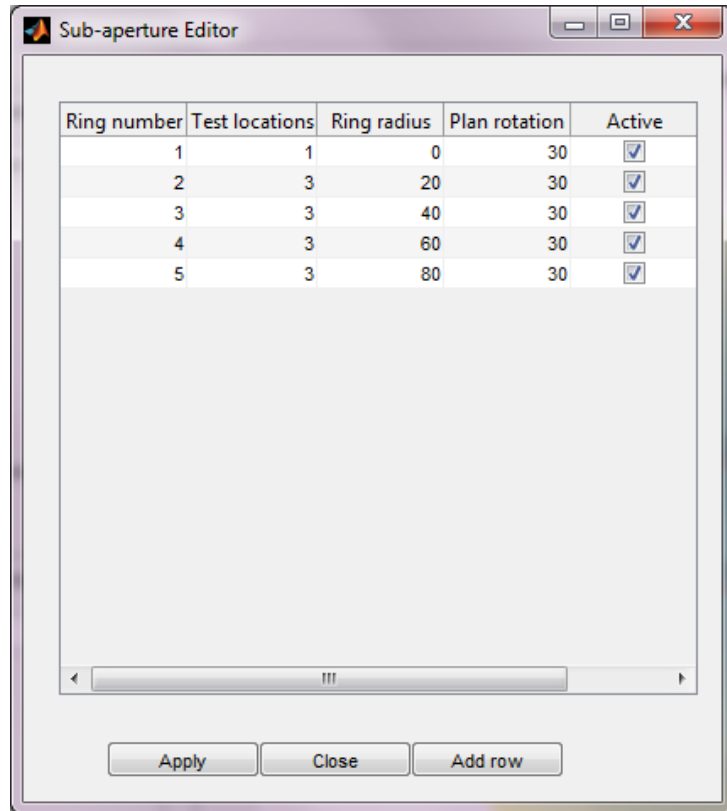


Figure 5.3: Modified test point locations table for STA automatic control testing

Following execution of the setup procedures, measurement was started with an alignment averaging level of 4 samples and measurement averaging of 16 samples. It was observed that the system took approximately 20 minutes to execute the measurement plan. 30% of this time was occupied with data acquisition for both measurement and alignment testing, which is less than expected. Much of the remaining time (14 minutes) was spent in coarse alignment and surface location. As mentioned in Section 4.5.2.1, due to the small depth of focus of the objective, small stage iterations must be made to ensure interferometric fringes are not missed. As has been established in testing, even with the application of non-linear correction, the measurement location may be $\pm 30 \mu\text{m}$ from the predicted location.

The measurement data collected is saved as 4D data files (.h5 format) and must be interpreted manually by the operator. However, as with sub-aperture stitching

measurement, a summary of the measurement statistics (PV, RMS, valid pixels) is produced in a text file. In the case of the example automated measurement, the data showed < 0.3 nm RMS variation in texture across the surface. As this surface is a development part for the ESO E-ELT project, it had previously been treated with a rigid pitch tool, providing a good finish (typically < 3 nm RMS). Figure 5.4 provides an example dataset from automatic measurement. Although, a treatment using the pitch tool has been applied, visible artefacts of the previous process, using LP-66 polyurethane, remain. The fine diagonal left-right marks indicate bonnet rotation direction as it moved against the surface, leaving some perpendicular waviness of small amplitude (< 1 nm). Some underlying, lower spatial-frequency content is also present which shows that insufficient smoothing has been carried out.

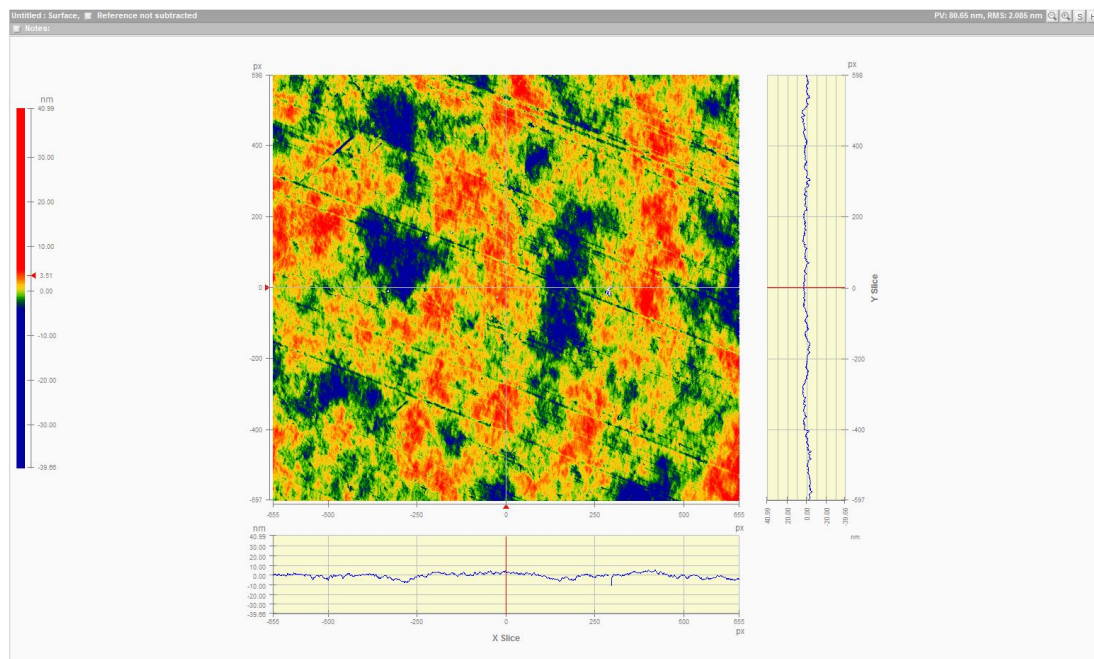


Figure 5.4: STA on-machine automatic measurement example of a small-scale E-ELT process development component

This example illustrates the benefits of using automatic metrology to check surface texture. It is possible for such texture to occur on the surface non-uniformly. This is

particularly problematic for the aspheric ESO E-ELT segments, where the rigid pitch tools exhibit aspheric mismatch. Such a mismatch can cause the smoothing process to be more effective in some areas of the surface, where better conformity occurs, causing a variation in texture. Measuring texture in a small number of locations on a surface of this size poses a risk of areas of poor texture remaining. If such defects go undetected, a degradation in optical performance of the completed system will occur, particularly in stray light. The use of automated on-machine texture measurement therefore provides improved characterisation of both the application of the polishing process and the effectiveness of the final texture treatment.

5.1.3 Comparison of STA with Existing Texture Analysis Techniques

This section will present comparison between the on-machine STA measurement system developed in this thesis and existing texture measurement techniques. This comparison will demonstrate the viability of automated on-machine texture measurement when compared with laboratory based metrology.

5.1.3.1 ADE Phaseshift White Light Interferometer

The Author's paper previous work [81] provided comparison data between the STA and the ADE Phaseshift device, used in small scale process development at OptIC Glyndwr. The dominant reason for the numerical discrepancy between the two measurements was considered to be the different device spatial sampling levels, thought to be principally determined by the CCD resolution. In order to investigate this further, a two dimensional Fast Fourier Transform (FFT) was taken of the two datasets, prior to pixel re-sampling (Figure 5.5 and Figure 5.6). In order to allow direct comparison, the FFT images have been reduced to a plot of power against spatial frequency, with the -3dB points also displayed, shown in Figure 5.7. From

the FFT images, it can be observed that the ADE device does not contain power to the edge of the FFT plot, indicating that the CCD cut-off frequency is not the limiting factor in the system. If the CCD were the performance limiting factor, one would expect to see the data truncated at the edge of Figure 5.5, and containing the same power as the corresponding region of the STA FFT plot.

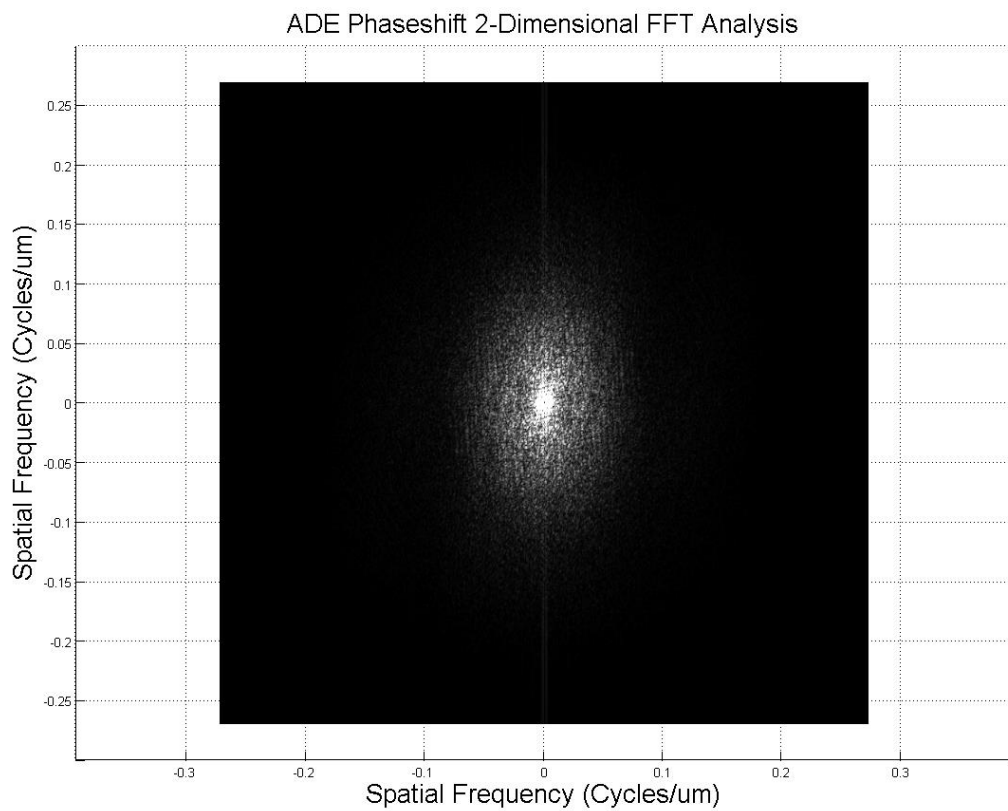


Figure 5.5: Phaseshift ADE FFT analysis result

4D Technology Surface Texture Analyser 2-Dimensional FFT Analysis

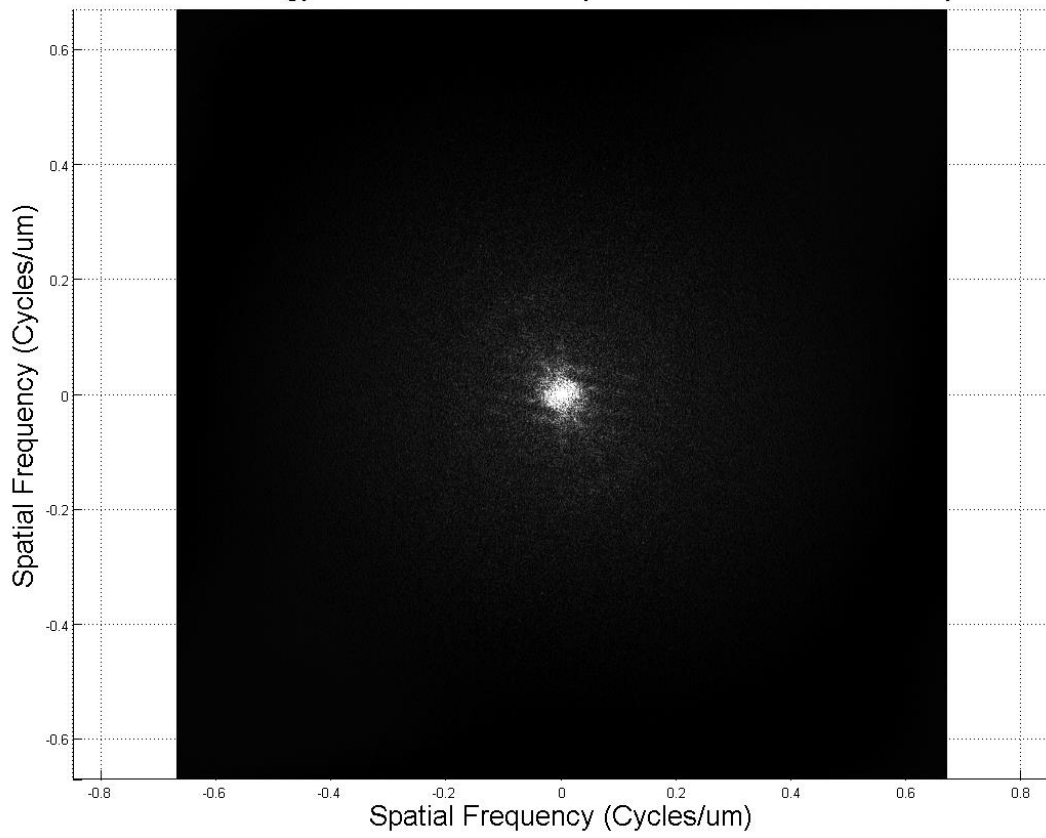


Figure 5.6: 4D Technology Surface Texture Analyser FFT result

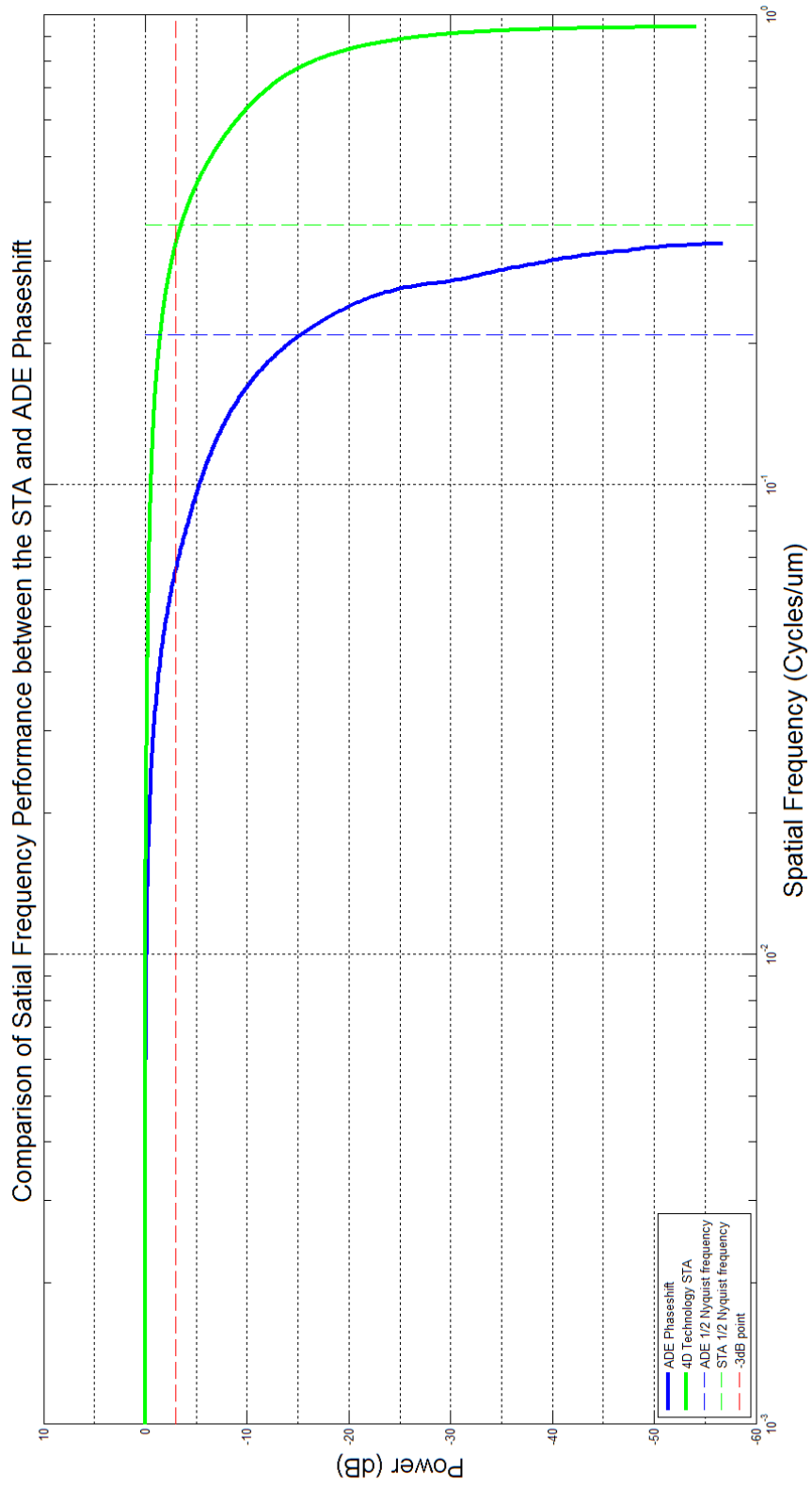


Figure 5.7: Spatial frequency performance comparison between ADE Phaseshift and 4D Technology devices.

Therefore, the optical transfer function (OTF) of the ADE system optics also contributes to the system cut-off frequency. The FFT analysis performed here also reveals the tendency of both systems to low-pass filter spatial frequencies, causing their under reporting in data statistics. The metrologist must therefore be aware of device performance limitations, especially when comparing data taken with different instruments.

The characteristics presented in Figure 5.7 cannot be considered absolute OTF characterisations for the systems compared. The data presented contains not only the instrument characteristic but also the local spatial frequency content of the SUT. Figure 5.7, therefore, serves only as a direct comparison of the two instruments tested, as all data were obtained from the same SUT, which exhibits uniform texture. Full characterisation would require the use of a periodic artefact. This analysis demonstrates why the two devices produce differing numerical results when measuring the same surface. The STA -3dB point occurs at $0.3270 \mu\text{m}^{-1}$ while that of the ADE at $0.0660 \mu\text{m}^{-1}$.

5.1.3.2 Surface Replication

As well as comparing the STA against existing optical techniques, work was also carried out to explore the viability of surface replication for texture characterisation. As mentioned in Section 1.3.2, though surface replication has proven a viable technique for texture characterisation, there is little published material applying the technique to smooth surfaces ($< \sim 100 \text{ nm Sa}$) similar to those required by the ESO E-ELT. In order to make a more thorough comparison, a small Zerodur sample was pitch polished to provide a texture similar to that of a

completed E-ELT prototype segment produced at OpTIC. Two separate replication techniques were then applied to assess their effectiveness. The ADE Phaseshift device was used during this test to provide a demonstration of how replication might be used as an alternative to the STA. Without the use of replication, the ADE device alone cannot measure E-ELT segments due to the physical configuration of the instrument. Figure 5.8 is a direct measurement of the sample SUT using the ADE device, to serve as a control sample for the replicated results. A result of 0.64 nm Sa was obtained over an area of 1.38 mm x 1.02 mm with tilt, power, astigmatism and coma removed. Such a result is representative of measured surface texture of an E-ELT segment.

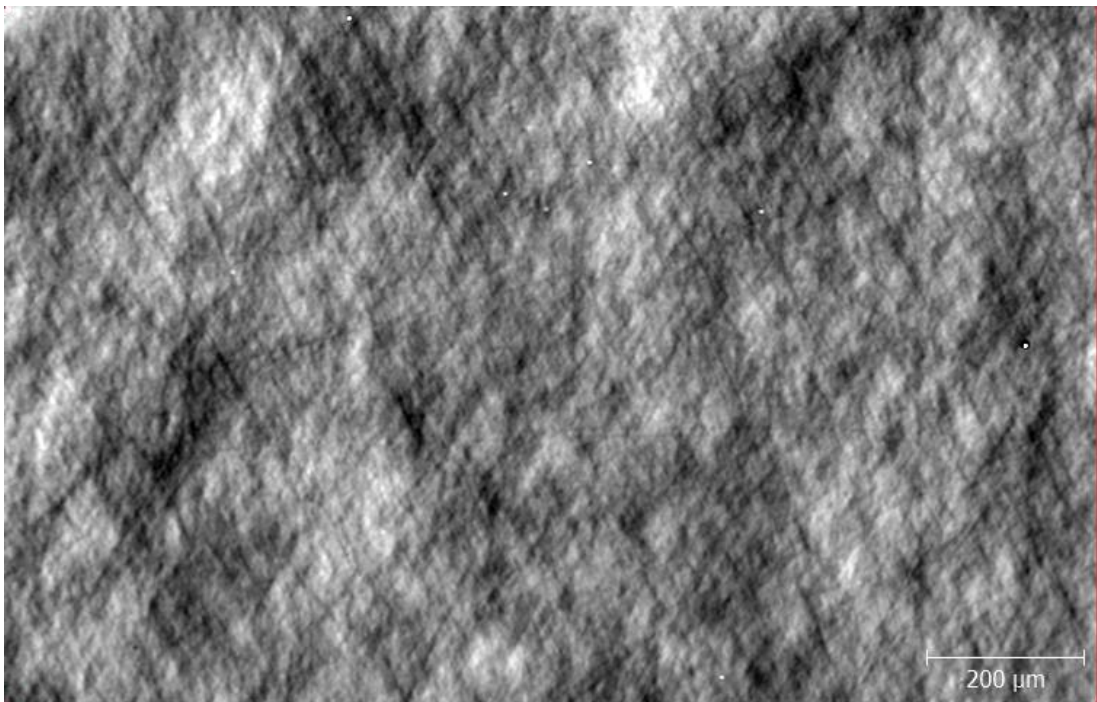


Figure 5.8: Direct measurement of Zerodur sample using ADE Phaseshift

Figure 5.9 shows an image of a result obtained by measuring a sample replicated from the surface of the Zerodur sample SUT. A polymer replication medium (similar to dental polymer) was deposited and, while still workable, a rigid substrate was

pressed against the side of the polymer not in contact with the SUT. The substrate forces the polymer into good contact with surface detail, as well as providing rigidity to the polymer when the sample is removed for testing. The polymer sample took 3 hours to cure and was subsequently removed to the ADE for testing. The result in Figure 5.9 provides a result of Sa 40.20 nm (compared with 0.64 nm by direct measurement) when measured over the same area as the previous result with the same terms removed. The red regions in the image represent data loss. The discrete black regions in the image are likely to be air bubbles trapped between the polymer and the SUT. These artefacts contribute significantly to the numerical result, making discerning the underlying texture difficult. Compared with the result shown in Figure 5.8, there is significant loss in high spatial frequency content and it is unlikely that the polymer could provide a suitable replication for smooth surface characterisation.

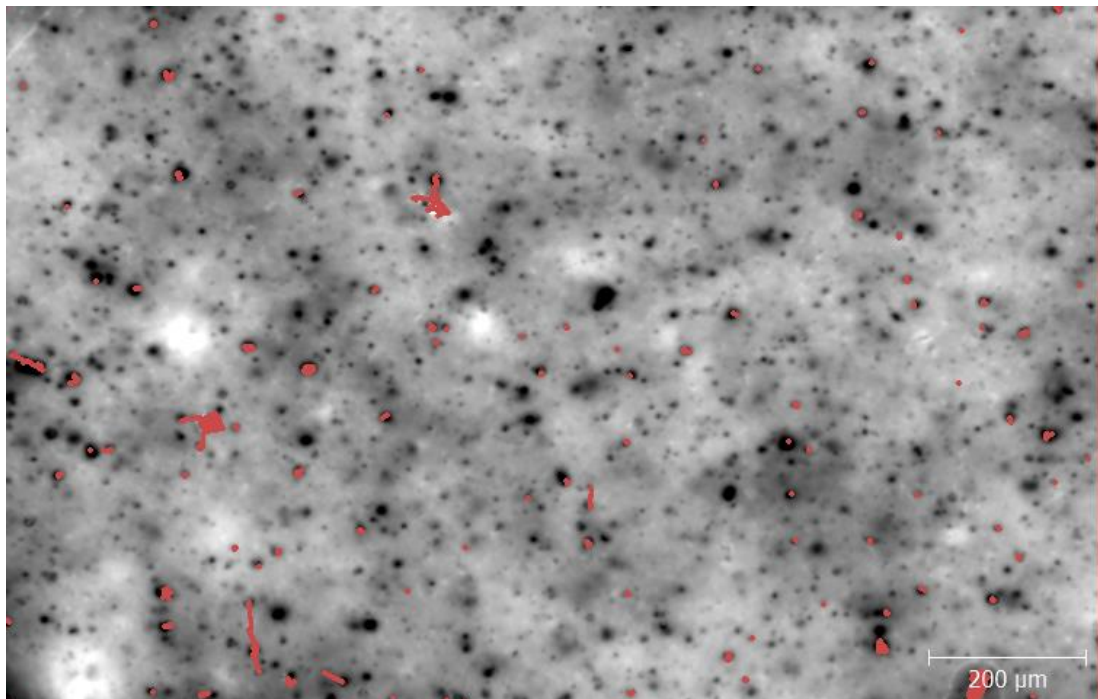


Figure 5.9: Polymer replication measurement using ADE Phaseshift

The second replication medium used in this trial was a UV curing compound. The compound was deposited onto the SUT and a wire used to draw a fine layer across the surface, providing a well-controlled layer. A transparent plastic backing is applied as a substrate to the UV compound, while still workable, and pressure applied with a roller to force the compound into the microstructure of the SUT and provide good adhesion between the compound and substrate. The compound is then exposed to UV light, through the substrate, for several minutes in order to cure. The UV cured compound was measured using the ADE Phaseshift and produced a result of 0.80 nm Sa over 1.38 mm x 1.02 mm with tilt, power, astigmatism and coma removed. Again, there is some evidence of loss of high spatial frequencies between direct and replicated measurement, however, the comparison is more favourable than that with the polymer replication.

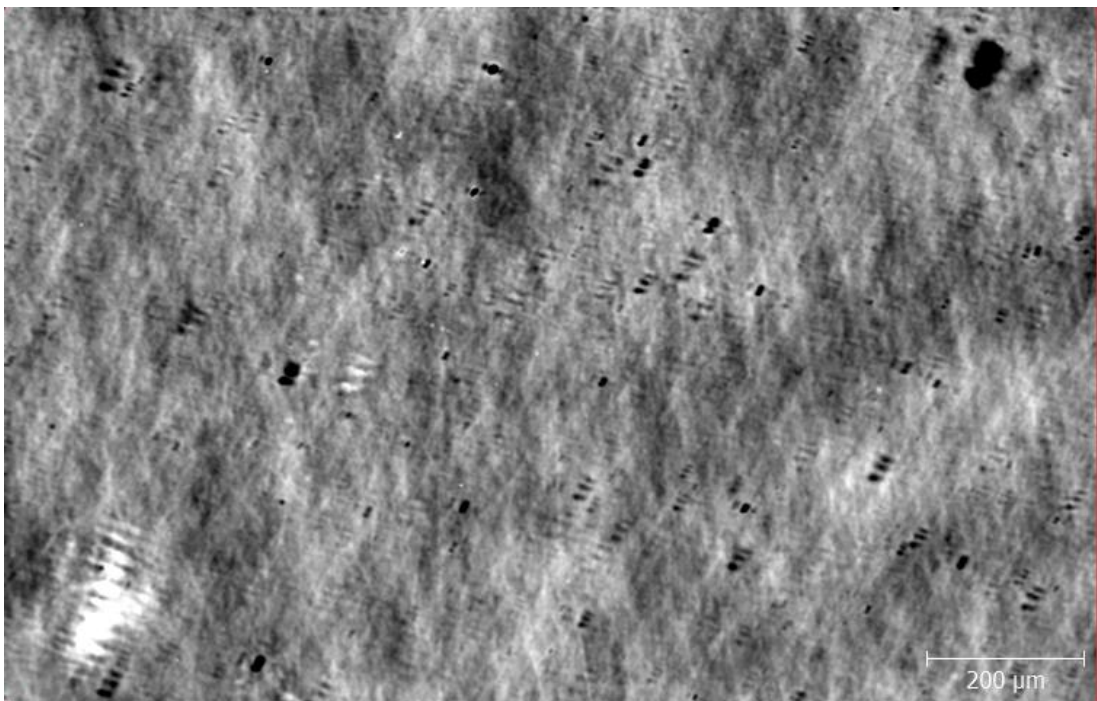


Figure 5.10: UV cure replication measurement using ADE Phaseshift

Although there is some evidence to suggest that characterisation of surface texture through replication is viable on smooth surfaces, the SUT used in this test had a small magnitude, random texture imparted by a pitch tool. In order to assess the linearity of the process, a known structured surface should be replicated and measured to display the accuracy of the replication. The test carried out here, therefore, does not prove conclusively that the material can produce a representative replication of a smooth surface, only that it has potential. It was also found that the UV compound samples lacked rigidity once removed from the original sample, causing them to distort. Such distortions affected the stability of measurement, requiring a low averaging level to minimise acquisition duration. This was mitigated during testing by bonding the plastic substrate of the UV compound to rigid cardboard.

In summary, this section has presented an initial test assessment of the use of replication, combined with a lab based instrument, as an alternate to STA for the in-situ measurement of large surfaces. Two materials, an air curing polymer and a UV curing compound have been applied to a smooth Zerodur sample and subsequently measured using the ADE Phaseshift device. It has been demonstrated that the UV curing compound exhibits a texture of comparable magnitude, although omitting the high spatial frequency features. However, this analysis does not take into account that the replication process requires manual handling of the original sample. In the case of large, 1.45 m diameter E-ELT segments, accessing the central region of the surface may still prove challenging and risky. Furthermore, even an

accurate replication technique will introduce extra error into the measurement process, which cannot easily be separated from that of the SUT.

5.1.4 Conclusion

This section has studied the performance of the 4D Technology STA device when used automatically on the IRP1200 machine in order to assess the performance of the instrument itself and the *Metrology Control Suite* detailed in the thesis. The automatic testing carried out here did not make use of the tilted spigot arrangement, designed to remove the effects of the machine [0,0,1] condition. A 3 m ROC SUT was therefore chosen, requiring that only a single, central measurement location be skipped. It was observed that the system is capable of carrying out measurement automatically and obtaining data which compared well both with that obtained manually and in the metrology lab. Further assessment of automatic system performance is made in Section 5.3.

Further analysis was also carried out of the STA and Phaseshift ADE devices to understand why the devices produce differing results when measuring the same calibration artefact. By analysing the spatial frequencies contained in measurement data, it was observed that the factors dictating system performance are more complex than originally considered. The system OFT contributes heavily to the overall instrument transfer function, especially in the case of the ADE. Selection of measurement device may become critical for projects where observed wavelength approaches the spatial frequency of the SUT texture. In such cases, measurement device attenuation, which causes texture at high spatial frequencies could indirectly lead to reduced optical performance.

This section has also presented a brief overview of surface replication as an alternative to on-machine metrology using the STA. A sample with texture similar to that of an E-ELT segment was replicated using two different materials and measured using the ADE device. While it was found that the UV cured sample may have the potential to be suitable for E-ELT measurement, the techniques used require manual working in proximity to the SUT, and likely contribute error to the measurement process. Also, due to the flexible nature of the thin UV cure compound layer, the technique tends to contribute to the low spatial frequency content of the texture measurement. This form cannot be discerned from that of the SUT and increases retrace error in subsequent optical measurement.

Following the development of the *Metrology Control Suite*, the STA is considered a suitable device for projects such as the ESO E-ELT due to the high level of automation and ease of obtaining good quality data. However, full automatic measurement of ESO segments does require an IRP machine with an H-axis configured with an encoder, to allow the use of the tilted spigot. The STA also has the ability to characterise texture of higher spatial frequency than the other techniques observed here and so is likely to be suitable for characterisation of optics designed to image at shorter wavelengths.

5.2 Metrology Station

The Metrology Station system was designed to allow the measurement of optical components which could not be measured in a full-aperture regime, for example large ROC convex and large diameter plano parts. The system can also measure optics which are too large to be accommodated by other commercial stitching

systems, such as the QED SSI. Though the Metrology Station table cannot support an ESO E-ELT segment for measurement, the techniques and software developed can be applied to hardware capable of supporting these components, such as the OpTIC testing tower. To demonstrate the combined performance of the Metrology Station and the software developed by the author, this section compares measurements performed with the Metrology Station and state-of-the-art systems, which produce comparable performance. As the Metrology Station was developed as a customer project, these measurements were used to pass-off the machine against the specification agreed with the customer.

Although this section focuses on the quality of the output data, the work presented in this thesis is also concerned with the automation of metrology. Therefore, an assessment of the automatic capabilities of the system is presented in Section 5.3.

5.2.1 Application of Automatic Sub-Aperture Stitching Interferometry

When developing a customer system, it is common practice to perform a pass-off trial before shipping, and repeat this trial with the system installed at the customer site. The pass-off trial is a series of measurements designed to confirm system performance against that indicated in the product specification. In the case of the Metrology Station, the tests are also designed to evaluate the performance of *Metrology Control Suite* in terms of correctly calculating a valid metrology plan, applying machine kinematic calculations, and controlling system elements in order to position the surface and acquire data. With the data acquired, the *Stitching Toolkit*, developed by Dr Christopher King, accepts the measurement data along with the sub-aperture configuration file and must stitch the data into a

representative synthetic full-aperture surface map. In order for the software to be able to perform the outlined tasks, the system hardware itself must also function properly, as any assembly error can cause both poor control and stitched measurement results.

This section presents sample results of the pass-off tests and discusses factors limiting system performance. Table 5.2 provides a summary of the specification for measurement pass-off of the Metrology Station and the results obtained from the tests discussed in the following sections. The system performance was tested for both plano and spherical surfaces, as high precision measurement of each presents unique challenges. The Metrology station was passed off successfully, surpassing the specification in all areas.

Table 5.2: Summary of Metrology Station pass-off specification and achieved results

Pass-off Test		Specification	Result Achieved
Plano	Repeatability	2 nm	0.57 nm
	Accuracy	$\lambda/20$	$\lambda/37$
Spherical	Repeatability	3 nm	1.45 nm
	Accuracy	$\lambda/20$	$\lambda/33$

5.2.1.1 Spherical Pass-Off Measurement

The cavity length of the full-aperture spherical test is defined by the ROC of the SUT and that of the reference optic. Tests of long ROC surfaces can therefore become impractical and suffer from poor SNR. Full-aperture measurement of large convex surfaces is generally limited by the interferometer aperture size. By using the Metrology Station, cavity length can often be chosen through selection of transmission sphere and so measurement can become more tolerant of air currents and vibration. Convex surfaces also become as simple as concave to measure.

The spherical pass-off tests were carried out on a 465 mm ROC convex surface of 300 mm diameter. This surface was affixed into an aluminium ring which was in turn secured to the Metrology Station rotary table by three peripheral clamps, as shown in Figure 5.11.



Figure 5.11: 465 mm ROC convex sphere used for Metrology Station pass-off testing

For measurement, it was decided that an f1.5 transmission sphere would be used to provide a sub-aperture of 86.11 mm. The surface design was generated using *Surface Designer* and loaded into *Metrology Designer*. The transmission optic specification parameters were entered into the optics database and a plan generated, as shown in Figure 5.12. Each red point on the figure represents the interferometer FOV centre at a test location and the blue circle shows the size of

the sub-aperture. It was found that the outer ring of sub-apertures was too far over the part edge and so the plan was manually adjusted using the sub-aperture angles editor menu.

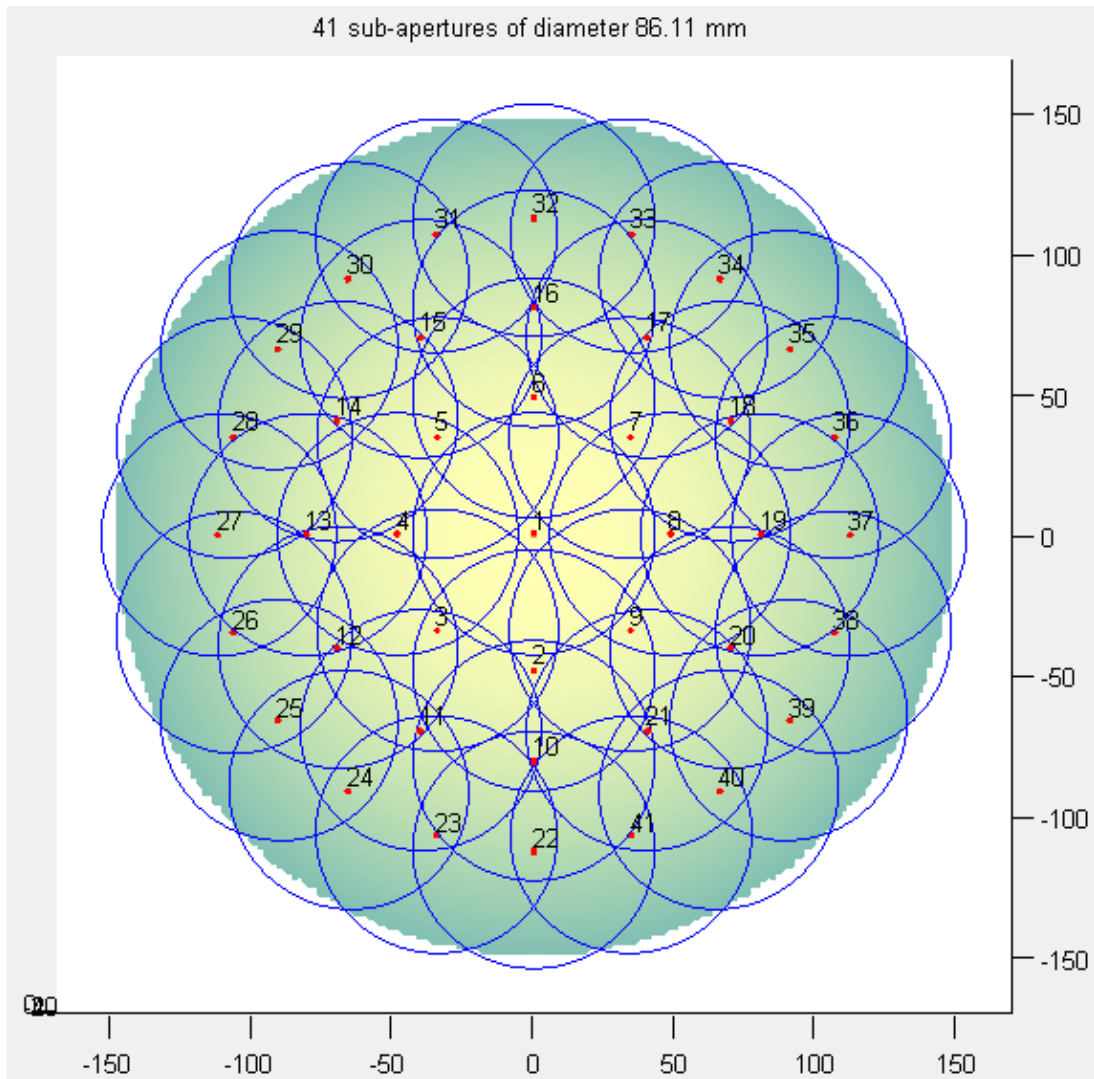


Figure 5.12: Measurement plan used for Metrology Station pass-off at customer site. SUT: 300 mm, 465 mm
ROC Convex

Figure 5.13 is a screen shot of the sub-aperture angles editor menu and shows the resultant sub-aperture ring configuration following plan optimisation. In the case of spherical measurements, only the elevation angle and number of sub-apertures column may be edited. The Y-axis offset is the calculated offset required to move the SUT between concentric rings.

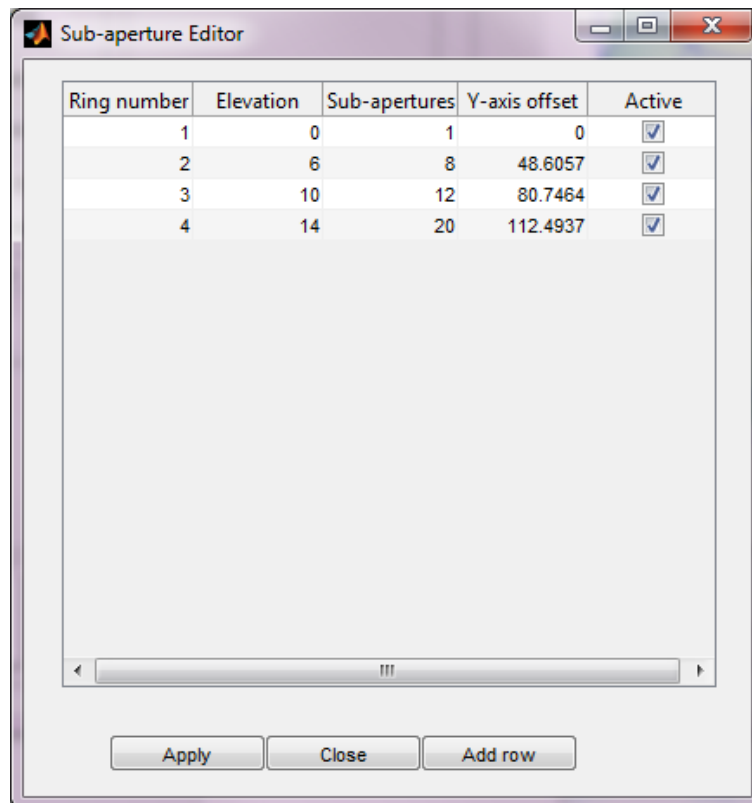


Figure 5.13: Sub-aperture angles editor configuration for pass-off test of Metrology Station

With the measurement plan designed, an OMM file was generated and saved. This allows the plan to be repeated at a later date but may also be used to modify the plan further.

The OMM file was loaded into *Metrology Controller*, displaying the plan for confirmation. The setup procedures outlined in Section 4.3 were carried out to clock and align the surface to the interferometer optical axis. The machine coordinate system was also set to zero to define the optical centre of the first sub-aperture as the machine origin. With the setup tasks complete, the machine was commanded to execute the measurement plan.

The system performed the measurement start up tasks, where tilt and focus sensitivities are measured at the position at which the operator has manually aligned the surface. This ensures that the sensitivity measurements are carried out

in an area of the SUT of known acceptable optical quality, maximising their accuracy. The Metrology Station then began the task of moving to, aligning with and measuring each of the 41 sub-apertures in the measurement plan. In order to provide repeatability data, the system was requested to repeat the overall measurement process 6 times. In between each measurement set, the system is not required to recalculate tilt and focus sensitivities as the previously calculated results are retained until the conclusion of measurement. The laboratory in which the measurement was carried out is able to regulate air temperature to approximately 0.1 °C.

It was found that the measurement of the 41 locations planned in the pass-off test took around 4 hours to complete, averaging 256 acquisitions per sub-aperture. With each acquisition recorded to take ~0.9 seconds to complete, this results in a total measurement acquisition time of 2 hours 37 minutes. However, during alignment, the system makes measurements by averaging 4 acquisitions in order to perform Zernike analysis to determine alignment. It was found that each measurement location requires, on average, two correction moves and therefore 3 alignment measurements. This gives a total acquisition time of ~2 hours 45 minutes. The Metrology Station therefore spends nearly 70% of the measurement period acquiring data. The rest of the time is spent moving between measurement locations and performing alignment corrections.

Following measurement acquisition, the data was saved and the machine coordinates at which measurement was acquired recorded in the sub-aperture configuration file. This file was then loaded into the Stitching Toolkit to describe the

configuration in which to reassemble the sub-aperture into the final synthetic dataset. Figure 5.14 shows the resultant stitched data set for the Metrology Station spherical pass-off measurement.

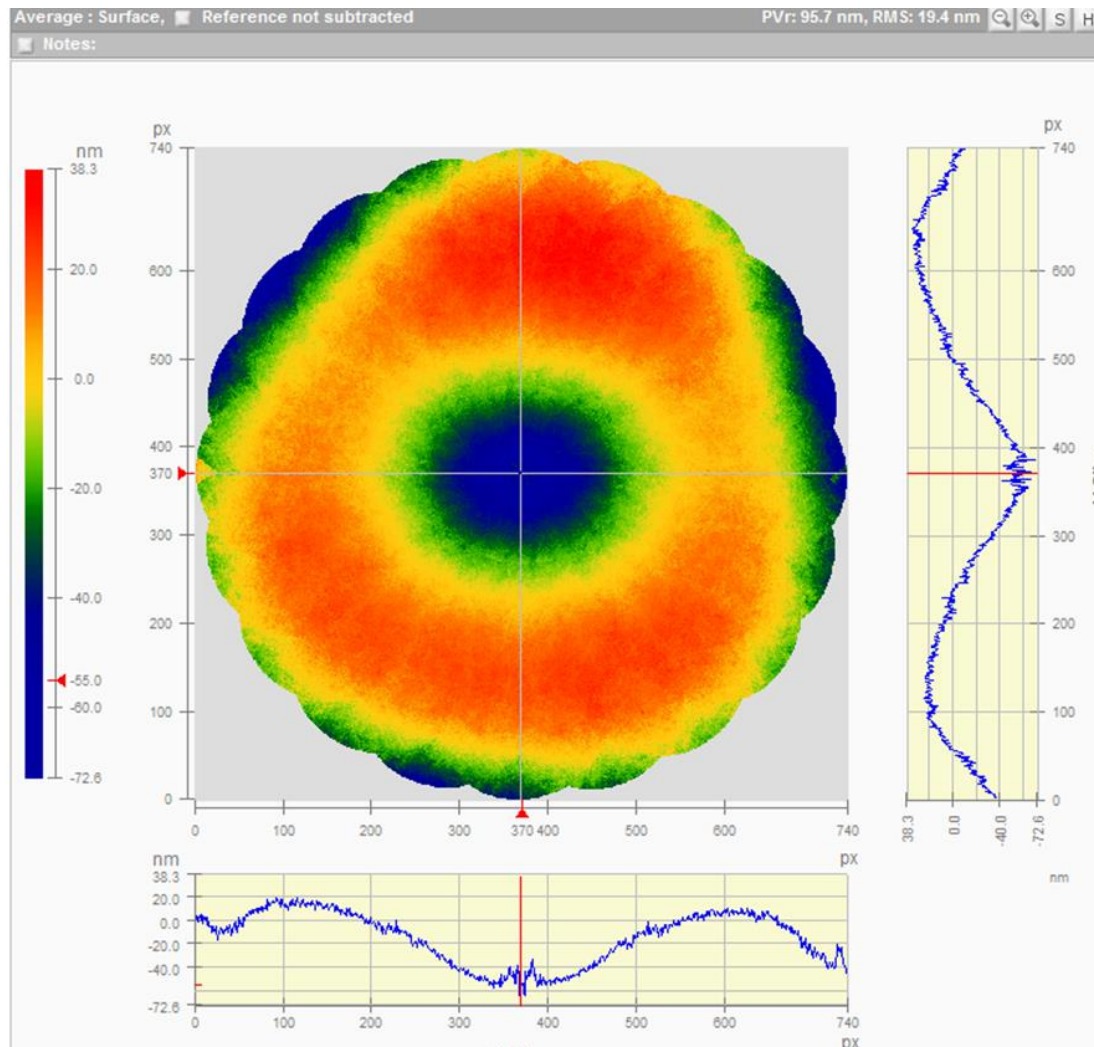


Figure 5.14: Stitched result of Metrology Station pass-off test (image by C.W. King)

When compared with a circular interferometer aperture, the synthetic dataset is immediately obvious due to the petal like patterning around the dataset periphery. When compared with the SUT design in Figure 5.12, some truncation was expected due to the sub-apertures overhanging the SUT edge. However, the surface diameter of the design underestimated the SUT, resulting in no such effect being visible. This approach of underestimation of the SUT diameter was deliberately used as a

method of avoiding sub-aperture edge overhang. At the left and right edges, two markers are visible to aid in orientation of the surface in the interferometer FOV. These also provide a key to allow the data and subsequent polishing tool path to be matched to the surface when setting up corrective polishing. The *Stitching Toolkit* also automatically estimates and subtracts the reference surface error from each sub-aperture, prior to stitching. The example shown in Figure 5.14 has a PVr of 95.7 nm and is representative of the 6 stitched measurements obtained during the spherical pass-off measurement.

Table 5.3 summarises the difference statistics between the computed mean and each of the six stitched results. The measurement repeatability has been computed as shown in Equation 5.1 and shows that the system falls within the repeatability specification of 3 nm RMS, given in Table 5.2 .

Table 5.3: Measurement statistics for the delta between the six repeat measurements and the computed mean

Delta	PV (nm)	PVr (nm)	RMS (nm)
1	19.4	7.2	1.2
2	12.9	6.5	0.9
3	15.1	7.1	1.3
4	20.0	6.9	1.3
5	18.7	7.1	1.12
6	21.7	8.4	1.2
Mean	17.97	7.19	1.17
Sigma	3.30	0.65	0.14
Repeatability	24.57	8.48	1.45

Equation 5.1: Measurement repeatability

$$Repeatability = \bar{x} + 2\sigma$$

An example dataset showing the delta between a stitched measurement and the computed mean dataset is shown in Figure 5.15. This dataset clearly demonstrates the propagation of the discontinuities caused by the orientation markers into the dataset. Although, the sub-aperture regions are clearly visible as a patterning across the surface, the magnitudes of these steps are numerically insignificant and barely visible on the lateral profiles shown.

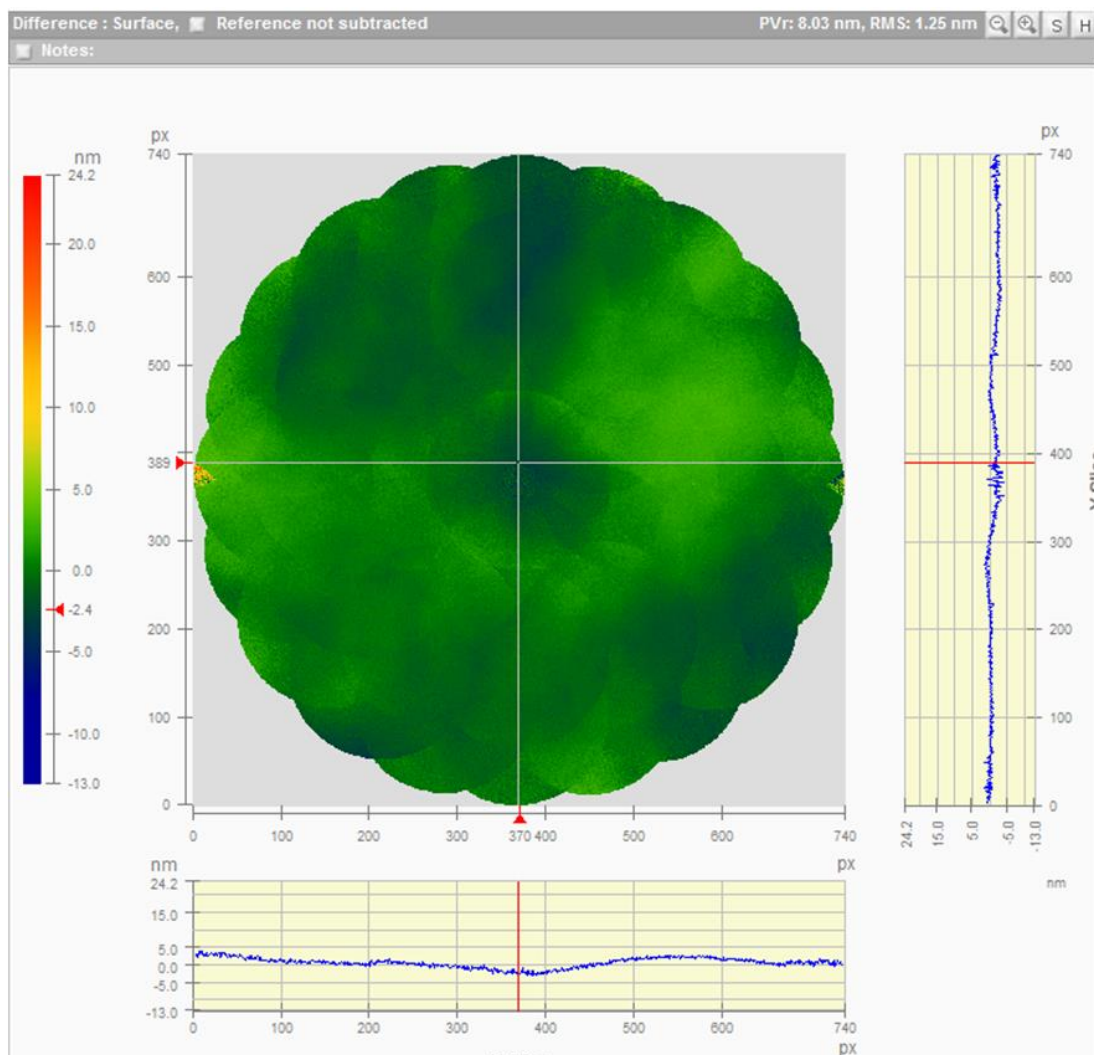


Figure 5.15: Example delta between stitched measurement and mean result for Metrology Station pass-off (image by C.W. King)

Following the spherical pass-off tests the Metrology Station was found to have met specification in terms of measurement repeatability. The system provides the

opportunity to perform metrology on spherical surfaces which cannot currently be accommodates on existing full-aperture measurement systems. In the case of the 465 mm ROC convex surface, the customer was unable to measure the SUT interferometrically, and so unable to complete polishing without the Metrology Station.

5.2.1.2 Plano Pass-Off Measurement

Measurement of large plano surfaces can be difficult due requiring either a large beam expander or the arrangement of a Ritchey Common Test (both requiring large optics). Sub-aperture stitching allows the use of standard interferometer configurations but requires known positioning of the SUT in order to achieve an acceptable stitched result. The Metrology Station therefore offers a simple and automatic method of measuring large plano surfaces without requiring other large surfaces.

The measurement process outlined in Section 5.2.1.1 was repeated for a plano surface. This section will outline the results of this test as well as the Metrology Station system performance during this trial. The measurement was performed on a 150 mm diameter transmission flat. As the Fizcam 3000 aperture supports up to 164 mm transmission optics, the aperture was stopped down to 100 mm to simulate the use of a 100 mm transmission optic, as agreed in the pass-off requirements. Figure 5.16 shows the measurement plan used for the plano pass-off test.

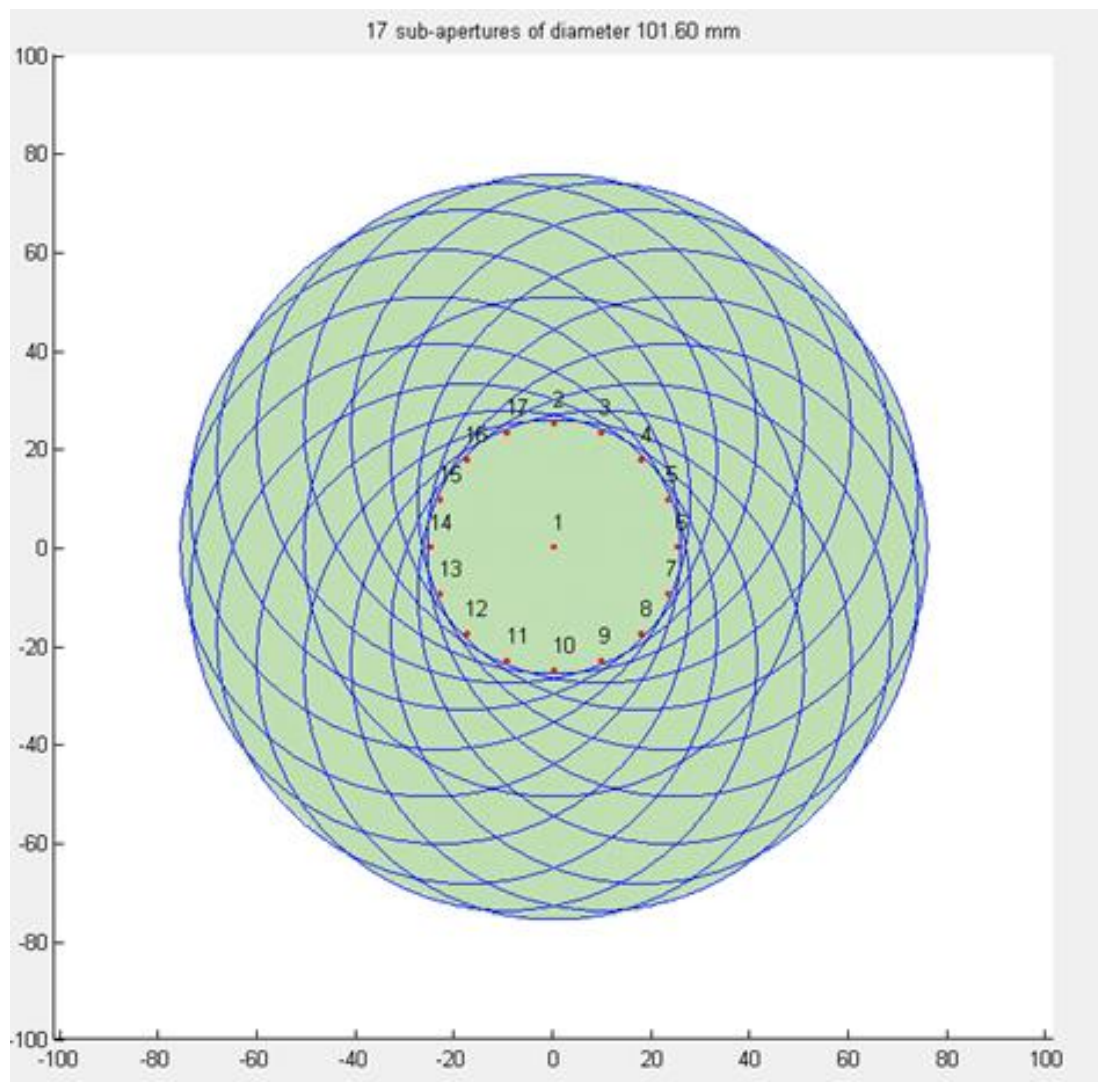


Figure 5.16: Metrology Station plano pass-off measurement plan

The sub-apertures were arranged in a single ring, with an offset of 30 mm from the central sub-aperture. Measurement setup tasks were carried out as per the spherical pass-off test, with the exception that no pivot distance measurement is required as the rotary table is not required to tilt during operation. The measurement was configured to repeat 4 times to provide sufficient data to make a study of measurement repeatability.

It was found that measurement duration scaled well with the number of sub-apertures, when excluding the tilt sensitivity measurement steps as these are of

constant duration. The plano measurement took around 2 hours to complete with a measurement acquisition level of 256 and alignment level of 4. Both spherical and plano measurement scripts largely perform the same tasks, the main difference being that different axes are used to align the part for measurement. Test duration should therefore be directly proportional with number of sub-apertures measured and acquisition level.

Following measurement, the *Stitching Toolkit* was used to compute synthetic datasets. A representative example of the results is shown in Figure 5.17. SUT orientation markers are visible at the top and bottom edges of the part, which have caused the noise visible in the Y-axis slice visible to the right of the image. This measurement has a PVr of 10.3 nm and RMS of 1.27 nm. The colour map used for the surface has been stretched to reveal surface detail.

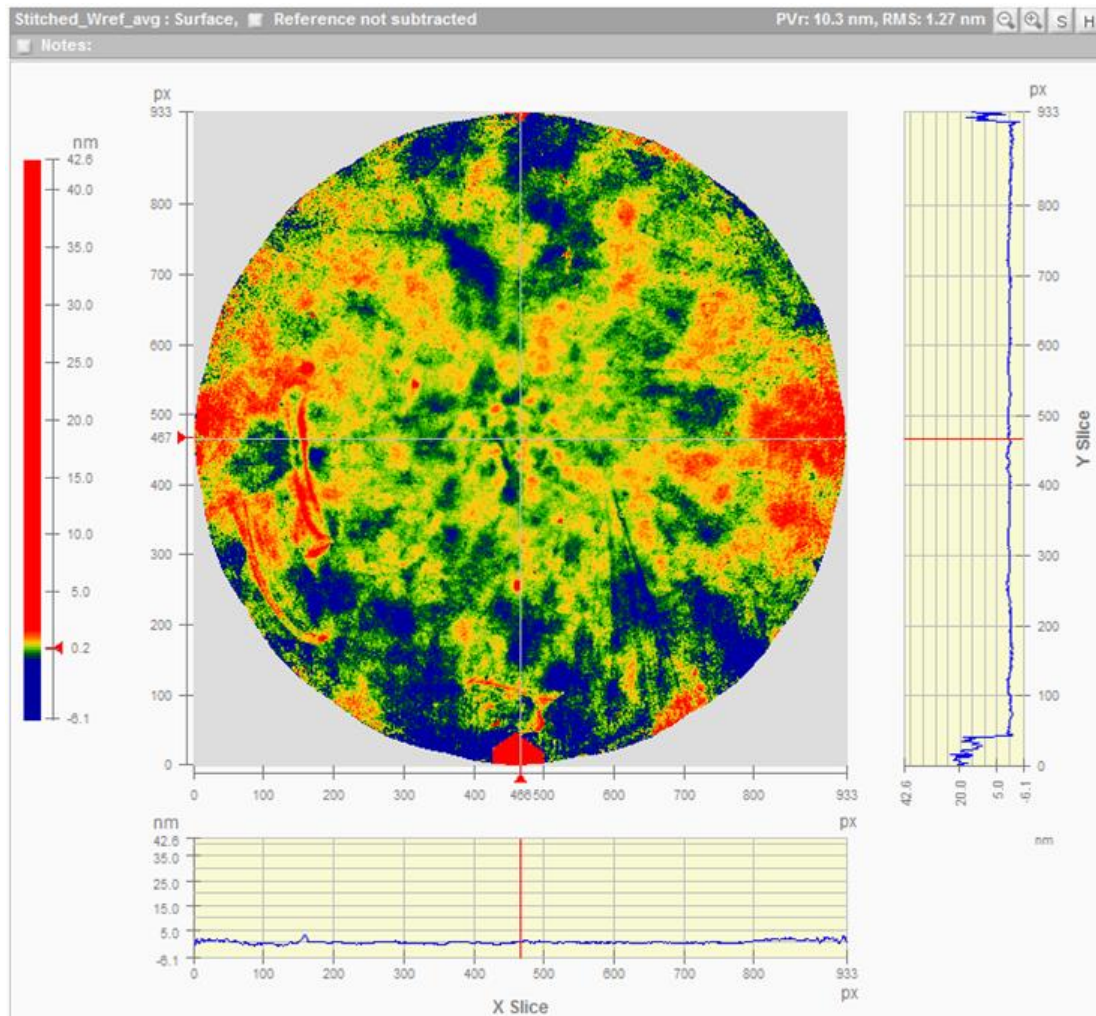


Figure 5.17: Plano pass-off measurement stitched result (image by C.W. King)

Table 5.4 shows a summary of the results obtained by taking a difference between the stitched result of each plano pass-off measurement and the computed mean. The value given for the system repeatability has been obtained using Equation 5.1. The plano repeatability was found to be 0.57 nm RMS, well within the 2 nm RMS given in the system specification.

Table 5.4: Metrology Station plano pass-off measurement delta results

Delta	PV	PVr	RMS
1	17.0	2.3	0.38
2	7.9	2.3	0.44
3	9.2	2.5	0.46
4	11.6	2.2	0.52
Mean	11.42	2.33	0.45
Sigma	4.03	0.15	0.06
Repeatability	19.47	2.63	0.57

Further to making an assessment of measurement repeatability, tests were carried out to establish the accuracy of measurement data. The plano SUT was measured using a 300 mm Zygo system located at the customer laboratory. The two measurements were registered using the orientation markers and subtracted. A difference of 4.43 nm PVr ($\lambda/37$) with reference errors estimated and subtracted was found, within the accuracy required in the specification. This measurement also serves to provide a comparison of the performance of stitching metrology against full-aperture, showing that there is little difference between the two techniques, as applied. It is also difficult to tell which measurement is correct. The next section provides a comparison between sub-aperture and full-aperture measurement of spherical surfaces and the reference estimation technique of *Stitching Toolkit*.

5.2.2 Comparison of sub-aperture and full-aperture metrology

In order to assess the accuracy of the Metrology Station when performing sub-aperture measurement acquisition, a comparison full-aperture and sub-aperture stitching measurement was made. In order to provide an assessment of the reference surface estimation performed in *Stitching Toolkit*, the full-aperture measurement was performed using a 3-sphere test [95] [96]. These measurements

were carried out on an 87.07 mm ROC convex Taylor Hobson calibration surface of 90 mm diameter. In order to accommodate the surface in the full-aperture test with available transmission optics, only the central 54 mm of the surface could be measured. Figure 5.18 shows the configuration for both the sub-aperture (left) and full-aperture 3-sphere (right) tests.

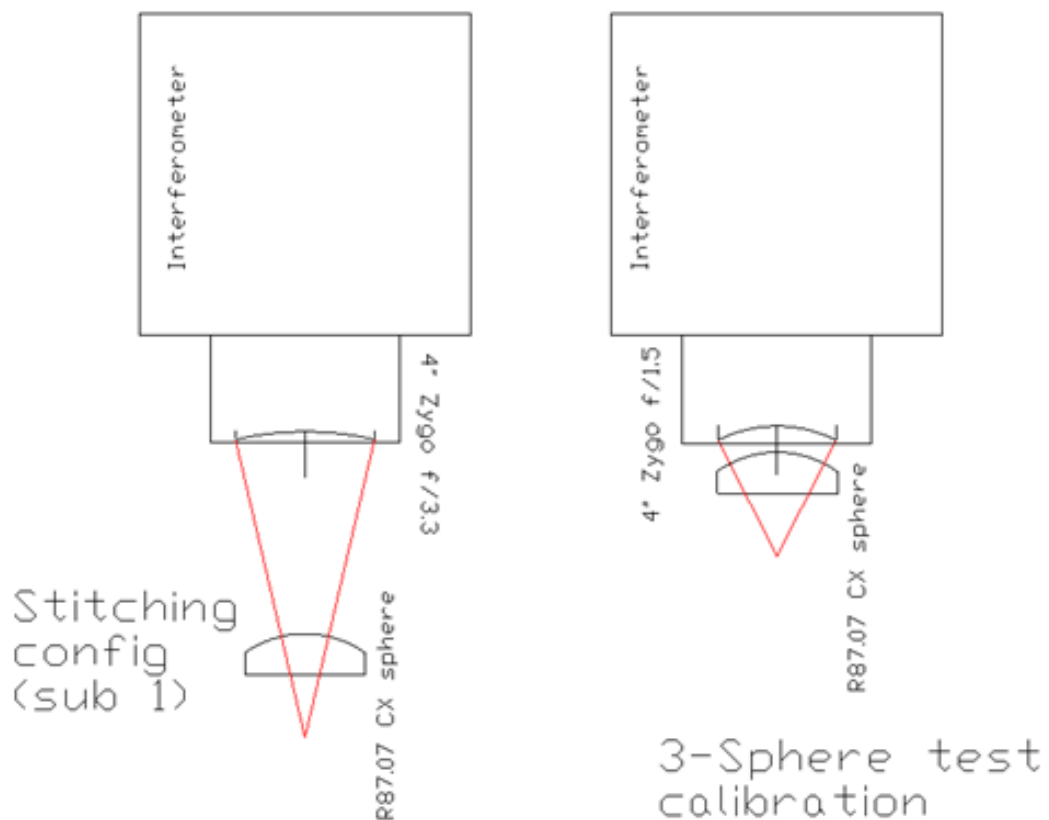


Figure 5.18: Schematic of test setup for comparison between stitched and full-aperture measurement (image by C.W. King)

The transmission optics used for both tests were also different, with the stitching measurement using an f3.3 and the 3-sphere test using an f1.5. The measurement plan for the stitching measurement is shown in Figure 5.19. Although the sub-apertures appear to overlap the edge of the SUT, the design represents only the target region of the central 54 mm region of the SUT.

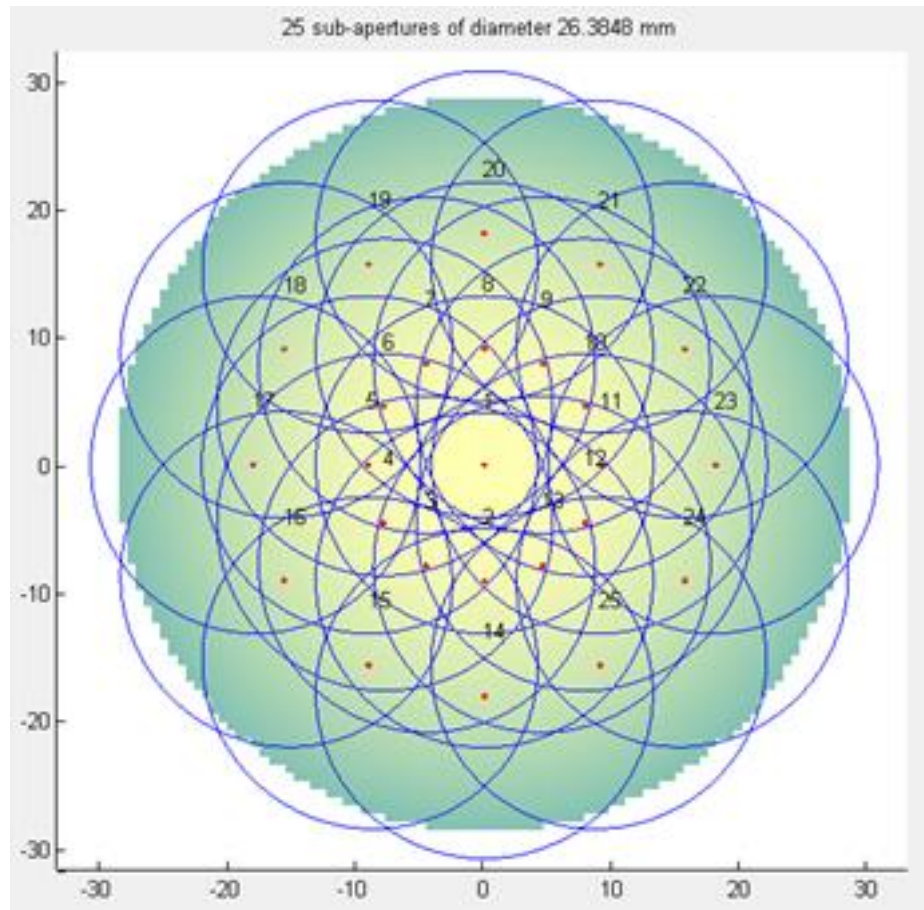


Figure 5.19: 3-sphere test measurement plan

The control application was configured to repeat measurement acquisition three times, providing sufficient data to compute repeatability statistics. Figure 5.20 shows the result of the 3-sphere measurement, giving a PVr of 67.3 nm and RMS of 11.3 nm. Figure 5.21 shows the averaged result of the three stitched measurement datasets and has a PVr of 68.9 nm and RMS of 11.6 nm. In both images, SUT orientation markers are visible at the top and bottom edge of the datasets as triangular regions of missing data.

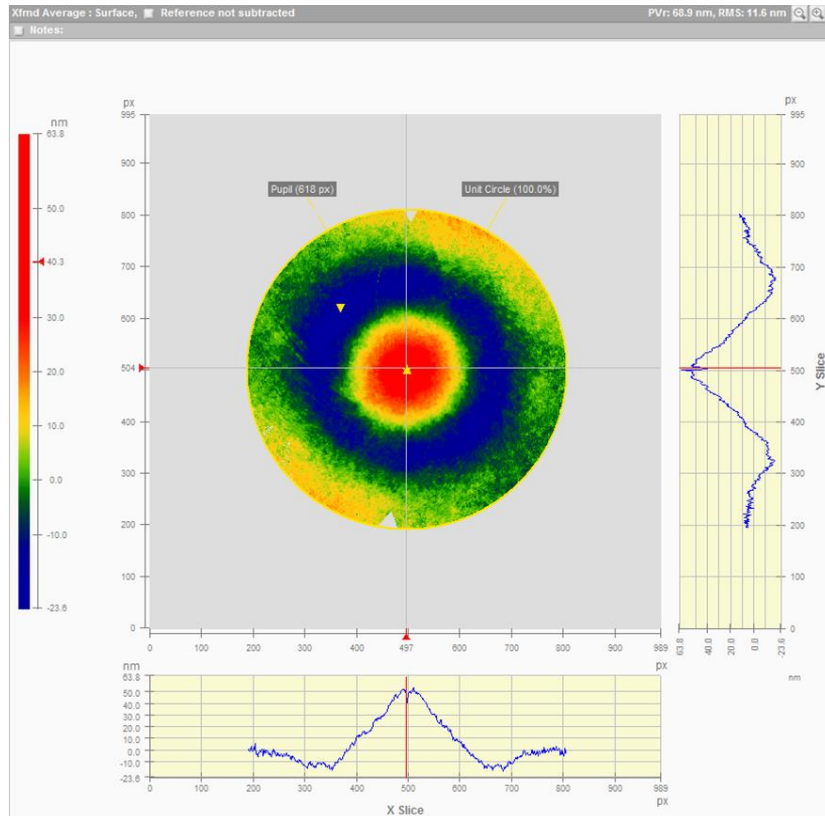


Figure 5.20: 3-sphere measurement result (image by C.W. King)

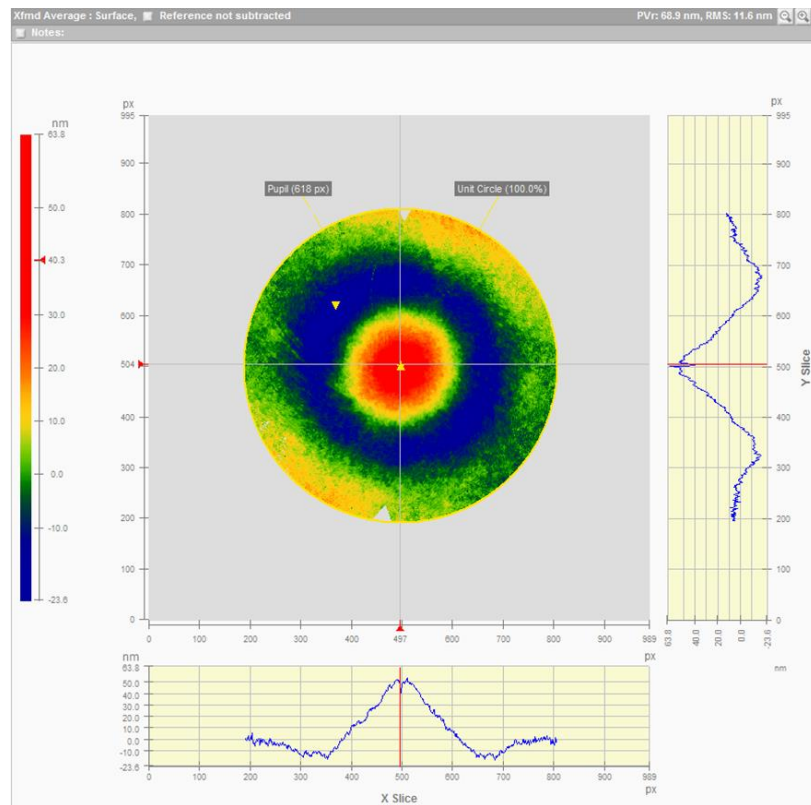


Figure 5.21: Stitched measurement result (image by C.W. King)

Figure 5.22 shows a resultant image of the subtraction of the 3-sphere and stitched measurement. The circular regions of concentric rings at the left and right of the image are diffraction rings caused by dust particles contained within the f1.5 transmission optics. Though clearly visible to the eye, they contribute little to the numerical result. The difference dataset has a PVr of 18.0 nm and RMS of 2.97 nm.

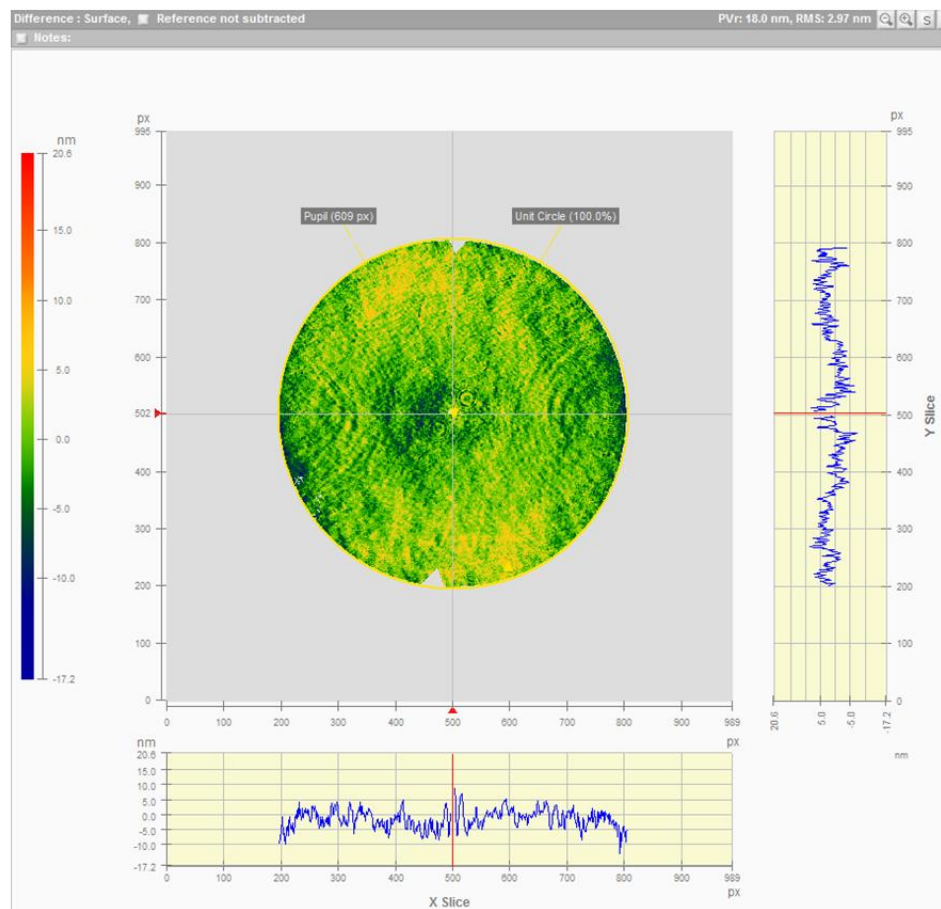


Figure 5.22: Difference between 3-sphere and stitched results (image by C.W. King)

The comparison measurement presented was carried out prior to shipment of the Metrology Station to the customer. As such, data acquisition of the stitching measurement data was carried out on the machine shop floor at the Zeeko facility

in Coalville, Leicestershire. The working volume temperature of the Metrology Station was observed to vary by around 3 °C during a 24-hour period as shown in Figure 5.23. It is expected that the results produced in this comparison could be improved upon in more stable conditions.

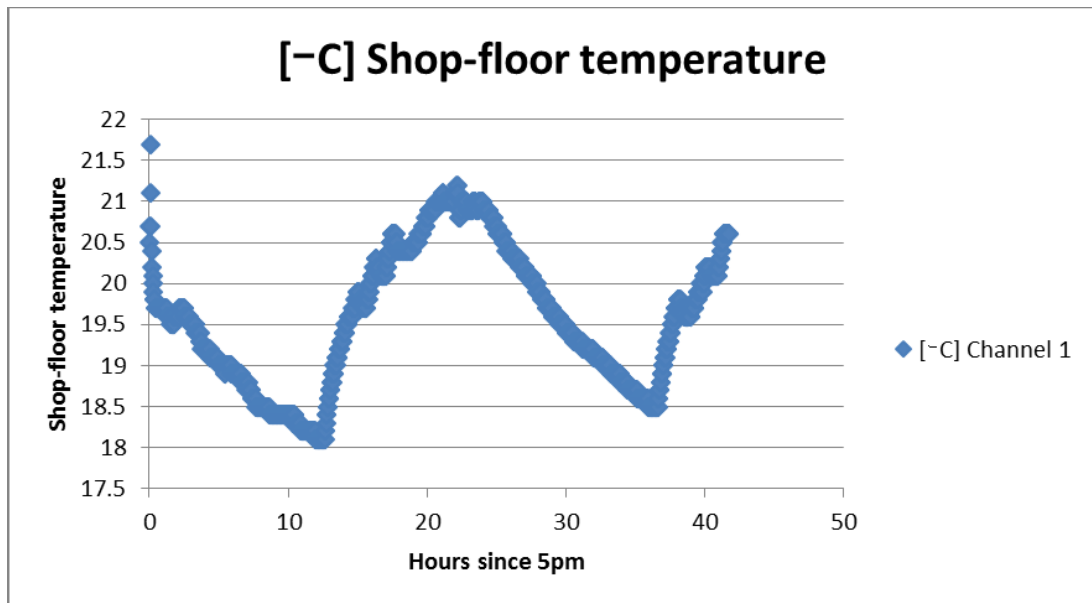


Figure 5.23: Metrology Station working volume temperature variation during stitching measurement for full-aperture and stitching comparison

Despite the instability of the atmospheric conditions, the stitching results provided a repeatability of PVr 7 nm and RMS 1.2 nm with good reference surface agreement between the two techniques, and within specification. This result demonstrates the reduced cavity lengths obtainable through sub-aperture stitching allow precision measurement in the presence of atmospheric instability.

5.2.3 Conclusion

This section has provided example data acquired using the Metrology Station in automatic measurement mode, which demonstrates the repeatability and accuracy of the system in stable laboratory conditions for both plano and spherical surfaces. Data allowing comparison between full-aperture and sub-aperture measurement

has also been presented, which serves to validate the sub-aperture positioning accuracy and ability of the control system to correctly align the device, minimising system retrace errors.

All of the sub-aperture data presented here has been obtained automatically, with user intervention only during the setup phases. Much of the time the system was left unattended during measurement, as this allowed for maximum atmospheric stability in the measurement volume. It was generally observed from the system error logs that errors did occur, most commonly interferometer timeouts, however these were correctly handled and measurement continued.

Many of the errors which continue to affect and limit system performance are the result of the interferometer Python interface. During long measurement cycles, it is observed that the 4D Technologies web service tends to occupy an increasing amount of system memory, causing all system operations to slow. This condition is only resolved by restarting 4Sight. The correct selection of measurement mask in 4Sight and metrology plan, i.e. such that little sub-aperture area overhangs the part edge can mitigate this affect. However, this can limit measurement design flexibility.

5.3 Automatic Operation

This chapter presented data which validates the combined performance of metrology devices and CNC positioning systems. These systems have been operated using the *Metrology Control Suite*, developed by the author. Although the driving force is the desire to obtain good quality data, it is appropriate that an assessment be made of system automation. Feedback from such examination can then drive

improvement in future versions of software. This section discusses the limitations of the on-machine metrology systems developed and suggests how these may be overcome.

As well as the principal motivation of reducing the risk of damage associated with the manual handling, automation of on-machine metrology can potentially reduce the overall measurement time. Figure 5.24 shows an overview of the process chain of the corrective polishing regime applied to the prototype ESO E-ELT segments. Toolpath calculation and polishing times are dependent upon residual surface error and so cannot be reduced by metrology. For the E-ELT prototypes, metrology is performed in-situ and so measurement setup times would remain constant with the use of automation. However, for other projects, SUT transport time would be eliminated as well as part clocking which would present a time saving of potentially several hours per process cycle. Metrology of E-ELT segments current varies between 8 and 36 hours, as better SNR is required as the segment nears specification which requires increased averaging. However, the adoption sub-aperture measurement techniques demonstrated in this thesis would allow a reduction in cavity length and so in improved SNR. Combined with automatic alignment, it is expected that automatic on-machine measurement of an E-ELT segment using a sub-aperture device would take approximately 8 hours to complete, based on testing duration of Metrology Station discussed earlier.

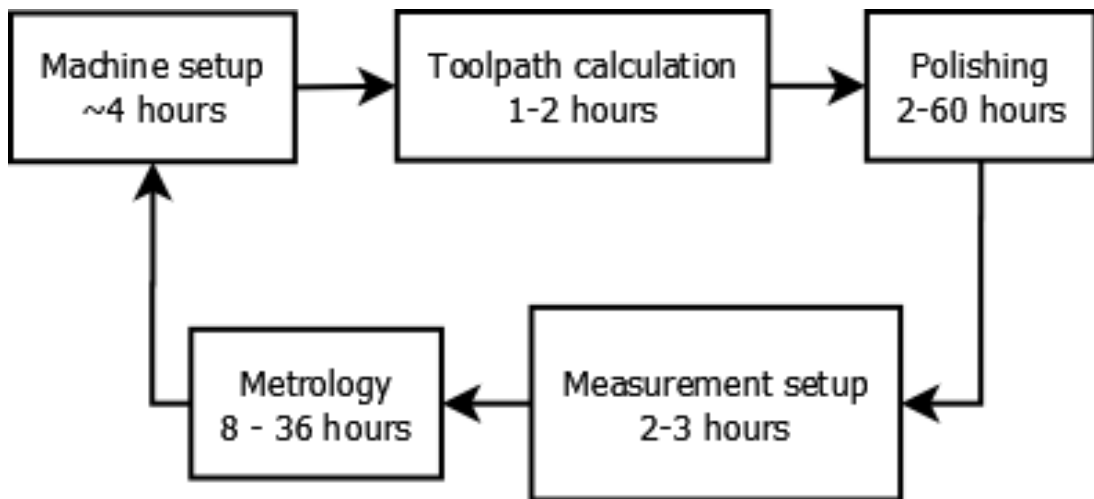


Figure 5.24: Time constraints associated with current ESO segment processing steps

5.3.1 Measurement Duration

One of the motivations of measurement automation is the potential for reduction in measurement duration. As mentioned earlier, the systems presented spend around 70% of the measurement duration acquiring data frames from the interferometer. The remaining time is spent either moving to new measurement location for performing alignment corrections. This section provides examples of how automatic metrology speed may be increased.

5.3.1.1 Measurement Acquisition

Measurement acquisition is composed partly of exposure, allowing light to enter the optical system and fall upon the CCD, and processing. Processing involves reading the data from the CCD and performing phase unwrapping to provide a surface map and the computation of statistics. With the current interferometer software, the processing period dominates measurement acquisition and cannot be adjusted as it requires the execution of functions over which the author has no control. The speed of execution of the phase unwrapping algorithms is also dependent upon surface quality. Discontinuities in the surface or edge overhang

can cause phase unwrapping errors, making it more difficult for the algorithm to solve. Processing time can be minimised through proper design of measurement plan by minimising edge overhang and the number of locations measured. A further option would be to split the interferometer video signal, and process images separately to provide tilt analysis using a 2-dimensional Fast Fourier Transform for alignment correction. However, this would not reduce the measurement acquisition period as unwrapping would still be required.

Similarly, the exposure duration period required to capture sufficient light is dependent upon both the interferometer light output and the surface reflectivity. As it is possible that the SUT is mid-process at the time of measurement, good surface reflectivity is beyond the control of the metrologist. An option for reducing exposure time is to increase the light output of the interferometer. The Fizcam 3000 installed on the Metrology Station uses a 2 mW Helium-Neon laser and during pass-off testing an exposure of around 0.18 seconds was used. Even if this unit were upgraded to a longer cavity 35 mW unit, requiring significant redesign of the system, this would reduce exposure to a minimum of 0.01 seconds, assuming a linear relationship between laser output power and exposure time. Overall this improvement would provide a 19% reduction in acquisition period. However such an improvement would be highly dependent upon surface reflectivity and thus, finish quality.

5.3.1.2 Device and SUT Positioning

The second major activity which dictates the duration of the overall measurement process is moving the SUT or device, either for alignment correction or between

measurement locations. For both the STA and Metrology Station, the maximum system feed rate is limited to 250 mm per second. This is done primarily to protect the interferometer from accelerations which could cause miss-alignment of the internal optics. In order to safely increase feed rate and reduce movement duration, either the interferometer design must be hardened against these increased accelerations or the system must be redesigned so that the interferometer does not move at all.

Either of these options would require a significant redesign. However, in the case of high-volume production, such work would be justified by the requirement to reduce measurement time as far as possible. Given that the instruments selected for use are third party systems, redevelopment of the interferometer for faster automatic operation may be unfeasible. Any redesign must also maintain manufacturing performance and so a trade-off must be made.

5.3.1.3 Setup Procedures

A further task which contributes to the measurement duration is the execution of setup procedures. Metrology Station is the most affected of the two systems presented, with setup usually taking up to an hour prior to execution of measurement. Such tasks must be performed properly for the measurement system to operate properly and safely in automatic mode. Poor performance of these procedures can greatly increase the measurement duration, if the system can operate at all.

In order to reduce the duration of setup procedures for the Metrology Station, further elements would need to be motorised. This would allow the system to

automatically clock the part to the interferometer optical axis without operator intervention. The measurement of the pivot distance may remain problematic, as prior to the co-ordinate system being zeroed, the system does not have knowledge of the part location. Automation of this procedure will require development work to ensure that the system does not pose a risk to the part, possibly using proximity detection.

There are some clear opportunities for reducing measurement time of the automated systems presented, in particular the Metrology Station. However, these require further investigation and development of both hardware and software and were not possible in the scope of this thesis. It is expected that as automated on-machine metrology becomes more prevalent in the manufacturing environment, there will be significant commercial drive to reduce operating times and increase throughput of such systems.

5.3.2 User Interface

Both the STA and Metrology Station provide utilise a common interface with *Metrology Control Suite*, which is designed to provide operator familiarity, even when using the application with a new metrology device.

However, when operating the system with a 4D Technologies interferometer, operators have commented that having to perform setup tasks in both the 4Sight software interface and the *Metrology Control Suite* GUI can be confusing. Due to the only interferometer interface available being the web service, which must be run from the 4Sight application, this cannot currently be avoided. It is possible that another interferometer manufacturer could provide an alternative interferometer

control method, allowing a single system interface. However, the 4D Technology systems are well suited to the on-machine environment due to the simultaneous phase acquisition allowing reduced vibration sensitivity. Other devices may require greater mechanical stability in order to produce comparable performance.

5.3.3 Software Requirements Compliance

Table 5.5 provides a summary of the compliance of the Metrology Control Suite application against the requirements specified in 2.6. The application developed is found to be fully compliant with the requirements discussed, however improvements can be made. For example, the pause and cancel features suffer some delay, as discussed in Section 4.5.1. This is found to be acceptable, given that safety critical inputs such as emergency stop are implemented in hardware. Removal of this delay would improve user experience when operating the interface which can influence confidence in effectiveness of the automation.

Table 5.5: Metrology Control Suite software compliance matrix

Metrology Designer	
✓	Allow specification of the surface to be tested
✓	Allow specification of device and optical setup to be used for testing
✓	Allow simple design of metrology plan which will provide useful data
✓	Provide customisation of plan for more demanding measurements
✓	Prevent generation of a metrology plan which will cause damage to the machine, SUT, or present danger to personnel
✓	Allow the plan to be saved for future use or modification
Metrology Controller	
✓	Allow the measurement plan to be loaded and reviewed
✓	Interface with machine controller(s)
✓	Query system axis positions
✓	Dynamically generate g-code and upload to the controller
✓	Execute and delete g-code files from control system
✓	Display measurement progress and system status clearly to the user
✓	Prevent the system making movements which could damage the machine, SUT or pose a danger to the operator
✓	Control the measurement device to make automatic measurement acquisitions and save the data to file
✓	Ensure acquired data is useful for either correction or SUT measurement
✓	Analyse device alignment and compute correction moves
✓	Summarise measurement information to allow operator to interpret progress
✓	Allow user to pause or cancel the measurement process
✓	Record any system errors to allow remote debugging

5.3.4 Conclusion

This section has reviewed the automatic operation of *Metrology Control Suite* with the aim of improving the system, primarily with regards to reducing measurement duration. Discussion has been taken as to how this may be achieved and the practical implications of such improvements.

Any improvement of such a system will require significant work as a change in any aspect of the integrated hardware has an effect on further system elements. No key part of the system hardware can be considered in isolation. Furthermore, the use of third party hardware, such as 4D Technology interferometers limits the extent of control over the device. The development of such systems in-house, while attractive, is a major undertaking in itself and will ultimately require further development of other aspects of the measurement system. The easiest way to dramatically reduce measurement duration is to both minimise the number of measurement locations and, in the case of sub-aperture metrology, minimise sub-aperture overlap. To date, most sub-aperture stitching measurements have been carried out using high overlap levels, with 30% overlap considered the minimum. However, to establish the trade-off between data quality and measurement speed, a further study must be carried out.

Measurement speed can be increased in the short term through better development of algorithms such as the fringe detection, and the application of this algorithm to the characterisation of tilt alignment. However, the expected reduction from this is expected < 5%.

5.4 Overall Conclusion

This chapter has presented measurement results obtained with the Surface Texture Analyser and Metrology Station systems. Both systems were tested using the *Metrology Control Suite* application to provide automatic measurement. The data presented demonstrates the viability of on-machine metrology and the suitability for integration into the manufacturing environment. Where possible, data has also been provided to compare performance between the on-machine systems and state-of-the-art metrology. It can be seen the systems developed as part of this thesis provide comparable measurement performance with existing systems. Should future projects demand measurement devices other than those presented in this thesis, the modular architecture of *Metrology Control Suite* would allow the integration of future hardware with minimal development work. Although sub-aperture measurement systems such as the QED SSI are in use, the control architecture presented in this thesis is capable of supporting on-machine metrology with various instruments and is therefore more versatile.

Automatic operation of the systems developed has also been assessed. Automatic on-machine metrology provides not only the potential benefits of saving time through not having to remove the SUT from the machine but also that of allowing unattended metrology in the same way that polishing does not require operator intervention during the process. This also reduces the risk of damage to the optic through handling and ensures good quality data, allowing measurement to be automatically reacquired if quality is insufficient.

Observations of how system automation may be further improved have also been given, focusing on increasing system measurement speed. The main limiting element in the systems presented is considered to be the control interface with the interferometer and the speed at which the device can acquire data.

6 Conclusions and Further Work

This thesis has demonstrated that many of the current limitations associated with state-of-the-art metrology may be overcome by carrying out measurement in-situ. Techniques such as sub-aperture stitching interferometry have been combined with commercial vibration insensitive interferometers to allow on-machine metrology. The application of metrology to the polishing machine also allows the automation of measurement device positioning and alignment, using the existing CNC axes. The author's *Metrology Control Suite* allows the design and execution of a measurement plan, for automatic on-machine metrology of both form and texture.

The introduction to this thesis presented a review of the techniques used for the production of optical surfaces, and how CNC has become fundamental to these processes. A review has also been provided of state-of-the-art methods of surface characterisation used to provide feedback during the manufacturing process, and certification afterwards. High precision optical manufacturing is an iterative process, cycling between polishing and measurement. The accuracy of polishing is affected by that of measurement, and so limitations in the performance of metrology will affect the ability to control surfaces, and therefore the optical performance of surface produced. Finally, the limiting factors of current metrology were discussed as well as how automation of metrology may provide a solution. Metrology of large surfaces is hampered either by the logistical issues of moving heavy components to the metrology facility or by the poor stability associated with large test cavities. However, new techniques such as stitching interferometry and

devices such as the STA provide an opportunity to integrate metrology into the manufacturing environment, while improving performance.

Chapter 2 went on to give an overview of the manufacturing systems used to provide actuation of the metrology device, such as the IRP machine in metrology mode. Metrology instruments viable for integration with CNC machine have been reviewed in order to establish the potential limitations of performing metrology in, what can be, a hostile environment. The devices selected for development were reviewed in detail and some initial experimental data presented to verify feasibility. While some difficulties were found during initial testing, it was decided that these could be overcome and that automated metrology was viable. Having reviewed the hardware in detail, an outline was made of additional technology was required in order to realise automated metrology. Software was identified as the largest deficit of the initial system and so a software specification was provided, which would form the basis for the development of *Metrology Control Suite*.

Chapter 3 detailed the development of the *Metrology Control Suite* planning application. *Metrology Designer* allows an operator to plan metrology to be performed. This application allows the specification of the surface under test, a measurement device, and a test optic, and their use to create a measurement plan. The design of measurements for various instruments is allowed for, with the addition of extra planning modules, thus minimising development time for future automatic metrology devices. The planning modules are selected using a series of configuration files.

The development of the *Metrology Controller* module, which allows the execution of metrology plans was discussed in Chapter 4. *Metrology Controller* is distinct from all software used during polishing as, instead of executing a polishing program generated prior to commencing the process, the application itself generates the G-code program automatically. These automatically generated programs are based upon either the measurement plan or feedback obtained from the measurement device. This process of using feedback to perform automatic alignment correction of an on-machine measurement device is a novel step for texture interferometry. The use of feedback also allows precise alignment of devices using a CNC system intended for manufacturing, while in an environment which is unstable compared with the metrology laboratory. *Metrology Controller* interfaces directly with the CNC system to upload and execute G-code programs without input from the operator. The development work presented in both Chapter 3 and Chapter 4 was discussed in the context of the two systems selected for development, the Surface Texture Analyser and the Metrology Station.

Having developed the *Metrology Control Suite*, a series of tests were carried out to validate the capabilities of the example systems. Chapter 5 presented and discussed this data, and made comparison between the new systems and state-of-the-art metrology devices. The presented systems were demonstrated to provide measurement performance comparable with devices sited in the metrology laboratory. The capability to measure components not accommodated by current systems, such as large plano and convex parts on the Metrology Station was also shown. Much of the data was obtained automatically, with the system measuring

overnight. Such capability to obtain measurements automatically allows data to be acquired in far greater quantity and of improved statistical quality.

The demonstrated systems consist of off-the-shelf interferometers which have been successfully integrated with CNC machines and the software applications presented here. The modular architecture of *Metrology Control Suite* provides scope for retrofitting into existing hardware, such as the OpTIC Glyndwr testing tower for the ESO E-ELT project, as well as new systems currently under development. Indeed, if a consortium are to progress to full scale fabrication of the segments required for the E-ELT, such automation will form a fundamental part of the process chain. It seems that, given the observed rise in automation of various forms, work such as this will become increasingly relevant in the future, both in support of the Science Base and industrial manufacturing.

This project has served as an initial step in the direction of automating on-machine metrology of precision optical components in the manufacturing environment. The next section will outline some of the projects to which the work presented here is already being applied.

6.1 Future Work

This section will outline the future work to improve the functionality and performance of the *Metrology Control Suite*. Some of the longer term projects into which this work will feed are also presented.

6.1.1 *Metrology Control Suite*

The *Metrology Control Suite* is currently being supplied as part of commercial Zeeko systems which feature automatic metrology. A secondary aim of developing the

architecture was to allow a separation between the low level functions communicating with the control system and the instrument developer. This allows the instrument developer to concentrate upon maximising instrument performance, while not becoming concerned with ensuring the performance of the underlying CNC system. At the time of writing, *Metrology Control Suite* is capable of supporting only three separate machine controllers simultaneously. This limitation will be removed in the near future, to ensure that the software is scalable to support more complicated system designs.

Though the systems presented offers time saving in metrology compared with manual measurement and transportation of the SUT, it is expected that further gains can be made. The current limitation arises because the control application requires processed measurement data in order to compute alignment corrections, and interferometers supplied by 4D Technology acquire around 1 frame per second. However, it has been shown that the Hough transform may be applied to detect interferometric fringes in the interferometer FOV. It is planned that further investigation be carried out into the viability of counting these fringes and thus calculating the required correction without performing data analysis in 4Sight. This would require the generalisation of the Hough functions applied here. The function used currently only detects lines, as the STA field of view is small and fringes do not typically appear curved. However, large FOV devices (such as the Fizcam 3000) are likely to encounter curved fringes and so circle detection will also be required. Furthermore, error handling will be needed for situations where unusual form is encountered and fringe shape becomes unpredictable.

An initial aim of this work was to develop on-machine sub-aperture stitching metrology, using the OMSI device. During the feasibility study, this device proved to be unstable and so the OMSI project was re-directed, using the Metrology Station as a test bed for sub-aperture stitching systems. While the base of the commercial implementation was identical to that of an IRP 600 machine, this constitutes a standalone metrology system and so is not strictly on-machine metrology. However, *Metrology Control Suite* is now being applied to a project involving placing a test tower over an IRP machine, as shown in Figure 6.1. This system allows on-machine sub-aperture stitching metrology, and so will exhibit improved versatility compared with full-aperture measurement. It is expected that there will be some variation in measurement repeatability due to the increased height of the test tower and larger metrology loop. However, software and control performance is expected to remain unchanged.



Figure 6.1: IRP600XL combined with metrology testing tower

6.1.2 Automatic Measurement of Aspheric Surfaces

Although the work presented supports the automatic form measurement of both plano and spherical surfaces, aspheres are not supported. In order for the systems developed to allow sub-aperture measurement on surfaces such as the E-ELT prototype segments, support for aspheric surfaces must be included in *Metrology Control Suite*. Potential methods of adding support for aspheres are discussed in Section 6.1.2.1 and Section 6.1.2.2.

6.1.2.1 Non-Null Testing

When carrying out sub-aperture measurement on mild aspheres, it is possible to carry out non-null testing provided that interferometric fringes are not aliased and

the residual retrace error is tolerable. Due to the varying local ROC, it cannot be assumed that the local surface normal vector will offer the best null, unlike spherical and plano measurement. In the non-null testing regime the system should minimise the number of fringes in the interferometer FOV, which may require some residual tilt and power to remain. Therefore, the automatic alignment procedures developed for plano and spherical measurement cannot be used. In order to compute the best null position ray tracing software, such as Zemax, could be used. Maintaining a simple software interface would require that Metrology Controller handle all interfacing and operation of the ray tracing application in the background (Dynamic Data Exchange), allowing the operator to interact only with Metrology Designer.

It is expected that a ray tracing model of each sub-aperture would be produced automatically and examined to determine a set of target Zernike terms which would offer the best null. The automatic alignment routine would then use these Zernike terms as a target for the alignment process.

6.1.2.2 Wavefront Correction

When null testing an aspheric optic it is normal to use some type of wavefront correction, such as a CGH. A CGH is typically custom made optical element and only suitable for a single aspherical prescription. When performing sub-aperture testing using a CGH, typically only rotationally symmetrical optics may be accommodated by a single CGH. Sub-aperture measurement of optics such as the ESO E-ELT prototypes would not be carried out this way as segments are typically off-axis apsheres and so off no rotational symmetry. In order to allow a maximise system flexibility, it is desirable to use wavefront correction which may be reconfigured for

each sub-aperture, based upon a ray tracing model, as discussed in Section 6.1.2.1. Instead of computing the best orientation along which to address the surface, the ray tracing application would compute the required wavefront correction to allow null testing at each sub-aperture location. Upon arriving at each sub-aperture the wavefront corrector would be reconfigured with the predicted correction and the alignment correction system can operate in a manner similar to that of spherical testing but including minimisation of astigma and coma Zernike terms arising due to aspherical mismatch.

An example variable wavefront correction device is the liquid crystal display (LCD) spatial light modulator [97]. Such a device could be fitted to the front of the Fizeau interferometer, to allow wavefront correction without the modification of other elements in the measurement system. Reflective spatial light modulators can also be used as a reference generator in a Twyman-Green based interferometer, however, the Fizeau is preferred due to the benefits of common path error cancellation.

For surface texture measurement, requiring only discrete point spaced across the surface, no such limitation exists. At the scale of the device FOV, residual error due to aspheric mismatch with the objective wavefront is expected to be negligible, although some adjustment of nulling algorithm may be required for steeper parts.

This chapter has drawn together the main developments presented in this thesis. Two example automated metrology systems have been proven, but these are a precursor to what is likely to be many more, which will be developed using, and amalgamated into, the *Metrology Control Suite*. The aim of this work is to provide

improved quality measurement data more quickly, in order to further develop our control of precision surfaces. Development of the *Metrology Control Suite* eases the practical problems of measurement by allowing a generalised approach to be applied to a range of surfaces. This removes the requirement for specialist configurations which are suitable for only a single, or limited number of projects. By demonstrating that automatic on-machine metrology is viable for demanding projects such as the ESO E-ELT, it is evident that the work presented has the potential to revolutionise the field of optical manufacturing.

7 List of publications

7.1 Papers

Bibby, M.; King, C.W., “Development of an On-Machine 3D Texture Analyser”, Proc. ICAM2012, Jiaoxi, Taiwan, March 2012.

Bibby, M.; King, C.W., “Development of an On-Machine 3D Texture Analyser”, Advanced Materials Research, Vol. 579, p. 338-347, Trans Tech Publications, 2012.

King, C.; **Bibby, M.**, 2013. Development of a metrology workstation for full-aperture and sub-aperture stitching measurements, JSPE, International symposium on application of precision engineering to support the next generation astronomical telescopes, Proc. JSPE March 2013.

Walker, D.D.; Beaucamp, A.; **Bibby, M.;** Fox-Leonard, T.; Gray, C.; King, C.; Rees, P.; Yu, G., “Interactions Between Manufacture and Measurement of Off-Axis Aspheres”, Proc. ASPE/ASPEN Summer Topical Meeting: Manufacture and Metrology of Freeform and Off-axis Aspheric Surfaces, p 72-77, 2014.

7.2 ESO Certification Documents

Bibby, M.; Rees, P., “Procedure – Measurement of Microroughness”, ESO document number: E-PRO-OPT-300-0318/10042-10318, Issue 3, October 2013.

Rees, P.; **Bibby, M.**, “Test Report – Segment SPN04 Microroughness Results”, ESO document number: E-TRE-OPT-300-0119/10042-10119, Issue 1, October 2013.

Rees, P.; **Bibby, M.**, “Test Report – SPN01 Microroughness Results”, ESO document number: E-TRP-OPT-300-0126/10042-10126, Issue 1, June 2014.

8 Bibliography

- [1] Oxford English Dictionary, "Surface, n," Oxford University Press, Oxford , 2014.
- [2] C. Narbeth, "The Cowry Shell as Money," *Molusc World*, 22 May 2013.
- [3] N. H. Jones, "The Origins of Hypodermic Medication," *Scientific American*, Vols. 224, , no. 1, pp. 96-102, 1970.
- [4] S. A. Layard, in *Discoveries in the ruins of Nineveh and Babylon; with travels in Armenia, Kurdistan and the desert: being the result of a second expedition undertaken for the Trustees of the British Museum*, New York, G.P. Putnam and Co., 1853, pp. 197-198.
- [5] G. Sines and Y. A. Sakellarakis, "Lenses in Antiquity," *American Journal of Archaeology*, vol. 91, no. 2, pp. 191-196, 1987.
- [6] J. M. Enoch, "First Known Lens Originating in Egypt About 4600 Years Ago," *Documenta Ophthalmologica*, vol. 99, no. 3, pp. 303-314, 1999.
- [7] H. C. King, *The History of the Telescope* pp.30-33, Mineola, New York: Courier Dover Publications, 1955.
- [8] A. Edited by Van Helden, S. Dupre, R. Van Gent and H. Zuidervaart, *The Origins of the Telescope*, Amsterdam: Amsterdam University Press, 2010.
- [9] A. Boccaletti, "Direct Imaging of Extrasolar Planets: Overview of Ground and Space Programs," in *eprint arXiv:0910.4339*, Ithaca, New York, 2009.
- [10] European Southern Observatory, "E-ELT Publications and Documentation," European Southern Observatory, 2010. [Online]. Available: http://www.eso.org/sci/facilities/eelt/docs/e-elt_constrproposal.pdf. [Accessed 29 July 2014].
- [11] T. De Zeeuw, R. Tamai and J. Liske, "Constructing the E-ELT," *The Messenger*, pp. 3-6, December 2014.
- [12] B. Burke, J. Gregory, M. Cooper, A. Loomis, D. Young, T. Lind, P. D. P. Doherty, D. Landers and C. J., "CCD Imager Development for Astronomy," *Lincoln Laboratory Journal*, vol. 16, no. 2, pp. 392-412, 2007.
- [13] A. Greve and M. Bremer, "Radiative Heat Transfer," in *Thermal Design and Thermal Behaviour of Radio Telescopes and their Enclosures*, London, UK, Springer , 2010, pp.

141-143.

- [14] R. A. Paquin, in *Handbook of Optomechanical Engineering*, Boca Raton, CRC Press, 1996, p. Chapter 3.
- [15] Newport, "Optical Materials," Newport, [Online]. Available: <http://www.newport.com/Optical-Materials/144943/1033/content.aspx>. [Accessed 30 July 2014].
- [16] A. J. Leistner, E. G. Thwaite, F. Lesha and J. M. Bennett, "Polishing Study using Teflon and Pitch Laps to Produce Flat and Supersmooth Surfaces," *Applied Optics*, vol. 31, no. 10, pp. 1472-1482, 1992.
- [17] F. W. Preston, "The Theory and Design of Plate Glass Polishing Machines," *Journal of the Society of Glass Technology*, vol. XI, no. V11, pp. 214-257, 1927.
- [18] M. J. Cumbo, D. Fairhurst, S. D. Jacobs and B. E. Puchebner, "Slurry Particle Size Evolution During the Polishing of Optical Glass," *Applied Optics*, vol. 34, no. 19, pp. 3743-3755, 1995.
- [19] R. Williamson, "Overarm spindle machine," in *Field Guide to Optical Fabrication*, Bellingham, WA, SPIE, 2011, p. 43.
- [20] D. Brooks and A. Gee, "Manufacture of Large Optics: Materials and Processes," in *Proc. of the 23rd Meeting of the ASPE and the 12th ICPE*, 2008.
- [21] D. Brooks, "PhD Thesis Chapter: The Reconstruction of the Birr Telescope," in *The Production of Metal Mirrors for Use in Astronomy*, London, University College London, 2001, pp. 88-149.
- [22] W. Pease, "An Automatic Machine Tool," *Scientific American*, vol. 187, no. 3, pp. 10-23, 1952.
- [23] S. C. West, H. M. Martin, R. S. Nagel, D. W. B., T. J. Trebisky, S. T. DeRigne and B. B. Hille, "Practical Design and Performance of the Stressed-lap Polishing Tool," *Applied Optics*, vol. 33, no. 34, pp. 8094-8100, 1994.
- [24] L. Haitao, Z. Zhige, W. Fan, F. Bin and W. Yongjian, "Study on Active Lap Tool Influence Function in Grinding 1.8 m Primary Mirror," *Applied Optics*, vol. 52, no. 31, pp. 7504-7511, 2013.
- [25] B. E. Gillman and D. Jacobs, "Bound-abrasive Polishers for Optical Glass," *Applied Optics*, vol. 37, no. 16, pp. 3498-3505, 1998.
- [26] R. Williamson, "Designing Aspheres for Manufacturability," in *Field Guide to Optical Fabrication*, Bellingham, WA, SPIE, 2011, p. 12.

- [27] S. Bambrick, M. Bechtold and A. Farnung, "Process Control With Sub-Aperture Polishing," *Optics and Photonics News*, pp. 12-13, July 2009.
- [28] International Standards Organisation, ISO6983: Numerical control of machines - program format and definition of address words - Part 1.Data format for positioning, line motion and contouring control system, 2009.
- [29] S. D. Jacobs, "International Innovations in Optical Finishing," *Proc of the SPIE: Current Developments in Lens Design and Optical Engineering*, vol. 264, p. doi:10.1117/12.557274, 2004.
- [30] S. Bambrick, M. Bechtold, S. DeFisher and D. Mohring, "Ogive and Free-Form Polishing with Ultraform Finishing," in *Proc. of the SPIE - International Society of Optical Engineering*, Orlando, FL, USA, 2011.
- [31] S. Jacobs, W. Kordonski, I. Prokhorov, D. Golini, G. Gorodkin and T. Strafford, "Deterministic Magnetorheological Rinishing". New York, US Patent EP0858381B1, 11 October 1996.
- [32] J. E. DeGroot, A. E. Marino, J. P. Wilson, A. L. Bishop, J. C. Lambropoulos and S. D. Jacobs, "Removal Rate Model for Magnetorheological Finishing of Glass," *Applied Optics*, vol. 46, no. 32, pp. 7927-7941, 2007.
- [33] C. Miao, J. C. Lambropoulos and S. D. Jacobs, "Process Parameter Effects on Material Removal in Magnetorheological Finishing of Borosilicate Glass," *Applied Optics*, vol. 49, no. 10, pp. 1951-1963, 2010.
- [34] A. Swat, M. Cayrel and P. Dierickx, "E-ELT Programme: E-SPE-ESO-300-0150 Issue 4," ESO, Garching bei München, Germany, 2009.
- [35] M. Schinhaerl, C. Vogt, A. Geiss, R. S. P. Stamp, L. Smith, G. Smith and R. Rascher, "Forces Acting Between Polishing Tool and Workpiece Surface In Magnetorheological Finishing," *Proc. of the SPIE: Current Developments in Lens Design and Optical Engineering*, vol. IX, p. doi:10.1117/12.794196, 2008.
- [36] M. Tricard, P. R. Dumas, D. Golini and J. T. Mooney, "SOI Wafer Polishing with Magnetorehological Finishing (MRF)," in *2003 IEEE International SOI Conference*, Newport Beach, California, 2003.
- [37] D. Golini, W. I. Kordonski, P. Dumas and S. J. Hogan, "Magnetorheological Finishing (MRF) in Commercial Precision Optics Manufacturing," *Proceedings of the SPIE: Optical Manufacturing and Testing III*, vol. 3782, no. 80, p. doi: 10.1117/12.369174, 1999.
- [38] D. Golini, M. Demarco, W. Kordonski and J. Druning, "MRF Polishes Calcium Fluoride to High Quality," *Laser Focus World*, vol. 37, no. 7, 2001.

- [39] D. D. Walker, G. Yu, H. Li, W. Messelink, R. Evans and A. Beaucamp, "Edges in CNC Polishing: From Mirror-Segments Towards Semiconductors, Paper 1: Edges on Processing the Global Surface," *Optics Express*, vol. 20, no. 18, pp. 19787-19798, 2012.
- [40] D. D. Walker, R. Freeman, G. McCavana, R. Morton, D. Riley, J. Simms, D. Brooks, E. Kim and A. King, "Zeeko/UCL Process for Polishing Large Lenses and Prisms," *Proceedings of the SPIE: Large Lenses and Prisms*, vol. 4411, no. 106, p. doi:10.1117/12.454877, 2002.
- [41] A. Beaucamp, R. Freeman, R. Morton and D. D. Walker, "Metrology Software Support for Free-form Optics Manufacturing," in *Proceedings of JSPE*, Chubu, 2007.
- [42] G. Yu and D. D. L. H. Walker, "Research on Fabrication of Mirror Segments for E-ELT," in *Proc. of the SPIE - 6th International Symposium on Advanced Optical Manufacturing and Testing Technologies*, Xiamen, China, 2012.
- [43] D. walker, A. Daldwin, R. Evans, R. Freeman, S. Hamidi, P. T. X. Shore, S. Wei, C. Williams and G. Yu, "A Quantitative Comparison of Three Groishing Techniques for the Precessions Process," *Proceedings of the SPIE - The International Society for Optical Engineering*, vol. 6671, no. 1, pp. 1-9, 2007.
- [44] R. Youngworth, B. Gallagher and B. Stamper, "An Overview of Power Spectral Density (PSD) calculations," *Proc. of the SPIE - Optical Manufacturing and Testing*, vol. VI, p. doi: 10.1117/12.618478, 2005.
- [45] H. Karow, "Interferometric Testing in a Precision Optics Shop: A Review of Testplate Testing," *Proc. of the SPIE: Interferometry*, vol. 56, p. doi: 10.1117/12.957837, 1979.
- [46] D. Malacara, "Newton Interferometer," in *Optical Shop Testing, 3rd ed*, Hoboken, New Jersey, Wiley & Sons, 2007, pp. 1-4.
- [47] P. Hariharan, "CCD image capture," in *Basics of Interferometry, 2nd Edition*, Sydney, Australia, Elsevier, 2007, pp. 51-53.
- [48] W. Hao-ming and T. Xing, "Vibration Errors in Phase-Shifting Interferometer," in *Proc. of the SPIE International Conference on Optical Instruments and Technology: Optoelectronic Measurement Technology and Systems*, 2009.
- [49] M. Yamauchi, "Measurement of Air Turbulence for On-Machine Interferometry," *Applied Optics*, vol. 42, no. 34, pp. 6869-6876, 2003.
- [50] D. M. Sykora, "Instantaneous Measurement Fizeau Interferometer With High Spatial Resolution," *SPIE Optical Manufacturing and Testing*, vol. 8126, no. IX, 2001.
- [51] C. Zhao and J. Burge, "Optical Testing with Computer Generated HologramsL

Comprehensive Error Analysis," *Proc of the SPIEL Optical Manufacturing and Testing*, vol. X, p. doi: 10.1117/12.2024742, 2013.

- [52] C. Kreischer, "Retrace Error: Interferometry's Dark Little Secret," in *SPIE - The International Society for Optical Engineering*, Rochester, NY, USA, 2013.
- [53] D. Malacara, "Common-Path interferometers," in *Optical Shop Testing, 2nd Ed*, Wiley & Sons Inc, 2007, p. 97.
- [54] S. O'Donohue, P. Murphy, J. Fleig and G. Devries, "Stitching Interferometry for Flexible Asphere Metrology," in *Proc. of the 21st Annual ASPE Meeting*, Monterey, CA, 2006.
- [55] B. Catanzaro, J. Thomas and E. Cohen, "Comparison of Full-Aperture Interferometry to Sub-Aperture Stitched Interferometry for a Large Diameter Fast Mirror," in *Optomechanical Design and Engineering*, San Diego, CA, USA, 2001.
- [56] M. Tricard, A. Kulawiec, M. Bauer, G. DeVries, J. Fleig, G. Forbes, D. Miladinovich and P. Murphy, "Subaperture Stitching Interferometry of High-Departure Aspheres by Incorporating a Variable Optical Null," *CIRP Annals - Manufacturing Technology*, vol. 59, no. 1, pp. 547-550, 2010.
- [57] S. Zeng, Y. Dai and S. Chen, "Subaperture Stitching Interferometer for Large Optics," in *Proc. of the SPIE 4th International Symposium on AOMATT: Large Mirrors and Telescopes*, Chengdu, China, 2009.
- [58] T. Hagino, Y. Yokoyama, Y. Kuriyama and H. Haitjema, "Sphericity Measurement Using Stitching Interferometry," *Key Engineering Materials*, vol. 883, pp. 523-524, 2012.
- [59] C. King, G. Davies, J. Mitchell, P. Mitchell, A. Rees and D. Walker, "Fusing Data From Multiple Interferometers for the Measurement of Off-Axis Aspheres," in *ASPE ASPEN: Manufacture and Metrology of Freeform and Off-Axis Aspheric Surfaces*, Kohala Coast, HI, USA, 2014.
- [60] C. King and M. Bibby, "Development of a Metrology Workstation for Full-Aperture and Sub-aperture Stitching Measurements," in *2nd CIRP Conference of Surface Integrity*, Nottingham, UK, 2014.
- [61] Agilent, "Accuracy and Repeatability," in *Agilent Laser and Optics User Manual: 5th Ed.*, Santa Clara, CA, Agilent Technologies Inc., 2007, pp. 168-179.
- [62] J. E. Harvey and A. K. Thompson, "Scattering effects from residual optical fabrication errors," in *International conference on optical fabrication and testing*, Tokyo, 1995.
- [63] R. J. Noll, "Effect of Mid- and High -Spatial Frequencies on Optical Performance,"

Optical Engineering, vol. 18, no. 2, pp. 137-42, 1979.

- [64] M. C. Weisskopf, "Chandra x-ray optics," *Optical Engineering*, p. DOI: 10.1117/1.OE.51.1.011013, 2012.
- [65] D. Vernani, G. Borghi and e. al, "Performance of supersmooth x-ray mandrels for new hard x-ray missions," in *Optics for EUV, X-ray and gamma-ray astronomy IV*, San Diego, 2009.
- [66] R. Leach, L. Brown, X. Jiang, M. Conroy and D. Mauger, "Introduction," in *A National Measurement Good Practice Guide No. 108: Guide for the Measurement of Smooth Surface Topography using Coherence Scanning Interferometry*, Middlesex, National Physical Laboratory, 2008, pp. 2-9.
- [67] D. Malacara, "Lyot Test," in *Optical Shop Testing, 3rd Ed.*, Hoboken, NY, Wiley and Sons, 2007, pp. 305-306.
- [68] R. Parks, "In Situ Surface-roughness Measuring Topographer," *SPIE Newsroom*, p. DOI: 10.1117/2.1231102.003555, 28 March 2011.
- [69] B. Kinbrough, N. Brock and J. Millerd, "Dynamic Surface Roughness Profiler," *Optical Manufacturing and Testing IX*, vol. 8126, p. DOI: 10.1117/12.893557, 2011.
- [70] Y. C. Liu, C. Y. Ling, A. A. Malcom and Z. G. Dong, "Accuracy of replication for non-destructive surface measurement," in *Singapore International NDT Conference & Exhibition*, Marina Bay, Singapore, 2011.
- [71] D. Walker, H. Yang and D. Brooks, "Interferometry Applied to Testing Large Optics," in *Applied Optics and Optoelectronics*, Brighton, UK, 1998.
- [72] D. Walker and R. Bingham, "Unspecified," in *Proceedings of the International Workshop on Mirror Substrate Alternatives*, Grasse, France, 1995.
- [73] D. Brooks, "Chapter 5: Parabolising," in *The Production of Metal Mirrors for use In Astronomy (PhD Thesis)*, London, University College London, 2001, p. 138.
- [74] T. Wang, H. Cheng, Y. Feng, Z. Dong and H. Tam, "Correction of Remounting Errors by Masking Reference Points in Small Footprint Polishing Process," *Applied Optics*, vol. 52, no. 33, pp. 7851-7858, 2013.
- [75] 4D Technology, "4D Technology Nanocam Product Page," 4D Technology, [Online]. Available: <http://www.4dtechnology.com/products/NanoCamSq.php>. [Accessed 16 November 2014].
- [76] P. Rees and M. Bibby, "Test Report - Segment SPN04 Microroughness Results," OpTIC Glyndwr, St Asaph, 2013.

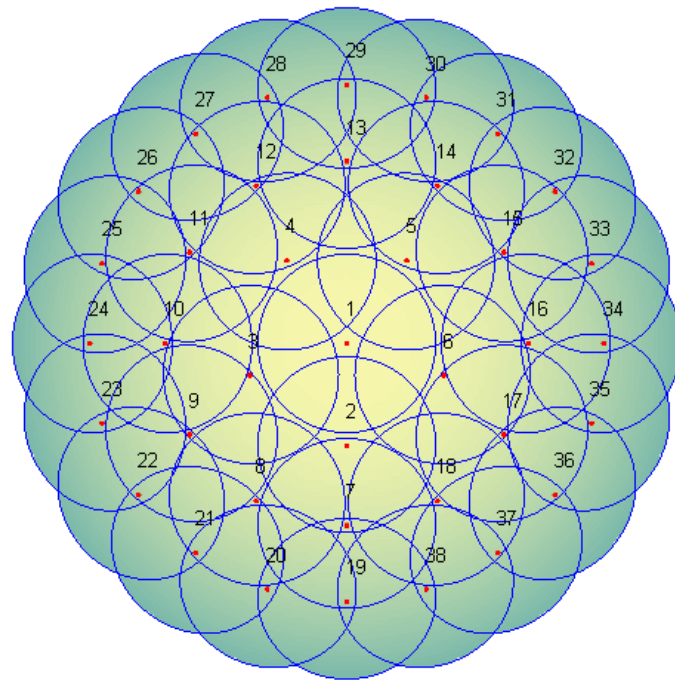
- [77] C. W. King, "Integrated On-Machine Metrology Systems," in *JSPE International Symposium: Autumn Meeting*, Tokyo, 2010.
- [78] Zeeko, "Zeeko product webpages," 2000. [Online]. Available: http://www.zeeko.co.uk/site/tiki-index.php?page=IRP+Machine+Brochures&no_bl=y. [Accessed 28 June 2014].
- [79] B. Kimbrough, N. Brock and J. Millerd, "Dynamic Surface Roughness Profiler," in *Proc. SPIE International Society for Optical Engineering*, San Diego, CA, USA, 2011.
- [80] *Discussion with Neal Brock, 4D Tehcnology*, 2013.
- [81] M. Bibby and C. W. King, "Development of an On-Machine 3D Texture Analyser," *Advanced Materials Research*, vol. 579, pp. 338-347, 2012.
- [82] 4D Technology, "4D Technology FizCam3000 Product Page," 4D Technology, [Online]. Available: <http://www.4dtechnology.com/products/fizcam3000.php>. [Accessed 16 November 2014].
- [83] B. Kimbrough, E. Frey and J. Millerd, "Instantaneous Phase-Shifting Fizeau Interferometer Utilizing a Synchronous Frequency Shift Mechanism," in *Proc SPIE The Internatioal Society for Optical Engineering: Interferometry XIV: Techniques and Analysis*, San Diego, CA, USA, 2008.
- [84] QED, "QED SSI-A Product Specification Sheet," QED, Rochester, NY, USA, 2011.
- [85] O. Boubaker, "The inverted pendulum: A fundamenteel benchmark in control theory and robotics," in *2012 International Conference on Education and e-Learning Innovations*, Sousse, Tunisia, 2012.
- [86] R. Henselmans, L. Cacace, G. Kramer, P. Rosielle and M. Steinbuch, "The NANOMEFOS Non-Contact Measurement Machine for Freeform Optics," *Precision Engineering*, vol. 35, no. 4, pp. 607-624, 2011.
- [87] Mathworks, "Matlab Support Page: Data Types," Mathworks, 2014. [Online]. Available: http://uk.mathworks.com/help/matlab/data-types_data-types.html?nocookie=true. [Accessed 22 November 2014].
- [88] J. Snyman, "Line Search Descent Methods for Unconstrained Minimization," in *Practical Mathematical Optimization*, Springer US, 2005, pp. 34-35.
- [89] NIST, "National Institute of Standards of Technology: Computer Security Division Computer Security Resource Center," July 2001. [Online]. Available: <http://csrc.nist.gov/publications/fips/fips197/fips-197.pdf>. [Accessed 26 November 2014].

- [90] IEEE, "IEEE 802.3 Ethernet Working Group," IEEE, 7 November 2014. [Online]. Available: <http://www.ieee802.org/3/>. [Accessed 26 November 2014].
- [91] V. Mahajan, "Zernike Polynomials and Wavefront Fitting," in *Optical Shop Testing, 3rd ed.*, New York, USA, Wiley, 2007, pp. 498-521.
- [92] D. Greenhill and G. Jones, "Analysis of Interferometric Images Using the Hough Transform," *Electronic Letters*, vol. 32, no. 3, pp. 199-201, 1996.
- [93] D. Walker and R. Freeman, "TSB Project 101550 - Developing and Integrated System to Enable a Robot to Speak With a Zeeko Machine to Automate Currently Manual Operations," Zeeko Ltd, Coalville, Leicestershire, UK, 2013.
- [94] R. Parasuraman and V. Riley, "Humans and Automation: Use, Misuse, Disuse, Abuse," *Human Factors*, vol. 39, no. 2, pp. 230-253, 1997.
- [95] K. Creath and J. Wyant, "Absolute Measurement of Spherical Surfaces," *Proceedings of the SPIE - The International Society for Optical Engineering*, vol. 1332, no. 1, pp. 2-7, 1990.
- [96] B. Truax, "Absolute Interferometric Testing of Spherical Surfaces," *Proceedings of the SPIE - The International Society for Optical Engineering*, vol. 1400, pp. 61-68, 1991.
- [97] M. Cashmore, "Phd Thesis: Interferometric Metrology Using Reprogrammable Binary Holograms," Durham University, Durham, UK, 2013.
- [98] C. H. Eyraud, "European Association for Astronomy Education," Institut National de Recherche Pédagogique, 2009. [Online]. Available: http://www.eaae-astronomy.org/WG3-SS/WorkShops/pdf/ws2_2009.pdf. [Accessed 29 27 2014].
- [99] H. H. Karow, *Fabrication Methods for Precision Optics*, New York: Wiley-Blackwell, 2004.
- [100] General Electric, *GE-225 Programming Reference Manual*, Phoenix, Arizona: General Electric Company, 1966.
- [101] J. Burge, Z. Chunyu and M. Dubin, "Measurement of Aspheric Mirror Segments Using Fizeau Interferometry with CGH Correction," *Proc. of the SPIE - Optical Engineering*, vol. 7739, pp. 773902-773917, 2010.
- [102] The Economist Newspaper Limited, "The Onrushing Wave," *The Economist*, p. Briefing, 18 January 2014.
- [103] S. L. (Editor), "Crofton - Crophthorne," in *A Topographical Dictionary of England*, London, Institute of Historical Research, 1848, pp. 729-733.

- [104] W. Farrer and J. Brownbill, "Townships: Middleton," in *A History of the County of Lancaster: Volume 5*, British History Online, 1911, pp. 161-169.
- [105] T. Hult, "Presentation of a New High Speed Paper Tape Reader," *BIT Numerical Mathematics*, vol. 3, no. 2, pp. 93-96, 1963.
- [106] C. Harley and N. Crafts, "Cotton Textiles and Industrial Output Growth During the Industrial Revolution," *The Economic History Review*, vol. 48, no. 1, pp. 134-144, 1995.
- [107] Economic History Society, "Economic History Society," 1987. [Online]. Available: <http://www.ehs.org.uk/dotAsset/15457c19-e7bd-4045-a056-30a3efac2d47.pdf>. [Accessed 19 November 2014].
- [108] J. Postel, "Internet Engineering Task Force: User Datagram Protocol," IETF, 28 August 1980. [Online]. Available: <http://tools.ietf.org/html/rfc768>. [Accessed 26 November 2014].
- [109] E. J. Evans, "PVr - A Robust Amplitude Parameter for Optical Surface Specification," *Optical Engineering*, vol. 48, no. 4, p. DOI: 10.1117/1.3119307, 2009.

9 Appendices

9.1 *Metrology Control Suite* User Manual



Zeeko Metrology Control Suite

Operating Manual Ver. 1.0

1 Introduction

The Zeeko Metrology Control Suite is designed to allow measurement design and execution using one of the range of Zeeko metrology products. The software allows the user to define a surface and use this to generate a measurement plan. The plan can either be saved for later execution (.OMM or On Machine Metrology file) or used immediately.

Metrology Control Suite has been developed to allow simplified measurement, which much of the process being automatic. Once the initial set-up procedures are complete, the system can carry out measurement without further user input.

2 Installation

The following steps demonstrate the installation or upgrade of Zeeko Metrology Control Suite.

1. Ensure that no previous versions of Zeeko Metrology Control Suite are installed on the system.
2. Select 'Zeeko Metrology Control suite Setup.exe' on the disc provided. This will install Zeeko Metrology Control Suite, Metrology Designer and Zeeko Axis Position Display. Note the selected installation path, e.g. C:\Program Files (x86)\Zeeko\
3. Select 'Config Setup.exe'. This will install the metrology system configuration files required for operation. This must be installed to the same path as that used for step 2 and within the program directory, e.g. C:\Program Files (x86)\Zeeko\Metrology_Control_Suite
4. Double click 'Zeeko Metrology Control Suite' icon on the desktop. If not already set up, the user will be prompted to install the Zeeko software license key. Contact Zeeko with the hardware key provided in the pop up box.
5. Once a license has been obtained, select browse to locate the key and select to install. This completes installation and will activate the application for use.

3 Metrology Control Suite Module Overview

Metrology Control Suite consists of the following main modules;

- Metrology Control interface. This is the main software window through which the user controls the measurement system. Useful information regarding progress is displayed to the user.
- Measurement Designer. The measurement design module allows a measurement plan to be developed using a surface design (Zeeko .design file) and a test optic specification.
- Surface Designer. This module allows the test surface parameters to be defined and saved for future use. This the same module included in other Zeeko applications such as TPG and Metrology Toolkit.

4 Metrology Control Interface

During measurement, metrology is controlled from the graphical user interface (GUI) of the Metrology Controller (Figure 2). Additional windows which may be displayed depending upon user selection are also shown below.

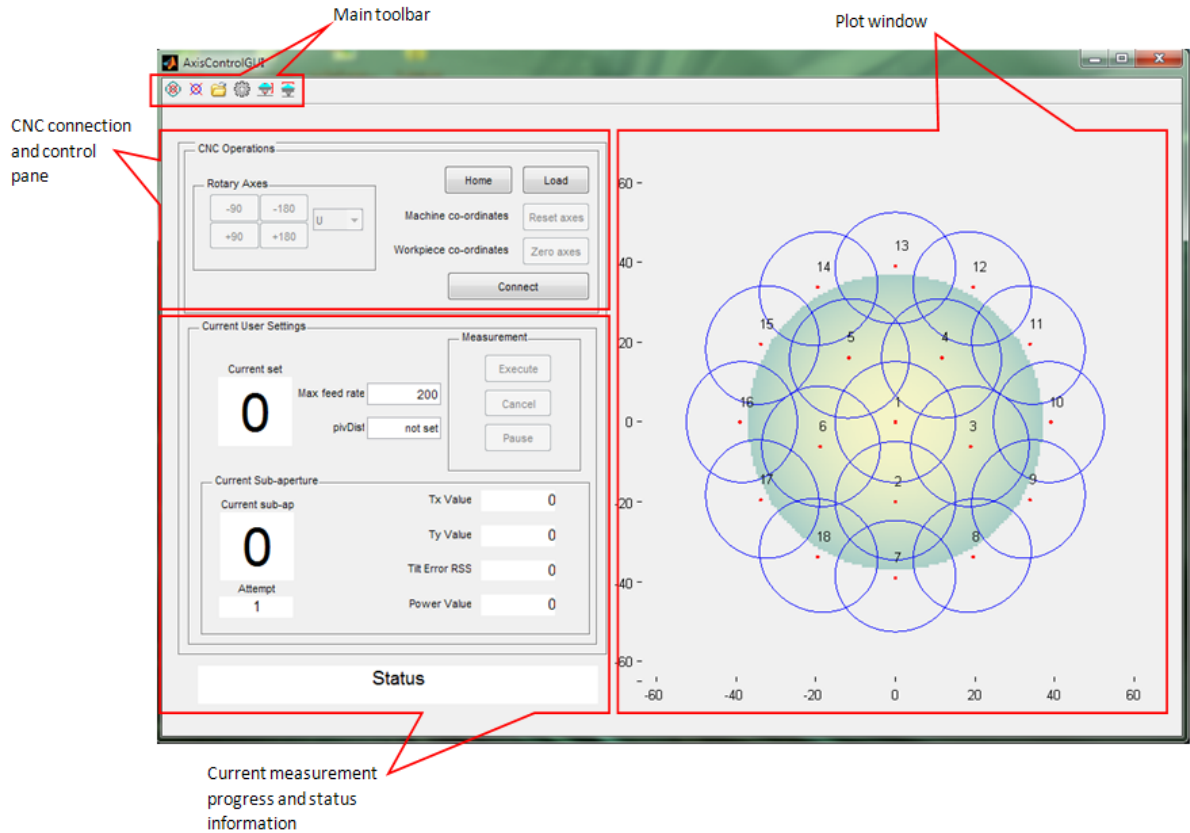


Figure 2: Metrology Control main window.

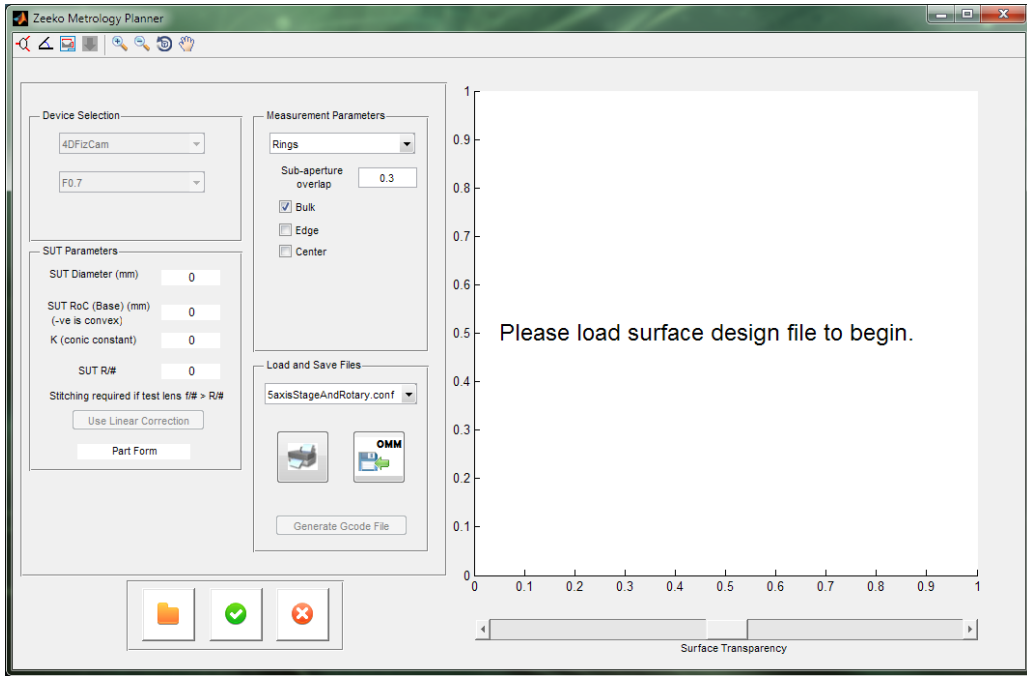


Figure 3: Metrology Planner.

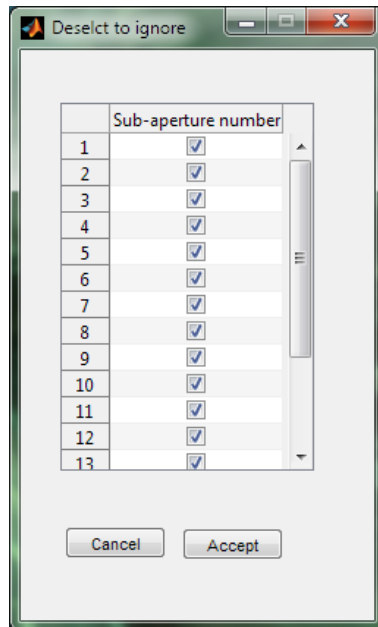


Figure 4: Ignore sub-aperture menu.

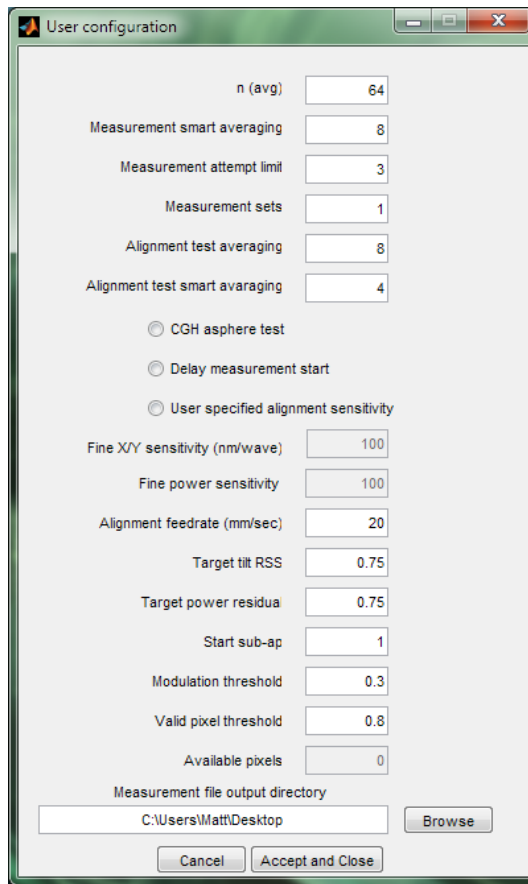









Figure 5: User configuration menu.

5 Main Toolbar Icon Functions

Most of the control functions are available via the main software GUI (Figure 2) however sub-menus and system set up procedures are accessible from the main toolbar. The functionality of these buttons is outlined below.

Table 6: Main GUI toolbar functions.

Icon	Function	Description
	Start Metrology Designer	Opens Metrology Designer to allow the user to design a metrology plan (OMM) or edit an existing one.
	Edit ignored sub-apertures	Opens a window to allow user to edit sub-apertures which will be measured.
	Open an On-Machine Measurement (OMM) file	Allows the user to select an OMM file for loading.
	Start pivDist calculation assistant	Begins the pivDist calculation procedure.
	Open user configuration menu	Opens a window to allow the user to edit the system configuration.
	Start the part alignment assistant	Begins the semi-automatic part alignment procedure.
	Start the Axis Position Display	Starts the Axis Position Display module.

5.1 Start Metrology Planner

Selection of the start Metrology Planner toolbar button will activate the planner module in a new window, as shown in Figure 3. Metrology Planner is covered in detail in chapter 8.

5.2 Edit ignored sub-apertures

When a measurement plan is loaded, the ignore sub-aperture menu will be displayed in a new window. Each available sub-aperture is displayed with an associated check box. Un-checking a box will ignore this sub-aperture during measurement. Select the 'Accept' button to modify the measurement plan with this selection.

Loading a measurement plan will clear any selections in this menu. Changes made do not modify the OMM file in any way. The user must select sub-apertures to ignore every time the OMM file is loaded.

5.3 Open user configuration menu

A new window is opened, displaying the user configuration menu (Figure 5). From this menu the user can adjust system behaviour. The function of each parameter is outlined below.

5.3.1 N(avg)

Number of acquisitions to average during a sub-aperture measurement.

5.3.2 Measurement smart averaging

Sets minimum number of valid pixels across measurements to be averaged in order for pixel to be considered valid (see 4D 4Sight manual). This allows a certain amount of data dropout while still returning data for analysis. This parameter must be less than n(avg) to be valid. The user will receive a warning if the entered value is invalid.

5.3.3 Measurement attempt limit

If poor quality data is acquired during measurement, the acquisition may be repeated. This parameter is the maximum number of attempts before the measurement location is skipped. Skipped measurements are noted in the measurement log file and measurement report.

5.3.4 Measurement sets

Parameter specifies the number of times to repeat the measurement plan. No user input is required between repetitions.

5.3.5 Alignment test averaging

Specifies the number of acquisitions to average when determining the interferometer/part alignment. If an inappropriate value is chosen here, alignment may not converge. Proper value selection depends upon surface finish and environmental conditions. If in doubt, the user should manually perform several acquisitions to determine an averaging value at which Zernike terms 2, 3 and 4 may be reliably determined.

5.3.6 Alignment test smart averaging

As for 5.3.2 but used during alignment testing. This value must be smaller than the alignment test averaging level.

5.3.7 CGH asphere test

When testing a rotationally symmetrical aspherical surface using a computer generated hologram (CGH), the user is required to make initial alignment. Selection of this option will turn off auto-alignment during the measurement process, ensuring the surface/CGH alignment stays constant. This option also enables the '*Available pixels*' parameter.

5.3.8 Delay measurement start

Selection of this option allows the user to specify a delay time upon commencement of the measurement process (HH:MM from pressing execute). When the '*Execute*' button is pressed to begin measurement a window is displayed (Figure 6), giving the user the option to enter the required time delay.

Selecting 'OK' begins the delay counter (Figure 7) and 'cancel' will abort the measurement start. This option allows the user to schedule measurement outside working hours, when the laboratory environment may be more stable.

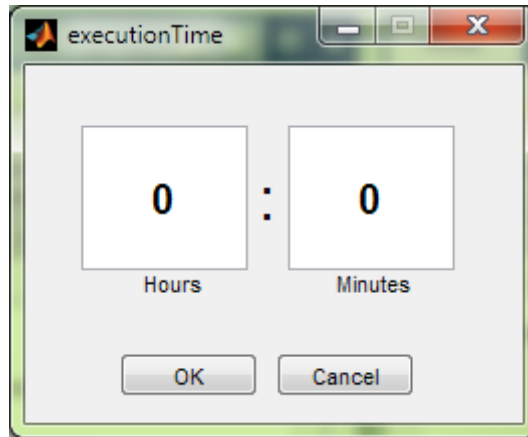


Figure 6: Measurement delay entry window.

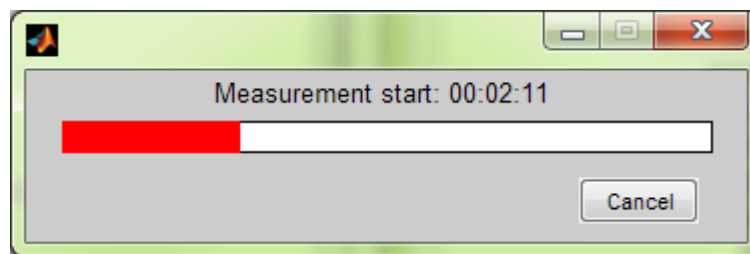


Figure 7: Measurement delay counter.

5.3.9 User specified alignment sensitivity

When this option is disabled (default) the measurement system will perform an automatic calculation to establish the sensitivity of the current reference/test optic configuration to tilt and power for both coarse and fine correction regimes.

When this parameter is enabled, the fine tilt/power sensitivity calculation is skipped and the user is required to enter these parameters in the two entries below (Fine X/Y sensitivity and Fine power residual) in waves/radius error. It is recommended that the user make a series of measurements manually, moving one axis at a time to establish the correct values for these entries.



Warning

Where possible, it is recommended that automatic sensitivity calculation mode be used. Miscalculation of alignment/power sensitivities can result in non-convergence.

5.3.10 Fine X/Y sensitivity

Fine sensitivity of current test/reference optical set up to tilt, specified in waves/radius. This entry is only enabled when '*User specified alignment sensitivity*' is active (See 5.3.9).

5.3.11 Fine power sensitivity

Fine sensitivity of current test/reference optical set up to power, specified in waves/radius. This entry is only enabled when '*User specified alignment sensitivity*' is active (See 5.3.9).

5.3.12 Alignment feed rate

This is the maximum rate at which any part of the system may move during an alignment procedure, specified in mm/sec. Alignment moves typically involve movement of the measurement device and so it is desirable to limit federate and therefore accelerations to which the device is subjected.

5.3.13 Target tilt RSS

This entry is the maximum allowable level of tilt error allowed for the system to consider the surface under test (SUT) well aligned enough for measurement. This figure is the root sum squared result of Zernike terms 2 and 3 and expressed in waves/radius tilt error;

$$T_{RSS} = \sqrt{Z_2^2 + Z_3^2}$$

If the analysed Zernike terms of an alignment measurement are less than the entered value, surface alignment will be deemed sufficient for measurement.

5.3.14 Target power residual

This entry is the maximum allowable level of power error allowed for the system to consider the surface under test (SUT) sufficiently nulled for measurement. Target power is expressed in waves of defocus. During measurement of a plano surface power is not tested.

5.3.15 Start sub-ap

The user may specify the first sub-aperture the system should address during measurement. Measurement will proceed from the specified location numerically, ignoring all measurements before that specified.

5.3.16 Modulation threshold

Interference modulation is computed during the alignment process as an indicator of data quality and allows the system to decide when to switch between coarse and fine alignment. By specifying a modulation value, the user can adjust the point at which the system will change alignment mode (see 4D 4Sight manual).

An average modulation value greater than that entered must be achieved for the system to switch to fine alignment. This value is set by determining the minimum value at which the interferometer will return reliable tilt and power information.

5.3.17 Valid pixel threshold

Following the acquisition of measurement data the number of valid pixels is queried to evaluate measurement quality. If the number of valid pixels in the data set is less than the total available pixels multiplied by the valid pixel threshold factor, the measurement is discarded. The measurement is repeated until the measurement attempt limit (5.3.3) is reached.



Note!

If part of the measurement field of view overlaps the SUT edge, the resulting missing data may cause false valid pixel result. The user must either avoid overhanging measurement locations or reduce the valid pixel threshold.

5.3.18 Available pixels

When running measurement of an aspherical surface (5.3.8) the user must manually specify the number of available pixels. This entry is then used in the valid pixel threshold test for measurement quality.

5.3.19 Measurement file output directory

This entry contains the output location for data and log files generated during measurement. The user may select 'browse' to locate a suitable directory. The software must have read/write permissions for this location in order to save data and logs.

At the commencement of measurement a time stamped folder is created for the current measurement. The user will also note the following files;

- Measurement data – numbered files containing measurement data (e.g. 1.h5)
- Measurement report – a text file containing a summary of measurement results and data quality.
- Measurement log – a text file containing a log of all events carried out during measurement.

5.4 Start pivDist calculation assistant

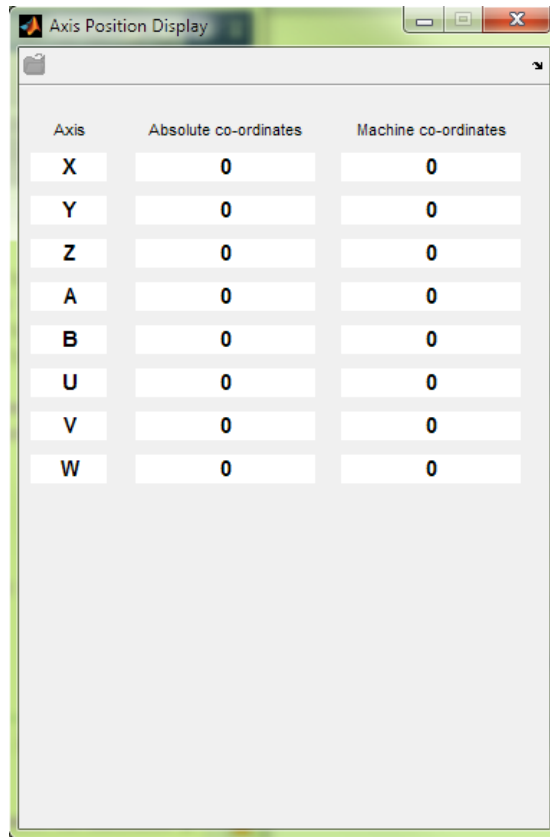
This button forms part of the machine setup procedure prior to starting measurement and enables the user to calculate the offset between the machine T-axis and the SUT CoC. This is required to allow multiple ring measurements to be made on spherical surfaces.

5.5 Start part alignment assistant

Activates the Metrology Control Suite semi-automatic SUT clocking procedure.

5.6 Start Axis Position Display

The Axis Position Display module allows the operator to view the position of all of the system axes in both absolute and machine co-ordinates.



The screenshot shows a window titled "Axis Position Display" with a table containing the following data:

Axis	Absolute co-ordinates	Machine co-ordinates
X	0	0
Y	0	0
Z	0	0
A	0	0
B	0	0
U	0	0
V	0	0
W	0	0

Figure 8: Axis Position Display GUI

The axis position display lists each axis with associated absolute and machine values.



Note!

When running Axis Position Display module from within the Zeeko Metrology Control Suite, program execution is paused. This operation mode is designed for checking position during the set up procedures. For continuous operation, Axis Position Display should be executed separately.

When running the Axis Position Display from executable, the application will require system configuration information in order to connect to the system and provide position information. This may be provided by selecting the load button from the toolbar and selecting either a system configuration file or a compatible OMM file for the system to be queried.

6 CNC Operations Panel

The panel labelled '*CNC Operations*' allows the user to manage the connection between Zeeko Metrology Control Suite and the measurement system. This panel (Figure 9) is located in the upper left corner of the main Metrology Control GUI.

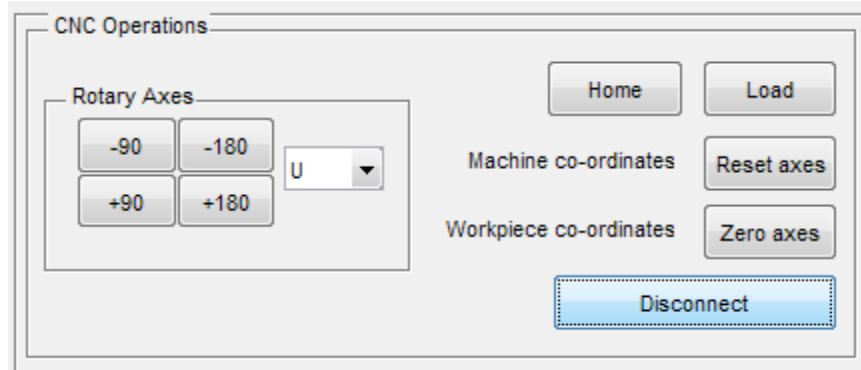


Figure 9: CNC Operations panel.

The functions of the buttons are outlined below;

- Home – Move system to the home parking position. The feed rate of this move is fixed and defined in machine configuration.
- Load – Move system to the part loading position. The federate of this move is fixed and defined in machine configuration.
- Reset axes – As part of the set up procedure for measurement, the user must define the part centre. The '*Reset axes*' button clears this offset.
- Zero axes - As part of the set up procedure for measurement, the user must define the part centre as [0,0,0]. The '*Zero axes*' button defines the current machine location as the origin.
- Connect/Disconnect – This instructs the control software to establish or close a connection to the metrology system. When connecting, the system also performs a check to ensure communication is functioning normally.
- Rotary axes panel
 - The dropdown box shows the selected rotary axis controlled by the four relative move buttons. Axes such as rotary tables will be displayed here and are defined by their axis names.

- The four buttons to the left allow the user to instruct a relative move of either -180, -90, +90 or +180. The feed rate for this move is entered in the '*Max feed rate*' entry on the '*Current measurement*' panel.

7 Current Measurement Panel

The 'Current User Settings' panel allows the user to control and view progress of metrology. This panel (Figure 10) is located on the lower left side of the main Metrology Control GUI. Many of the elements in this panel simply provide user feedback on metrology and are not editable.


The screenshot shows the 'Current User Settings' panel. It is divided into several sections. The top left section, 'Current set', displays a large '0' in a white box. To its right are two input fields: 'Max feed rate' with the value '200' and 'pivDist' with the value 'not set'. The top right section, 'Measurement', contains three buttons: 'Execute', 'Cancel', and 'Pause'. The bottom section, 'Current Sub-aperture', displays a large '0' in a white box, an 'Attempt' field with the value '1', and four input fields: 'Tx Value' (0), 'Ty Value' (0), 'Tilt Error RSS' (0), and 'Power Value' (0). At the bottom of the panel is a 'Status' field.


Figure 10: Current User Settings panel.

The function of each element in the above panel is described below;

- Current set – non-editable indicator of which set or repetition of the measurement plan is currently being processed.
- Max feed rate – this is the maximum feed rate any axis may travel at when moving between measurement positions. The measurement device is not typically moved during non-alignment moves so the feed rate may be higher than that indicated in 5.3.12. This value is limited by the CNC controller internal hardware limit.
- PivDist – This value describes the vertical offset between the table horizontal rotation axis and the SUT CoC. This entry is required in order to allow the measurement system to make multiple ring measurements on a non-plano surface. This value may be calculated with the aid of the pivDist calculation assistant (5.4).

- Measurement panel:
 - Execute – Instructs the measurement system to begin metrology of the specified plan. Following selection of the execute button, there is a short start up procedure which requires user input.
 - Cancel – Instructs the measurement system to abort metrology. All data already collected is retained and the system will not make further movements.
 - Pause/Resume – Toggles the machine between running and paused moves. Pause move halts the machine where it is and holds the current measurement plan. On resumption, the system will continue with measurement.

 Warning **The cancel and pause buttons are not to be used as a replacement for emergency stop (EMG) under any circumstances.**

 Warning **When these items are used, the system will complete the last internal task before responding. There may be a small delay before the system responds.**

- Current sub-aperture Panel
 - Current sub-ap – Displays the current measurement sub-aperture being addressed. This value corresponds to the plot label numbers on the right hand plot window. The current surface area under test is circled in red.
 - Attempt – Shows the current attempt value for this measurement location. If measurements continually require more than one attempt to obtain valid data, this may indicate a measurement set-up or environmental problem.
 - Tx/Ty Value – These displays show the tilt-X and tilt-Y values respectively in waves/radius.
 - Tilt error RSS – This shows the root sum squared value of tilt-X and tilt-Y (see 5.3.13).
 - Power value – Indicates the residual power term in waves. Both the tilt error RSS and power residual must be less than those specified in the user configuration menu for the system to commence measurement of the current sub-aperture.

8 Measurement Designer application

The Measurement Designer application allows the user to develop a measurement plan based upon a Zeeko part design file and knowledge of the test optic to be used. Measurement Designer is started by selecting the icon on the main toolbar on the Metrology Control Suite GUI and opens into the main window.

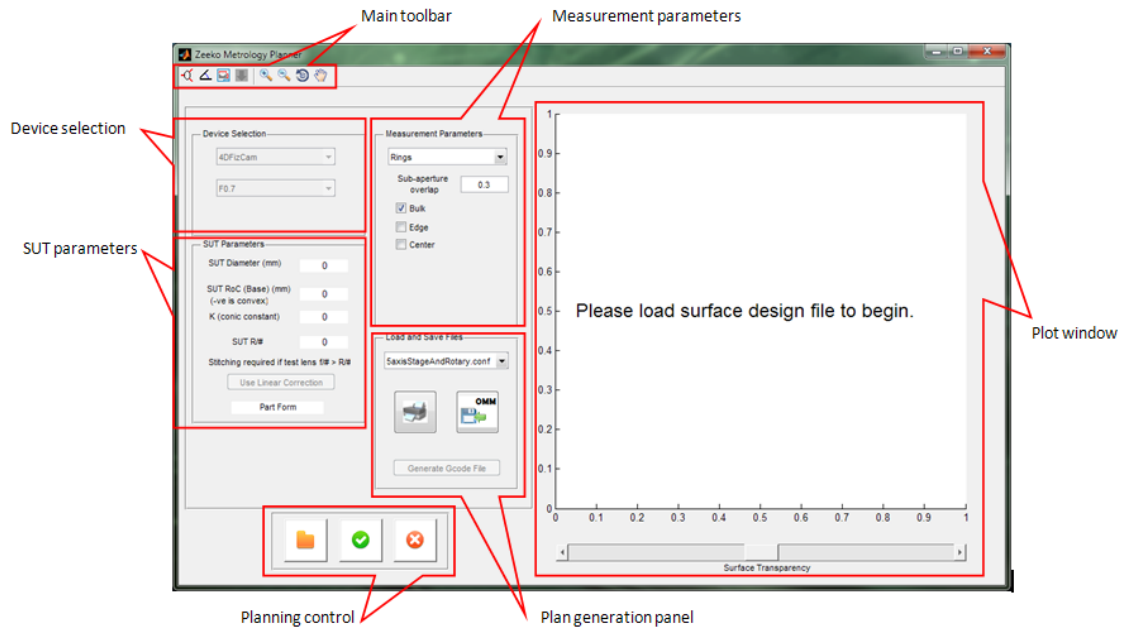
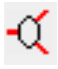









Figure 11: Measurement Designer main GUI

8.1 Main toolbar functions

Most of the features of Measurement Designer are accessed through the GUI main toolbar. These are outlined below.

Table 7: Measurement Designer main GUI toolbar.

Icon	Function	Description
	Edit optics database	Opens the optics database editor to allow the user to add/remove/modify optics which can be used to design measurements.
	Open sub-aperture angles editor	Opens a window to allow user to manually edit sub-aperture placement to allow plan optimisation.
	Open surface designer	Opens surface designer. This allows the user to generate a surface design file.
	Pass measurement plan back	Allows the user to pass the metrology plan back to Metrology Control program without saving.
	Zoom in plot window	Selecting zoom and clicking on the plot window will zoom in on current image.
	Zoom out plot window	Selecting zoom and clicking on the plot window will zoom out on current image.
	Rotate plot window	Selecting this mode, the user can click and hold the left mouse button while moving to rotate the surface plot.
	Pan plot window	Selecting this mode, the user can click and hold the left mouse button while moving to pan the surface plot.

8.1.1 Edit optics database

In order for a metrology plan to be developed, the application must have knowledge of optic parameters. The optics database allows the user to store optics for future use. The optics database editor allows the user to view the database contents, add, edit and remove optics as required. The database editor GUI is shown in Figure 12.

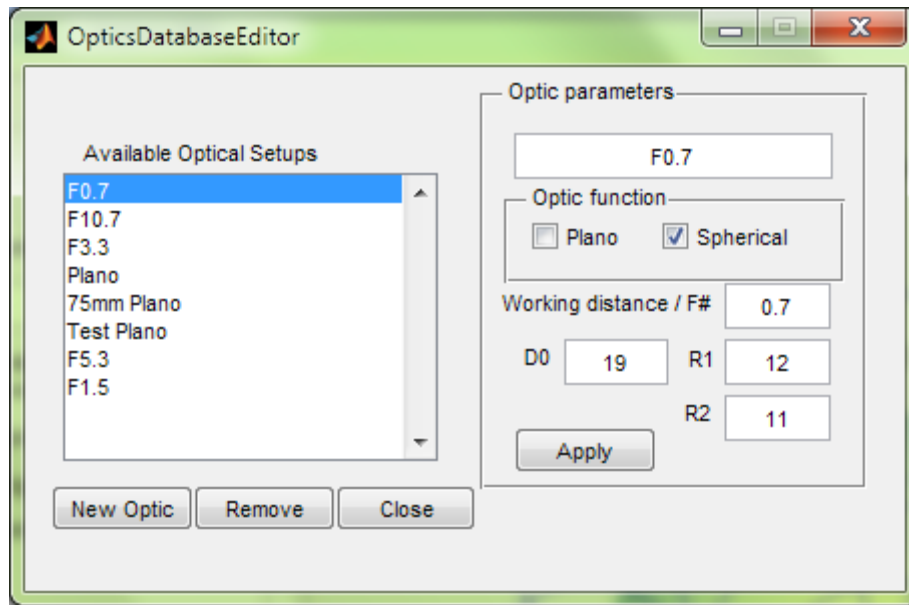


Figure 12: Optics database editor.

Available Optical Setups list – The available setups list shows all optics currently available in the database. Selecting any of the optics listed will highlight it and populate the parameters panel (to the right) with the associated information.

New Optic – This button will add a new entry to the optics database. This will be shown as *'new optic'* in the list. This should be selected to begin editing.

Remove – This will delete the selected item from the list.

Close – This will close the optics database editor and return to Metrology Designer.

Optic parameters panel –

Optic title – This is a description of the optic. This must contain at least one character and may be made up of alphanumeric characters and symbols such as underscore (), dash (-) and period (.).

Optic function – The user should select whether the optic is intended for plano or spherical measurement.

Working distance/f# - For spherical surfaces, the user should enter the reference optic F#. For plano surfaces this entry is unused but it is suggested that the user enter a working distance as a reference.

D0 – This is the reference surface diameter.

R1 – Reference surface radius of curvature (RoC), used in calculation of sub-aperture size at the test surface.

R2 – Effective RoC of the objective front face, taking into account the optics mounting chassis. This is used to check the offset between the reference objective front face and the test optic to ensure there is sufficient clearance to allow testing. Should there be insufficient space between the two optics during planning a warning will be displayed.

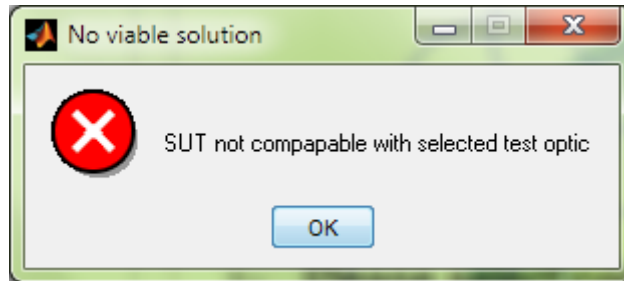


Figure 13: Insufficient reference/test optic clearance.

8.1.2 Sub-aperture angles editor

Following the initial measurement design, it is often the case that the user will wish to modify the measurement plan. This may be done using the sub-aperture angles editor (Figure 14).

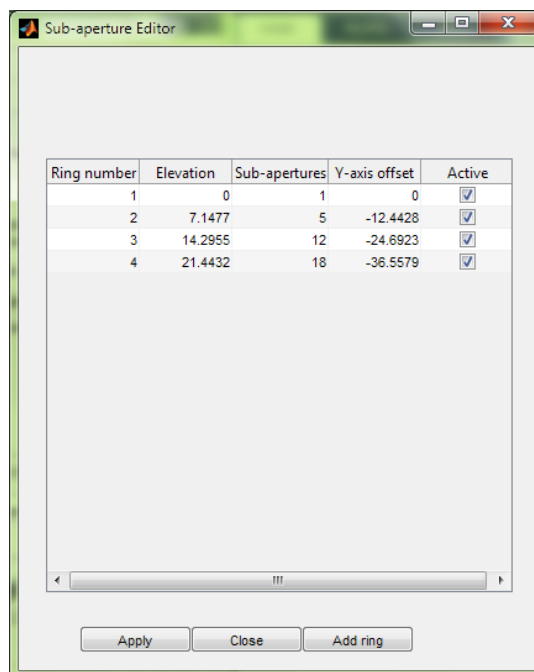


Figure 14: Sub-aperture angles editor.

When the sub-aperture angles editor is opened, the user will note that each ring of sub-apertures is represented by a row in the list. Each column from left to right is explained below;

Ring Number – This refers to the sub-apertures in groups of rings numbered from centre to SUT edge.

Elevation – This indicates the angular elevation change in degrees from the centre ring to that of interest. If a spherical surface design is loaded, this entry may be edited in order to allow the ring position to be changed.

Sub-apertures – This is the number of sub-apertures on any given ring. This value may be edited to change the number of measurement points on a ring. Sub-apertures are placed at $360/n$ degrees.

Y-axis offset – This is the amount of lateral offset between the rings for the first sub-aperture in each ring. When designing measurement using a plano surface, this value may be changed to adjust the spacing between sub-aperture rings. For spherical testing, this value is fixed.

Active – This allows the user to toggle the ring on and off. This can be used should the user wish to avoid certain areas of the surface or look solely at the centre or edge.

Apply – The apply button will recalculate the measurement design using the updated parameters. The sub-aperture angles editor will be reopened following calculation.

Cancel – The changes will be abandoned and the editor window will be closed, returning to the Metrology Designer main GUI.

Add ring – An extra row will be added to the list table. The user may edit this row to provide an extra ring.

8.1.3 Open Surface Designer

This button opens the Zeeko Surface Designer application, which allows the user to create a surface design file. Please see separate Zeeko documentation for operation of this module.

8.1.4 Pass measurement plan back

When a measurement design is generated, the '*pass back*' button is enabled. This allows the plan to be passed back to the Metrology Control application without saving and reopening. It should be noted that using this button will close Metrology Designer without saving the plan. Should the plan be required again, the save button on the plan generation panel should be used.

8.2 Device selection panel

The device selection panel allows the user to select the device to be used to carry out measurement and chose an appropriate optic from the database.

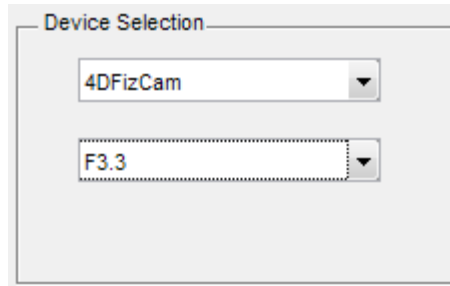


Figure 15: Device selection panel.

Device selection - The upper dropdown list provides all available measurement devices. When a device is selected the associated configuration is loaded and compatible optics from the optics database are listed into the lower list menu.

Optic selection – Depending upon the surface and device type selected, the optics database is filtered and only appropriate optics for the set up are displayed for selection. Selection of an optic loads the configuration ready for planning.

8.3 SUT parameters

The SUT parameters panel is non-user editable and serves to provide confirmation of the surface upon which measurement is being planned. This panel is shown in detail in Figure 16.

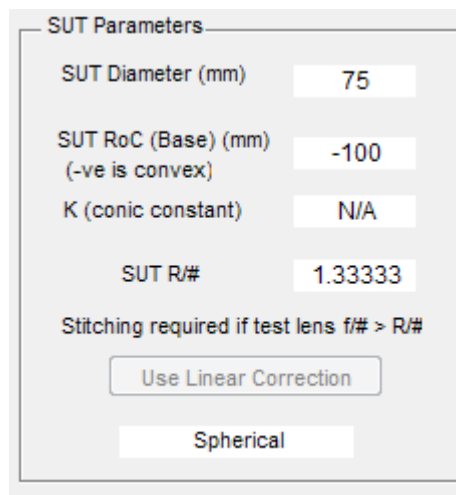


Figure 16: SUT parameters panel.

The elements of the SUT parameters panel are outlined below;

- SUT diameter – the minimum diameter circle, concentric with the SUT, which can enclose the SUT at the widest extents, expressed in millimetres.
- SUT RoC – The base radius of curvature to which the surface conforms, expressed in millimetres.
- K – Conic constant of the SUT.

- SUT R# - Effectively the F# number of the SUT. This is displayed to give the user an indication of when stitching measurements are required with a given reference optic.
- Use linear correction – When measuring on an IRP machine, linear correction allows a plane to be fitted to the SUT to correct for any mounting error. A window is opened to allow the user to select a non-linear file. This feature is disabled when not applicable.
- Form confirmation – This text box confirms the form of the current design and therefore the design mode under which the application is operating. Valid values are *'sphere'* and *'plano'*

8.4 Measurement parameters

The measurement parameters panel (Figure 17) allows the user to configure initial measurement planning.

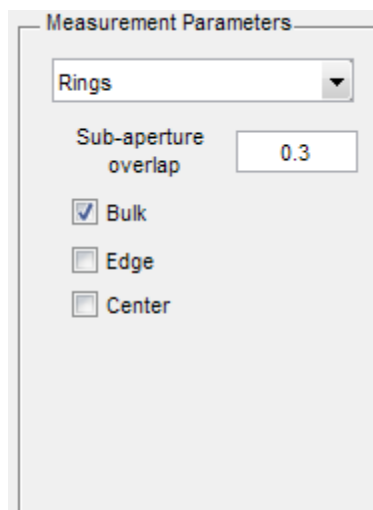


Figure 17: Measurement parameters panel.

- Measurement point configuration – The dropdown list at the top of the panel allows the user to select the measurement point organisation. Spherical surfaces only feature concentric rings at present. Plano surfaces can accommodate a square raster layout.
- Sub-aperture overlap – The user may enter a required overlap value (0.01-0.99) for the planner to use. Should the value entered result in a plan which does not cover the whole surface; the overlap value is increased until a viable solution is found. The entry is then updated for reference.
- Coverage check boxes – The three lower check boxes allow the user to specify regions of the surface to ignore. This allows inspection of just the edge or centre using the entered rules. Selection of *'edge'* or *'centre'* will display further entries, allowing the user to enter exclusion distances from the part centre in millimetres.

8.5 Plan generation panel

Following creation of a valid measurement design the user can return the plan back to the Metrology Control application via the toolbar button. However, if the plan will be required again in the future the user may save it via the plan generation panel.

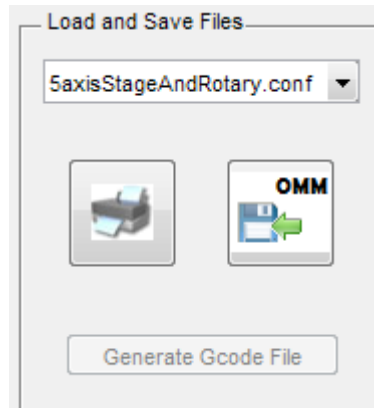


Figure 18: Plan generation panel.

- Configuration selection – The upper dropdown menu allows selection of the measurement system configuration. This is the description of the equipment which makes up the measurement system (e.g. IRP machine, 5-axis stage, rotary table, etc).
- Metrology plan report – The print button displays a window containing a diagram of the metrology plan along with information about the SUT.
- OMM save button – This allows the user to save the plan as an OMM file for future use. Metrology Designer also allows OMM files to be reopened for modification.
- Generate G-code – Metrology planner also supports part fiducial and grid placement for interferometer characterisation (IRP machine only). This requires generation of a g-code file.

8.6 Planning control

The planning control section (Figure 19) of the Metrology Designer GUI allows the initiation of planning as well as the discarding of any results. This is also where the user may access the load OMM/design file button.



Figure 19: Planning control panel.

- Open – The left button opens a window which allows the user to select either an OMM plan file or a surface design file for loading.
- Begin planning – The green check button starts the planner based upon the parameters set in the rest of the GUI.
- Discard results – The red cross button will discard any results and reset the plot window to contain only the surface design.

8.7 Plot window

The plot window displays the surface design, along with any planned measurement points. The plot window in Metrology Designer is different to that of the Metrology Control application in that it may be rotated, zoomed and panned using the main toolbar functions. The slider to the bottom of the window also allows the adjustment of the surface translucence. This allows greater visibility of measurement points when rotating the surface.

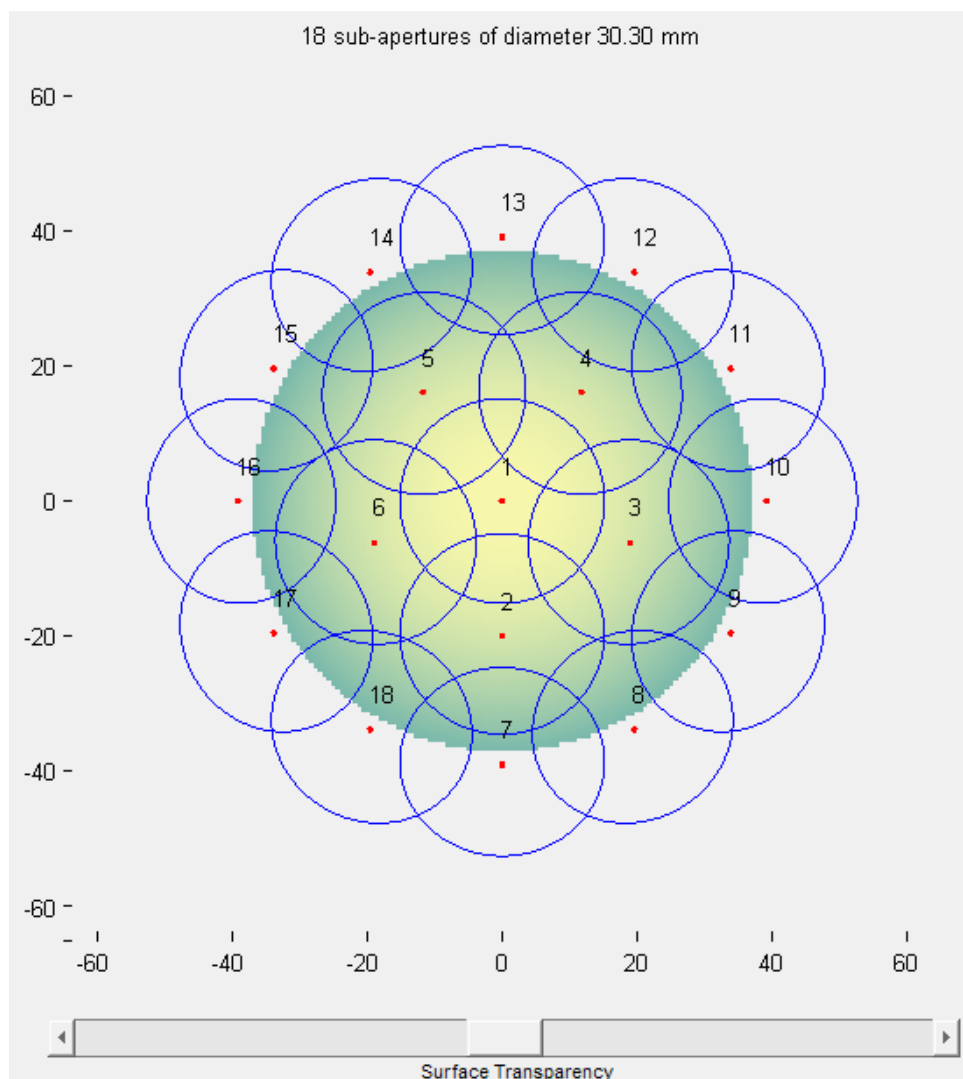


Figure 20: Metrology Design plot window.

All plot window axes are displayed in millimetres.

9 Operating Procedures

Many of the setup operations of Metrology Suite require user intervention to ensure safe and correct execution of measurement. This section details how these procedures are to be carried out and add further detail to the user prompts displayed.

9.1 Start-up

Each time any auto-execution task is started, the automatic sub-aperture measurement system will perform the tasks described below, which require some user intervention. Auto-execution tasks which complete this procedure are listed below and are required each time one of these operations is requested.

- Auto-clocking assistant.
- Auto-clocking while using the pivDist assistant.
- Execution of automatic measurement.

This procedure is as follows;

1. Alignment screen – The system will remove the test and reference return spots from the alignment screen by activating a solenoid located at the rear of the interferometer. This will produce two audible sounds spaced around 2 seconds apart.
2. Alignment screen reference only – A user prompt will be displayed as shown in Figure 21.

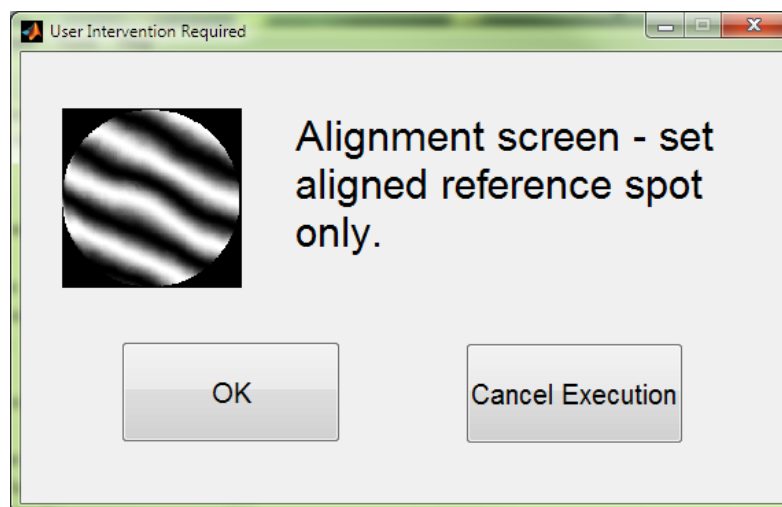


Figure 21: Reference spot only user prompt.

The operator should obscure the SUT from the interferometer with a non-reflective material (e.g. paper). This should be held between the reference optic and the SUT at an angle to minimise any stray reflection to return into the interferometer. This should

cause only the reference return to be visible on the alignment screen. With the beam blocked the user should press the 'OK' button and wait for the next prompt to be displayed before removing the block. Selection of the 'Cancel Execution' button aborts operation.

3. Check mask – Following the acquisition of the alignment screen images, a second user prompt screen is displayed as shown in Figure 22.

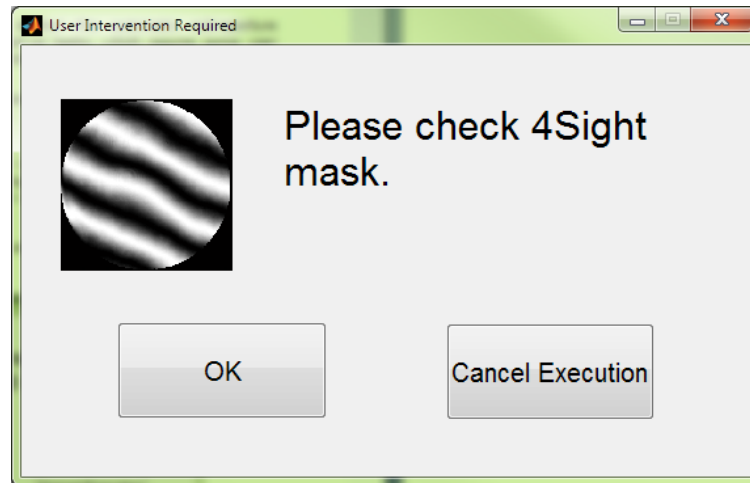


Figure 22: Check 4Sight mask prompt.

The operator may remove the beam block used for the previous step. The 4Sight detector mask should be set to the appropriate size so as to be slightly smaller than the interferometer field of view. This ensures that the interferometer does not suffer from data discontinuities at the edge of the pupil. Once the detector mask is appropriately set, the user should select 'OK'. Selection of the 'Cancel Execution' button aborts operation.



Note!

See 4Sight user manual for guidelines on setting the detector mask.

4. Webservice and HMOP – The third user prompt instructs the operator to start the 4Sight webservice and set the HMOP switch into the off position.

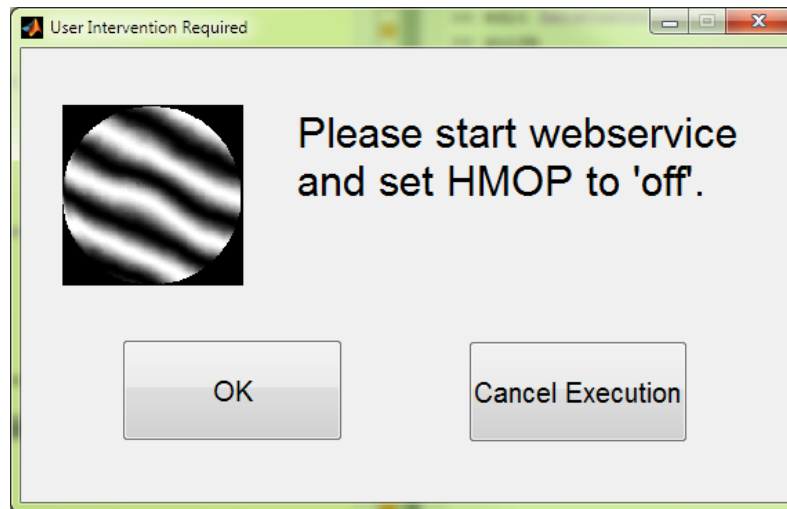


Figure 23: Webservice and HMOP prompt.

The operator should start the 4Sight webservice and confirm that it is running. The HMOP switch should be set into the off position (See OMSI Metrology Station Operation Manual). The operator may then select the 'OK' button. Selection of the 'Cancel Execution' button aborts operation.

The system should now proceed with the requested operation.

9.2 Auto-clocking assistant

In order to maximise the speed and accuracy of measurement it is desirable to minimise the amount of alignment corrections required at each measurement location. This may be achieved by ensuring the optical centre of the SUT and measurement device are coaxial.

The auto-clocking assistant is a user aid which allows this process to be carried out with minimal user interaction. The auto-clocking assistant is started by selecting the 'alignment assistant' button located on the GUI main toolbar (Table 6: Main GUI toolbar functions..



Note!

Auto-clocking is only intended for spherical measurement set up. Selection of the auto-clocking feature with a non-supported OMM file will result in a warning message and the operation being aborted.

1. Before selecting the auto-clocking button from the main GUI toolbar, the operator should centre the rotary table lateral adjustment screws to provide maximum adjustment during clocking. Also ensure that the tilt screws are secure.

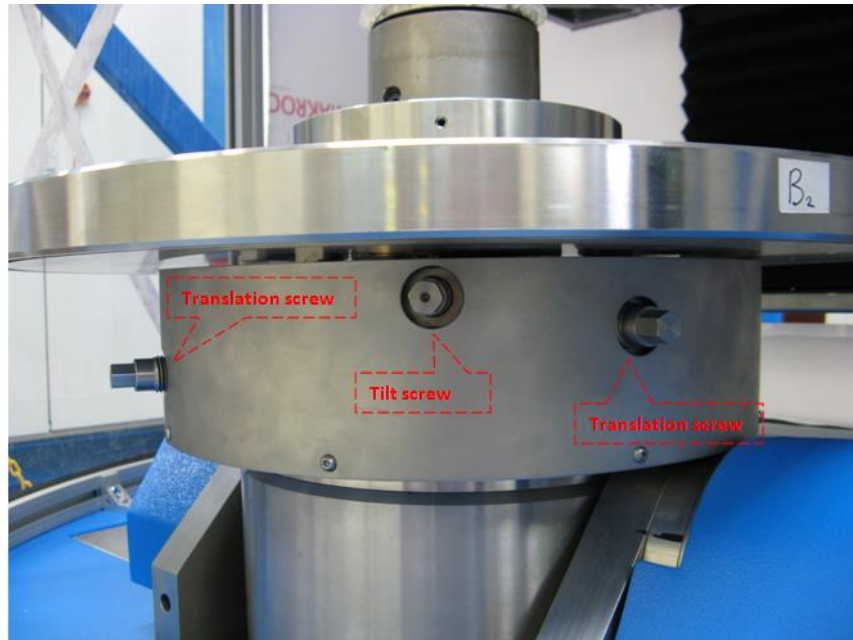


Figure 24: Rotary table screws.

2. Auto-locking initiates with the Start-up procedure (9.1).
3. The system will enter auto-alignment. If this is the first procedure to be run since the OMM file has been loaded, this procedure may take several minutes to complete.
4. Following auto-alignment, the machine table will rotate by 180°. The system will then check part alignment. If required, a screen will be displayed containing the reference and SUT return spots along with a suggested position (green cross) for the SUT return spot (Figure 25). The operator should open the machine door and use the table lateral translation screws to align the SUT return to the indicated position.

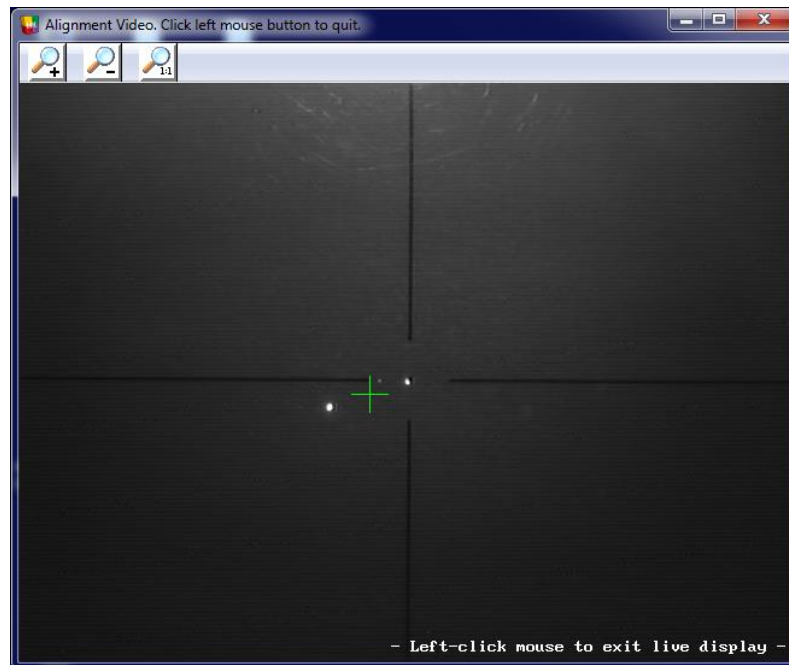


Figure 25: Auto-clocking alignment screen.

When the SUT return and the suggested position indicator are adequately aligned, the user should left-click the alignment screen. The image will be closed.



Note!

Following the alignment of the SUT return and the suggested position, the operator is not required to close the machine guard. For best results, it is advised that the guard is left open for the remainder of this procedure.

Should the SUT be seriously misaligned and the return spot is lost from the alignment screen during the 180° rotation, the system will make a series of rotations while attempting to continue the procedure. If the system cannot find a solution which allows the continuation of the auto-clock procedure, a user prompt (Figure 26) is displayed and operation is cancelled. In this case, the user should manually improve SUT clocking and restart the procedure.

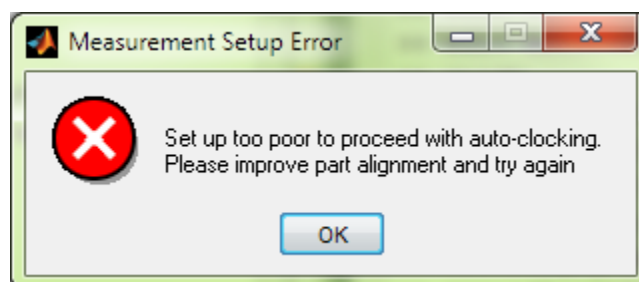


Figure 26: Auto-clock set up failure.

5. Following realignment, the system will enter auto-alignment.
6. Steps 3 – 4 are repeated as required until the SUT and interferometer optical axes are sufficiently coaxial for measurement. A user prompt is then displayed to indicate the procedure has completed (Figure 27).

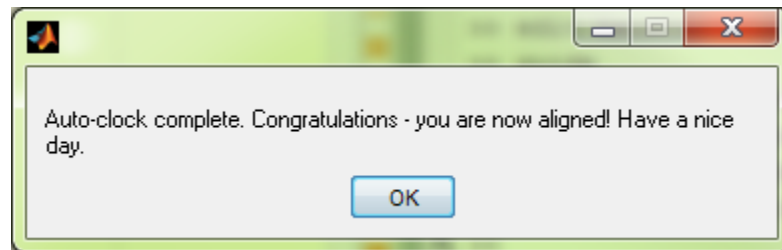


Figure 27: Auto-clock completed user prompt.

9.3 pivDist calculation assistant

When measuring spherical surfaces using multiple rings, the Metrology Station must rotate the T-axis in order to place the relevant ring in the correct orientation for measurement by the interferometer. This rotation requires a correction of the W and Z axes to ensure the SUT is located within the interferometer FOV (Figure 28).

When using a previously calculated pivDist value the number is placed in the pivDist entry on the Metrology Control Suite main GUI (chapter 7). The pivDist procedure may then be skipped.

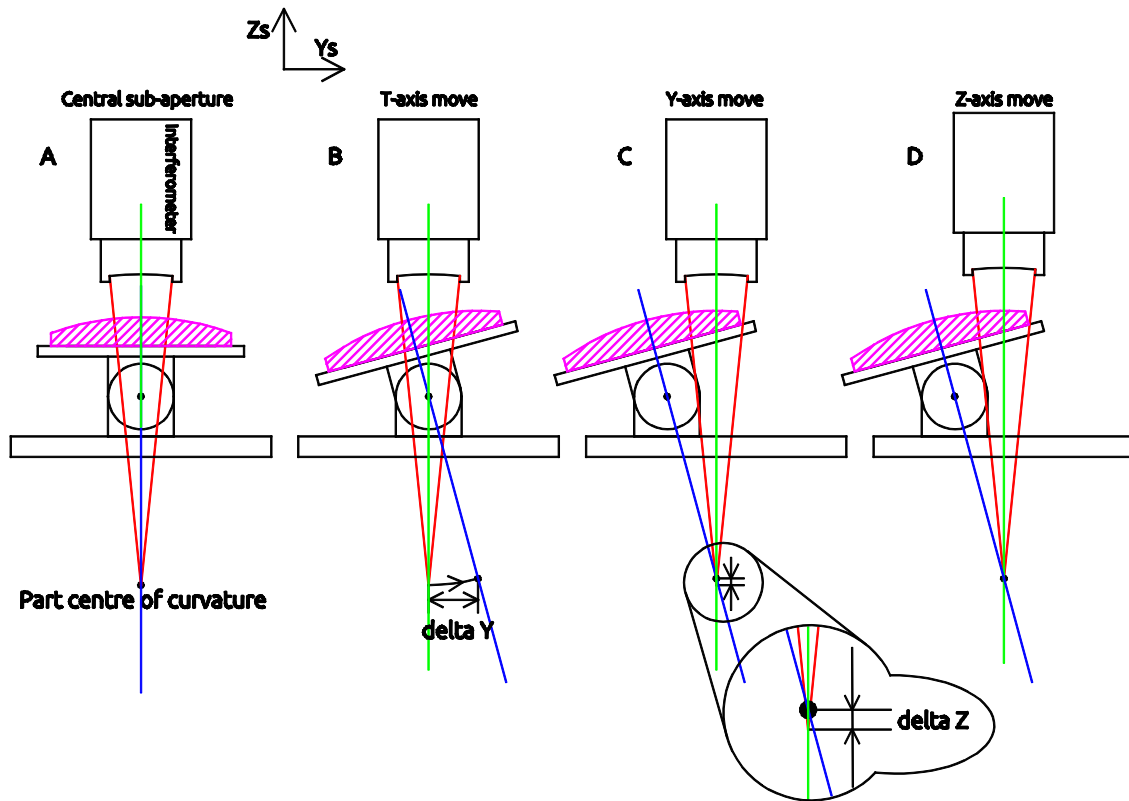


Figure 28: pivDist correction during multiple ring measurement.

In order to make accurate correction moves the distance between the T-axis pivot and the part centre of curvature must be found. The pivDist calculation assistant allows this calculation to be carried out during measurement set up. The pivDist calculation assistant is started by selecting the button located on the main GUI toolbar (Table 6).

1. The user should ensure that the rotary axis is placed at the machine zero position, with one translation screw parallel to the Y-axis of the machine chassis. The table-top must also be horizontal. i.e. $V=0$, $A=0$, $B=0$, and the table-top must be clocked to be perpendicular to the U-axis.
2. Table cat's eye – A user prompt is displayed instructing the operator to place the interferometer cat's eye at the rotary table surface.



Figure 29: Table cat's eye.

The user should switch the HMOP into manual mode and manually move the system to place the interferometer focal point at the rotary table. This can be verified by observing the fringes using 4Sight. When at the cat's eye position, the operator should observe a null or tilt fringes only. These tilt fringes indicate the reference surface alignment and not the table alignment. The operator should seek to remove any power from the fringes to ensure proper positioning at cat's eye.

With the interferometer positioned at cat's eye the operator should select the 'OK' button to complete this step. Selection of 'Cancel Execution' will abort the process.

3. Auto-clocking – Although step 0 of this procedure may be performed with the part secured to the machine, it is not required. For large parts, it may be impossible to position the cat's eye at the machine table with the SUT in place. Therefore, auto-clocking has been incorporated into the pivDist procedure. A user prompt will be displayed as shown in Figure 30.

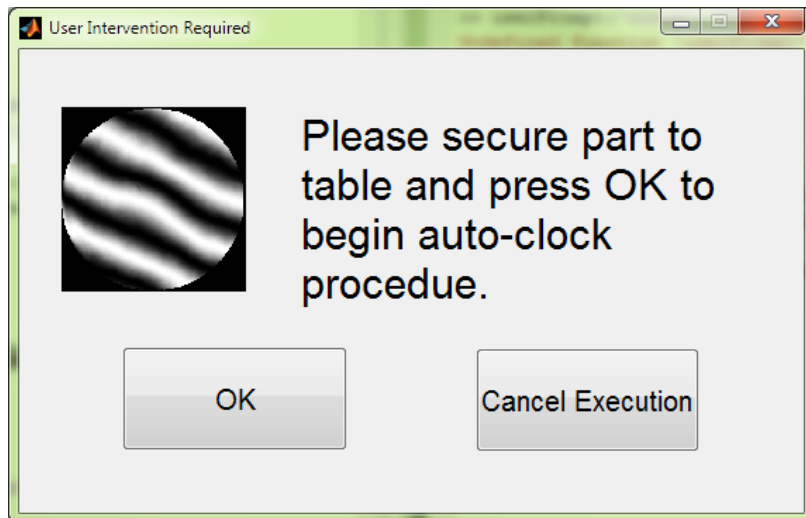


Figure 30: pivDist auto-clock user prompt.

The user may select 'OK' to enter the pivDist procedure as detailed in 9.2. If the operator does not require auto-clocking, 'Cancel Execution' should be selected. In this case the procedure will be continued with only this step being skipped. A further user prompt will be displayed to confirm this.

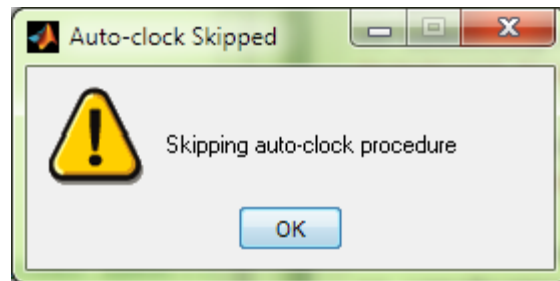


Figure 31: Auto-clock skip prompt.

4. Position confocal – Following either skipping or completing auto-clocking a user prompt will be displayed to request the interferometer be positioned confocal with the SUT.

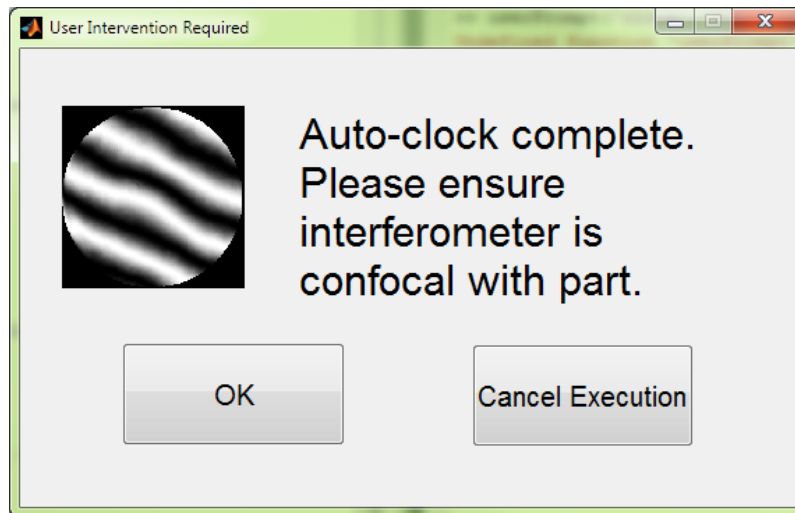


Figure 32: Request confocal positioning prompt.

The user should place the HMOP switch on and select the manual mode. The interferometer should be positioned with the T-axis level and nulled (both tilt and power) at the centre sub-aperture position. When the system is nulled, the operator may select 'OK' to move to the next step. Selection of 'Cancel Execution' will abort the procedure.

5. Part vertex cat's eye – A user prompt is displayed to request that the user place the interferometer cat's eye at the part vertex.



Figure 33: Part vertex cat's eye prompt.

Following step 4, the operator should only need to move the Z-axis. The move should be the same size and sign as the part radius of curvature (-ve for concave, +ve for convex). When at cat's eye, the operator should seek to null only power from the interferogram. The residual tilt represents reference surface misalignment and does not require adjustment.

With the part cat's eye positioned correctly, the operator should select the 'OK' button. Selection of 'Cancel Execution' will abort the procedure.

6. pivDist calculation – Following positioning the interferometer at the three positions, the system has enough information to calculate the pivDist value. This is done automatically and a user prompt is displayed to confirm the process was successful.

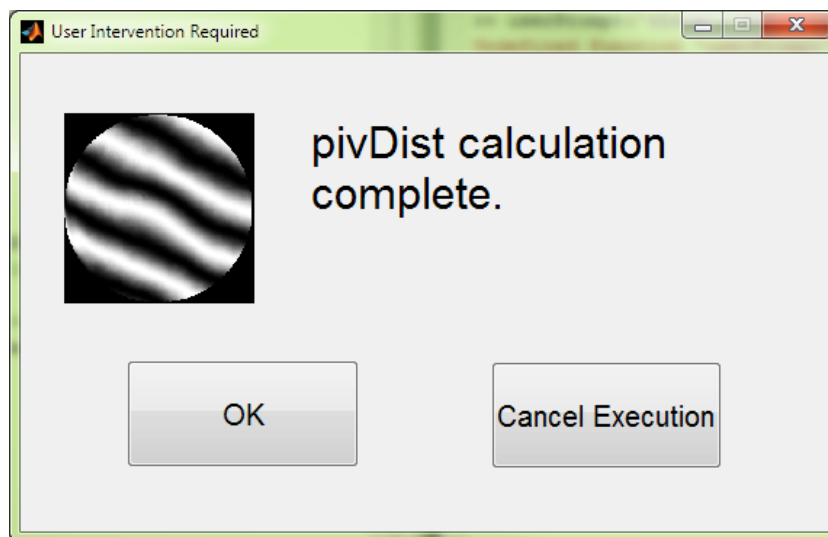


Figure 34: pivDist calculation complete prompt.

The user should select the 'OK' button to complete the process. This will update the pivDist entry on the current measurement panel (Chapter 7) with the calculated value.



Note!

It is possible for the pivDist value to be negative when measuring long RoC convex parts.

7. Following pivDist calculation, the operator should lower the Z-axis back to the confocal position and re-null the interferometer. The 'Zero axes' button on the CNC Operations panel should be selected (Chapter 6). This will zero the machine axes ready for measurement.

The pivDist value may be retained for future use without carrying out the above procedure. However, the test set up must be the same including SUT, part support and securing. It is advised that when a part is removed and replaced the assistant be used to ensure the value entered is accurate.

9.4 Measurement initiation

In order to initiate measurement, the user must have a valid OMM file loaded and have completed any required setup procedures (auto-locking and pivDist calculation for spherical surfaces).

1. The user should place the system at the measurement location 1 in the plan. The interferometer should be nulled at this position.
2. Zero the system axes by selecting the '*Zero axes*' button on the CNC operations panel.
3. Select the '*Execute*' button from the Measurement panel. The system will now carry out the start-up procedure (9.1).
4. The system will now enter auto-alignment. This process may take several minutes to complete. Following alignment sensitivity calculation, the system will enter measurement.

10 Example Workflow of Metrology Control Suite

Having covered the functions of the Metrology Control Suite and the associated sub-modules we can examine the overall procedure of using a metrology system.

- 1) Either load an OMM file directly or generate one using Metrology Designer (Chapter 11). The user will note the *'connect'* button is enabled on the *'CNC operations'* panel when a valid measurement design is loaded.
- 2) Select the *'connect'* button to establish communications.
- 3) Fit the same reference optic as specified during the design of the OMM file.
- 4) For spherical surfaces, perform the pivDist calculation procedure (9.3). For plano place the part on the rotary table.
- 5) For spherical surfaces, perform the auto-clocking procedure (9.2), if required (if not already done). For plano designs, manually centre the surface using traditional clocking techniques.
- 6) Check user configuration and make any required changes.
- 7) Part should now be optically clocked and pivDist value acquired (spherical only). Place measurement device confocal with centre of optical surface.
- 8) Select *'zero axes'* button in *'CNC operations'* panel.
- 9) Set maximum feed rate entry as required.
- 10) Select any sub-apertures to be ignored in the *'Ignore sub-apertures'* menu on the main toolbar.
- 11) Follow the measurement initiation procedure (9.4).

11 Example workflow of measurement design

- 1) Load a surface design file by selecting the '*open*' button (8.6).
- 2) Confirm surface specification against that shown in SUT parameters panel (8.3).
- 3) Select device to be used for plan generation from the '*device selection*' panel (8.2).
- 4) Select optic from dropdown menu.
- 5) Set overlap value to required level in the '*measurement parameters*' panel (8.4). Any value that is too low will be modified to minimum acceptable value by optimiser.
- 6) Select begin planning button on planning control panel (8.6).
- 7) Select sub-aperture angles editor to modify ring spacing as required (8.1.2).
- 8) Confirm correct configuration file for measurement system is selected in plan generation panel (8.5).
- 9) Either save plan to OMM file or pass data back to Metrology Control GUI via the main toolbar.
- 10) Close Metrology Designer.

12 Troubleshooting

Occasionally during operation the user may encounter error messages or note that the system does not perform as expected. This section aims to provide an explanation of these messages to aid issue resolution.



Note!

During unexpected operation the user must focus on machine operation and SUT safety. When attempting to troubleshoot the user should pause or cancel operation prior problem solving.



Warning

If in any doubt about machine performance during unexpected operation the user should operate the emergency stop button. Do not allow continued improper operation.

12.1 Coarse alignment spot oscillation/loss

If the coarse alignment spot is observed to oscillate or leave the spot screen during sensitivity calculation, the user should immediately stop the measurement process by selecting the 'Cancel' button.

This condition can occur due to improper performance of item 2 of the start-up procedure (9.1). It is recommended that the operator selects the 'Cancel' button to abort the measurement procedure. Measurement may be restarted without further action while ensure proper execution of the start-up procedure.

12.2 System unable to null at measurement location

The system fine alignment error displays may be observed to either oscillate around the null position or remain near static but not fall below the threshold error level.

This may occur due to either the operator selecting an error threshold below the measurement/actuation noise level or the fine alignment sensitivity calculation being inaccurate. In either case the measurement must be aborted by selecting the 'Cancel' button on the CNC operations panel. The operator should complete the following procedure;

1. The user is advised to restart measurement while observing the Axis Position Display (separately executed).

2. If the null issue recurs, observe if the axis positions are changing.
3. If the positions do not change over several updates of the error values on the current measurement panel, the user should restart measurement using higher tolerance values for the axis which could not be sufficiently nulled.
4. If the axis values are changing but the system does not null, the user should check the set up of the 4Sight software and interferometer. In particular:
 - Manually make a measurement and select the '*Terms Removed*' item in the '*Processing Options*' pane on the right hand side of the measurement screen. Select '*None*' in the Aberration Removal menu and select '*Copy to Future*'.
 - Ensure the detector mask is set appropriately for the measurement to be undertaken.
 - Ensure that the measurement locations do not over hang the edge of the SUT by more than ~5% of the interferometer field of view. When nearing the SUT edge it is advised that the user increase the number of measurement locations and minimised edge overhang to ensure system reliability.

12.3 Measurement locations skipped/ large slope error in data

The user may observe, in the measurement report, that measurement locations have been skipped with multiple attempts or have a large error (usually slope) on the resultant data.

Skipping of measurement locations indicates a significant amount of pixels have returned poor modulation during testing. This can be due to poor surface finish resulting in the scattering of the testing beam, dirt or scratches on the surface or measurement locations overhanging the SUT edge.

- The user should check the detector masking to ensure a single mask is defined which covers the area up to a few pixels from the interferometer field of view edge.
- Ensure that the SUT is clean and clear of any debris.
- Ensure that the measurement locations do not over hang the edge of the SUT by more than ~5% of the interferometer field of view. When nearing the SUT edge it is advised that the user increase the number of measurement locations and minimised edge overhang to ensure system reliability.
- The user can reduce the valid pixel threshold (5.3.17) to require less valid data to give a good measurement result. However, this will increase the likelihood of poor measurements no being repeated. If measurement is set up as advised, a measurement threshold of ~90% should be suitable.

12.4 Incorrect mode error

The system will not operate or has ceased operation and is displaying an error dialog box.

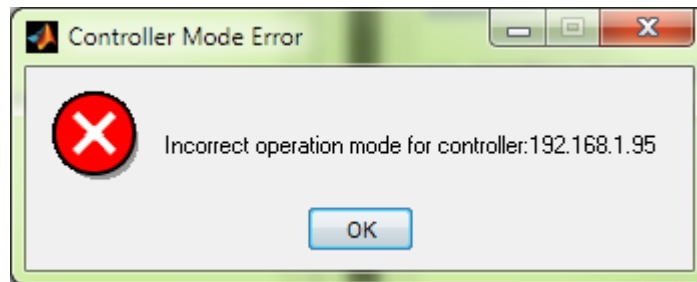


Figure 35: Controller mode error message

This error is caused by the system being in the incorrect operation mode for automatic operation. Before selecting 'OK' to close this message, the user should ensure that the system is placed in the automatic mode. (See OMSI Metrology Station Operation Manual)

9.2 Metrology Control Suite Debug Mode Application Note

Zeeko Metrology Control Suite

System Debugging Mode Application Note

1 INTRODUCTION

Zeeko Metrology Control Suite includes a debugging mode to enable internal system messages to be printed and viewed by the operator. Debugging mode allows to analysis of system operation and diagnosis potential errors. This application note describes how to place the system into debug mode and what to do with any output data.

2 STARTING DEBUGGING MODE

Metrology Control Suite can be placed in debugging mode as follows;

1. To enable debugging mode to print messages, Metrology Control Suite should be started from a command prompt. To start a command prompt in MS Windows, click the 'Start' button and type 'cmd' into the search box, as shown in Figure 1. Select cmd.exe from the list to start the command prompt. An example window is shown in Figure 2.

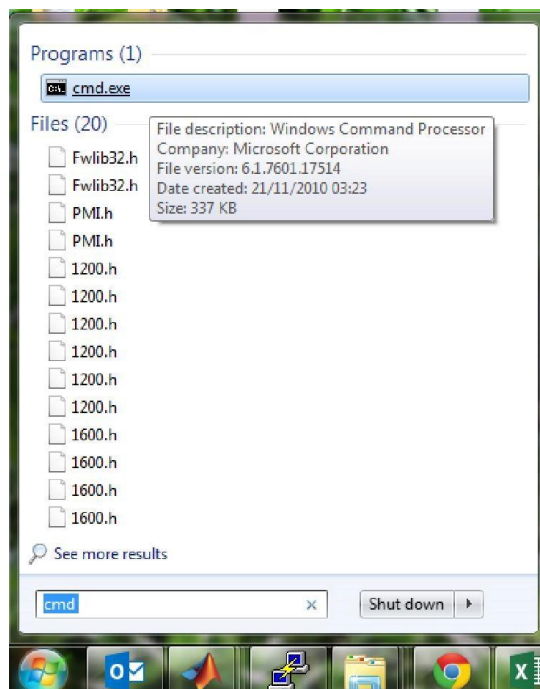


Figure 1: Start a command prompt

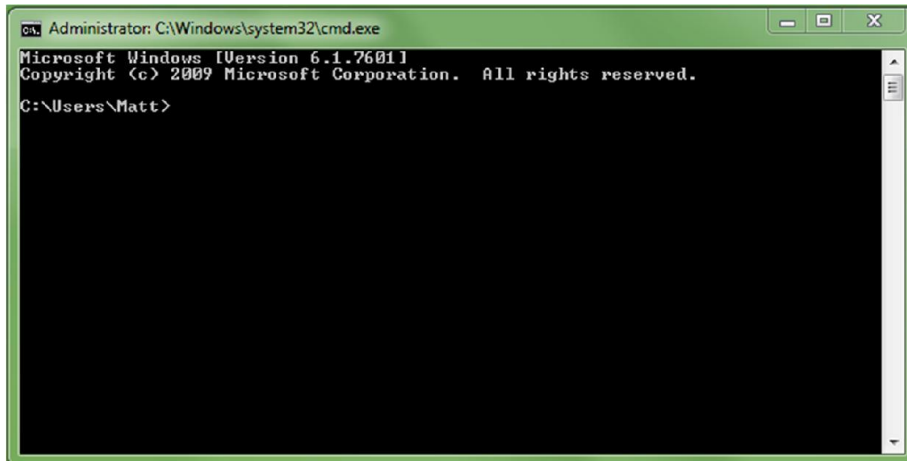


Figure 2: Command prompt window

2. With the command prompt window open, the user should navigate to the Metrology Control Suite executable folder using the window. Tip: The quickest way to do this is to use the Windows explorer window to locate the target directory. Click on the navigation bar at the top of the window and copy the folder location.

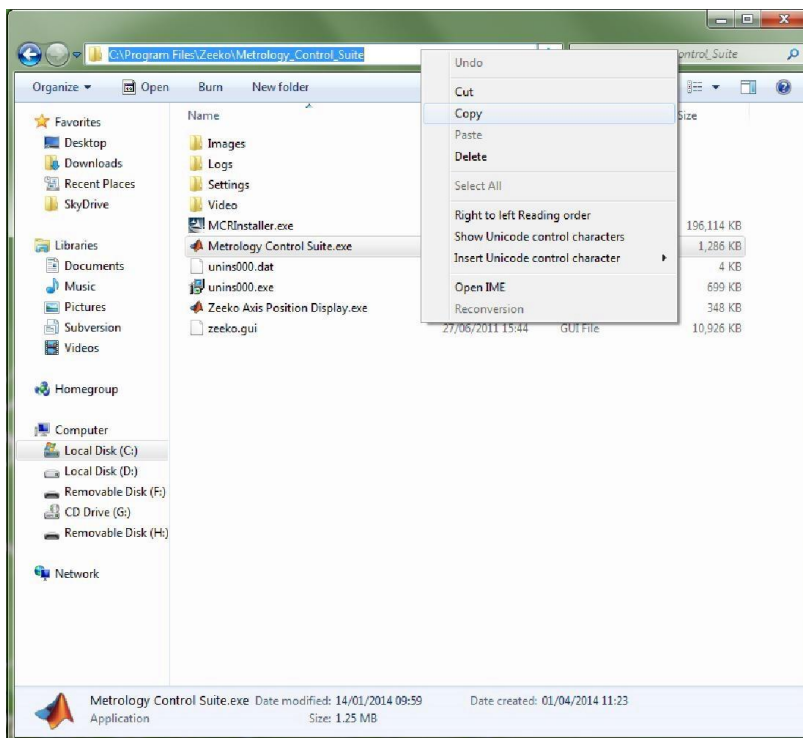


Figure 3: Windows explorer navigation bar

In the command prompt window, enter 'cd' followed by a space. Then paste the copied folder location and press enter. This will change the current directory into the Metrology Control Suite path. This can be confirmed by typing 'dir' followed by the enter key. A file listing should be produced which matches that in Windows explorer, as shown in Figure 4.

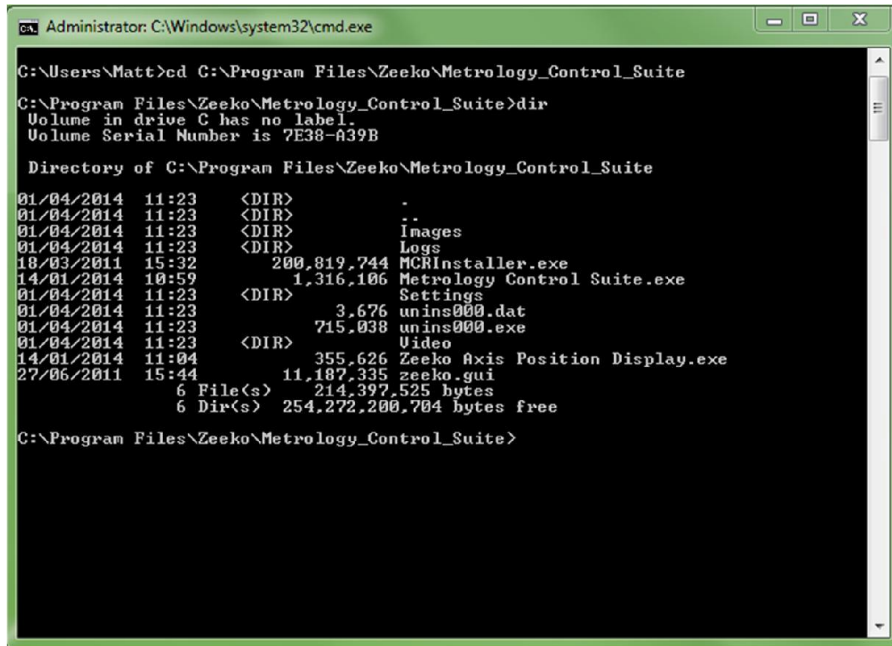


Figure 4: Directory listing

To start Metrology Control Suite, the user must enter “Metrology Control Suite.exe”, including the inner quotation marks. With Metrology Control Suite loaded, the operator should load or create an OMM file in the normal way.

3. When a valid OMM file is loaded, the user can enter debugging mode by selecting the blank button on the main graphical user interface (GUI) toolbar. This is indicated by the red box in Figure 5. A password entry box will be displayed to the user. Please enter the password provided by Zeeko personnel.

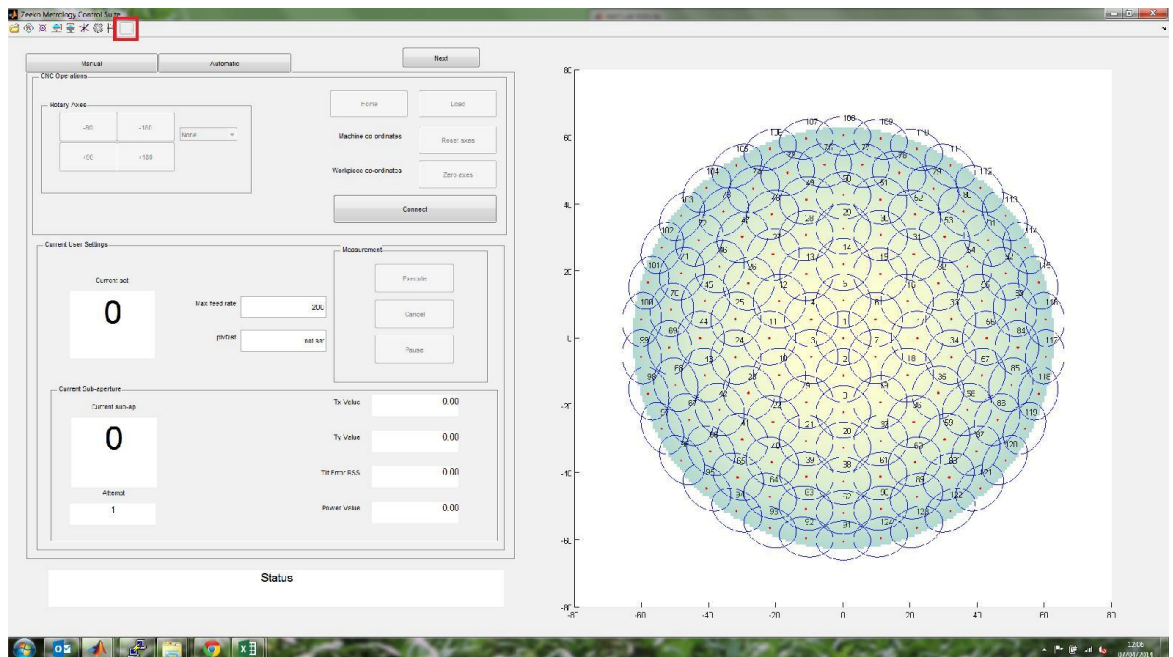


Figure 5: Debug mode toolbar button

4. Correct entry of the password will place the system into debug mode. This will be indicated by the command prompt window, shown in Figure 6. This window should remain open in order to view all debug mode messages.

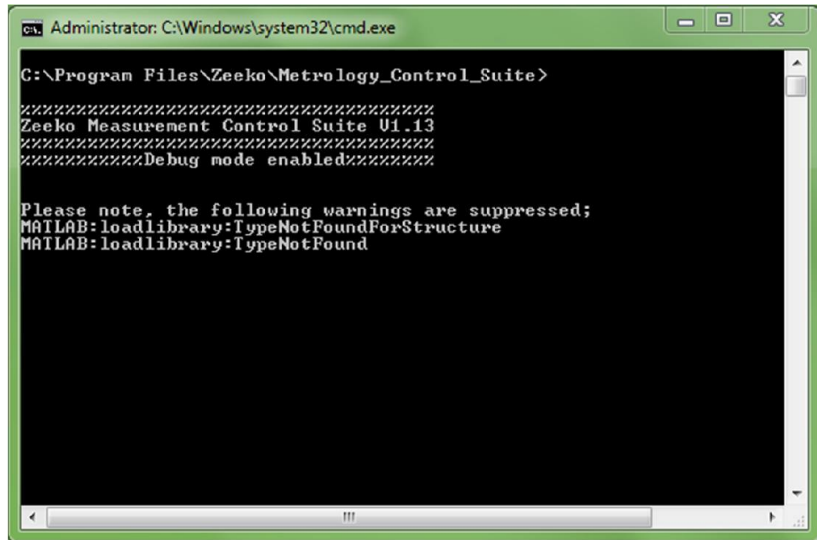
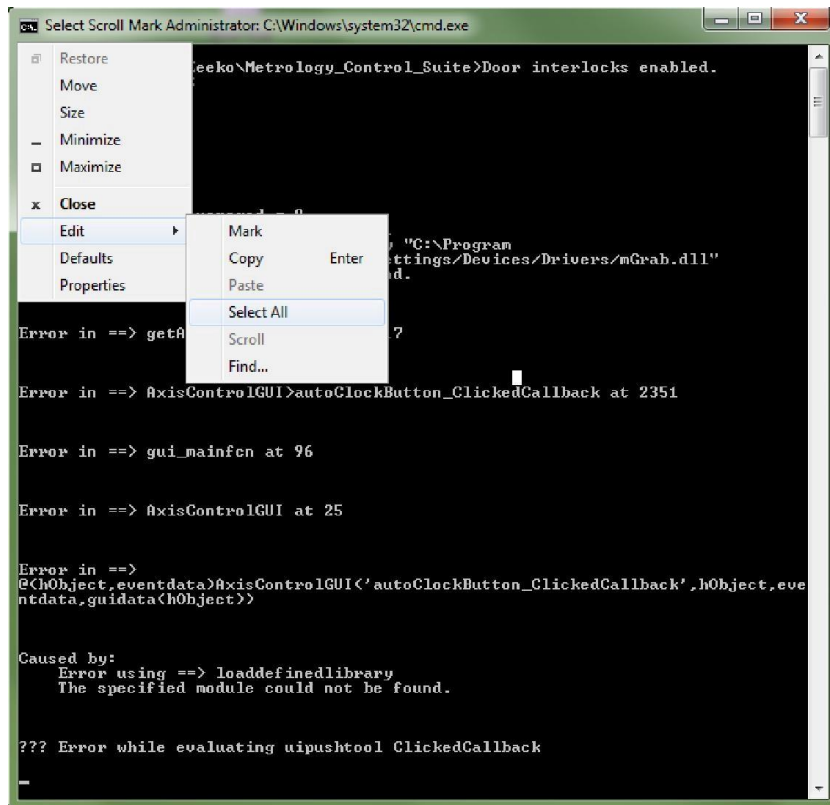


Figure 6: Successful password entry

3 USING DEBUG MODE

With debug mode enabled, all operation data will be reported on the command prompt window. The system operator can monitor performance and observe any errors which occur. While using this mode, the system will perform normally and all features remain available.

Should the system halt for any reason, the text within the command prompt window should be copied into a document and emailed to Zeeko personnel for analysis. This may be done by clicking the icon at the top left corner of the command prompt window and selecting 'select all' followed by 'copy', as shown in Figure 7.



9.3 STA Tilted Spigot Assembly

